The Mathematics of Foam

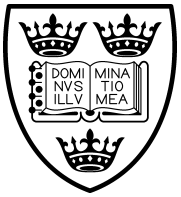

Christopher James William Breward
St Anne's College
University of Oxford

A thesis submitted for the degree of
Doctor of Philosophy

June 1999

Contents

List of Figures

Acknowledgements

I should like to thank a number of important people who have assisted me in many areas during my research time at Oxford. I'll start with my official supervisors: John Ockendon, and Richard Darton. They have both been extremely useful: John has continued to ensure that I perform to the best of my mathematical ability, while Richard has always endeavoured to 'keep me on the straight and narrow'. Peter Howell, while not an official supervisor, has been an invaluable and irreplaceable source of ideas. He has ensured that I remained focussed on the task in hand, no matter how often I attempted to stray from the path.

We have been in close collaboration with Colin Bain and Samantha Manning-Benson, from the Physical and Theoretical Chemistry Laboratory, who have provided us with insight into the behaviour of surfactants at surfaces, and a wealth of experimental data from the overflowing cylinder.

I should also like to thank Kui-Hua Sun from Engineering Department, for the high speed camera picture of a foam, Andy Kraynik for the pictures of the Kelvin cell and the random foam and Warrick Cooke, from OCIAM, for developing some mathematica code to enable the plotting of vector fields between two free surfaces.

There are numerous other people have made my DPhil time pleasant: My family; the old and not-so-old DH9 crew Keith, Mark, Dave, John and Jim; the rest of OCIAM; the members of St Anne's, especially Ele, Jason, Clare and Dr Hilary Priestley; and the members of my air cadet unit, 2267 (Lechlade) Detached Flight.

Finally I should like to finish by thanking Dr Mary Kearsley. Without her unending stories, I would never have remembered a whole host of mathematical concepts, including my favourite vector identity: *curl curl equals grad div minus del squared.*

The Mathematics of Foam

Christopher James William Breward

St Anne's College
University of Oxford

A thesis submitted for the degree of Doctor of Philosophy

June 1999

The aim of this thesis is to derive and solve mathematical models for the flow of liquid in a foam. A primary concern is to investigate how so-called "Marangoni stresses" (*i.e.* surface tension gradients), generated for example by the presence of a surfactant, act to stabilise a foam. We aim to provide the key microscopic components for future foam modelling.

We begin by describing in detail the influence of surface tension gradients on a general liquid flow, and various physical mechanisms which can give rise to such gradients. We apply the models thus devised to an experimental configuration designed to investigate Marangoni effects.

Next we turn our attention to the flow in the thin liquid films ("lamellae") which make up a foam. Our methodology is to simplify the field equations (*e.g.* the Navier-Stokes equations for the liquid) and free surface conditions using systematic asymptotic methods. The models so derived explain the "stiffening" effect of surfactants at free surfaces, which extends considerably the lifetime of a foam.

Finally, we look at the macroscopic behaviour of foam using an *ad-hoc* averaging of the thin film models.

Chapter 1

Introduction

Liquid foams occur in a wide variety of contexts. In everyday life, they form the froth in a washing-up bowl, and the head on a pint of beer. Practically, they are important, for example, in dampening explosions, collecting radioactive dust, dyeing materials and crop spraying. In all these applications, the ability of a foam to spread a small amount of liquid over a wide area is crucial. Foams are also used in the mineral recovery industry (the largest industry in the world). Here, it is the foam's ability to preferentially select one mineral over another which is important. This process has also been used to separate proteins. However, the presence of a foam is not always beneficial. For example, in the brewing industry, the presence of a foam during beer production is undesirable because it both reduces vessel capacity and lessens the foam potential of the finished product (see Bamforth [4]). Also, the presence of unwanted foam in a distillation column can cause substantial problems such as loss of throughput or deterioration in product quality throught loss of separation efficiency. In any case, it is desirable to understand the bulk properties of a foam and how they depend on those of its constituents.

1.1 What is a foam?

A foam is a gas-liquid mixture in which the volume fraction of the liquid phase is small. Foams are broadly divided into 'wet' and 'dry', depending on the proportion of liquid contained in them. In a wet foam (where the liquid volume fraction is typically between 10% and 20%) the bubbles are approximately spherical, while in a dry foam (where the volume fraction of liquid is less than 10%), the bubbles are more polyhedral in shape as in Figure 1.1. In a dry foam (as shown in a high speed photograph in Figure 1.2), the thin films forming the faces of the roughly polyhedral bubbles are called lamellae and the "tubes" of liquid at the junctions of these films are called Plateau borders, named after

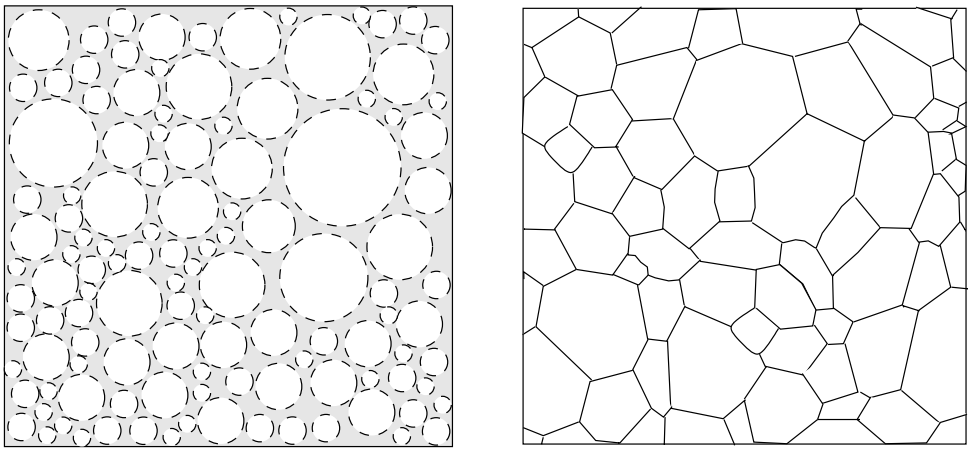

(a) (b)

Figure 1.1: Schematic of (a) a wet foam and (b) a dry foam.

Plateau, following his paper [66] discussing the angle at which three soap films meet. The vertices where typically four Plateau borders meet are called nodes.

We warn that pictures of foam are often misleading, since they are two-dimensional representations of three-dimensional structures. For example, in the photograph in Figure 1.2, the dark lines are Plateau borders, the lamellae span these dark lines and the nodes are the junctions of these lines. In the two-dimensional schematics of Figure 1.1, however, the lines represent the *lamellae* and the junctions of the lines represent *Plateau borders*; we cannot easily depict the nodes in these two dimensional representations. We show three dimensional schematics of the liquid distribution within a dry foam in Figures 1.3 and 1.4.

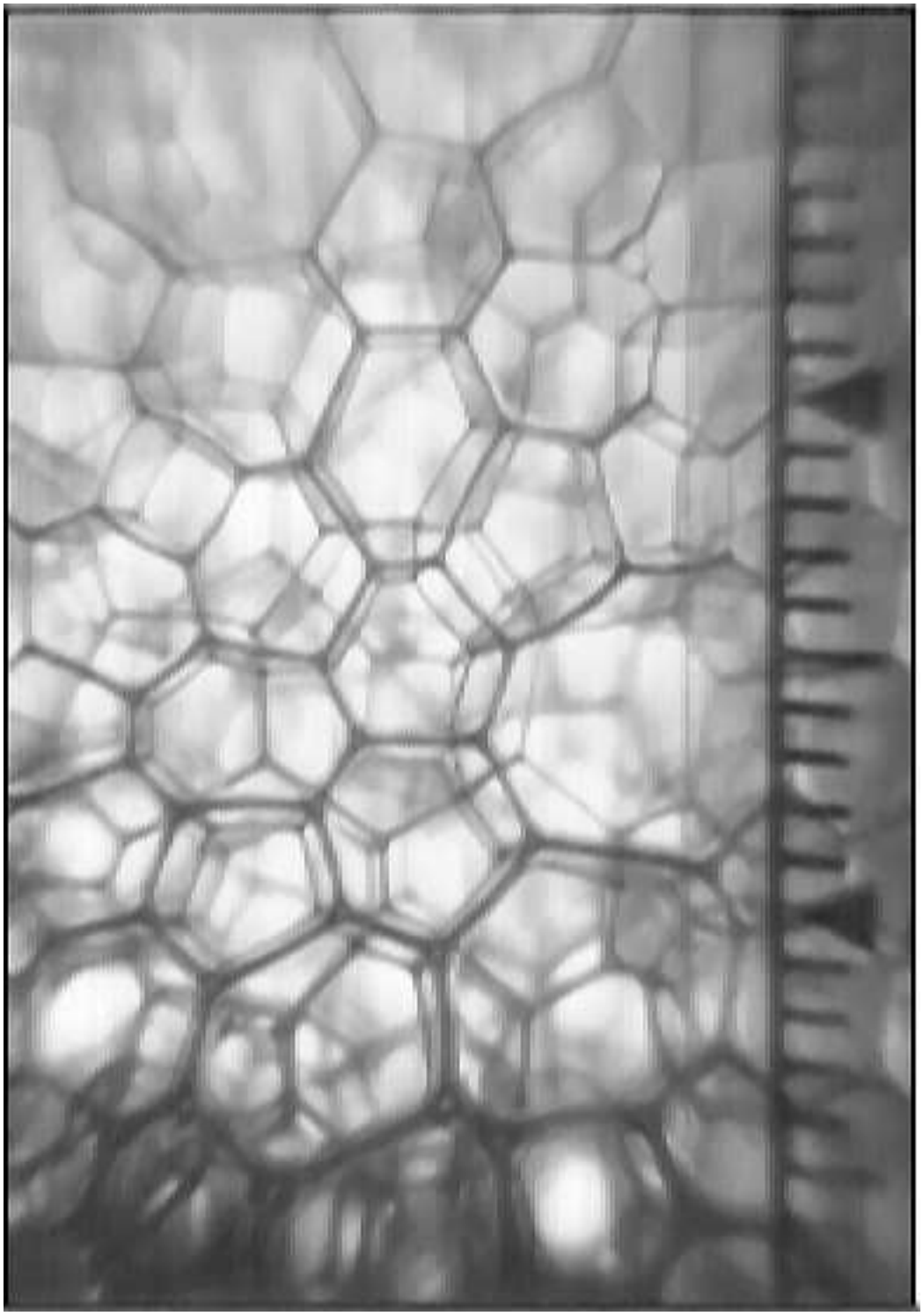

Figure 1.2: High speed photograph of a foam (courtesy of Kui-Hua Sun, Engineering Department, University of Oxford).

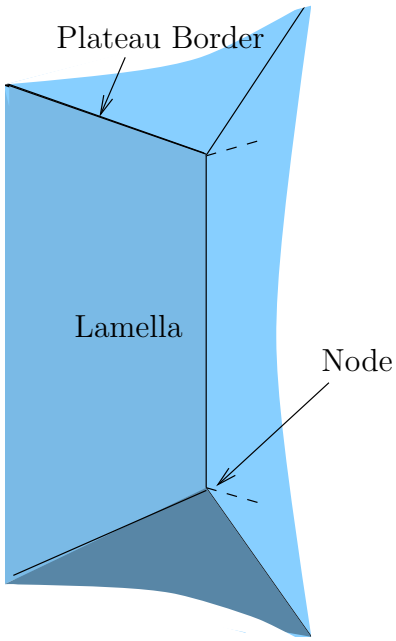

Figure 1.3: Schematic of liquid within a foam.

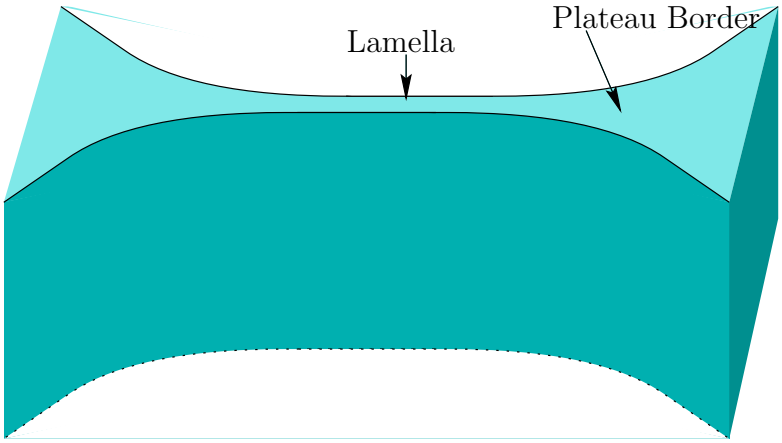

Figure 1.4: Close up of a lamella between two Plateau borders.

1.2 How do foams form?

Foams are formed when a gas and liquid are mixed. There are many ways in which this can occur, including:

- when a gas passes through a liquid, such as in a distillation column;
- when a gas and liquid are mixed and the gaseous phase is entrained, for example, when generating bubble bath foam;
- when a gas is released from solution due to a change in pressure, such as upon opening a bottle of fizzy pop.

Once a foam has been formed, its lifetime is determined by the flow of liquid, and the subsequent distribution of the various chemical components, through the microstructure. In general, a foam starts wet and becomes dryer as the liquid drains out of it. For some systems, this process proceeds until a stable volume fraction is reached after which the foam can last virtually indefinitely (due to intermolecular interactions). In others, the foam has a finite lifetime and when it becomes sufficiently dry, the lamellae become unstable and rupture and eventually the foam collapses.

1.3 Why does a foam persist after it has been formed?

Foam consisting of a pure liquid (*e.g.* pure water) is relatively short–lived. Since the curvature of the Plateau borders causes them to have a much lower pressure than the lamellae, the liquid drains rapidly from the lamellae into the Plateau borders. We call the effect of this pressure the 'Plateau border suction'. The lifetime of such a foam may be extended, however, by the addition of surface-active agents (*e.g.* washing up liquid) or volatile components, which generate surface effects that oppose the drainage of liquid from the lamellae.

1.3.1 Surfactants

A molecule of a surface-active agent (surfactant) is amphiphilic: it has both a hydrophobic and a hydrophilic part. The hydrophobic part often has an organic structure, while the hydrophilic part contains a group which either has charges which separate when dissolved in water or is polar. At sufficiently high bulk concentrations, the surfactant molecules associate with each other in the bulk and form micelles. These are 'balls' of surfactant molecules arranged in such a way that the hydrophobic 'tails' are completely surrounded by hydrophilic 'heads', see Figure 1.5(a).

Surfactant molecules prefer to be present at an interface, rather than remaining in the bulk. They arrange themselves so that the tail groups are in contact with the air, while keeping the head groups within the liquid, see Figure 1.5(b). Adsorption of surfactant

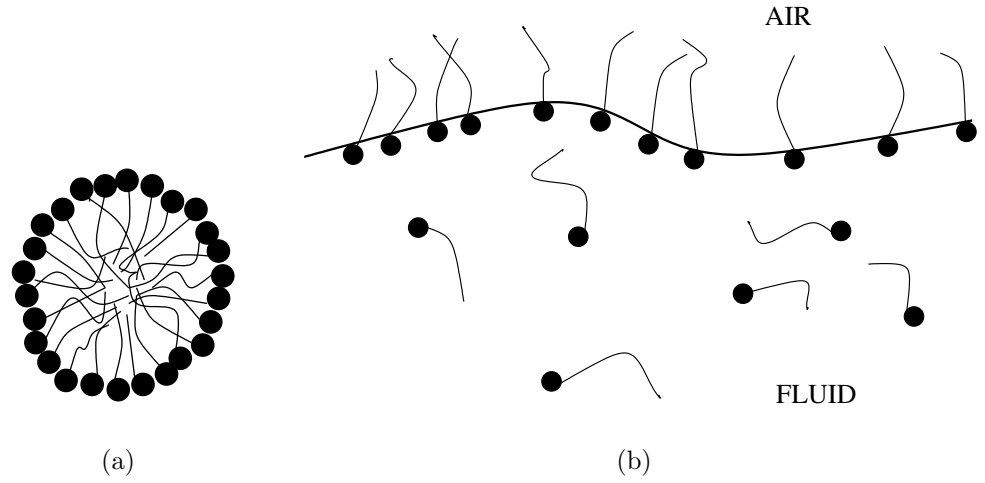

Figure 1.5: Surfactant molecules (a) forming a micelle and (b) at a free surface.

in this manner reduces the surface tension of the interface. We must thus consider two species of surfactant molecules, namely those in the bulk liquid and those residing in the surface.

Once the bulk concentration reaches the 'critical micelle concentration' (CMC), that is, the concentration at which micelles first form, the surface tension does not change with concentration. The surfactant molecules form more micelles rather than adsorbing at the interface. Nonuniform adsorption due, for example, to an expanding surface, can therefore result in a surface tension gradient.

1.3.2 How does a surface tension gradient affect a liquid flow?

A gradient in surface tension results in a surface shear stress acting on the liquid at the surface. Viscosity transmits this shear into the liquid and hence the liquid is accelerated or retarded, depending on the direction of the gradient relative to the bulk liquid flow. This effect will tend to stabilise foam if the surface shear opposes the Plateau border suction and conversely, the foam will be destabilised if the surface shear enhances the Plateau border suction.

1.3.3 Volatile Components

A foam may also be stabilised if it contains a second, volatile, liquid component which has a different surface tension from that of the primary liquid (*e.g.* in a heptane/toluene mixture). Higher evaporation in one part of the system compared to another can lead to depletion of the volatile component and hence a surface tension difference between the two locations. If such a gradient of surface tension exists between the lamella and Plateau border in a foam, the film may either be stabilised or destabilised, depending on whether the volatile component has a higher or lower surface tension than the inert component. In the Chemical Engineering literature, if the volatile component has the lower surface tension, then the system is known as *Marangoni Positive* while if it has the higher tension, then the system is known as *Marangoni Negative* (see Zuiderweg and Harmens [82]). Marangoni positive systems readily foam, while Marangoni negative systems do not foam at all. The former typically occur within distillation columns, where their persistence is highly undesirable.

1.4 What happens to lamellae when they become thin?

If a lamella is allowed to drain in a controlled environment, it may become so thin that molecular forces arising from the interaction of the two free surfaces come into play. If these forces are repulsive, this culminates in the formation of a stable "black" film of thickness between 10 and 100 Angstroms.[1] A very thin lamella may also be stabilised by the formation of a solid surface layer, for example, in an ageing washing-up liquid foam. Stabilisation of lamellae by these mechanisms will not be considered in this thesis. Our concern is with foam that is fundamentally unstable, but whose lifetime may be extended considerably by the mechanisms presented in §1.3.1 and §1.3.3.

1.5 How does a lamella rupture?

It is well known that a purely viscous film cannot break in finite time under the action of a finite force. In practice, films spontaneously rupture when they become sufficently thin. This may be due to random external fluctuations or to physical effects other than viscosity and surface tension. Indeed, numerous authors have incorporated attractive long-range intermolecular forces into thin-film models and thus predicted rupture at a

[1] One Angstrom is equal to 10^{-10}m.

critical thickness. We do not concern ourselves here with the mechanics of the rupture: we simply take this critical thickness to be a known material property.

1.6 How are foams destroyed in industrial situations where they are not wanted?

There are two methods that are often used in industrial situations to break down foams.

1. Chemical breakdown: Chemicals that disperse foams are known as antifoams, and are often oils or highly surface active materials. The choice of suitable antifoam for a given foaming system is empirical, and an antifoam which works well for one system may not work for another, similar system.[2]

2. Mechanical breakdown: Various mechanical methods can also be employed to breakdown foams. These range from the use of beaters (large stirring paddles within the piece of industrial equipment) to using ultrasound, where the frequency is determined to maximise foam destruction. Other methods include the use of heat transfer.

Obviously, the method used depends crucially on the constitutive parts in the foam. Attempting to break down a petrochemical foam using heat could be disastrous, for example. Also these methods are all potentially costly, and it would be preferable to avoid producing large quantities of foam in the first place.

1.7 Background material

There is a vast amount of literature on foams, both experimental and theoretical. We present details of the work which is most relevant to this thesis in the appropriate chapters that follow. General reviews of foam and its behaviour have been presented by Bikerman [11], Kraynik [46] and Aubert, Kraynik and Rand [3]. Bikerman's book focusses on experimental observations and *ad-hoc* models for foams. Kraynik's review includes more theoretical aspects, while Aubert et al. provides an 'easy-to-read' account of foaming phenomena.

Here, for completeness, we present an overview of some historically important and interesting areas of foam research that we will not have space to touch on in the rest of this thesis.

[2] "*When a plant has a foaming problem, the antifoam salesman is called, who turns up with a briefcase full of chemicals. These chemicals are, in turn, introduced to samples of the foam in question. If the foam is substantially reduced by one chemical, then it is introduced to the foaming solution.*"-Darton [18].

More exotic foams

There are a variety of non-aqueous and non-volatile systems which foam. For example, foams form on the top of molten baths of metal (such foams are known as Slag Foams). It is not clear whether such foams are stabilised by the presence of surface-active impurities or by small differences in temperature between the lamellae and Plateau borders. Experimental work studying such foams is being undertaken by Nexhip [61].

Geometric work

The characteristic shape of foam bubbles depends on the coarseness of the foam. As noted earlier, in a wet foam, bubbles are nearly spherical, while in a dry foam, the bubbles are more polyhedral. Numerous authors have attempted to determine bubble shapes, all trying to generate ideal cells: ones that tesselate space and minimise surface area.

Two-dimensional foams

As previously mentioned, Plateau [66] studied the joining of three lamellae (experimentally), and concluded that they always meet at 120^o. Weaire and Kermode [78, 79] describe von Neumann's bubble law which arises from a model to describe the change in area of a two-dimensional bubble acting under only gas diffusion between bubbles and capillary forces. The model predicts that bubbles with fewer than six sides shrink in area, whereas bubbles with more sides grow.

Three-dimensional foams

When four lamellae meet, in three-dimensional space, they always join at an angle of $\cos^{-1}(1/3)$ (see Kraynik [46]). Planar films cannot satisfy this constraint, and so lamellae must be curved. At the end of the last century, Lord Kelvin [74] created a tetrakaidecahedron; a structure with six planar quadrilateral faces and eight non-planar faces, all with curved edges, see Figure 1.6. He showed that it both tesselates space and minimises surface area for a given volume. More recently, Weaire and Phelan [80] found that such cells were present within a real foam. They also noted, from Matzke [57], that in practice the commonest films in a foam are pentagonal. They constructed a collection of eight polygonal bubbles which contains many pentagonal faces, fills space, and also has fractionally less surface than a Kelvin cell. Kraynik and Reinelt [50, 47, 48, 49, 68] carried out extensive work on the deformation of various theoretical foams. They used a surface evolver, which computed the minimal surface at each stage of deformation, to find the shape of a spatially periodic foam when shearing forces are applied.

Figure 1.6: The Kelvin Cell (courtesy of Andy Kraynik).

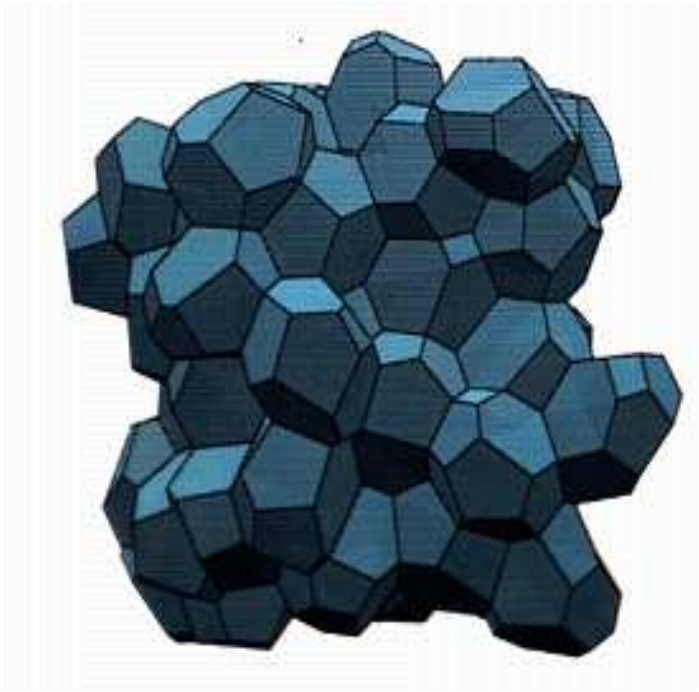

Figure 1.7: A random foam structure (courtesy of Andy Kraynik).

They used this to obtain shear moduli for the foams under consideration, which could then be used to describe macroscopic properties of the foam. Of course, real foams are often a random collection of bubbles, of various shapes and sizes, as shown schematically in Figure 1.7.

Foam flow

The mechanism for foam flow is the slip of each bubble over its neighbours to a corresponding position further along, see Figure 1.8. A critical yield stress is required to make this

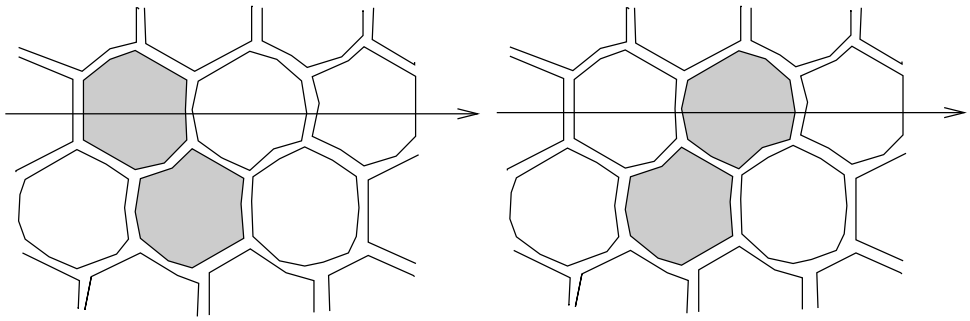

Figure 1.8: Schematic of a layer of bubbles moving over the top of another layer.

step. Thereafter, the effective viscosity decreases with shear rate. As noted in Kraynik [46], foams are macroscopically "multi-phase fluids which are compressible, nonlinear and viscoelastic" and, typically, foam is consituted as a shear-thinning viscoplastic material. A foam also exhibits *slip* at rigid boundaries. This can easily be seen as a macroscopic description of flow of bubbles over a wetted surface. These properties should be derivable from the microscopic flows that occur between the lamellae and Plateau borders.

There is a vast amount of work concerning foam flows in oil recovery processes. Here, the size of the channel in which the foam flows may be only a few bubble diameters across. Kornev et al. [22, 44], and Shugai [70] have discussed the flow of a foam within a porous medium. The former performed experiments on bubble trains through a cavity as shown in Figure 1.9. When the characteristic size of the bubbles was the same size as the inlet, the bubbles moved through the cavity without disturbing those bubbles around the edge of the chamber. When the characteristic size of the bubbles was much smaller than the inlet, the motion of the bubbles in the cavity appeared totally random. A mathematical study of flow of a bubble train through a porous medium was carried out in Kornev and Kurdyumov [45].

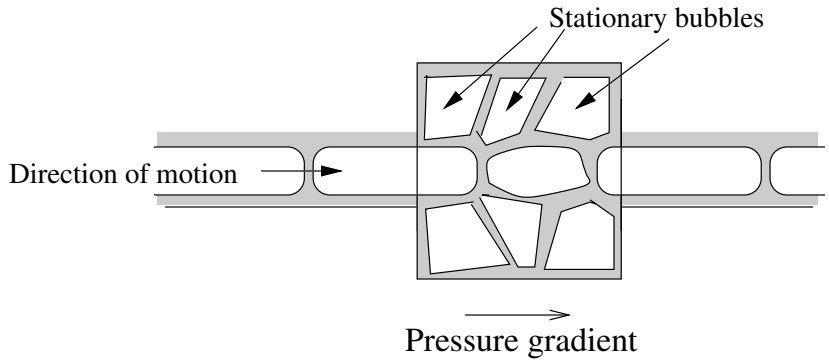

Figure 1.9: Schematic of experiment to study a bubble train moving through a cavity.

1.8 Thesis plan

In Chapter 2, we present the basic models that underpin all the work that we carry out in this thesis. We state the model for an incompressible Newtonian liquid, and we give details of the boundary conditions at both rigid and free surfaces. We then state the model for a soluble surfactant and formulate the boundary conditions for a surfactant adsorbed at a free surface. Finally, we state the model for a volatile component in a volatile-inert mixture, and discuss the boundary conditions that arise when we allow for mass transfer across an interface.

In Chapter 3, we present details of an experiment to study how a surfactant affects a dynamic interface in an easily accessible geometry, that of the overflowing cylinder. We model both the liquid and the surfactant, and the interaction between the two. We include the effects of gravity, capillarity, surface tension gradients, inertia and viscosity, convection and diffusion of the surfactant, and diffusion-controlled adsorption onto the surface. We have a high Reynolds number and high Péclet number flow and both diffusive and viscous boundary layers exist at the free surface. A crucial observation is that the diffusive boundary layer is typically much thinner than the hydrodynamic boundary layer. We solve the outer problems for the liquid and the surfactant, and then solve the inner problems close to the free surface, and in the vicinity of the stagnation point.

In Chapter 4, we develop the theory for thin films evolving under the action of Marangoni, capillary and viscous forces. We derive the distinguished limits of the model, defined as those regimes in which as many forces as possible balance. We also present other limits in which two forces balance or one force dominates. We further describe the distribution of the Marangoni inducing term, whether it is a surfactant or a volatile component.

In Chapter 5, we apply the thin film models derived in Chapter 4 to the problem of liquid

drainage from a lamella into a Plateau border. This involves decomposing the liquid domain into a time-dependent lamella, a capillary-static Plateau border and a quasi-steady transition region between the two. We first illustrate our procedure by considering the evolution of a pure liquid film, for which an explicit solution to the problem has been found. We solve the transition region problem to give the flux of liquid flowing from the lamella into the transition region as a function of lamella thickness, and then, assuming that the lamella is spatially independent, we are able to find the lamella thickness as a function of time. We then turn our attention to a lamella stabilised by a well-mixed surfactant, and we follow the same decomposition of the liquid domain as for the pure liquid case. Our numerical solutions produce some interesting behaviour, which we explain by an asymptotic analysis of the governing equations. We repeat the procedure using parameters for the soluble surfactant CTAB, and for an insoluble pulmonary surfactant. We present, but do not solve, the model for a lamella stabilised by a volatile component. Finally, we show that we may make progress and obtain an explicit solution to the problem if we assume that the system exhibits a constant surface viscosity rather than a Marangoni stress.

In Chapter 6, we present an *ad-hoc* model for the flow in a single Plateau border. We use this building block in a macroscopic model for a foam. We also discuss foam destruction by a self-generated antifoam and by using hot wires.

In Chapter 7, we round off by presenting the important results from the previous chapters, and by discussing extensions to our work. We finish by discussing experiments that we feel would aid the advancement of the theory.

1.9 Statement of Originality

In Chapter 3, §3.4 onwards is original work. In Chapter 4, the identification of the velocity scalings is original work, as are the models including Marangoni terms. The surfactant and volatile models are original, except for the models where $\epsilon^2\mathrm{Pe} \sim O(1)$ and the insoluble surfactant model. The modelling has been presented in Breward, Darton, Howell and Ockendon [14]. The work in Chapter 5 is all original, but the work in §5.2 is very similar to that presented in Howell [38]. With the exception of the presentation of the so-called Foam Drainage Equation, the work in Chapter 6 is all original.

Chapter 2

Modelling of liquids, surfactants and volatile systems

In this chapter, we discuss the modelling of liquids, surfactants and volatile systems. Our aim is to present the fundamental models for surfactant solutions and mixtures of volatile and inert liquids flowing beneath a free surface. As noted in the introduction, the surface tension of such solutions is not necessarily constant, and we describe the interplay between the surface tension and the concentration field in each case. In general, the bulk properties (such as density and viscosity) of a surfactant solution also vary with the bulk concentration; see Pandit and Davidson [64]. Here we only consider the case where such effects are negligible, and so we can treat the mixture as an incompressible Newtonian liquid.

In the section that follows, we present an uncontroversial model and boundary conditions to describe the velocity and pressure within the liquid. However, when we come to modelling the surfactant, while the field equation (the convection-diffusion equation) is well-known, the boundary conditions and the relationship between surface tension and surfactant concentration are less obvious. We present a chemical justification for these conditions, which, while not rigorous, gives some insight into the processes taking place. Our faith in the conditions that we arrive at is born out by their ability to fit experimental data (see Manning-Benson [52]). The model for a volatile component and the associated boundary conditions are reasonably well established in the paint-drying literature (see below).

For simplicity, we restrict ourselves to a two-dimensional geometry in this chapter. The equations generalise to three dimensions in fairly obvious ways, and indeed, in Chapter 3 we employ the axially-symmetric version.

2.1 Liquid modelling

2.1.1 Field Equations

We employ the incompressible Navier-Stokes equations (see, for example, Ockendon and Ockendon [62]) to describe the flow of our liquids. Thus $\mathbf{u} = (u(x, y, t), v(x, y, t))$, the velocity, and p, the pressure in the liquid, satisfy

$$\nabla.\mathbf{u} = 0, \tag{2.1}$$

$$\rho(\mathbf{u}_t + (\mathbf{u}.\nabla)\mathbf{u}) = -\nabla p + \mu\nabla^2\mathbf{u} - \rho g\mathbf{j}, \tag{2.2}$$

where ρ is the density, μ is the constant viscosity and g is the acceleration due to gravity (which we assume acts in the $-\mathbf{j}$ direction). The first of these equations represents conservation of mass while the second represents conservation of momentum.

2.1.2 Boundary conditions

At any rigid boundaries, we impose the usual no-slip condition that the liquid in contact with the boundary must move with the same velocity as the boundary. At a free surface $y = H(x, t)$, however, the boundary conditions are more complicated than the no-slip condition, and involve force balances and kinematics. We utilise the unit tangent and unit normal to the surface, defined by

$$\mathbf{t} = \frac{\pm 1}{(1 + H_x^2)^{\frac{1}{2}}} \begin{pmatrix} 1 \\ H_x \end{pmatrix}, \qquad \mathbf{n} = \frac{\pm 1}{(1 + H_x^2)^{\frac{1}{2}}} \begin{pmatrix} -H_x \\ 1 \end{pmatrix}, \tag{2.3}$$

where we choose the sign of $\mathbf{t}$ and $\mathbf{n}$ so that the normal points outward from the liquid. We denote the liquid stress tensor by τ, so for a Newtonian liquid we have

$$\tau = \begin{pmatrix} -p + 2\mu u_x & \mu\,(u_y + v_x) \\ \mu\,(u_y + v_x) & -p + 2\mu v_y \end{pmatrix}. \tag{2.4}$$

If σ is the surface tension of the liquid-gas interface, then balancing forces on a small element of the surface, we obtain the relationships

$$\pm\sigma\kappa = \mathbf{n}.\tau.\mathbf{n}, \tag{2.5}$$

$$\frac{\partial\sigma}{\partial s} = \mathbf{t}.\tau.\mathbf{n}, \tag{2.6}$$

where the (two-dimensional) curvature, κ, is given by

$$\kappa = \frac{H_{xx}}{(1 + H_x^2)^{\frac{3}{2}}}, \tag{2.7}$$

and s is arc length. Here, the liquid is on the right of the interface, when viewed along the direction of s increasing, and we choose the sign in (2.5) to be consistent with the definition of the normal in (2.3). We break with our usual convention of writing derivatives as subscripts when we consider $\frac{\partial}{\partial s}$ and $\frac{\partial}{\partial n}$. This is because s is a useful subscript to denote surface quantities, and we wish to avoid confusion. Also, we use the quantity s to denote volatile component later. On substituting for the stress tensor in these boundary conditions, we find

$$\pm\sigma\kappa = -p + 2\mu\frac{v_y - (u_y + v_x)H_x + u_x H_x^2}{1 + H_x^2}, \tag{2.8}$$

$$\frac{\partial\sigma}{\partial s} = \mu\frac{(u_y + v_x)(1 - H_x^2) - 2(u_x - v_y)H_x}{1 + H_x^2}. \tag{2.9}$$

We shall refer to these two boundary conditions as the 'normal force balance' and the 'tangential force balance'. The gradient of surface tension in the tangential force balance is commonly known as a Marangoni stress.

We also require a third condition to locate the free surface. Assuming that there is no evaporation, we employ the kinematic condition, which may be written as

$$v = H_t + uH_x. \tag{2.10}$$

We show how the kinematic condition can be modified to take account of evaporation in §2.3 to follow.

2.2 Surfactants

We have previously mentioned that a surfactant has an affinity for a surface. Here, we show how to model the transport of surfactant both in the bulk and on the surface. There are two ways of describing the concentration. We choose to follow the surface chemistry approach and to think of surfactant concentration as the number of moles of surfactant in a unit volume (bulk surfactant) or area (surface surfactant). The other approach is to use the volume fraction of surfactant molecules present in the solution.

As described in the previous chapter, some surfactants contain charged head groups which dissociate when dissolved in water. Adsorption of surfactant at the free surface results in the formation of an "electrical double layer". Such a layer can hinder further transport of surfactant to the surface. For simplicity, in this thesis we shall henceforth neglect such effects.

We assume that the bulk surfactant is transported by convection and diffusion, and that the concentration is below the critical micelle concentration, so that the dimensional model for the bulk surfactant concentration, $C(x, y, t)$ reads

$$C_t + (\mathbf{u}.\nabla)C = \nabla.\left(D(C)\nabla C\right), \tag{2.11}$$

where $D(C)$ is the diffusivity of the surfactant which can, in general, vary with the concentration of surfactant. We assume in this thesis, however, that the diffusivity is a constant.

We assume that the concentration of surface surfactant $\Gamma(x, t)$ (also known as the surface excess) is also transported by convection and diffusion, but now we also allow for an interchange of molecules with the bulk. We assume that such an interchange is controlled by diffusion (although the process may also be controlled by activation energies see Manning-Benson [52] or Chang [15] for a review), and so the flux from the bulk onto the surface is

$$j = -D\frac{\partial C}{\partial n}. \tag{2.12}$$

The equation for conservation of surfactant in the surface then reads

$$\Gamma_t + \frac{\partial(u_s\Gamma)}{\partial s} - D_s\frac{\partial^2\Gamma}{\partial s^2} = j, \tag{2.13}$$

where u_s is the surface velocity

$$u_s = \mathbf{u}.\mathbf{t}|_{y=H(x,t)}, \tag{2.14}$$

and D_s is the surface diffusivity. In practice, surface diffusion is often negligible, and we will neglect it henceforth, although we briefly examine its effects in the case of an insoluble surfactant in §4.5.6 and §5.5. We call (2.13) the "replenishment condition". The model is closed by the constitutive relation for the flux j, which is in general of the form

$$j = j(C, \Gamma). \tag{2.15}$$

The most common such model in the chemistry literature (see Chang [15]) sets the rate of adsorption of surfactant at the surface to be proportional to the sub-surface concentration, $C(x, H, t)$, and to the amount of space available at the surface. The rate of desorption is set proportional to the amount of surfactant on the surface, Γ. Hence we have the relation

$$j = k_1\left(C(\Gamma_\infty - \Gamma) - k_2\Gamma\right), \tag{2.16}$$

where Γ_∞ is the "surface saturation concentration", that is, the largest concentration of surfactant that can be present at the surface, and k_1 and k_2 are material parameters.

Equation (2.13) along with the flux given by (2.16) is known as the Langmuir-Hinshelwood equation (Chang [15]).

The three boundary conditions (2.12), (2.13) and (2.16) are sufficient to close the model for C and Γ. They are often simplified further. Often, in practical situations we can assume that the adsorption process described by (2.16) takes place very rapidly, and thus k_1 is, in some sense, large and (2.16) leads to a thermodynamic relation between Γ and C known as the Langmuir isotherm (see Adamson [1]),

$$\Gamma = \frac{\Gamma_\infty C}{k_2 + C}, \tag{2.17}$$

which is then coupled with (2.12) and (2.13).

Another simplification occurs if the surfactant is insoluble (as is often the case for pulmonary surfactant) in which case we can set $j \to 0$ in (2.13) and ignore the problem for C completely (see Gaver and Grotberg [29], for example).

2.2.1 Effect of surfactant on the surface tension

At a free surface, a surfactant is able to expel its hydrophobic tail from the solution and this reduces the surface energy of the system. For our purposes, it is necessary to impose the resulting constitutive relation between the surface tension and the surface concentration. These relations are typically obtained experimentally, but to help explain the origin of these effects, we present a "chemists' model". Our starting block is the modified Gibbs equation which relates changes in surface tension to the surface concentration and to changes in bulk concentration (Denbigh [24], Levich [51]),

$$\delta\sigma = -RT\Gamma\frac{\delta C}{C}, \tag{2.18}$$

where R is the universal gas constant and T is the temperature.[1] Now, assuming thermodynamic equilibrium, we use the Langmuir isotherm (2.17) to relate C to Γ, we let the infinitesimals tend to zero, and integrate the equation to read

$$\sigma^* - \sigma = -RT\log\left(1 - \frac{\Gamma}{\Gamma_\infty}\right), \tag{2.19}$$

where σ^* is the surface tension of pure water. Equation (2.19) is known as the Frumkin equation (see Chang [15]). The term $\sigma^* - \sigma$ is sometimes called the "surface pressure".

[1] Chemists use the concepts of (a) chemical potential and (b) an ideal-dilute solution to formulate this relationship. The RT factor in (2.18) arises because, at the surface, the surfactant is assumed to be in equilibrium with its vapour phase.

If the concentration of surfactant is above the critical micelle concentration (see §1.3.1), we must include diffusion of micelles and interplay between the bulk and micellar concentrations. Such modelling is beyond the remit of this thesis.

2.3 Volatile and Inert systems

In general a foaming mixture may be formed by mixing any number of chemicals with differing surface tensions and evaporation rates. In this thesis, we confine our attention to the simplest case in which we have one volatile and one inert component. We model the volatile component of an inert-volatile mixture by assuming that it forms a concentration field within the liquid as a whole. Here, we define the concentration $s(x, y, t)$ to be the mole fraction of the volatile component, that is, the number of moles of the volatile component compared to the total number of moles (of both the volatile and inert component) present. We use this definition of concentration to be consistent with the experimentalists. We propose that the mass transfer is controlled by convection and diffusion, and the model reads

$$\nabla.\left(D(s)\nabla s\right) = s_t + (\mathbf{u}.\nabla)s. \tag{2.20}$$

Again, the diffusion coefficient may vary with the concentration of volatile component, but in our modelling we will assume that it is constant.

2.3.1 Volatile component at the free surface

We must model two effects at the free surface: the first is evaporation of the volatile, and the second is the dependence of the surface tension on the concentration s. We assume that there is negligible adsorption of the volatile at the free surfaces, *i.e.*, $\Gamma \sim 0$, and we only have to consider the bulk concentration. We consider the liquid evaporating at a rate $e(s)$ at a surface $H(x, t)$, which moves with velocity V_n. At the surface we conserve both volatile and inert components:

$$-Ds_n + s\left(\mathbf{u}.\mathbf{n} - V_n\right) = e, \tag{2.21}$$

$$Ds_n + (1-s)\left(\mathbf{u}.\mathbf{n} - V_n\right) = 0. \tag{2.22}$$

We eliminate the terms multiplying the velocities and we obtain

$$-Ds_n = (1-s)e, \tag{2.23}$$

which we may re-write as

$$-D(s_y - H_x s_x) = (1-s)e\sqrt{1+H_x^2}. \tag{2.24}$$

If we eliminate the diffusion terms then we find

$$\mathbf{u}.\mathbf{n} - V_n = e. \tag{2.25}$$

Noting that $V_n = H_t/\sqrt{1+H_x^2}$, and that $\mathbf{u}.\mathbf{n} = (v - uH_x)/\sqrt{1+H_x^2}$, we can we-write (2.25) as

$$v = H_t + uH_x + e\sqrt{1+H_x^2}, \tag{2.26}$$

which is the kinematic condition re-written to include evaporation.

We denote the surface tension of the inert component by σ^I and that of the volatile component by σ^V. We require our mixture to have these surface tensions when s is zero or one respectively. However, the precise relationship that the surface tension follows depends on the two components and how they interact (see Atkins [2] for a discussion of how the partial pressures of binary mixtures behave). We assume that there is a linear variation between the two values, and so we have

$$\sigma = \sigma^I + \left(\sigma^V - \sigma^I\right) s. \tag{2.27}$$

2.3.2 Model for evaporation

We must also pose a constitutive relation for how the evaporation rate e varies with the concentration of volatile component s. Often, in applied mathematics literature, the rate is taken to be equal to a constant, *e.g.*, Howison et al. [39]. However, this does not adequately take account of the fact that there is a finite amount of the volatile and that the evaporation rate must be zero if the chemical potential in the liquid is the same as in the vapour phase. We call s^* the relevant concentration which makes the chemical potentials equal. We introduce a mass transfer coefficient, E_0, which is the velocity associated with the movement of the free surface in the case when there is only volatile present and the movement is due to evaporation alone. The simplest model that describes this phenomenon is $e = E_0(s - s^*)$, but we assume that the gaseous mole fraction is small and so work with

$$e = E_0 s. \tag{2.28}$$

2.4 Summary

We have presented the models that underpin the rest of this thesis, with a chemical justification of several of the conditions. We proceed to the next chapter where we hope to check that, using the surfactant conditions presented here, we can describe the flow

of a surfactant solution in an experiment to measure the properties of an expanding free surface.

We have closed our models by introducing extra chemistry relating to the surfactant or volatile component. Another approach that is employed by some authors is to suppose that the effect of a surfactant is to effectively stiffen the surface. Thus they pose a relationship between the surface tension and the surface velocity. The simplest such model sets the surface velocity equal to zero (for example, Schwartz and Princen [69]), while more elaborate, but still phenomenological models propose the use of a "surface viscosity", *i.e.*, the surface layer is treated as a viscous liquid with a different viscosity from the bulk liquid (for example Dey et al. [27]). In such a case, the surface tension is set to be equal to the surface viscosity multiplied by the rate of strain of the surface. Another similar approach is to model the surface as a elastic membrane, with a corresponding "surface elasticity". We believe that these effects can be thought of in terms of the surface tension gradient and hence do not need to be introduced if the chemistry and thermodynamics of §2.2 is justifiable macroscopically. At appropriate points through this thesis, we shall discuss our model's relationship to those in which surface viscosity is used in place of the Marangoni term.

Chapter 3

Modelling expanding free surfaces

3.1 Introduction

In Chapter 5 we will explore the way in which surfactant acts to stabilise a foam. A crucial property of surfactant in this respect is the way in which it resists expansion of the gas/liquid interface. However, making experimental measurements on such free surfaces is a difficult task since the lamellae are not only very thin, but are often also inaccessible. However, some ingenious experiments have been devised whereby expanding free surfaces can be studied and the effect of surfactant on them determined, the idea being to verify the boundary conditions proposed in Chapter 2. In these systems, the presence of surfactants affects the properties of the flow close to the free surfaces.

We turn our attention to two experiments that have been carried out within the Physical and Theoretical Chemistry Laboratory at Oxford University. The first experiment, using an overflowing cylinder, will be described in detail below. We shall also briefly describe the second experiment, which uses a jet of liquid, in Chapter 7. Both these experiments exhibit surface lifetimes comparable to those in foams.

3.2 The overflowing cylinder

The overflowing cylinder (OFC) is a device to measure the properties of an expanding free surface. It consists of a glass or metal cylinder (longer than it is wide) mounted with its axis vertical on a platform designed to minimise externally induced vibrations. Liquid is forced by a pump up the cylinder at a low flow rate so that, on reaching the top, it flows outward towards the rim of the cylinder and then smoothly overflows down the outside. It is then collected and re-circulated (see Figure 3.1). Flow straighteners near the base of the cylinder aim to ensure that uniform plug flow is achieved at a distance from the free surface. Using various techniques (including Laser Doppler Anemometry, Neutron

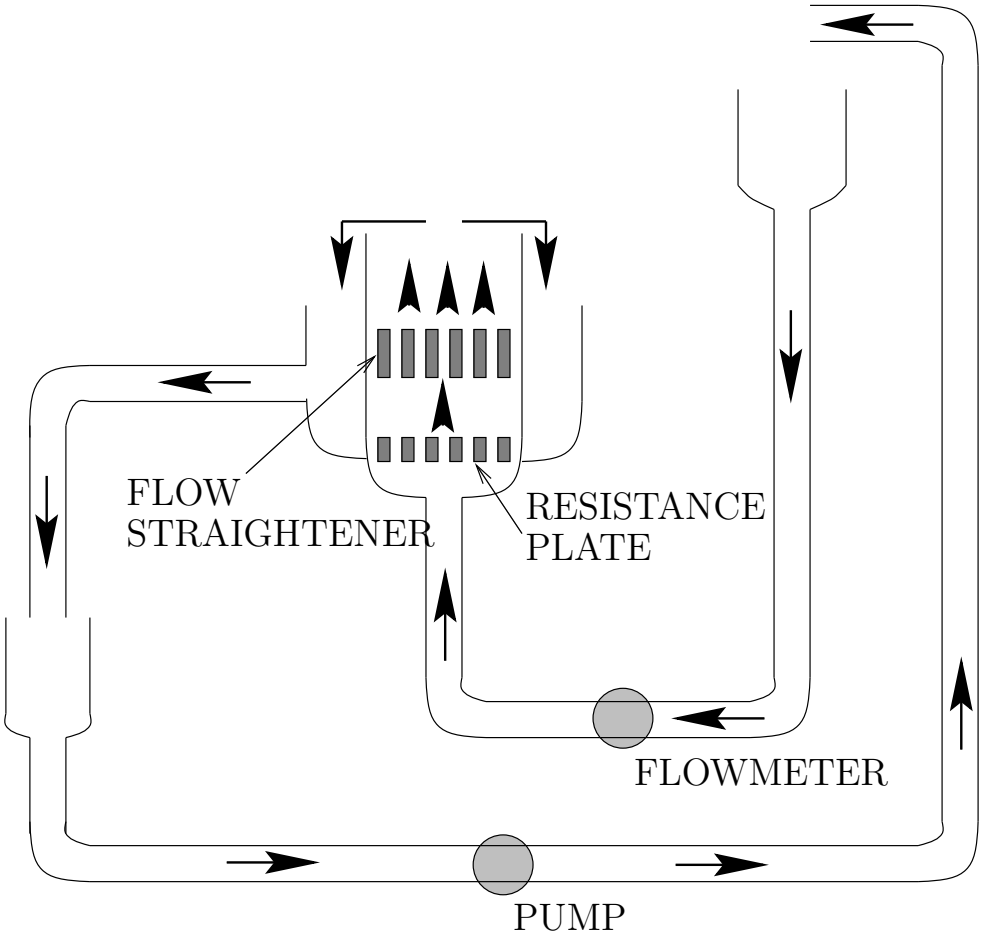

Figure 3.1: The overflowing cylinder.

Scattering and Ellipsometry), the shape of the top surface, the surface tension, the surface velocity and the surface concentration of any added surfactant can be determined at various points on the surface. These techniques are non-invasive, *i.e.*, they do not disturb the flow (unlike conventional techniques such as the Wilhelmy plate, see Manning-Benson [52]). The experimental techniques are reviewed in Manning-Benson et al. [52, 54, 55, 56]. We show a close-up of the overflowing cylinder in Figure 3.2. The arrows indicate the direction of the flow at the bottom of the cylinder, close to the free surface, and in the wetting film on the outside wall. The free surface at the top of the OFC is continually expanding, and, when a surfactant is present, surface tension gradients at this surface may be generated. By taking measurements of these gradients in a controlled system, we hope to learn about surface shear forces and adsorption of surfactant.

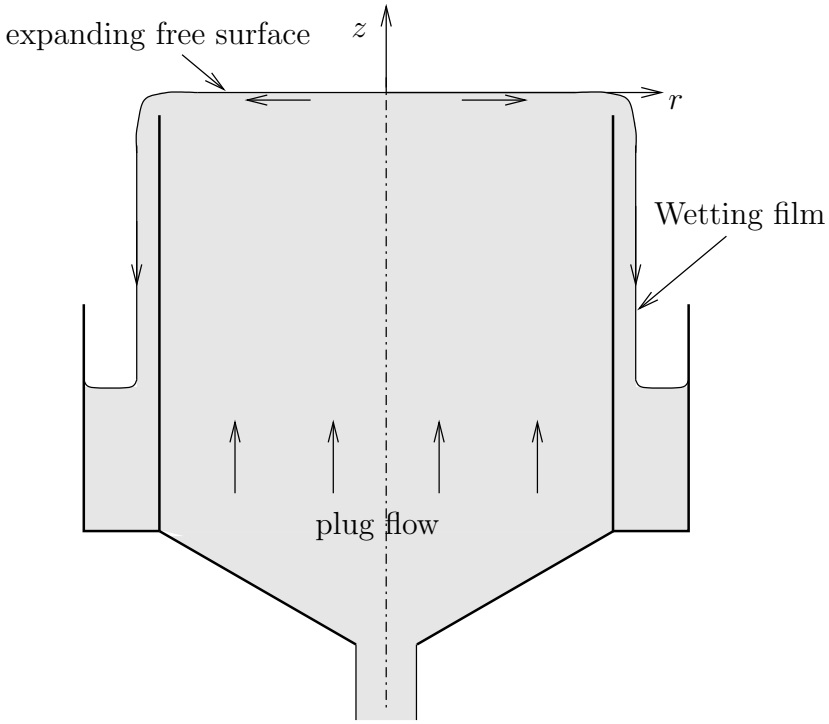

Figure 3.2: Close-up of the overflowing cylinder.

3.3 Previous work

Several authors have published details of experimental and theoretical work on the overflowing cylinder. Bergink-Martens et al. [7, 8, 9] formulated a boundary-layer model for the flow close to the surface, assuming that the flow at depth was given and that the surface tension gradient was known. Darton et al. [31] also attempted a boundary-layer approach in the modelling of their experiments. Gillow [30] formulated inviscid models in both two-dimensional and axially-symmetric geometries and solved these using analytical and numerical methods. Manning-Benson has described her recent experiments in the papers mentioned above.

Jensen [41] has formulated a model in the related area of insoluble surfactants on deep water and Harper [33, 35] has formulated a model in the related area of a bubble rising in a dilute solution of soluble surfactant.

Our new contribution is to couple the hydrodynamic problem (incorporating an inviscid outer flow and a viscous boundary layer at the free surface) with the surfactant problem via the momentum and mass balances and the continuity of shear and replenishment boundary conditions.

3.3.1 Experimental observations

Manning-Benson has carried out a variety of experiments using hexadecyltrimethylammonium bromide (CTAB), which is a cationic surfactant, and is shown in Figure 3.3. We

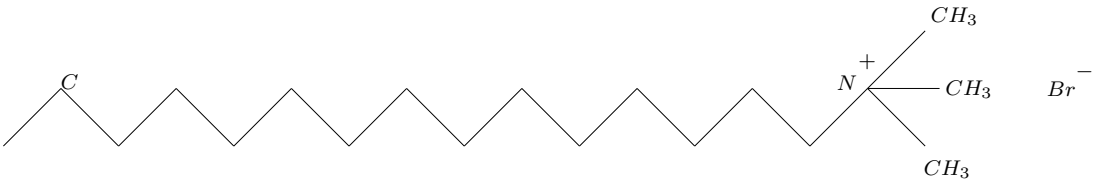

Figure 3.3: Display formula for CTAB.

present some of her experimental results and observations below. The measurements were restricted to a region within 2–3 cm of centre of the cylinder (whose radius was 4 cm). We comment that the measurements were made in a line across the free surface, and r here denotes distance from the centre, measured along this line (*i.e.* r can be negative).

1. Speed

   Figure 3.4 shows surface speed measurements versus the distance r from the axis, for a number of bulk surfactant concentrations and Figure 3.5 shows the surface speed for pure water.

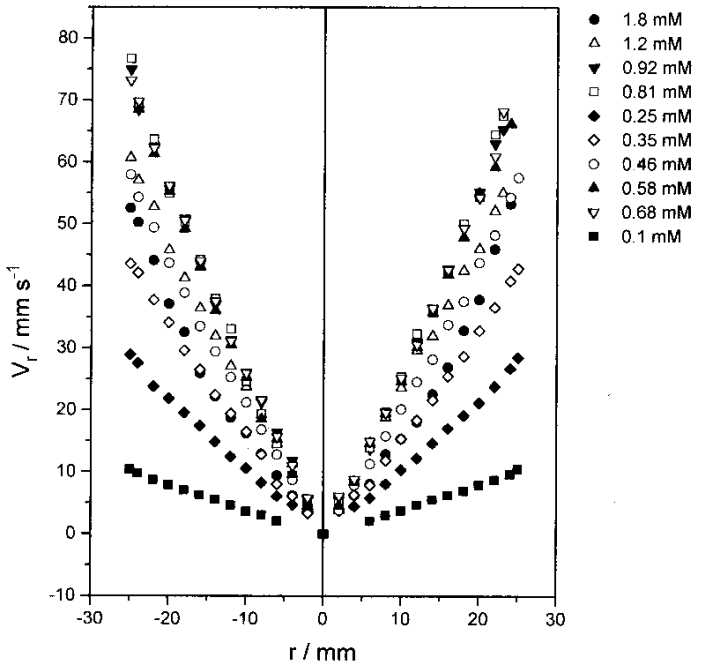

Figure 3.4: Surface speed measurements (V_r measured in mm s^{-1}) against distance (r measured in mm), for a number of bulk concentrations.

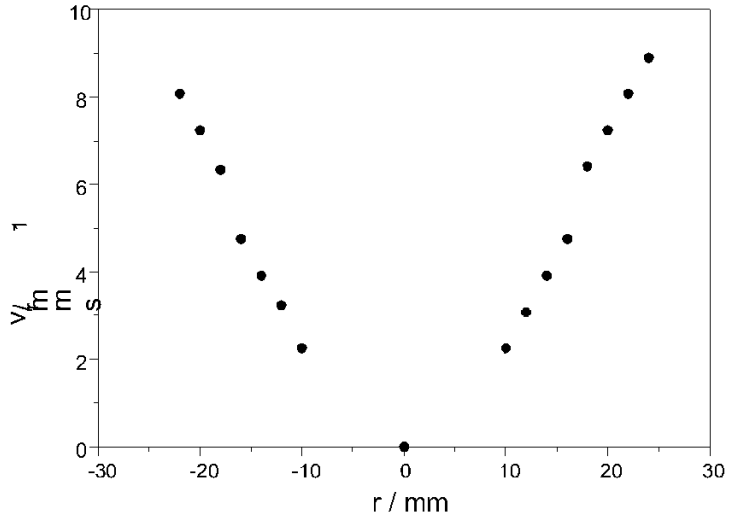

Figure 3.5: Surface speed measurements (V_r measured in mm s^{-1}) against distance (r measured in mm), for pure water.

We note that:

- with surfactants in the system, the speed of the liquid at the free surface is markedly faster than the surface speed associated with pure water;
- the surface velocity appears to vary approximately linearly with distance.

We attribute the apparant 'kink' in the pure water speed profile in Figure 3.5 to experimental error. Figure 3.6 shows the change of horizontal speed with distance away from the surface, at different stations across the cylinder. The concentration of CTAB is 0.58 mol m^{-3} in this case. We note that the liquid is accelerated in a small region close to the top surface of the liquid.

2. Bulk concentration versus surface concentration

   Figure 3.7 shows the variation of surface concentration with bulk concentration, measured under static conditions. The data have been fitted with a Langmuir isotherm. As mentioned in Chapter 2, there is a timescale associated with the adsorption onto the surface. We hope that this timescale is much shorter than any other timescale in the problem, so that the Langmuir isotherm may be employed under our dynamic conditions.

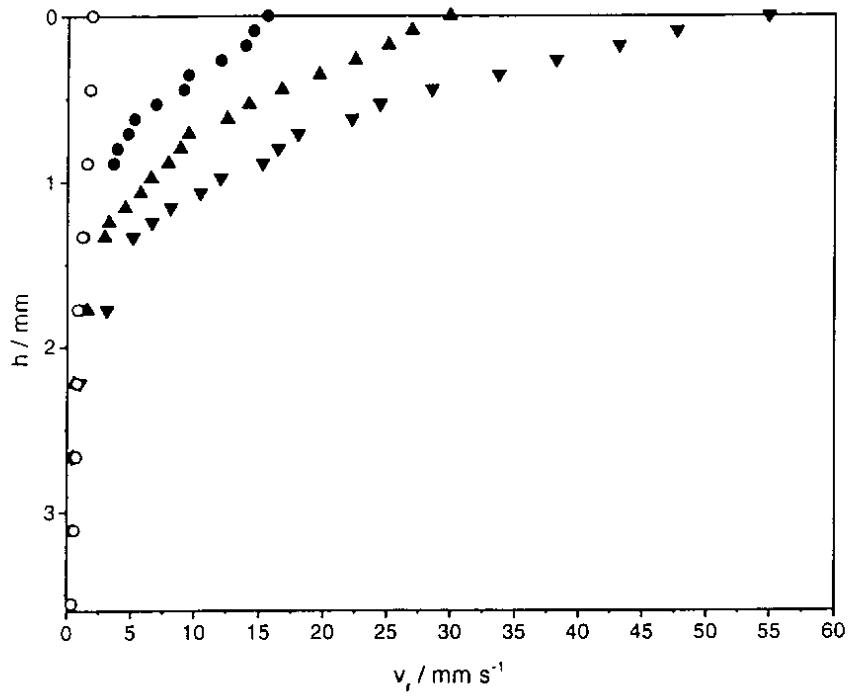

Figure 3.6: Horizontal speed (V_r in mm s^{-1}), for a number of depths (h in mm), at $r = 6$mm (circles), $r = 12$mm (triangles) and $r = 20$mm (upside down triangles).

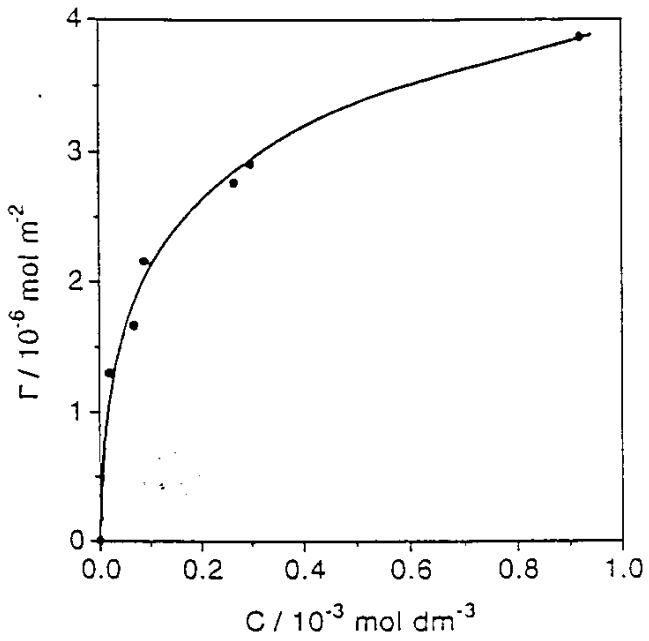

Figure 3.7: The Langmuir isotherm.

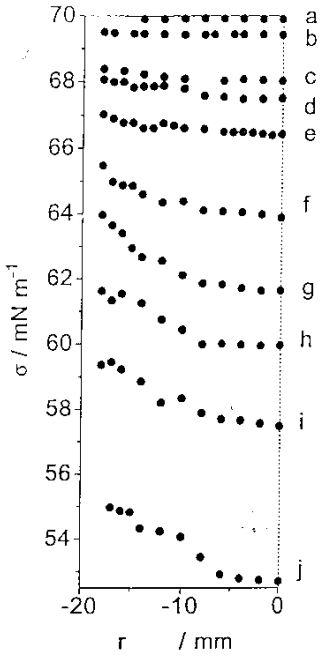

Figure 3.8: Variation of surface tension (σ in mN m^{-1}) with distance across the cylinder (r in mm), for various bulk concentrations: (a) 0.1, (b) 0.17, (c) 0.25, (d) 0.31, (e) 0.35, (f) 0.46, (g) 0.51, (h) 0.58, (i) 0.68, (j) 0.81 mol m^{-3}.

3. Surface Tension

   Figure 3.8 shows the surface tension, measured under dynamic conditions, for various bulk concentrations (from Manning-Benson [52]). We note that:

   - the surface tension varies only slightly across the cylinder and does so roughly quadratically;
   - the surface tension is lowest at the centre of the surface.

   We show the variation of surface tension with *bulk* concentration, measured under static conditions, in Figure 3.9. Note that, in experiments, it is the bulk concentration of the surfactant solution that is initially known, rather than the surface concentration. By comparing the data in Figure 3.9 with the surface tension at the centre of the cylinder in Figure 3.8, we see that the surface tension at the centre is *higher* when the measurement is made under dynamic conditions than when the measurement is made under static conditions.

4. Surface Concentration

   Figure 3.10 shows the variation of surface concentration across the cylinder, for various values of the bulk concentration. We note

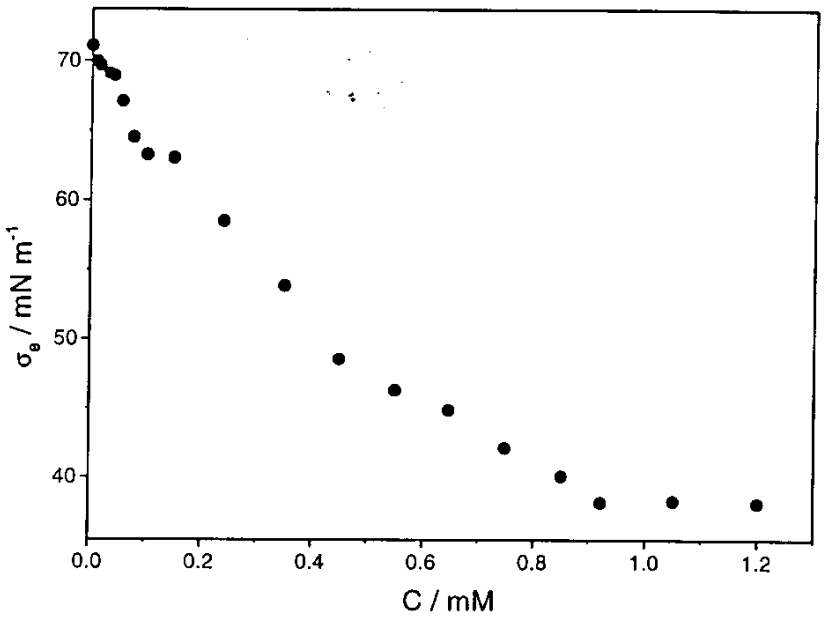

Figure 3.9: Variation of surface tension (σ_0 in mN m^{-1}) with bulk concentration (C in mol m^{-3}) measured under static conditions.

- the concentration appears to be almost constant, and the variation to this constant appears quadratic;
- the concentration is largest in the centre of the surface;

Using the Langmuir isotherm to convert bulk concentration to surface concentration, and then comparing this surface concentration to the central values in Figure 3.10, we can infer that the surface concentration is *lower* under dynamic conditions than under static conditions.

5. Other experimental observations

   - Experiments were performed using cylinders with different radii (3, 4 and 5 cm). The velocity and concentration profiles were virtually unaffected by these changes.
   - Various flanges were inserted into the cylinder to change the curvature at the rim. Such changes did not affect the measurements on the surface.
   - It was found that, so long as the wetting film on the outside of the cylinder was sufficiently long, it did not affect the behaviour on the expanding free surface. Subsequently, all experiments were performed above this critical length.

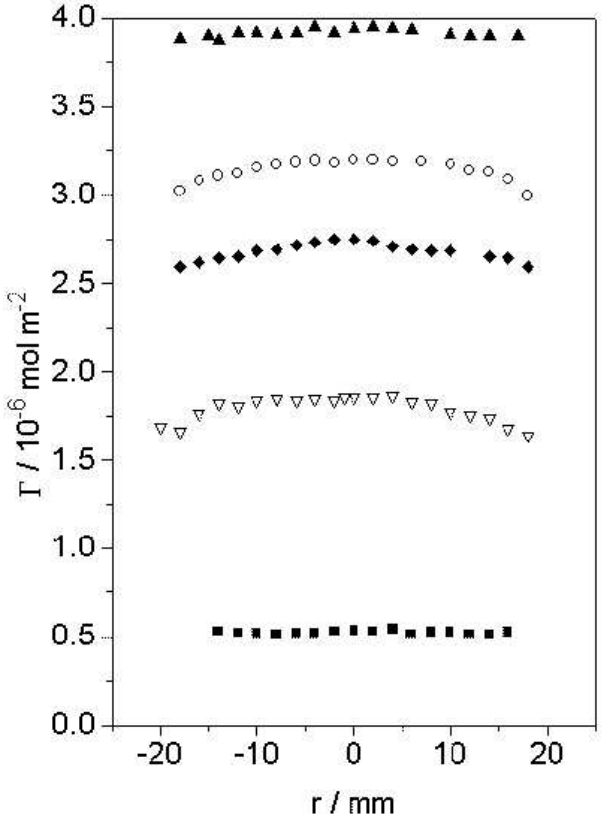

Figure 3.10: Variation of surface concentration (Γ in mol m^{-2}) with distance across the cylinder (r in mm), for various bulk concentrations: 0.1 mol m^{-3} (black triangles), 0.31 mol m^{-3} (open circles), 0.58 mol m^{-3} (black diamonds), 0.81 mol m^{-3} (open triangles) and 1.73 mol m^{-3} (black squares).

- The flow rate was varied, and above a critical flow rate, the surface velocity did not change as the flow rate was altered. The experiments were carried out above this critical flow rate.
- In the case of pure water, the deviation of the free surface from horizontal was more pronounced than in the surfactant cases, where the deviation was very small.

3.3.2 Plan

We model both the liquid velocity and the distribution of surfactant, and show that the model exhibits the qualitative experimental behaviour described above. We then compare our results for surface tension, surface velocity and surface concentration with those obtained experimentally.

3.4 Model formulation: velocity distribution

We consider the situation shown in Figure 3.2. We use the axially symmetric form of the model presented in Chapter 2, and, since all the measurements at the surface are made in a steady state, we assume that the velocities and the height of the free surface do not vary with time. The steady axially symmetric Navier-Stokes equations are

$$\rho\left(uu_r + wu_z\right) = -p_r + \mu\left(\frac{1}{r}\left(ru_r\right)_r - \frac{u}{r^2} + u_{zz}\right), \tag{3.1}$$

$$\rho\left(uw_r + ww_z\right) = -p_z + \mu\left(\frac{1}{r}(rw_r)_r + w_{zz}\right), \tag{3.2}$$

$$\frac{1}{r}(ru)_r + w_z = 0, \tag{3.3}$$

where p is the reduced pressure (see Batchelor [6]), and the boundary conditions at free surface $z = H(r)$ read

$$\sigma\kappa = -p + \rho g H + 2\mu\frac{w_z - (u_z + w_r)H_r + u_r H_r^2}{1 + H_r^2}, \tag{3.4}$$

$$\sigma_r = \mu\frac{(u_z + w_r)(1 - H_r^2) - 2H_r(u_r - w_z)}{\sqrt{1 + H_r^2}}, \tag{3.5}$$

$$w = uH_r, \tag{3.6}$$

where u is the horizontal velocity, w is the vertical velocity, H is the free surface shape, and r and z are as shown in Figure 3.2. At depth, we assume plug flow,

$$w \to U_d, \qquad u \to 0, \qquad z \to -\infty. \tag{3.7}$$

and at the cylinder walls we apply the no-slip condition

$$\mathbf{u} = \mathbf{0}, \qquad \text{at} \qquad r = a, \tag{3.8}$$

where a is the radius of the cylinder. Finally, we assume symmetry about the centre-line of the cylinder:

$$u = w_r = H_r = 0, \qquad \text{at} \qquad r = 0. \tag{3.9}$$

We note that (3.7) and (3.8) are inconsistent. In place of (3.7) we should really pose the condition that the flow straighteners give rise to plug flow at a finite depth in the cylinder. However, the actual flow through the straighteners is unknown, and is likely to be much more complicated than just plug flow. Hence, to stay clear of having to address this flow problem, we assume that the flow straighteners are at "$-\infty$". Of course, if we were concerned with flow close to the wall, we would have to deal properly with these inconsistencies, but we do not bother since we are most interested in the flow at the free surface, where all the available evidence suggests that the flow at depth is unimportant.

We proceed by nondimensionalising the field equations and boundary conditions (3.1)–(3.9), setting

$$\begin{aligned} u = U_d u', \qquad & v = U_d v', \\ r = a r', \qquad & z = a z', \\ p = \rho U_d^2 p', \quad & \sigma = \gamma_0 + \sigma' \Delta\gamma, \end{aligned} \tag{3.10}$$

where γ_0 is the (unknown *a priori*) surface tension of the surfactant solution at the centre of the cylinder, and $\Delta\gamma$ is the size of the surface tension change across the cylinder (which we will later relate to the change in surface concentration). The field equations become (dropping primes)

$$u u_r + w u_z = -p_r + \frac{1}{\mathrm{Re}} \left(\frac{1}{r} (r u_r)_r - \frac{u}{r^2} + u_{zz} \right), \tag{3.11}$$

$$u w_r + w w_z = -p_z + \frac{1}{\mathrm{Re}} \left(\frac{1}{r} (r w_r)_r + w_{zz} \right), \tag{3.12}$$

$$\frac{1}{r} (r u)_r + w_z = 0, \tag{3.13}$$

while the boundary conditions are

$$\left(\frac{1}{\mathrm{CaRe}} + \frac{\mathrm{Ma}}{\mathrm{Re}} \sigma \right) \kappa = -p + \frac{H}{\mathrm{Fr}^2} + \frac{2}{\mathrm{Re}} \frac{w_z - (u_z + w_r) H_r + u_r H_r^2}{1 + H_r^2}, \tag{3.14}$$

$$\mathrm{Ma} \sigma_r = \frac{(u_z + w_r)(1 - H_r^2) - 2 H_r (u_r - w_z)}{\sqrt{1 + H_r^2}}, \tag{3.15}$$

$$w = uH_r, \tag{3.16}$$

on $z = H$, and

$$w \to 1, u \to 0, \qquad z \to -\infty, \tag{3.17}$$

$$\mathbf{u} = \mathbf{0}, \qquad r = 1, \tag{3.18}$$

$$u = 0, H_r = 0, \qquad r = 0. \tag{3.19}$$

We have introduced four dimensionless groups describing various force balances: the Marangoni number Ma, the Reynolds number Re, the capillary number Ca and the Froude number Fr, given by

$$\mathrm{Ma} = \frac{\Delta\gamma}{\mu U_d} \qquad \mathrm{Re} = \frac{\rho a U_d}{\mu} \qquad \mathrm{Ca} = \frac{\mu U_d}{\gamma_0} \qquad \mathrm{Fr}^2 = \frac{U_d^2}{ga}. \tag{3.20}$$

The behaviour of the system of equations depends crucially on the size of these groups, and so we now consider typical physical parameter sizes.

3.4.1 Typical non-dimensional parameter sizes based on flow at depth

We use the following values, based on the Manning-Benson experiments, in calculating the sizes of the nondimensional groups:

$$\begin{aligned}
\rho &\sim 1 \times 10^3 \text{ kg m}^{-3}, \\
\mu &\sim 1 \times 10^{-3} \text{ kg m}^{-1} \text{ s}^{-1}, \\
\gamma_0 &\sim 5 \times 10^{-2} \text{ N m}^{-1}, \\
\Delta\gamma &\sim 2 \times 10^{-3} \text{ N m}^{-1}, \\
a &= 3 \times 10^{-2}\text{–}5 \times 10^{-2} \text{ m}, \\
Q &= \text{flux at depth} = 1.6 \times 10^{-5} \text{ m}^3 \text{ s}^{-1}, \\
U_d &= Q/(\pi a^2) = 3.2 \times 10^{-3} \text{ m s}^{-1} \quad \text{when} \quad a = 0.04 \text{ m},
\end{aligned} \tag{3.21}$$

whence,

$$\mathrm{Re} \sim 130, \qquad \mathrm{Ma} \sim 630, \qquad \mathrm{Ca} \sim 6.4 \times 10^{-5}, \qquad \mathrm{Fr}^2 \sim 2.5 \times 10^{-5}. \tag{3.22}$$

We use the size of these parameters to make qualitative statements about the flow.

- Since Re >> 1, the flow is inertia dominated away from the free and fixed surfaces.
- In (3.14), the capillary term $1/(\mathrm{CaRe}) \sim 10^2$, the gravity term $1/\mathrm{Fr}^2 \sim 4 \times 10^4$ and the viscous term $1/\mathrm{Re} \sim 10^{-2}$. Hence the normal force balance is dominated by

gravitational forces, and since, from (3.14), $H_x \sim O(\mathrm{Fr}^2/(\mathrm{CaRe})) = O(3 \times 10^{-3})$, the free surface is forced to be flat to lowest order, as seen in the experiments. Henceforth, we shall assume that the free surface is flat at $z = 0$, without loss of generality, and we no longer need to work with the normal force balance. We consider relaxing this assumption in §3.10.2.

- In (3.15), the Marangoni term $\mathrm{Ma} \sim 630$ and so we conclude that surface tension gradients dominate the flow close to the free surface.

3.5 Model formulation: surfactant distribution

We now formulate the convection–diffusion problem for the surfactant. We work with the axially-symmetric form of the equations and boundary conditions presented in Chapter 2, which read

$$D\left(\frac{1}{r}\left(rC_r\right)_r + C_{zz}\right) = uC_r + wC_z, \tag{3.23}$$

with boundary conditions at the free surface

$$\Gamma = \frac{\Gamma_\infty C}{k_2 + C}, \tag{3.24}$$

$$DC_z = -\frac{1}{r}(ru\Gamma)_r. \tag{3.25}$$

At depth, we assume that the concentration of surfactant is constant,

$$C \to C_b, \qquad z \to -\infty, \tag{3.26}$$

where C_b is the known concentration of the surfactant solution added to the system. At the edge of the cylinder there is zero flux:

$$C_r = 0, \qquad r = a, \tag{3.27}$$

and we assume symmetry about the centre-line, so that

$$C_r = 0, \qquad \Gamma_r = 0, \qquad r = 0. \tag{3.28}$$

We nondimensionalise the bulk concentration with its value at depth,

$$C = C_b C'. \tag{3.29}$$

However, more care is needed in choosing the most appropriate scaling for the surface concentration. Experimental observations indicate that Γ varies by a fairly small amount across the surface, but its value at the axis, Γ^* say, is unknown *a priori*. We suppose

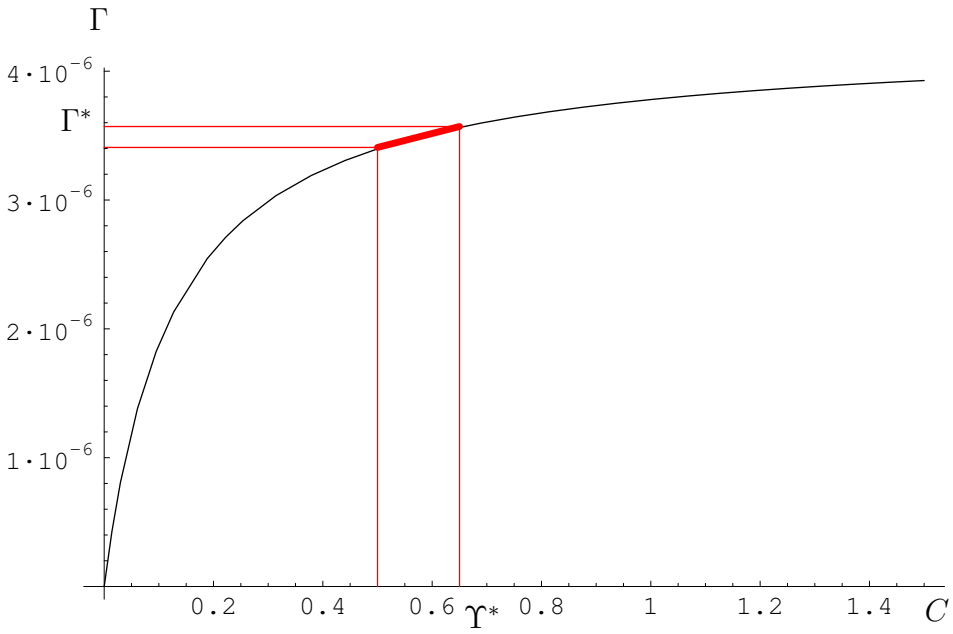

Figure 3.11: Langmuir isotherm showing Υ^*, Γ^* and the variation of Γ and C at the surface (in red).

that the sub-surface concentration corresponding to Γ^* is Υ^*, see Figure 3.11. We nondimensionalise Γ in such a way that the *slope* of the graph of Γ and C at $\Gamma = \Gamma^*$ is 1. We therefore set

$$\Gamma = \frac{k_2 \Gamma_\infty C_b}{(k_2 + C_b \Upsilon)^2} \Gamma', \tag{3.30}$$

where $\Upsilon = \Upsilon^*/C_b$ is the dimensionless value of the subsurface concentration at the centre of the cylinder (which we emphasise is unknown *a priori*).

The field equation becomes (dropping primes)

$$\frac{1}{r}\left(rC_r\right)_r + C_{zz} = \mathrm{Pe}\left(uC_r + wC_z\right), \tag{3.31}$$

with boundary conditions at the free surface $z = 0$

$$\Gamma = \frac{(k_2 + C_b\Upsilon)^2 C}{k_2(k_2 + C_b C)} = \lambda\Upsilon^2 + C - \frac{\lambda(C-\Upsilon)^2}{1+\lambda C}, \tag{3.32}$$

$$SC_z = -\frac{1}{r}(ru\Gamma)_r, \tag{3.33}$$

while

$$C \to 1 \qquad \text{as} \qquad z \to -\infty. \tag{3.34}$$

We introduce three further dimensionless groups: the Péclet number Pe, the replenishment number S, and λ given by

$$\mathrm{Pe} = \frac{U_d a}{D} \qquad S = \frac{D(1+\lambda\Upsilon)^2}{U_d \Gamma_\infty} \qquad \lambda = \frac{C_b}{k_2}. \tag{3.35}$$

We close the model by specifing the relationship between the surface tension and surface concentration, which, after the chosen nondimensionalisation, reads

$$\frac{\sigma^* - \gamma_0}{RT\Gamma_\infty} - \frac{\Delta\gamma}{RT\Gamma_\infty}\sigma = -\log\left(1 - \frac{\lambda\Gamma}{(1+\lambda\Upsilon)^2}\right), \tag{3.36}$$

3.5.1 Linearisation

Now we simplify the above problem further by linearising the Langmuir isotherm (3.32) and the Frumkin equation (3.36). Our aim is to obtain more tractable boundary conditions which still retain the important physical mechanisms of coupling between the bulk concentration, surface concentration and surface tension.

We use the experimental observation in §3.3.1 that Γ does not vary much across the cylinder to motivate our linearisation. We shall check *a posteriori* that this assumption is correct in §3.9.3.

We linearise (3.32) about the sub-surface centre concentration Υ to obtain

$$\Gamma = \lambda\Upsilon^2 + C, \tag{3.37}$$

and from here onwards we work with (3.37) in place of the more complicated (3.32). We note that this is equivalent to replacing the Langmuir isotherm with the straight line segment shown in red in Figure 3.11. We substitute Γ into the replenishment condition, which then reads

$$SC_z = -\frac{1}{r}\left(ru\left(\lambda\Upsilon^2 + C\right)\right)_r. \tag{3.38}$$

Finally, we substitute Γ from (3.32) into (3.36),

$$\frac{\sigma^* - \gamma_0}{RT\Gamma_\infty} - \frac{\Delta\gamma}{RT\Gamma_\infty}\sigma = -\log\left(\frac{1}{1+\lambda C}\right). \tag{3.39}$$

We linearise (3.39) about $C = \Upsilon$, and we find

$$\frac{\sigma^* - \gamma_0}{RT\Gamma_\infty} - \frac{\Delta\gamma}{RT\Gamma_\infty}\sigma = -\log\left(\frac{1}{1+\lambda\Upsilon}\right) + \frac{\lambda}{1+\lambda\Upsilon}(C - \Upsilon), \tag{3.40}$$

and so, setting

$$\gamma_0 = \sigma^* + RT\Gamma_\infty \log\left(\frac{1}{1+\lambda\Upsilon}\right), \tag{3.41}$$

and

$$\Delta\gamma = \frac{RT\Gamma_\infty\lambda}{1+\lambda\Upsilon}, \tag{3.42}$$

we obtain the simple relation between σ and C

$$\sigma = \Upsilon - C. \tag{3.43}$$

3.5.2 Nondimensional parameter sizes based on flow at depth

In addition to the values given in §3.4.1, we also use

$$\begin{aligned} D &\sim 5 \times 10^{-10} \text{ m}^2 \text{ s}^{-1} \\ k_2 &\sim 0.127 \text{ mol m}^{-3} \\ \Gamma_\infty &\sim 4.26 \times 10^{-6} \text{ mol m}^{-2}. \end{aligned} \tag{3.44}$$

To calculate Pe, S and λ, we must choose a value of C_b and use the experimental results to estimate Υ. For $C_b = 0.58$ mol m^{-3}, we have $\Upsilon = 0.4$. Hence we find

$$\text{Pe} \sim 2.5 \times 10^5, \qquad S \sim 3.7 \times 10^{-2}, \qquad \lambda \sim 4.6. \tag{3.45}$$

These parameters indicate that convection dominates the problem away from the free surface.

3.6 Outer (Inviscid) Problem

We first consider the "outer" region where the flow is inviscid to leading order. We expand the dependent variables in terms of Re^{-1} and the leading-order outer liquid problem becomes

$$u_0 u_{0r} + w_0 u_{0z} = -p_{0r}, \tag{3.46}$$

$$u_0 w_{0r} + w_0 w_{0z} = -p_{0z}, \tag{3.47}$$

$$\frac{1}{r}(r u_0)_r + w_{0z} = 0. \tag{3.48}$$

These are the Euler equations for an inviscid flow, which are a singular limit of the Navier-Stokes equations in which the highest derivatives have been dropped. Thus, the only boundary conditions that we can apply are the kinematic condition (the normal force balance has already led to the conclusion that $H = 0$), the normal velocity condition at the edge of the cylinder, the matching condition at depth and the symmetry condition at the axis. The tangential components can only be applied when we consider viscous boundary layers. The associated boundary conditions therefore read

$$w_0 = 0 \qquad \text{on} \qquad z = 0, \tag{3.49}$$

$$w_0 \sim 1 \qquad \text{as} \qquad z \to -\infty, \tag{3.50}$$

$$u_0 = 0 \qquad \text{on} \qquad r = 1, \tag{3.51}$$

$$u_0 = 0 \qquad \text{on} \qquad r = 0. \tag{3.52}$$

We recast the problem in terms of a stream function ψ, so that $u_0 = \frac{1}{r}\psi_z$, $w_0 = -\frac{1}{r}\psi_r$. Since the flow is clearly irrotational, we arrive at the following model for ψ

$$\psi_{rr} - \frac{\psi_r}{r} + \psi_{zz} = 0, \tag{3.53}$$

with

$$\psi = 0 \qquad \text{on} \qquad z = 0, \tag{3.54}$$
$$\psi \sim -\frac{1}{2}r^2 \qquad \text{as} \qquad z \to -\infty, \tag{3.55}$$
$$\psi = -\frac{1}{2} \qquad \text{on} \qquad r = 1, \tag{3.56}$$
$$\psi = 0 \qquad \text{on} \qquad r = 0. \tag{3.57}$$

3.6.1 Inviscid solution

To solve the system (3.53)-(3.57), it is useful to make the substitution $\chi = \psi + \frac{1}{2}r^2$. The problem becomes

$$\chi_{rr} - \frac{\chi_r}{r} + \chi_{zz} = 0, \tag{3.58}$$

with

$$\chi = \frac{1}{2}r^2 \qquad \text{on} \qquad z = 0, \tag{3.59}$$
$$\chi = 0 \qquad \text{on} \qquad r = 0, \tag{3.60}$$
$$\chi = 0 \qquad \text{on} \qquad r = 1, \tag{3.61}$$
$$\chi \to 0 \qquad \text{as} \qquad z \to -\infty. \tag{3.62}$$

We can find the solution, for example, by letting $z = -z'$ and then peforming a sine transform, *i.e.* setting

$$\bar{\chi}(r,k) = \int_0^\infty \chi(r,z')\sin(kz')dz'. \tag{3.63}$$

The equation for $\bar{\chi}$ is

$$\bar{\chi}_{rr} - \frac{\bar{\chi}_r}{r} - k^2\bar{\chi} = -\frac{k}{2}r^2, \tag{3.64}$$

and, after applying the boundary conditions we find the solution is

$$\bar{\chi} = \frac{r^2}{2k} - \frac{rI_1(kr)}{2kI_1(k)}, \tag{3.65}$$

where I_1 is the modified Bessel function of the first order. So, inverting,

$$\chi = \frac{2}{\pi}\int_0^\infty \sin(kz)\left(\frac{r^2}{2k} - \frac{rI_1(kr)}{2kI_1(k)}\right)dk, \tag{3.66}$$

which gives us

$$\psi = \frac{r}{\pi}\int_0^\infty \frac{I_1(kr)\sin(kz)}{kI_1(k)}dk. \tag{3.67}$$

Hence, the liquid velocities are given by

$$u_0 = \frac{1}{\pi}\int_0^\infty \frac{I_1(kr)\cos(kz)}{I_1(k)}dk, \qquad w_0 = -\frac{1}{\pi}\int_0^\infty \frac{I_0(kr)\sin(kz)}{I_1(k)}dk. \tag{3.68}$$

The velocity field given by (3.68) is shown in Figure 3.12. For subsequent matching, we require the velocity at the top surface, say

$$u_{out}(r) = \frac{1}{\pi}\int_0^\infty \frac{I_1(kr)}{I_1(k)}dk. \tag{3.69}$$

Near to the origin this has the behaviour

$$u_{out}(r) \sim \frac{r}{2\pi}\int_0^\infty \frac{k}{I_1(k)}dk + \frac{r^3}{16\pi}\int_0^\infty \frac{k^3}{I_1(k)}dk + O\left(r^5\right), \tag{3.70}$$

which, on evaluating, becomes

$$u_0(r,0) \sim 0.89r + 0.67r^3 + \ldots. \tag{3.71}$$

A comparison between the expansion and the exact solution, for r between 0 and 0.5 is shown in Figure 3.13.

We may also examine the behaviour of the solution near to the rim. Firstly, we substitute $s = kr$ and then we let $r = 1 - \epsilon r'$ and $z = \epsilon z'$. Then u becomes

$$u = \frac{1}{\pi(1-\epsilon r')}\int_0^\infty \frac{I_1(s)}{I_1\left(\frac{s}{1-\epsilon r'}\right)}\cos\left(\frac{\epsilon z' s}{1-\epsilon r'}\right)ds. \tag{3.72}$$

To proceed we must split the range of integration since the integrand has different asymptotic behaviour when $s \sim O(1)$ and when $s \sim O(1/\epsilon)$. We choose to split the range of integration into $(0, 1/\sqrt{\epsilon})$, $(1/\sqrt{\epsilon}, \infty)$, although any power of ϵ between zero and one will do. We also utilise the asymptotic form for $I_1(s)$ when s is large:

$$I_1(s) \sim \frac{1}{\sqrt{2\pi s}}e^s. \tag{3.73}$$

After some grisly algebra, we find

$$u \sim \frac{1}{\pi(1-\epsilon r')}\int_0^{1/\sqrt{\epsilon}} \frac{I_1(s)}{I_1\left(\frac{s}{1-\epsilon r'}\right)}\cos\left(\frac{\epsilon z' s}{1-\epsilon r'}\right)ds + \frac{e^{-\frac{\sqrt{\epsilon}r'}{1-\epsilon r'}}\left(r'\cos\frac{\sqrt{\epsilon}z'}{1-\epsilon r'} - z'\sin\frac{\sqrt{\epsilon}z'}{1-\epsilon r'}\right)}{\pi\epsilon\sqrt{1-\epsilon r'}(r'^2+z'^2)}, \tag{3.74}$$

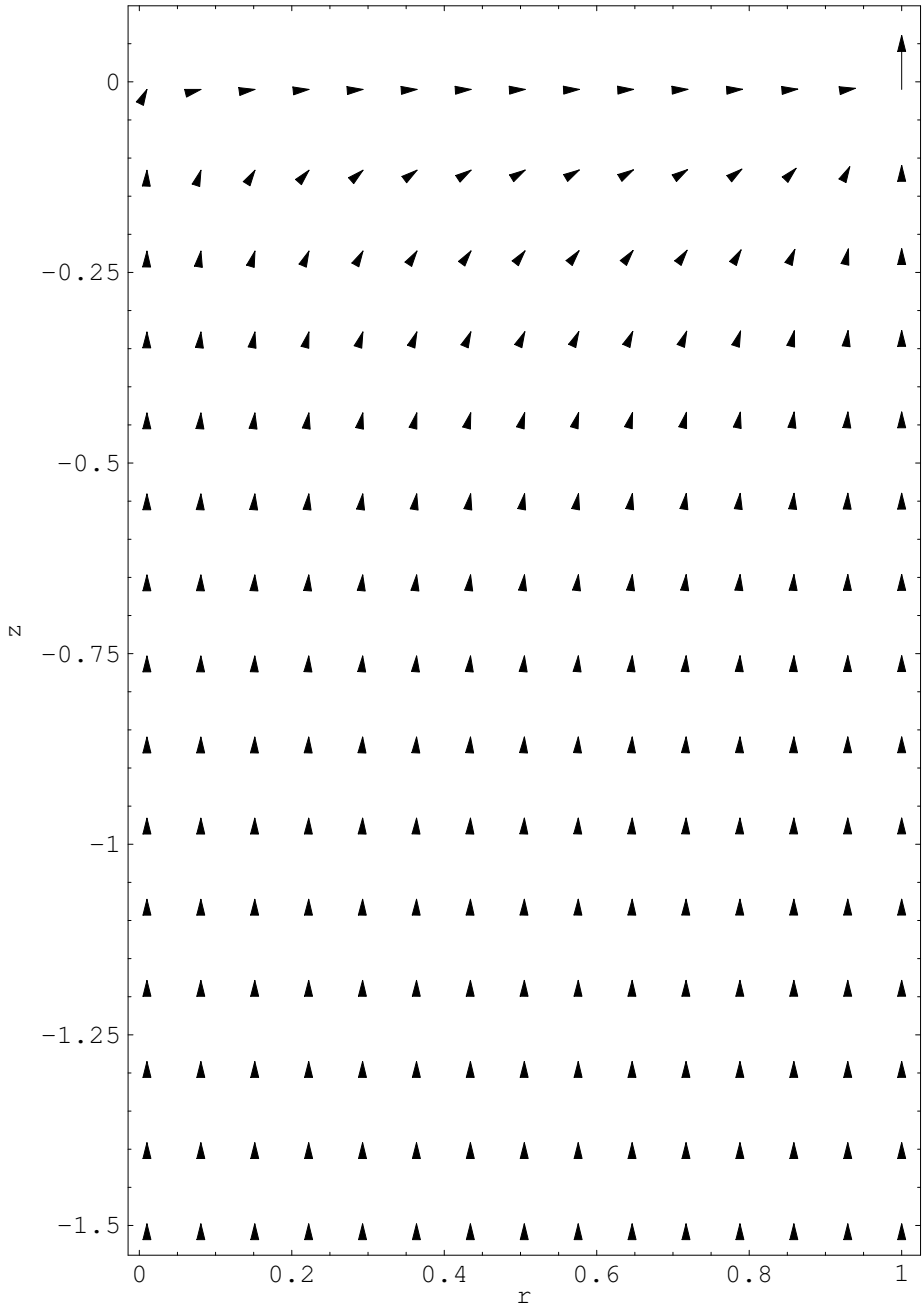

Figure 3.12: Plot showing the inviscid velocity field.

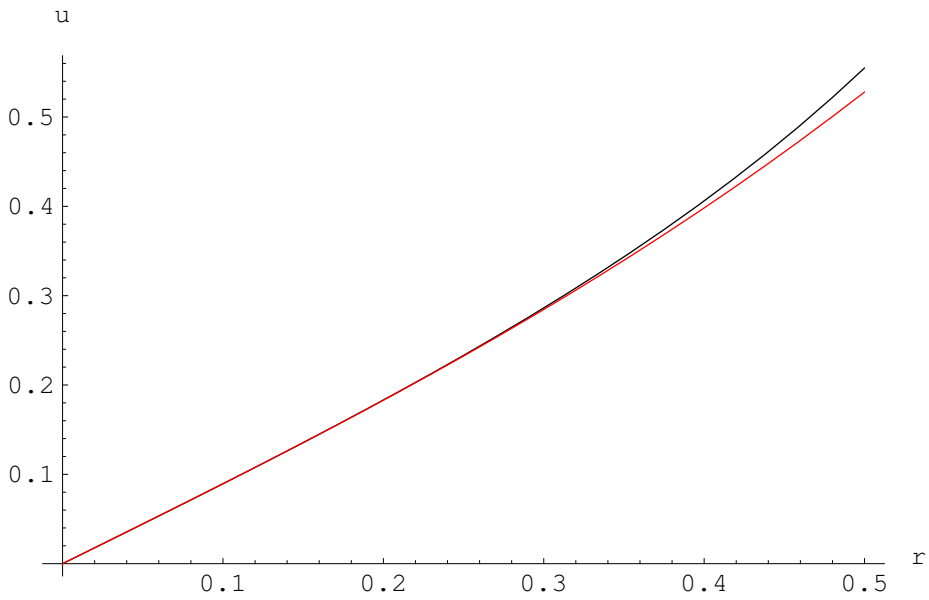

Figure 3.13: Graph showing the solution, (3.69), for u (in black), compared with the expansion (3.71), for u (in red).

and, expanding both the integral and the second term in powers of ϵ and then substituting for the original variables, we find that

$$u(r,z) \sim \frac{1-r}{\pi((1-r)^2+z^2)}. \tag{3.75}$$

We may also find the form of w in a similar way,

$$w \sim -\frac{z}{\pi((1-r)^2+z^2)}. \tag{3.76}$$

The rim may therefore be viewed as a sink, strength 2 (as might have been anticipated from the boundary conditions).

We note that

- the solution satisfies $u_z = 0$ on $z = 0$. Thus this condition satisfies the tangential boundary condition on $z = 0$ exactly if the Marangoni number is zero (*i.e.* if there is no surfactant present). However, when $\mathrm{Ma} \neq 0$, (3.15) is not satisfied and so we must introduce a viscous boundary layer near $z = 0$. We consider the boundary layer problem in §3.8.1.

- the inviscid solution does not satisfy the boundary condition $w_0 = 0$ on $r = 1$. In order to satisfy this condition, we should reintroduce the viscous terms close to the edge. However, since our main interest is in the free surface we hope we will not need to analyse flow near $r = 1$ in detail.

3.7 Outer (surfactant) Problem

In (3.31) the Péclet number, which we recall is large, plays the same role as the Reynolds number does in the hydrodynamic problem. As in the liquid case, the limit $\mathrm{Pe} \to \infty$ is singular, since Pe multiplies the highest derivative in the system. Thus, again, we will not be able to satisfy all of the boundary conditions at the free surface and at the edge of the cylinder with this "outer" solution. We introduce a diffusive boundary layer near $z = 0$ in §3.8.2. Here, we expand (3.31) in powers of $1/\mathrm{Pe}$, and we find that to leading-order, the surfactant concentration satisfies

$$u_0 C_{0r} + w_0 C_{0z} = 0, \tag{3.77}$$

and so C_0 is constant along the streamlines. So, since we have

$$C_0 \to 1 \qquad \text{as} \qquad z \to -\infty, \tag{3.78}$$

we deduce that the concentration must be $C_0 = 1$ everywhere in the outer region.

3.7.1 Solution to the problem in the limit $\mathrm{Ma} \to 0$ and $S \to \infty$

In §3.6.1 we noted that the leading-order outer solution actually satisfies the correct boundary conditions on $z = 0$ when $\mathrm{Ma} = 0$. Similarly, the solution $C = 1$ satisfies the replenishment condition in the limit $S \to \infty$. Thus in the limit $\mathrm{Ma} \to 0$ and $S \to \infty$, we have $u \to u_0$ and $w \to w_0$, as given by (3.68) and the solution to the surfactant problem reads

$$C_0 = 1, \qquad \Gamma_0 = 1 + \lambda, \qquad \sigma = 0. \tag{3.79}$$

We note that, for example, for $C_b = 0.58$ mol m^{-3}, we have $\Gamma = 5.57$, which corresponds to a dimensional value of 3.5×10^{-6} mol m^{-2}. This is the value that we would have expected for the surface concentration if it had been measured under static conditions. However, if we read off the experimental value of Γ at the centre of the free surface from Figure 3.10, we find that $\Gamma \sim 2.75 \times 10^{-6}$ mol m^{-2}. Hence, we conclude that the value of Γ given by (3.79) is higher than the experimentally observed value.

3.8 Boundary layers at the free surface

When we have nonzero Marangoni and inverse replenishment numbers, the solutions above fail to satisfy the continuity of shear and the replenishment boundary conditions. We therefore seek both hydrodynamic and diffusive boundary layers beneath the free surface. Recall that in the outer solutions described above, the velocity is scaled with U_d and

lengths all scale with a. However, as indicated in §3.3.1 the behaviour of the surface velocity and concentration is observed experimentally to be independent of both U_d and a. This motivates us to allow the boundary layer problems to select not only the thicknesses of the two boundary layers, but also the velocity scaling and the lengthscale of the problem. We scale the vertical hydrodynamic length and the vertical velocity by ϵ, and the corresponding diffusive length by δ. We replace the radius, a by L, and the velocity U_d by U in each of the dimensionless groups (namely Re, Ma, Pe and S). Setting $\epsilon^2\mathrm{Re} = 1$, $\delta^2\mathrm{Pe} = 1$, $\epsilon\mathrm{Ma} = 1$ and $S/\delta = 1$, we have four equations for the four unknowns L, U, ϵ and δ, and we find that the relevant scalings are

$$\begin{aligned} U &= \left(\frac{DR^2T^2C_b^2}{\rho\mu}\right)^{\frac{1}{4}}(1+\lambda\Upsilon)^{\frac{1}{2}}, \\ L &= \left(\frac{R^2T^2C_b^2\Gamma_\infty^8}{D^3\rho\mu k_2^8}\right)^{\frac{1}{4}}(1+\lambda\Upsilon)^{-\frac{7}{2}}, \\ \epsilon &= \left(\frac{D\mu^3k_2^4}{\rho R^2T^2\Gamma_\infty^4C_b^2}\right)^{\frac{1}{4}}(1+\lambda\Upsilon)^{\frac{3}{2}}, \\ \delta &= \left(\frac{D^3\rho\mu k_2^4}{R^2T^2C_b^2\Gamma_\infty^4}\right)^{\frac{1}{4}}(1+\lambda\Upsilon)^{\frac{3}{2}}. \end{aligned} \tag{3.80}$$

All the scalings contain the (unknown) sub-surface centre concentration, Υ, which will be determined during the solution of the problem. We note before continuing that, using $\Upsilon = 0.4$, which is the nondimensionalised experimental value for $C_b = 0.58$ mol m^{-3},

$$U \sim 0.3 \text{ m s}^{-1}, \qquad L \sim 0.01 \text{ m}, \qquad \epsilon \sim 0.018, \qquad \delta \sim 4\times10^{-4}. \tag{3.81}$$

There are several interesting ratios that we can make from the above scalings. The first is the ratio of the two boundary layer thicknesses

$$\frac{\delta}{\epsilon} = \left(\frac{\rho D}{\mu}\right)^{\frac{1}{2}} = \mathrm{Pr}^{\frac{1}{2}}, \tag{3.82}$$

where Pr, the Prandtl number, is a property only of the surfactant-liquid system under consideration. For example, in an aqueous CTAB solution, $\mathrm{Pr}^{\frac{1}{2}} \sim 0.022$, and indeed we can expect all systems of practical interest to have $\mathrm{Pr} << 1$. We conclude that the diffusive boundary layer (known hereafter as DBL) is always *much* thinner than the hydrodynamic boundary layer (HBL). We will use this ratio when considering the coupling between the hydrodynamic and diffusive problems.

The next ratio of interest is $V = U_d/U$, the ratio of the velocity at depth to the intrinsic velocity scale. Using $\Upsilon = 0.4$, we calculate $V \sim 1\times10^{-2}$. Hence our intrinsic velocity

scale is much larger than the the velocity at depth, as supported by the experimental evidence.

The final interesting ratio is $l = L/a$, the ratio of the intrinsic lengthscale to the radius of the cylinder. Again we use $\Upsilon = 0.4$, and we find that $l = 0.2625$. Hence, our intrinsic length scale is less than the radius of the cylinder and this suggests the presence of an "inner region" close to the axis of the cylinder (where the experimental measurements are taken).

3.8.1 The hydrodynamic boundary layer

Now we re-nondimensionalise the equations and boundary conditions using the above scalings, *i.e.*, scaling $r = L\hat{r}$, $z = \epsilon L\hat{z}$, $u = U\hat{u}$ and $w = \epsilon U\hat{w}$. We only consider the leading-order solution in ϵ and thus simply set $\epsilon = 0$ in the resulting equations, which then read

$$\hat{u}\hat{u}_{\hat{r}} + \hat{w}\hat{u}_{\hat{z}} = -p_{\hat{r}} + \hat{u}_{\hat{z}\hat{z}}, \tag{3.83}$$

$$p_{\hat{z}} = 0, \tag{3.84}$$

$$\frac{1}{\hat{r}}(\hat{r}\hat{u})_{\hat{r}} + \hat{w}_{\hat{z}} = 0. \tag{3.85}$$

From (3.84), the pressure is only a function of $\hat{r}$ and, if we substitute for a stream function, $\hat{\psi}$ so that the conservation of mass equation (3.85) is automatically satisfied (*i.e.* $\hat{u} = \frac{1}{\hat{r}}\hat{\psi}_{\hat{z}}$, $\hat{w} = -\frac{1}{\hat{r}}\hat{\psi}_{\hat{r}}$ again), then we obtain

$$\hat{\psi}_{\hat{z}\hat{z}\hat{z}} = \frac{1}{\hat{r}}\left[\hat{\psi}_{\hat{z}}\hat{\psi}_{\hat{z}\hat{r}} - \hat{\psi}_{\hat{r}}\hat{\psi}_{\hat{z}\hat{z}} - \frac{1}{\hat{r}}\hat{\psi}_{\hat{z}}^2\right] + p'(\hat{r}). \tag{3.86}$$

Now, matching with the flow at depth gives

$$\hat{\psi} \sim V\hat{r}\hat{z}u_{out}(l\hat{r}) \qquad \text{as} \qquad \hat{z} \to -\infty, \tag{3.87}$$

where u_{out} is the outer velocity found earlier,

$$u_{out}(t) = \frac{1}{\pi}\int_0^\infty \frac{I_1(kt)}{I_1(k)}dk. \tag{3.88}$$

Thus,

$$p'(\hat{r}) = -V^2 l\hat{r}u_{out}(l\hat{r})u'_{out}(l\hat{r}). \tag{3.89}$$

In terms of the stream function, the boundary conditions at the free surface reduce to

$$\hat{\psi} = 0 \qquad \text{on} \qquad \hat{z} = 0, \tag{3.90}$$

$$\frac{1}{\hat{r}}\hat{\psi}_{\hat{z}\hat{z}} = \sigma_{\hat{r}} \qquad \text{on} \qquad \hat{z} = 0. \tag{3.91}$$

3.8.2 The diffusion boundary layer

In the diffusion boundary layer, height is scaled with δL, and so we set $z = \delta L\zeta$, and then the leading-order surfactant problem reads

$$C_{\zeta\zeta} = \hat{u}C_{\hat{r}} + \frac{\epsilon}{\delta}\hat{w}C_{\zeta}, \tag{3.92}$$

with boundary conditions

$$-C_{\zeta} = \frac{1}{\hat{r}}\left(\hat{r}\hat{u}\left(\lambda\Upsilon^2 + C\right)\right)_{\hat{r}}, \tag{3.93}$$

at the free surface $\zeta = 0$ and

$$C \to 1, \qquad \zeta \to -\infty. \tag{3.94}$$

At first glance it may appear inconsistent to keep in the ϵ/δ term in (3.92), but we note that $\hat{w}(\hat{r},\hat{z}) = \hat{w}(\hat{r},\delta\zeta/\epsilon) = O(\delta/\epsilon)$ as $\delta \to 0$ so that this term is $O(1)$ as $\delta \to 0$.

3.8.3 Coupling between the hydrodynamic and diffusive problems

The coupling between the hydrodynamic and diffusive problems works both ways. Firstly, the diffusive problem is driven by the velocity field $(\hat{u},\hat{w})$. This coupling can be simplified by using the fact that the ratio of the boundary layer thicknesses is small, *i.e.*, by expanding (3.92) in the limit as $\delta/\epsilon \to 0$. The result of this is that the diffusion problem only depends on the velocity field evaluated at the free surface:

$$C_{\zeta\zeta} = \frac{1}{\hat{r}}\left[\hat{\psi}_{\hat{z}}(\hat{r},0)C_{\hat{r}} - \hat{\psi}_{\hat{r}\hat{z}}(\hat{r},0)\zeta C_{\zeta}\right], \tag{3.95}$$

with

$$C_{\zeta}(\hat{r},0) = -\frac{1}{\hat{r}}\left(\hat{\psi}_{\hat{z}}(\hat{r},0)\left(\lambda\Upsilon^2 + C(\hat{r},0)\right)\right)_{\hat{r}} \qquad \text{on} \qquad \zeta = 0, \tag{3.96}$$

$$C \to 1 \qquad \text{as} \qquad \zeta \to -\infty. \tag{3.97}$$

The concentration C is coupled back to the hydrodynamic problem through the surface tension, given by (3.43). Thus, the streamfunction ψ satisfies

$$\hat{\psi}_{\hat{z}\hat{z}\hat{z}} = \frac{1}{\hat{r}}\left[\hat{\psi}_{\hat{z}}\hat{\psi}_{\hat{z}\hat{r}} - \hat{\psi}_{\hat{r}}\hat{\psi}_{\hat{z}\hat{z}} - \frac{1}{\hat{r}}\hat{\psi}_{\hat{z}}^2\right] - lV^2\hat{r}u_{out}(l\hat{r})u'_{out}(l\hat{r}), \tag{3.98}$$

$$\hat{\psi}(\hat{r},0) = 0, \tag{3.99}$$

$$\frac{1}{\hat{r}}\hat{\psi}_{\hat{z}\hat{z}}(\hat{r},0) = -C_{\hat{r}}(\hat{r},0), \tag{3.100}$$

$$\hat{\psi} \sim V\hat{r}\hat{z}u_{out}(l\hat{r}) \qquad \text{as} \qquad \hat{z} \to -\infty. \tag{3.101}$$

Having solved this system, we may then read off Γ, σ, and γ_0. A schematic of the system and the equations that hold in each region is shown in Figure 3.14.

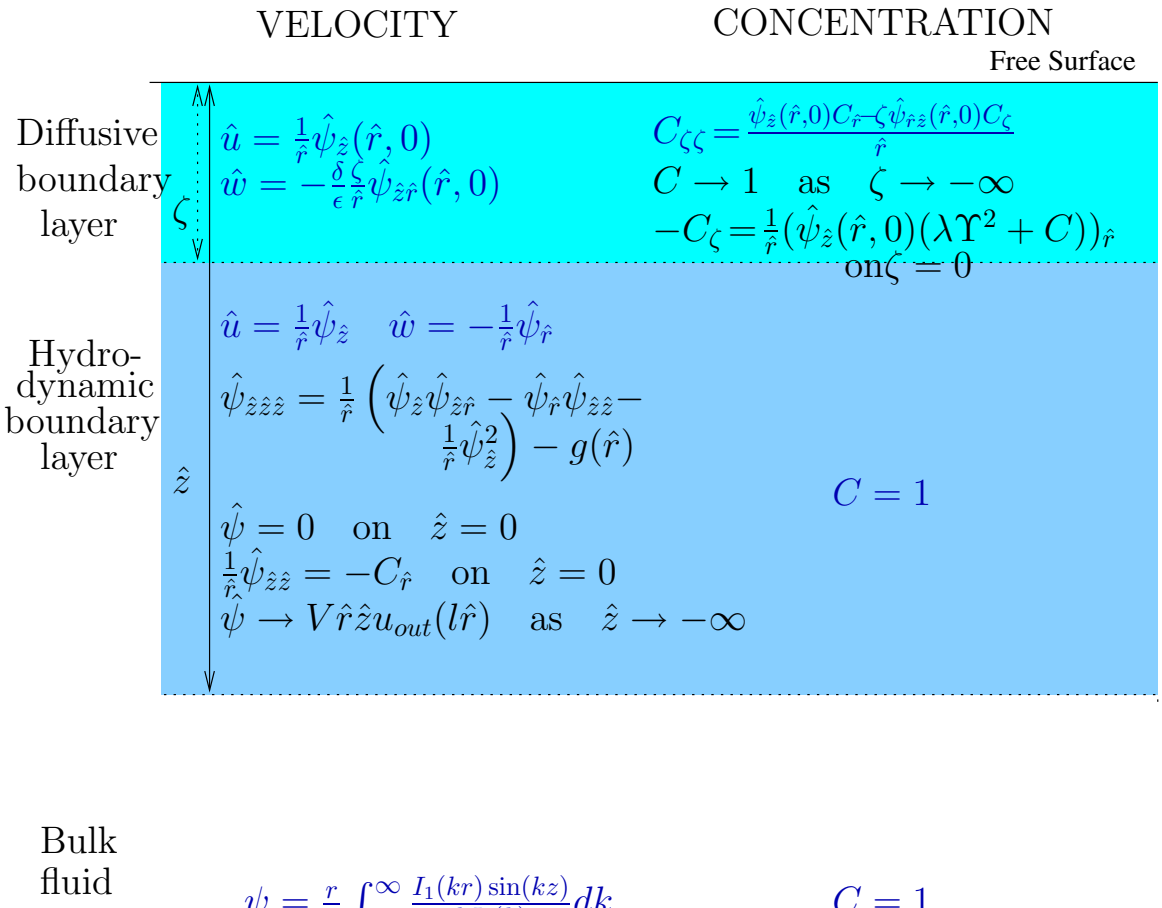

Figure 3.14: Schematic of the boundary layer structure: $g(\hat{r}) = V^2 l\hat{r}u_{out}(l\hat{r})u'_{out}(l\hat{r})$.

3.9 Series solutions to both the liquid and surfactant problems

In the previous section we derived the coupled problems for the stream function and the surfactant distribution. In general these must be solved numerically, but this does not appear straightforward and so we do not attempt to do so here. Moreover, it is not clear what to do at the edges of the cylinder, where the outer velocity becomes infinite. Our model certainly breaks down near to the rim, where gravity and surface tension probably play a dominant role, and the flow is extremely complicated. However, we have already mentioned that the experimental evidence suggests that the details of the behaviour at the rim appear to have negligible effect on the flow at the centre of the cylinder, and indeed the velocity and concentration profiles in the regions studied experimentally are entirely locally determined. Thus, we should hope that our solution depends mostly on the locally-determined scales L and U rather than the externally specified a and U_d.

As noted above, l and V are both small. We utilise the limit $l \to 0$ in the modelling that follows. This is analagous to an expansion about the axis and so is also consistent with the roughly linear behaviour of $\hat{u}$ and quadratic behaviour of C. We expand our 'outer' solution in powers of l^2, which, written in inner variables, reads

$$\hat{u} \sim 0.89Vl\hat{r} + 0.69Vl^3\hat{r}^3 + \ldots \tag{3.102}$$

In the limit $V \to 0$, the leading-order inner solution thus sees no flow at depth. Of course, in general we must also worry about the commutability of the limits $l \to 0$ and $V \to 0$. We discuss taking another limit in §3.10.2.

Now taking the limit $V \to 0$, we attempt to construct a solution of the form

$$\hat{\psi} = \sum_{n=1}^{\infty} \hat{r}^{2n} f_{2n-2}(\hat{z}) \qquad C = C^*(\zeta) + \sum_{n=1}^{\infty} C_{2n}(\zeta)\hat{r}^{2n}. \tag{3.103}$$

Substituting these series into the field equations and boundary conditions, and comparing terms of order r^{2n} yields the following system of problems:

$$f'''_{2n-2} = \sum_{k=0}^{n-1} \left[(2n-2k-1) f'_{2n-2k-2} f'_{2k} - (2n-2k) f_{2n-2k-2} f''_{2k} \right], \tag{3.104}$$

with

$$f_{2n-2}(0) = 0, \tag{3.105}$$

$$f'_{2n-2}(-\infty) = 0, \tag{3.106}$$

$$f''_{2n-2}(0) = -C_{2n}(0), \tag{3.107}$$

and

$$C''_{2n} + 2f'_0(0)\zeta C'_{2n} - 2nf'_0(0)C_{2n} =$$

$$\sum_{k=0}^{n-2}\left((2n-2k)f'_{2k}(0)C_{2n-2k} - (2k+4)\zeta f'_{2k+2}(0)C'_{2n-2k-2}\right) - (2n+2)\zeta f'_{2n}(0)C^{*\prime}, \quad (3.108)$$

where

$$-C'_{2n}(0) = (2n+2)\left(\sum_{k=1}^{n-1} f'_{2k}(0)C_{2n-2k} + f'_{2n}(0)\left(\lambda\Upsilon^2 + \Upsilon\right)\right), \quad (3.109)$$

$$C_{2n}(-\infty) = 0, \quad (3.110)$$

and C^* satisfies

$$C^{*\prime\prime} + 2\zeta f'_0(0)C^{*\prime} = 0, \quad (3.111)$$

$$-C^{*\prime}(0) = 2f'(0)\left(\lambda\Upsilon^2 + \Upsilon\right). \quad (3.112)$$

$$C^*(-\infty) = 1, \quad (3.113)$$

Our solution procedure is to solve first for C^* and then to solve iteratively the liquid and surfactant problems for each $n \geq 1$.

3.9.1 The Solution for C^*

The solution to (3.111) and (3.113) is

$$C^* = 1 + a_1 \int_{-\infty}^{\zeta} e^{-K\phi^2} d\phi, \quad (3.114)$$

where $K = f'_0(0)$. We recall that $C^*(0) = \Upsilon$, and so we have $a_1 = -2(1-\Upsilon)\sqrt{\frac{K}{\pi}}$. Finally, we find a relationship between K and Υ using (3.112),

$$K = \frac{(1-\Upsilon)^2}{\pi\Upsilon^2(\lambda\Upsilon+1)^2}. \quad (3.115)$$

Hence,

$$C^* = 1 - \frac{2(1-\Upsilon)^2}{\pi\Upsilon(\lambda\Upsilon+1)}\int_{-\infty}^{\zeta} e^{-\frac{(1-\Upsilon)^2\phi^2}{\pi\Upsilon^2(\lambda\Upsilon+1)^2}} d\phi, \quad (3.116)$$

and plots of this solution, varying Υ, are shown in Figure 3.15 below.

The relationship between Υ and K may be checked against experiments. However, we have limited data which is consistent between all the experiments, so we check the validity of this prediction using the data for $C_b = 0.58$ mol m^{-3}. First, it is useful to redimensionalise

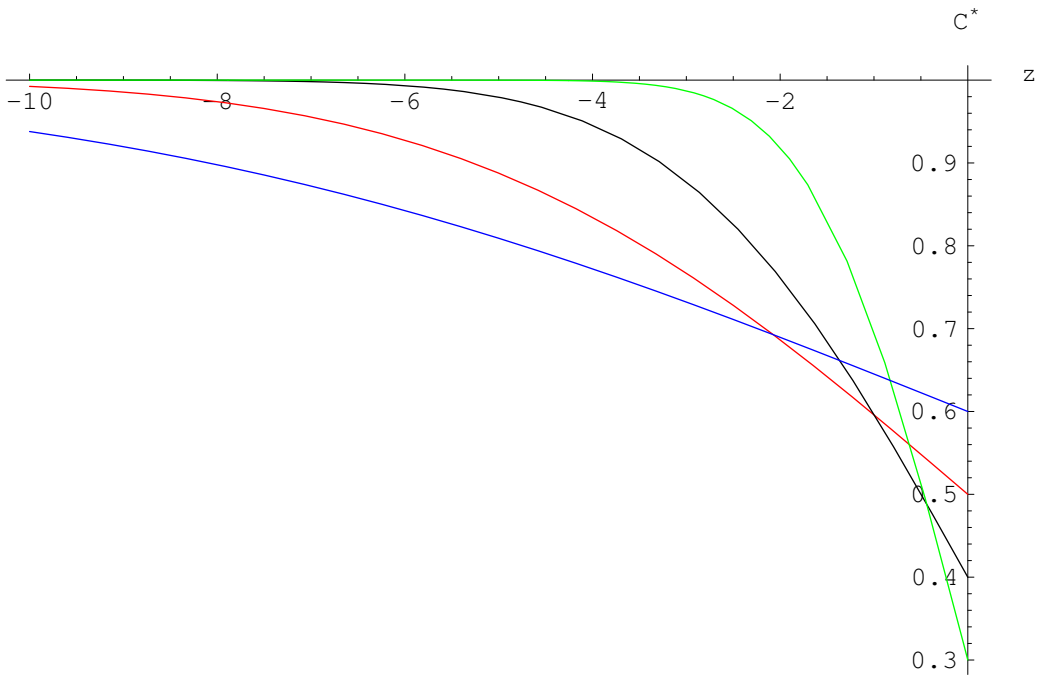

Figure 3.15: Graph showing $C^*(\zeta)$ versus depth ζ for $\Upsilon = 0.3$, 0.4, 0.5 and 0.6.

the relationship and re-form the velocity, and so, remembering that the dimensional sub-surface centre concentration is Υ^*, which we may obtain using the graphs of Γ vs r and Γ vs C, we have

$$u = \frac{D(k_2 + \Upsilon^*)^2(C_b - \Upsilon^*)^2}{\Gamma_\infty^2 \pi \Upsilon^{*2}} r. \tag{3.117}$$

Using the (consistent) set of data for $C_b = 0.58$ mol m^{-3}, we have $\Upsilon^* \sim 0.23$ – 0.24 mol m^{-3}, and $u \sim 2.44r$. Using (3.117), we find that $u \sim (2.37$ – $2.59)r$. We are encouraged by this agreement between the theory and experiment, but note that we have had to fix the solution using the measured value of Υ^*, rather than predicting Υ^* theoretically. This indeterminacy is going to be a thorn in our side henceforth.

3.9.2 Lowest order liquid problem and solution

We use the condition for K given above, assuming Υ is known, to close the leading order liquid model, which reads

$$f_0''' + 2 f_0 f_0'' - f_0'^2 = 0, \tag{3.118}$$

with boundary conditions

$$f_0(0) = 0, \tag{3.119}$$

$$f_0'(0) = \frac{(1-\Upsilon)^2}{\pi \Upsilon^2 (\lambda \Upsilon + 1)^2}, \tag{3.120}$$

$$f_0'(-\infty) = 0. \tag{3.121}$$

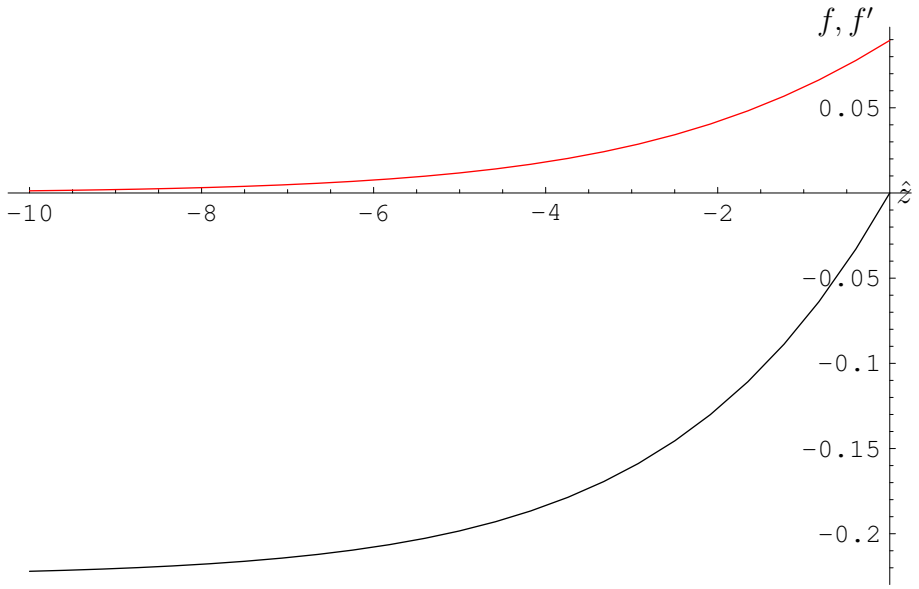

Figure 3.16: The solution f_0 (black) and f_0' (red) to (3.118)–(3.121), for $\Upsilon = 0.4$, $\lambda = 4.57$.

There is a one-parameter family of solutions to this problem which is parametrised by Υ, each solution having a different value of $f_0''(0)$. We show the general shape of the solution for f_0 and f_0' in Figure 3.16, given Υ which we choose to be 0.4 (which we have inferred from the experiments). We note that, with $\Upsilon = 0.4$, $\epsilon L \sim 1.87 \times 10^{-4}$ m and from Figure 3.16 we see that the velocity is effectively zero at $\hat{z} = -10$. Hence the dimensional thickness to which the hydrodynamic boundary layer extends is ~ 1.9 mm. This agrees well with Figure 3.6.

The shear at the free surface, $f_0''(0)$ is found to be 0.031, when $\Upsilon = 0.4$. We may compare this shear with that exhibited in the experiments, using the data in Figure 3.6. We take the gradients of the $r = 12$ mm and $r = 20$ mm plots (using pencil and ruler) and calculate the equivalent values of $f''(0)$ which are $f''(0) = 0.023$ and 0.026 respectively. We again have good agreement with experiments.

The behaviour of $f_0''(0)$ as Υ is varied is shown in Figure 3.17. It shows that, as the subsurface centre-concentration increases, the amount of shear at the surface decreases rapidly. We note that we have not yet appealed to the shear boundary condition (3.107). Indeed, we shall use this condition to pass information *from* the leading-order liquid problem into the surfactant problem for C_2. So the flow of information is as shown in Figure 3.18.

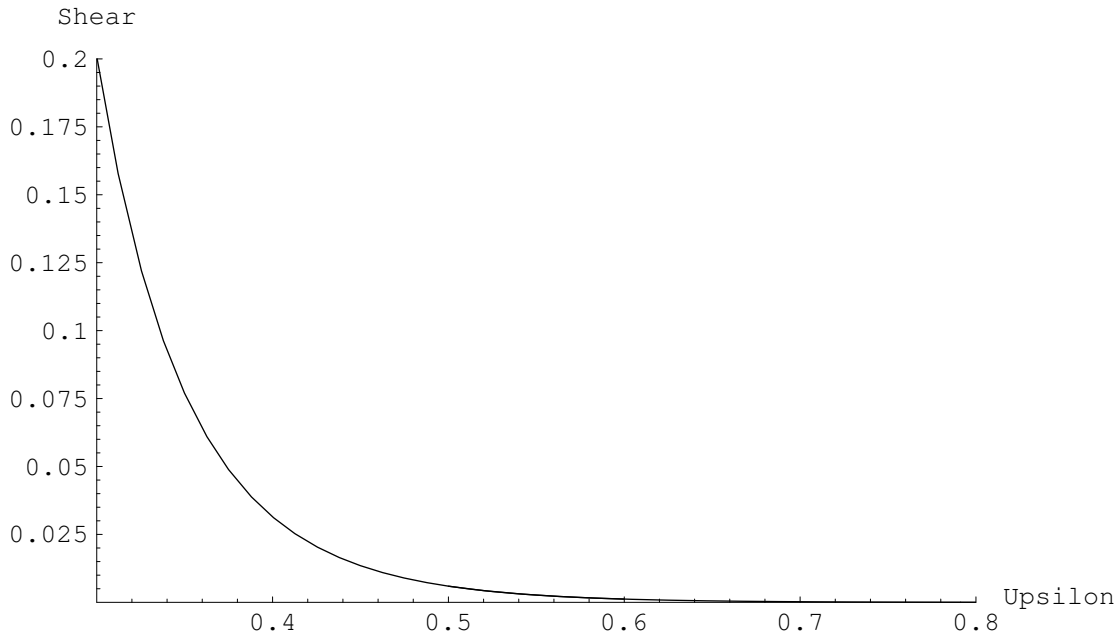

Figure 3.17: Graph showing how $f''(0)$ varies with Υ. $\lambda = 4.57$.

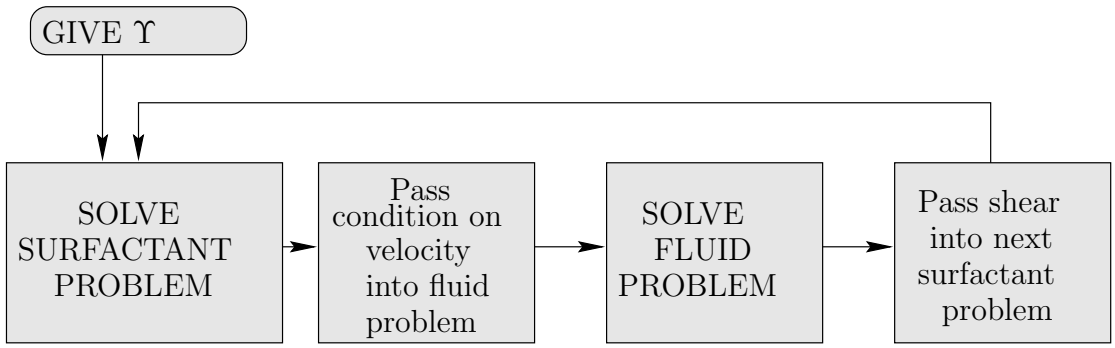

Figure 3.18: Flowchart showing transfer of information.

3.9.3 Problem and solution for C_2

We consider the model for C_2 to see if we can recover the experimentally observed behaviour that there is a small deviation to the constant concentration on the surface of the cylinder, and a small variation to the linear surface velocity profile. The $O(r^2)$ concentration problem described in §3.9.1 reads

$$C_2'' + 2KC_2' - 2KC_2 = -4\beta\zeta C^{*\prime}, \tag{3.122}$$

with

$$\begin{aligned} -C_2'(0) &= 4\beta(\lambda\Upsilon^2 + \Upsilon) + 4KC_2(0), & (3.123)\\ C_2(-\infty) &= 0, & (3.124)\\ C_2(0) &= -\frac{f_0''(0)}{2}, & (3.125) \end{aligned}$$

where $\beta = f_2'(0)$. The solution to (3.122), (3.124) and (3.125) is

$$C_2(\zeta) = -\frac{f_0''(0)}{2}\left(e^{-K\zeta^2} + 2K\zeta\int_{-\infty}^{\zeta} e^{-K\phi^2}d\phi\right) - \frac{4\beta(1-\Upsilon)}{3\sqrt{\pi K}}\zeta e^{-K\zeta}. \tag{3.126}$$

We then use (3.123) to find β, much as we did to find K (*c.f.* (3.115)):

$$\begin{aligned} \beta &= -\frac{3f_0''(0)\sqrt{\pi K}(4K + \sqrt{\pi K})}{8(1 - \Upsilon - 3\sqrt{\pi K}(\lambda\Upsilon^2 + \Upsilon))} & (3.127)\\ &= \frac{3f_0''(0)(1-\Upsilon)}{16\Upsilon^2(\lambda\Upsilon+1)^2}\left(1 + \frac{4(1-\Upsilon)}{\pi\Upsilon(\lambda\Upsilon+1)}\right). & (3.128) \end{aligned}$$

Since we have already found $f_0''(0)$ for $\Upsilon = 0.4$ in the previous section, we can immediately predict the variation in concentration at the surface (using (3.125)). The surface concentration reads

$$\Gamma = \lambda\Upsilon^2 + \Upsilon - \frac{f_0''(0)}{2}\hat{r}^2, \tag{3.129}$$

and we redimensionalise this to read

$$\Gamma_d = \frac{\Gamma_\infty\lambda}{(1+\lambda\Upsilon)^2}\left(\lambda\Upsilon^2 + \Upsilon - \frac{f_0''(0)}{2L^2}r_d^2\right). \tag{3.130}$$

We calculate that the variation from the constant (which we used to fix the value of Υ) in (3.130) is $3.4 \times 10^{-4} r_d^2$ and so, for example, at $r = 2$ cm, this gives a variation of 1.4×10^{-7} mol m^{-2}. We compare this with the experimental data shown in Figure 3.10, for $C_b = 0.58$ mol m^{-3}. We see that the actual variation from the constant at $r \sim 2$ cm is about 1.8×10^{-7} mol m^{-2} and we are encouraged by this agreement. We note that

- the smallness of the Γ variation has not resulted from l or V being small, but rather merely from the solution to the problem;
- our assumption that Γ does not vary much across the surface has been *a posteriori* verified.

We are also in a position to check whether the measured surface tension agrees with our predictions. We recall that

$$\gamma_0 = \sigma^* + RT\Gamma_\infty \log\left(\frac{1}{1+\lambda\Upsilon}\right), \tag{3.131}$$

and that

$$\sigma_d = \sigma\Delta\gamma = \frac{RT\Gamma_\infty\lambda}{1+\lambda\Upsilon}(\Upsilon - C) = -\frac{RT\Gamma_\infty\lambda}{2L^2(1+\lambda\Upsilon)}f_0''(0)r_d^2. \tag{3.132}$$

We calculate (with, as usual, $\Upsilon = 0.4$) $\gamma_0 = 0.059$ N m^{-1} and that, at $r = 0.02$ m, $\sigma_d = 1.05 \times 10^{-3}$ N m^{-1}. From Figure 3.8, we see that $\gamma_0 \sim 0.06$ N m^{-1} and that $\sigma_d \sim 2 \times 10^{-3}$ N m^{-1}. We are, again, in reasonable agreement with the experiments, and we note that we have, *a posteriori*, also verified our assumption that the change in surface tension across the surface is small.

Using (3.128), we calculate $\beta = 4.6 \times 10^{-3}$, and we redimensionalise the velocity to give the velocity on the surface, measured in m s^{-1},

$$u_d \sim 2.54r_d + 1192r_d^3. \tag{3.133}$$

The size of the second constant here is misleading, since it is measured in m^{-2} s^{-1}. We compare this to a best fit curve of the 0.58 mol m^{-3} data provided by Manning-Benson [53], in which the velocity in m s^{-1}, reads $u_d \sim 2.4r_d + 500r_d^3$. Again, we have reasonable agreement between the model and the experiment (up to a factor of 2 in this case).

The rest of the terms in the series can be generated in the same way. We do not generate any more of these terms here, our main conclusion being that, with the crucial proviso that Υ is fixed from the experiments, all the other experimental results are satisfactorily predicted by the mathematical model.

3.10 The lack of closure

To recap, to within a constant we have found solutions for the first two terms in the concentration field and for the leading-order liquid velocity in an expansion close to the

centre of the cylinder. We have also obtained a relationship for the second term in the surface velocity expansion. These all appear to give good qualitative agreement with the experiments, and indeed encouraging quantitative agreement once the free parameter Υ has been set (using experimental data). However, so far we have uncovered no way to select the value of Υ mathematically. We consider several possible closure mechanisms below.

3.10.1 Termination of the series

We could argue that, since there is no flow at depth in our model, we could terminate the series solution at some n and that this would give us a condition on Υ which would close the model. We contemplate that if we were to attempt such a termination after the first terms in the expansion, *i.e.*, we set $C_2(\hat{z}) \equiv 0$, then we must have $f_0''(0) = 0$ from (3.125) and so $f_0 \equiv 0$ and $C = 1$. If we attempt to set $f_2 \equiv 0$, then we must have $\beta = 0$ and so from (3.128) we are forced to conclude that $f_0''(0) = 0$ or $\Upsilon = 1$. In either case, the result is that $f_0 \equiv 0$ and $C^* = 1$. We have looked at the next terms in the series, and found that if we terminate there we are forced into the same conclusion, that $f_0 \equiv 0$ and $C^* = 1$. Since we know that this solution is physically unrealistic, we do not believe that termination of the series can be used to determine Υ.

We are forced to address the question "what is the behaviour of our expansion as $\hat{r} \to \infty$?". To answer this question, we have to consider the late terms in the series, but this is difficult because the problem is horridly nonlinear. To illustrate what mechanisms may be at work, we consider a simple, linear paradigm. We suppose that we are considering a problem with a finite solution whose "inner" formulation analogous to (3.92)-(3.94) is

$$C_{yy} = xC_x - yC_y, \tag{3.134}$$

with

$$-C_y = (xC)_x - C_{xx}, \qquad \text{on} \qquad y = 0, \tag{3.135}$$

$$C_x = 0 \qquad \text{on} \qquad x = 0, \tag{3.136}$$

$$C \to 1 \qquad \text{as} \qquad y \to -\infty. \tag{3.137}$$

With x replacing $\hat{r}$, the x factors in (3.134) and (3.135) represent $\hat{u}$, the factor of y in (3.134) represents $\hat{w}$ and we simulate the coupling between the hydrodynamics and the surfactant problem by introducing the $-C_{xx}$ term in (3.135).

As in our full problem, there is a solution to this problem which is independent of x, namely

$$C^* = 1 - \frac{1}{1+\sqrt{\frac{\pi}{2}}} \int_{-\infty}^{y} e^{-\frac{\eta^2}{2}} d\eta. \tag{3.138}$$

We seek a series solution which has C^* as the leading order term, *i.e.*, we set

$$C = C^* + \sum_{n=0}^{\infty} C_{2n}(y) x^{2n}, \tag{3.139}$$

and we formulate the problem for C_{2n} which reads

$$C''_{2n} - yC'_{2n} - 2nC_{2n} = 0, \tag{3.140}$$

$$C_{2n}(0) = \frac{C'_{2n-2}(0) + (2n-1)C_{2n-2}(0)}{2n(2n-1)}, \tag{3.141}$$

$$C_{2n} \to 0 \qquad \text{as} \qquad y \to -\infty. \tag{3.142}$$

The solution for C_{2n} reads

$$C_{2n}(y) = \alpha_{2n} S_{2n}(y) \left(I_{2n} - \int_y^0 \frac{e^{-\frac{\phi^2}{2}}}{S_{2n}(\phi)} d\phi \right), \tag{3.143}$$

where

$$S_{2n}(y) = \sum_{p=0}^{n} \frac{(2n)!! y^{2p}}{(2p)!!(2n-2p)!!} \qquad I_{2n-2-2q} = \int_{-\infty}^{0} \frac{e^{-\frac{\phi^2}{2}}}{S_{2n-2-2q}(\phi)} d\phi, \tag{3.144}$$

$$\alpha_{2n} = \frac{1}{(2n)!} \prod_{q=1}^{n-1} \left(2n - 1 - 2q + \frac{1}{I_{2n-2-2q}} \right) \frac{C_0(0)}{I_{2n}}. \tag{3.145}$$

We are interested in the behaviour of the solution on $y = 0$, where

$$C_{2n}(0) = \frac{1}{(2n)!} \prod_{q=0}^{n-1} \left(2n - 1 - 2q + \frac{1}{I_{2n-2-2q}} \right) C_0(0), \tag{3.146}$$

and so

$$C(x,0) \sim \frac{1}{1+\sqrt{\frac{\pi}{2}}} + C_0(0) \left[1 + \left(\frac{1}{2} + \frac{1}{2}\sqrt{\frac{2}{\pi}} \right) x^2 + \frac{1}{4!} \left(1 + \sqrt{\frac{2}{\pi}} \right) \left(3 + 2\sqrt{\frac{2}{\pi}} \right) x^4 + \ldots \right]. \tag{3.147}$$

We note that we have a one-parameter family of solutions, parametrised by $C_0(0)$. Thus $C_0(0)$ is analagous to the free parameter Υ in our nonlinear problem.

In order to match this solution to some "outer" solution we must consider the large x behaviour of C. We consider the ratio of $C_{2n}(0)/C_{2n-2}(0)$, which simplifies to

$$\frac{C_{2n}(0)}{C_{2n-2}(0)} = \frac{\left(2n-1+\frac{1}{I_{2n-2}}\right)}{2n(2n-1)}, \tag{3.148}$$

and, for large n, $I_{2n} \sim 1/\sqrt{2n}$, so in the limit $n \to \infty$, we have

$$\frac{C_{2n}(0)}{C_{2n-2}(0)} \sim \frac{1}{2n}. \tag{3.149}$$

By comparison with the ratio of the late terms in the power series expansion of $e^{x^2/2}$, we see that $C \sim e^{x^2/2}$ as $x \to \infty$. Since we wish to match to a finite value of C in the "outer" problem, we are thus forced to set $C_0(0) = 0$ and hence (3.138) is the only relevant solution of the inner problem. Thus we see that in this simple problem we can determine the solution uniquely, but only by looking at late terms in our local expansion, or by solving on a finite region.

We have looked at other more complicated problems where, for example, we introduce more velocity terms than just x and y, or by refining the simultation of the coupling between the hydrodynamic and diffusive problems. In these cases, we also find a one-parameter family of solutions and we are unable to find a condition which determines this constant in such a way as to give the solution some x dependence, and still enable us to match to the outer problem. Hence we conclude that the degenerate diffusion effects modelled by (3.134) are not responsible for our indeterminacy.

3.10.2 Neglected physical effects

In our modelling, we have made a number of assumptions about the underlying physics of the system. In this section we discuss several previously neglected mechanisms which might be necessary to close the model and allow us to predict Υ.

First we consider gravity. Recall that we supposed early on that gravity was strong enough to keep the top surface flat away from the rim, on the basis of the Froude number. In our scaled "inner region", it transpires that the reduced Froude number Fr^2/ϵ is typically $O(1)$. Instinctively, we do not expect gravity to be a determining factor in selecting Υ, but we discuss incorporating it here so that we can "rule it out". We perform modified scalings in the boundary layers to take account of undulations in the free surface (we set $\epsilon\hat{z} = z - H$ for example) and we find that the problem for the stream function ψ is unchanged: the problem for the free surface shape decouples from the rest of the problem.

The surfactant problem is, however, complicated by the introduction of the free surfaces, and, for example, we must modify (3.92) to read

$$\left(1+H_{\hat{r}}^2\right)C_{\zeta\zeta}=\hat{u}C_{\hat{r}}+\frac{\epsilon}{\delta}(\hat{w}-\hat{u}H_{\hat{r}})C_{\zeta}. \tag{3.150}$$

We are still able to employ our series expansions and regrettably, we obtain no extra information which enables us to close the problem.

We might think that neglecting the flow at depth has caused the indeterminacy, so here we consider the possibility of including this. We recall the expression for the flow at depth, written in boundary layer variables (3.102) reads

$$\hat{u}\sim 0.89Vl\hat{r}+0.69Vl^3\hat{r}^3+\ldots \tag{3.151}$$

Suppose that we take the (artificial) limit $l\to 0$, $Vl\sim O(1)$ so that we retain the first term in (3.151) but lose the successive terms. Our leading-order (in $\hat{r}$) velocity problem (3.118)-(3.121) must be modified to include a flow at depth. The behaviour of the solution to the modified problem is qualitatively the same as the solution that we have already presented, and, obviously, introduces no extra information into the system.

Next we consider surface diffusion. We must rescale $\hat{r}$ so as to bring in these terms, and the replenishment boundary condition becomes

$$-C_{\zeta}=\frac{1}{\tilde{r}}(\tilde{r}\hat{u}\Gamma)_{\tilde{r}}+\frac{1}{\tilde{r}}\left(\tilde{r}\Gamma_{\tilde{r}}\right)_{\tilde{r}}. \tag{3.152}$$

If we seek our similarity solution again, this boundary condition gives us, at lowest order in $\tilde{r}$, $-C^{*\prime}=2K\Gamma_0+2\Gamma_1$, *i.e.* an extra term has been introduced into the problem for C^* from higher up the expansion. Again, no extra information is introduced that will enable us to close the problem.

We encounter a similar problem if we attempt to include bulk lateral diffusion into the problem. The field equation reads

$$\frac{1}{\tilde{r}}\left(\tilde{r}C_{\tilde{r}}\right)_{\tilde{r}}+C_{\zeta\zeta}=\frac{1}{\tilde{r}}\left[\hat{\psi}_{\hat{z}}(\tilde{r},0)C_{\tilde{r}}-\hat{\psi}_{\tilde{r}\hat{z}}(\tilde{r},0)\zeta C_{\zeta}\right]. \tag{3.153}$$

This equation and the replenishment boundary condition still admit the series solution, with, as in the surface diffusion case, the $O(\tilde{r}^2)$ coefficient from the C expansion being drawn into the problem for C^*. We gain no extra information that enables us to predict Υ.

Finally, we suppose that the system is not in thermodyamic equilibrium, that is, that the Langmuir isotherm no longer holds. We must then consider the Langmuir-Hinschelwood equation (from Chapter 2)

$$\frac{1}{\hat{r}}(\hat{r}\hat{u}\Gamma)_{\hat{r}} = k_1(C(\Gamma_\infty - \Gamma) - k_2\Gamma), \tag{3.154}$$

for the evolution equation describing the transport of surface surfactant. Again, solving the system of equations using this boundary condition in place of the equilibrium isotherm fails to provide us with any extra information.

3.10.3 Edge Effects

In the light of the problem described above, we hypothesise that one can only close the model and predict the value of Υ by including edge effects in the model, even though the physical evidence seems to contradict this. The leading order outer flow at depth, while small at the centre of the cylinder, becomes infinite as the corner is approached. Thus the outer flow may have an effect close to the rim, and this effect may be transmitted back to the liquid and surfactant close to the axis. An important point to note is that in the simple, linear problem, if we did solve on a finite domain, it would not matter much what boundary conditions we actually impose at the edge. In our nonlinear problem, it is also possible that we need only to apply some matching condition with the outer problem. However, finding this condition might not be any more tractable than having to resort to a numerical solution of the full boundary layer equations on a finite r domain. Both these approaches would require a detailed knowledge of the flow over the rim of the cylinder, and so we do not attempt such solutions here.

3.11 Conclusions

We have formulated a model that describes the liquid motion and the surfactant distribution in the overflowing cylinder. We have solved both the liquid and surfactant problems away from the wall of the cylinder and the free surfaces. In this domain, the surfactant concentration is uniform and the liquid flows towards a sink at the rim.

We have also examined the structure of the problem close to the free surface. Here, we found both hydrodynamic and diffusive boundary layers. We noted the following

- The ratio of the two boundary layer thicknesses is the square root of the Prandtl number. For CTAB in water (and for surfactant systems in general), $\mathrm{Pr} << 1$, and the diffusive boundary layer is much thinner that the hydrodynamic boundary layer.

We concluded that the surfactant in the diffusion boundary layer only encounters the surface velocity.

- The problem selects its own length scale and velocity scale near to the free surface. The velocity scale is much larger than the pump velocity, and the lengthscale is a fraction of the cylinder's radius. We used the length scale to consider flow close to the centre of the cylinder, and we neglected edge effects in this 'inner' region. We used the ratio of the velocity scales to motivate "dropping" the outer flow from the model.

- We formulated a series solution for the liquid velocity and surfactant concentrations in this inner region.

- We found a relationship between the sub-surface centre concentration Υ and the coefficient of the linear component of the surface velocity, K, which reads

$$K = \frac{(1-\Upsilon)^2}{\pi\Upsilon^2(\lambda\Upsilon+1)^2}. \tag{3.155}$$

  Fixing Υ from experiments, the value of the leading-order surface velocity predicted by the (redimensionalised) relationship is in good agreement with experiments.

- We compared the surface concentration, surface tension and the surface shear predicted by our model with the experimental data for $C = 0.58$ mol m^{-3}, and, having fixed our solution with the appropriate value of Υ, we found good quantative agreement between the two.

- We were unable to determine the sub-surface centre concentration from our inner expansion. Adding in extra physics such as surface diffusion in this (or a smaller) region did not appear to determine Υ.

- We hypothesised that a full numerical solution of the boundary layer equations on a finite domain based on the radius of the cylinder would be required to determine the system completely, and that such a calculation would require in depth knowledge of the flow over the cylinder's rim. We noted that the conclusion that edge effects provide closure for the model near to the centre of the cylinder was counter-intuitive.

There are numerous extensions to the work presented in this chapter. Obviously, to completely describe the flow and surfactant distribution, the full numerical simulation of (3.86)-(3.91) and (3.92)-(3.94) must be carried out. Also the effects of surface diffusion, gravity, capillary forces and non-equilibrium adsorption, while small, could be included to

paint a fuller picture of what is going on. We could also attempt to model the system using a completely different adsorption isotherm: one that is activation controlled, for example. Since, once the sub-surface centre concentration has been fixed, the solution is in fair agreement with experiments, in the next chapter we proceed to apply the (validated) boundary conditions that we applied in this chapter, to the modelling of thin films in the presence of surfactants.

Chapter 4

Models for Marangoni flows in thin films with two free surfaces

4.1 Introduction

Thin liquid films arise in a large number of industrial and biological situations. For example, they are present in coating flows, bearing lubrication, and in the lining of the lungs. A recent review of a number of applications is given in Myers [59]. These films fall broadly into three types, depending on the number of constrained surfaces that they have. These are

- films between two solid surfaces, as in classical lubrication theory;
- films on substrates, such as in drop spreading or paint levelling;
- films with two free boundaries, such as those in foams or certain kinds of glass manufacture.

The stresses involved in moving a viscous liquid over a substrate, or between two solid surfaces, may demand a high pressure within the liquid. Our interest is in the flow of liquid between two free surfaces. In this case, even the presence of a small internally generated surface shear can generate a high pressure. As in the overflowing cylinder, the surface shear can be generated by the presence of a nonuniformly distributed surfactant, but it may also result from the presence of a nonuniformly distributed volatile component.

4.1.1 Thin films with two free boundaries

Work in this area has been carried out by a number of previous authors. Often, modelling is done with specific geometries in mind: those concerning foams are discussed at the start of Chapter 5. We briefly describe some of the work that is relevant to this thesis below.

1. Extensional thin layer flows

   Howell [36], [37] formulated a number of models for liquid flow under the action of viscosity, capillarity, inertia and gravity. We shall follow the procedure described there when we derive our thin film equations later in this chapter.

2. Extensional ultra thin layer flows

   Erneux and Davis [28] (E&D) and Ida and Miksis [40] (I&M) formulated models for ultra thin viscous layers where Van-der-Waals (intermolecular) forces become important. E&D found a time to film rupture using nonlinear stability analysis: the time depended on both the Hamaker number (ratio of intermolecular to viscous forces) and the capillary number. I&M extended this work by performing numerical simulations of the model to demonstrate film rupture. They concluded that Van-der-Waals forces and viscous forces dominated the evolution. We shall show how Van-der-Waals forces may be included into our model in §4.4.3.

3. Surfactants

   De Wit, Gallez and Christov [23] considered the rupture of a free film in the presence of insoluble surfactants. They included Marangoni terms and derived a system of three coupled nonlinear partial differential equations for the film thickness, velocity (uniform across the film) and the surfactant concentration. In the regime where inertial, capillary, Marangoni, viscous and Van-der-Waals forces all balance, they first found that the (linear) stability of the steady state depended on the capillary number and the Van-der-Waals number. They also found that the effect of the Marangoni number was to increase the time to rupture of the film. They integrated the system numerically to obtain profiles of the velocity, film thickness and concentration as the film thinned to rupture.

4.1.2 Films on substrates

The remaining literature involves flow over substrates. While the applications are not strictly relevant to this thesis, we briefly describe some of this work below, with the aim of illustrating approaches to surfactant and volatile modelling.

Gaver and Grotberg [29] considered the transport of insoluble surfactant, while Halpern and Grotberg [32] and Jensen and Grotberg [42] considered the transport of soluble surfactant. They derived coupled equations for the film thickness, and surfactant concentrations (in the insoluble case, they also included a surfactant source). In the first two papers, they solved their systems numerically to obtain the stream function, film thickness and

concentration field. The insoluble work highlighted a vortex within the liquid and that the surface flow was always in the same direction. The soluble work highlighted the presence of vortices rotating in opposite directions, giving rise to areas of 'outflow' and 'backflow' on the surface. Jensen and Grotberg's paper extended the soluble surfactant work to include non-equilibrium adsorption.

The main sources of (mathematical) literature about thin films containing volatile components concern paints. Howison et al. [39] modelled a drying paint layer acting under the influence of capillary, viscous and Marangoni forces. They formulated a diffusion dominated problem for resin concentration, while allowing solvent to evaporate at a *constant* rate E. Wilson [81] obtained an explicit solution to the leading-order film thickness and resin concentration in the limit of small evaporation, and then repeated the procedure for larger E. He then modified the evaporation model so that the rate was proportional to the volatile component. He solved the revised set of equations for the leading order film thickness and resin concentration in the limit of small E.

A number of the above models and results are summarised in Oron et al. [63].

4.1.3 Plan

We shall model the flow of a thin layer of viscous liquid residing between two free boundaries, and acting under viscous, capillary and Marangoni forces. We consider various sizes of the two important nondimensional parameter groups, the capillary and Marangoni numbers, and we catalogue the models that emerge in different parameter regimes. We then extend these models to include gravity, externally imposed pressures and Van-der-Waals forces. We repeat the procedure to derive models for surfactant concentration and volatile concentration, using the Péclet number and either repenishment or evaporation numbers to catalogue the models that result. We limit ourselves to considering two dimensional films for simplicity: generalisation to radially symmetric (or fully three dimensional) models are an extension to the work presented in this chapter. We shall use the models that we derive in this chapter in the next chapter when we model the drainage of foam lamellae.

4.2 Thin film equations for the liquid

Consider the flow of an incompressible liquid between two free surfaces denoted by $y = H(x,t) \pm \frac{1}{2}h(x,t)$, as shown in Figure 4.1. The notation is chosen so that H denotes the centre-line of the film, and h denotes the thickness. With liquid velocity given by

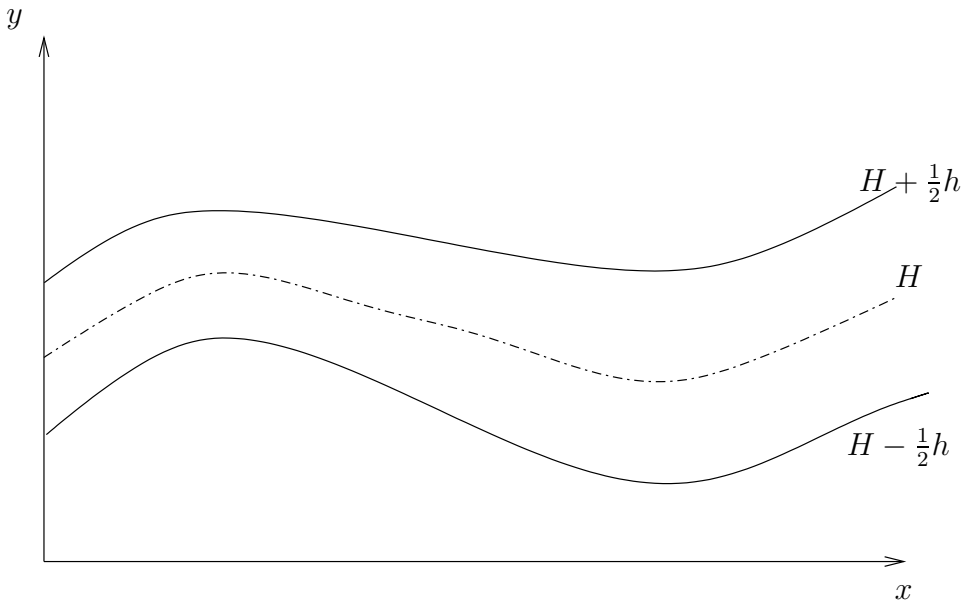

Figure 4.1: A thin film of liquid between two free surfaces.

$\mathbf{u} = (u, v)$, the liquid density, viscosity and pressure given by ρ, μ and p, and the surface tension on the top and bottom surfaces given by $\sigma^{\pm}$ respectively, the flow is governed by

$$\nabla.\mathbf{u} = 0, \tag{4.1}$$

$$\rho\left(\mathbf{u}_t + (\mathbf{u}.\nabla)\mathbf{u}\right) = -\nabla p + \mu\nabla^2\mathbf{u}, \tag{4.2}$$

assuming that gravity is negligible. The boundary conditions on the free surfaces are

$$\pm\sigma^{\pm}\kappa_{\pm} = -p + \mu\frac{\left(u_x\left(H_x \pm \frac{1}{2}h_x\right)^2 - (H_x \pm \frac{1}{2}h_x)v_x - 2u_y(H_x \pm \frac{1}{2}h_x) + 2v_y\right)}{1 + \left(H_x \pm \frac{1}{2}h_x\right)^2}, \tag{4.3}$$

$$\pm\sigma_x^{\pm} = \mu\frac{\left((u_y + v_x)\left(1 - \left(H_x \pm \frac{1}{2}h_x\right)^2\right) + 2(H_x \pm \frac{1}{2}h_x)\left(v_y - u_x\right)\right)}{\sqrt{1 + \left(H_x \pm \frac{1}{2}h_x\right)^2}}, \tag{4.4}$$

and

$$v = H_t \pm \frac{1}{2}h_t + u(H_x \pm \frac{1}{2}h_x), \tag{4.5}$$

which represent the normal and tangential force balance at each surface, and the kinematic condition respectively. We must also specify boundary conditions at the ends of the film (known hereafter as 'end conditions'). These depend on the situation under consideration. For example, in glass sheet stretching, we may fix one end (so that $u = 0$) and then extend the other at a fixed speed, *i.e.*, $u(l(t), t) = \dot{l}(t)$, where l is the length of the sheet.

We assume that the film is long and thin so that a typical lengthscale, L, is much larger than a typical thickness, ϵL say, where $\epsilon << 1$. We nondimensionalise equations (4.1)-(4.5) using the low Reynolds number scalings

$$\begin{aligned} x &= Lx', & y &= \epsilon L y', \\ u &= Uu', & v &= \epsilon U v', \\ p &= \frac{\mu U}{L} p', & t &= \tfrac{L}{U} t', \\ \sigma^{\pm} &= \gamma + \sigma'^{\pm} \Delta\gamma, & H \pm \tfrac{1}{2}h &= \epsilon L (H' \pm \tfrac{1}{2}h'). \end{aligned} \tag{4.6}$$

As in the previous chapter, we have decomposed the surface tension into a constant component γ and a variable component $\sigma'^{\pm}\Delta\gamma$, where $\Delta\gamma$ is a material property. The nondimensional equations read (dropping primes)

$$u_x + v_y = 0, \tag{4.7}$$

$$\epsilon^2 \mathrm{Re}(u_t + uu_x + vv_y) = -\epsilon^2 p_x + \epsilon^2 u_{xx} + u_{yy}, \tag{4.8}$$

$$\epsilon^2 \mathrm{Re}(v_t + uv_x + vv_y) = -p_y + \epsilon^2 v_{xx} + v_{yy}, \tag{4.9}$$

with

$$\pm \left(\frac{\epsilon}{\mathrm{Ca}} + \epsilon \mathrm{Ma} \sigma^{\pm} \right) \frac{(H_{xx} \pm \frac{1}{2}h_{xx})}{\left(1 + \epsilon^2 \left(H_x + \frac{1}{2}h_x\right)\right)^{\frac{3}{2}}} =$$

$$-p + \frac{2\epsilon^2 u_x (H_x \pm \frac{1}{2}h_x)^2 - 2\epsilon^2 v_x (H_x \pm \frac{1}{2}h_x) - 2u_y (H_x \pm \frac{1}{2}h_x) + 2v_y}{1 + \epsilon^2 (H_x \pm \frac{1}{2}h_x)^2}, \tag{4.10}$$

$$\pm \epsilon \mathrm{Ma} \sigma_x^{\pm} = \frac{(u_y + \epsilon^2 v_x)(1 - \epsilon^2 (H_x \pm \frac{1}{2}h_x)^2) + 2\epsilon^2 (H_x \pm \frac{1}{2}h_x)(v_y - u_x)}{\sqrt{1 + \epsilon^2 (H_x \pm \frac{1}{2}h_x)^2}}, \tag{4.11}$$

$$v = H_t \pm \frac{1}{2}h_t + u(H_x \pm \frac{1}{2}h_x), \tag{4.12}$$

where we have four nondimensional groups: the Reynolds number, Re, the capillary number, Ca, the Marangoni number, Ma, and the inverse aspect ratio ϵ, as defined in (3.20).

Note that we yet to define the velocity scaling U and there are two possible approaches. One is to choose U such as to balance as many different physical effects as possible. In this way the most general leading-order equations are obtained and any intermediate regimes can be identified as subsets of these "distinguished limits". In our case, it transpires that there are two distinct distinguished limits in which *three* physical effects balance.

Of course, in some cases U may actually be specified externally, for example through the end conditions or through the constitutive relationship for the surface tension. If so, we can regard U as given and calculate the resulting sizes of Re, Ca and Ma. Once U has been selected, the parameters are determined, and we can proceed with the asympotic analysis of (4.7)-(4.12).

Since we are not yet in a position to consider such external effects, we proceed for the moment with U unspecified and examine how the dominant balances shift as U varies. In fact, the character of the leading-order problem depends on the relative size of U compared with the "natural velocity scales" of the system. These are

- the velocity resulting from a balance between viscous and capillary forces,
$$U_c = \frac{\epsilon\gamma}{\mu}; \tag{4.13}$$
- the velocity resulting from a balance between viscous and Marangoni forces,
$$U_m = \frac{\Delta\gamma}{\epsilon\mu}; \tag{4.14}$$
- the velocity corresponding to a 'lubrication' style flow, that is a flow where the velocity is not uniform across the film,
$$U_l = \frac{\epsilon^3\gamma}{\mu} = \epsilon^2 U_c. \tag{4.15}$$

There are also velocity scales associated with a balance between inertial and viscous effects (*i.e.* based on the Reynolds number). Here, we assume that in the cases we are interested in (in line with the majority of thin film work), Re $<<$ 1, and so we do not discuss any inertial effects.

In classifying the possible regimes, the dimensionless group
$$T = \frac{\Delta\gamma}{\gamma\epsilon^2} = \frac{\mathrm{CaMa}}{\epsilon^2} = \frac{U_m}{U_c} \tag{4.16}$$
is particularly crucial. We note that $T = O(\epsilon^{-2})$ for consistency or it may be smaller, since the decomposition of the surface tension into a constant component and a variable component is meaningless if the second term is comparable to or larger than the first. We present a hierarchy of models, starting with the two distinguished limits, followed by those in which only two forces balance, and finish with those where only one force dominates over the other two. We illustrate the methodology involved in deriving all of the models in this section by formulating thin film equations from (4.7)-(4.12) in the $T \sim O(1)$ regime, where Ma $\sim O(\epsilon)$ and Ca $\sim O(\epsilon)$. In this parameter regime, $U \sim U_c \sim U_m$, and viscous, capillary and Marangoni forces all balance.

4.3 Reduction to thin film equations

4.3.1 Distinguished Limits: Three forces balancing

There are two distinct limits in which three forces balance, namely where viscous, capillary and Marangoni forces balance and where capillary, Marangoni and lubrication forces balance.

4.3.1.1 Viscous, capillary and Marangoni effects

In this regime, where $T \sim O(1)$ and $U \sim U_c \sim U_m$, we have $\mathrm{Ca} \sim O(\epsilon)$, $\mathrm{Ma} \sim O(\epsilon)$. To obtain a model for the film thickness, we expand the dependent variables as power series in powers of ϵ. We define $\mathcal{C} = \epsilon/\mathrm{Ca}$ and $\mathcal{M} = \mathrm{Ma}/\epsilon$. The leading–order problem reduces to

$$u_{0_x} + v_{0_y} = 0, \tag{4.17}$$

$$u_{0_{yy}} = 0, \tag{4.18}$$

$$v_{0_{yy}} = p_{0_y}, \tag{4.19}$$

with boundary conditions, on $y = H_0 \pm \frac{h_0}{2}$,

$$\pm\mathcal{C}(H_{0_{xx}} \pm \frac{1}{2}h_{0_{xx}}) = -p_0 + 2v_{0_y}, \tag{4.20}$$

$$u_{0_y} = 0, \tag{4.21}$$

$$v_0 = H_{0_t} \pm \frac{1}{2}h_{0_t} + u_0(H_{0_x} \pm \frac{1}{2}h_{0_x}). \tag{4.22}$$

Integrating (4.18) and applying (4.21) gives

$$u_0 = u_0(x,t), \tag{4.23}$$

i.e. the longitudinal velocity is uniform across the lamella. Such flows are often termed "extensional". Using this solution for u_0, (4.17) and (4.22) readily yield

$$v_0 = H_{0_t} + (u_0 H_0)_x - y u_{0_x}, \tag{4.24}$$

together with a relationship between u_0 and h_0 which represents conservation of mass

$$h_{0_t} + (u_0 h_0)_x = 0. \tag{4.25}$$

From (4.19) and (4.20), the equation for the centre-line is found to be

$$H_{0_{xx}} = 0. \tag{4.26}$$

This relationship forces the centre-line to be straight, and hence, without loss of generality, $H_0 = 0$. Including inertial effects, or a pressure difference across the film, will result in an equation for H_0 which must be solved alongside those for $\bar{u}$ and h. We consider the effect of a pressure difference later in this chapter.

We now also obtain the leading order pressure, p_0. Substituting for v_0 into (4.19), integrating, and applying (4.20) gives

$$p_0 = -2u_{0_x} - \frac{\mathcal{C}}{2} h_{0_{xx}}. \tag{4.27}$$

The pressure is therefore generated by a combination of extensional (viscous) and capillary effects.

To close the model for u_0 and h_0, we must examine the field equations and boundary conditions at the next order in the expansion. The relevant parts of the $O(\epsilon^2)$ problem are

$$u_{1_x} + v_{1_y} = 0, \tag{4.28}$$

$$u_{1_{yy}} = p_{0_x} - u_{0_{xx}}, \tag{4.29}$$

$$\pm \mathcal{M} \sigma_x^{\pm} = u_{1_y} + v_{0_x} \pm 2h_{0_x}(v_{0_y} - u_{0_x}) \qquad \text{on} \qquad y = \pm \frac{1}{2} h_0. \tag{4.30}$$

Integrating (4.29) between the upper and lower surfaces yields

$$(4h_0 u_{0_x})_x + \mathcal{M} \left(\sigma^+ + \sigma^-\right)_x + \frac{\mathcal{C}}{2} h_0 h_{0_{xxx}} = 0, \tag{4.31}$$

which, once the constitutive relations for $\sigma^{\pm}$ have been specified, provides a second nonlinear partial differential equation for h_0 and u_0 which must be solved in conjunction with (4.25) and with appropriate initial and end-conditions. This system requires two end-conditions for u and two for h. The factor of 4 in (4.31) is known as the "Trouton viscosity", see Howell [36]. We postpone discussion of the mathematical structure of this and all subsequent problems until we have formulated the related problems for the concentration of the Marangoni-inducing component.

The longitudinal force balance (4.31) includes contributions from the motion of the bulk liquid and from the surface forces present, and may be integrated once to give

$$4h_0 u_{0x} + \mathcal{M} \left(\sigma^+ + \sigma^-\right) + \frac{\mathcal{C}}{2} \left(h_0 h_{0xx} - \frac{h_{0x}^2}{2} \right) = \tau(t), \tag{4.32}$$

where $\tau(t)$ is the tension in the film.

4.3.1.2 Capillary, Marangoni and lubrication effects

In this regime, where $T \sim O(1)$ and $U \sim \epsilon^2 U_c \sim \epsilon^2 U_m$, we have Ma $\sim O(\epsilon^{-1})$ and Ca $\sim O(\epsilon^3)$. Here, surface forces are strong enough that the longitudinal liquid velocity can no longer remain uniform across the film, and it becomes parabolic, as in lubrication theory. To obtain a nontrivial leading-order balance, we must rescale the pressure via $p = p/\epsilon^2$. In contrast with §4.3.1.1, we can obtain all the information we require from the leading-order expansions. The resulting equations governing the flow are

$$h_t + (\bar{u}h)_x = 0, \tag{4.33}$$

$$\mathcal{M}\left(\sigma^+ + \sigma^-\right)_x + \frac{\mathcal{C}}{2} h h_{xxx} = 0. \tag{4.34}$$

The capillary dominated pressure is given by

$$P = -\frac{\bar{\mathcal{C}}}{2} h_{xx}, \tag{4.35}$$

and the liquid velocity is now given by

$$u = \bar{u} + \frac{\bar{\mathcal{C}}}{4} h_{xxx}\left(\frac{h^2}{12} - y^2\right) + \frac{\bar{\mathcal{M}}}{2}\left(\sigma^+ - \sigma^-\right)_x y. \tag{4.36}$$

where $\bar{\mathcal{C}} = \epsilon^3/\text{Ca}$, $\bar{\mathcal{M}} = \epsilon\text{Ma}$ and $\bar{u}$ is the cross-sectionally averaged velocity of the flow.

Since capillary and Marangoni forces dominate the flow, the film thickness and velocity are controlled purely by what is happening at the surface. Given the surface tension gradient, we solve (4.34) to find h and then (4.33) to find $\bar{u}$. This requires three end-conditions and an initial condition for h and an end-condition for $\bar{u}$. The velocity u is then given by (4.36). The increase in pressure within the film is due to the surface tension gradient exerting a shear at the free surfaces which the liquid must overcome in order to move.

We note that we either get plug flow, in which $u = u(x,t)$ and extensional viscous effects are important, or a parabolic flow, when extensional viscous effects must necessarily be negligible. There is no regime in which both effects are present.

4.3.2 Intermediate regimes where two forces balance

4.3.2.1 Capillary and Marangoni

In this parameter regime, where $T \sim O(1)$ and $U << U_m \sim U_c$, we have Ma $\sim O(1)$ and Ca $\sim O(\epsilon^2)$. We find that the liquid velocity is uniform across the lamella, we must scale the pressure by a factor of $1/\epsilon$ in order to balance surface forces, and we must work to

$O(\epsilon)$ in the field equations and boundary conditions to close the model. We find that the the resulting equations are identical to (4.33)-(4.35), viz

$$h_t + (uh)_x = 0, \tag{4.37}$$

$$\mathcal{M}\left(\sigma^+ + \sigma^-\right)_x + \frac{\mathcal{C}}{2} h h_{xxx} = 0, \tag{4.38}$$

$$p = -\frac{\mathcal{C}^*}{2} h_{xx}, \tag{4.39}$$

where $\mathcal{C}^* = \epsilon^2/\mathrm{Ca}$. In this regime, assuming that the constitutive relation for the surface tension is known, the solution strategy is to solve (4.38) to determine the shape of the free surfaces, and then to find the liquid velocity u using (4.37). Here, we need three boundary conditions on h to solve (4.38), and then an initial and boundary condition to solve (4.37).

4.3.2.2 Capillary and viscous effects

Here we have $T << 1$, $U \sim U_c >> U_m$, $\mathrm{Ma} \sim O(\epsilon^2)$ or less and $\mathrm{Ca} \sim O(\epsilon)$. Viscous forces now enter the problem at $O(\epsilon^2)$, but the Marangoni component is weak enough so that it does not affect the leading order model. We have

$$h_t + (uh)_x = 0, \tag{4.40}$$

$$(4hu_x)_x + \frac{\mathcal{C}}{2} h h_{xxx} = 0, \tag{4.41}$$

where the longitudinal force balance is now between viscous and capillary effects. We require an initial condition and two end conditions for h and two end conditions for u. In this case, the pressure is generated by both curvature changes and viscous effects

$$p = -2u_x - \frac{\mathcal{C}}{2} h_{xx}. \tag{4.42}$$

We note that this model may be used to describe the flow of a pure liquid devoid of any Marangoni inducing impurities.

4.3.2.3 Marangoni and viscous effects

Here, $T >> 1$ and $U \sim U_m >> U_c$ and we have $\mathrm{Ma} \sim O(\epsilon)$ and $\mathrm{Ca} \sim O(1)$ for example. We find

$$h_t + (uh)_x = 0, \tag{4.43}$$

$$(4hu_x)_x + \mathcal{M}\left(\sigma_x^+ + \sigma_x^-\right) = 0. \tag{4.44}$$

Given σ, we solve (4.44), with two end conditions for u, to obtain u, and then solve (4.43) with an initial condititon, to find h. The pressure here is viscous-generated

$$p = -2u_x. \tag{4.45}$$

4.3.2.4 Marangoni and lubrication effects

Here, $T >> 1$ and $U \sim \epsilon^2 U_c, U_m >> U_c$ and for example, we take Ma $\sim O(\epsilon^{-2})$ and Ca $\sim O(\epsilon^3)$. The longitudinal force balance is dominated by the Marangoni term, while the liquid velocity becomes nonuniform across the film. We have

$$h_t + (\bar{u}h)_x = 0, \tag{4.46}$$

$$\sigma_x^+ + \sigma_x^- = 0, \tag{4.47}$$

where

$$u = \bar{u} + \frac{\bar{\mathcal{C}}}{4} h_{xxx} \left(\frac{h^2}{12} - y^2 \right). \tag{4.48}$$

On first inspection, it seems as if we are an equation short. However, (4.47) is really a condition on the shear-inducing component of the system. For example, in §5.3.3, we will see that such a restriction informs us that the concentration in part of the film must be a function of time and not position. We impose this condition on the shear-inducing component and then we find u from that problem. The thickness h is then found from (4.46), and an initial condition.

4.3.3 Intermediate regimes where one force dominates

4.3.3.1 Capillary effects

Here, $T << 1$ and $U_c >> U_m, U$ and we have CaMa $\sim O(\epsilon^3)$ or less, Ca $\sim O(\epsilon^2)$ or less. In these regimes, the capillary forces outweigh both the viscous and the Marangoni forces, and we recover the familiar equation of linear capillary–statics

$$h_{xxx} = 0. \tag{4.49}$$

This has the obvious solution

$$h = a(t)x^2 + b(t)x + c(t), \tag{4.50}$$

where we must find the coefficients by applying end-conditions for h which are appropriate to the geometry under consideration. We require three end-conditions to fully specify the solution.

4.3.3.2 Viscous effects

Here, T has any size and $U >> U_c, U_m$ and for example, we may take Ma $\sim O(\epsilon^2)$ or less, Ca $\sim O(1)$ or larger. We find that surface tension forces do not enter the model at either

leading order or $O(\epsilon^2)$. In this case we recover the well-known Trouton model for the film thickness and the extensional velocity:

$$h_t + (uh)_x = 0, \tag{4.51}$$

$$(4hu_x)_x = 0. \tag{4.52}$$

This is the model for a thin liquid layer driven entirely by viscous forces. The pressure, again, decouples from the rest of the problem, and is entirely due to viscous effects,

$$p = -2u_x. \tag{4.53}$$

We require two end conditions for u to solve (4.52), and then an initial condition for h to solve (4.51). The general solution to this model has been presented in Pearson [65], Dewynne et al. [26] (using a partial hodograph transformation), and in Howell [36] (by transforming to Lagrangian coordinates).

There is no dependence of this model on the constitutive relation for surface tension, and we note that the system is hyperbolic, and that it can be solved by applying two boundary conditions for u and an initial condition for h. In the case of sheet stretching, for example, where one end of the film is assumed fixed, and the other end is pulled so that the length of the film is known, we apply conditions such as

$$\begin{aligned} h(x,0) &= h_0(x), & (4.54)\\ u(0,t) &= 0, & (4.55)\\ u(l(t),t) &= \dot{l}(t), & (4.56) \end{aligned}$$

where l is the length of the film.

4.3.3.3 Marangoni effects

Here $T >> 1$ and $U_m >> U_c, U$ and we illustrate these problems by considering the case where Ca $\sim O(\epsilon^2)$ and Ma $\sim O(\epsilon^{-1})$. In this situation, we must scale the pressure by $1/\epsilon$ and our leading order field equations become

$$\begin{aligned} u_{0yy} &= 0, & (4.57)\\ p_{0y} &= 0, & (4.58)\\ u_{0x} + v_{0y} &= 0, & (4.59) \end{aligned}$$

with

$$v = H_t \pm \frac{1}{2}h_t + u_0\left(H_x \pm \frac{1}{2}h_x\right), \tag{4.60}$$

$$-p = \pm\mathcal{C}^*\left(H_{xx} \pm \frac{1}{2}h_{xx}\right), \tag{4.61}$$

$$u_{0y} = \pm\bar{\mathcal{M}}\sigma_{0x}^{\pm}, \tag{4.62}$$

on $y = H \pm h/2$. We may solve for u_0 using (4.57) and (4.62) and we find that

$$u_0 = \frac{\bar{\mathcal{M}}}{2}(\sigma_0^+ - \sigma_0^-)_x y + \bar{u}, \tag{4.63}$$

and also

$$\bar{\mathcal{M}}(\sigma_0^+ + \sigma_0^-)_x = 0, \tag{4.64}$$

$$p_0 = \frac{\mathcal{C}^*}{2}h_{xx}. \tag{4.65}$$

We also obtain the conservation of mass equation as in all the other cases. As in §4.3.2.4, (4.64) provides a condition on the shear-inducing component of the system. We solve (4.64) to give information about the (so-far unspecified) model for Marangoni-inducing component, and then we solve this problem to give u. Finally, we then solve the mass-conservation equation using an initial condition for h.

4.3.4 Summary

We have derived the leading-order equations governing the evolution of both the velocity and the film thickness in a variety of parameter regimes. In Figure 4.2, we show how each of these models fits into the U, T parameter space,[1] and in Figure 4.3 we present a table of the models. We have set $\sigma_+ = \sigma_- = \sigma$ here for illustrative purposes. Once U has been determined, Ca and Ma can be calculated and the appropriate model "lifted" from this catalogue.

4.4 The effects of gravity, pressure drops across the film, disjoining pressure, and surface viscosity

In this section we shall show how the thin film equations of §4.2 may be modified to take account of gravity, pressure drops across the film, disjoining pressure, and surface viscosity. We shall set Ma $\sim O(\epsilon)$, Ca $\sim O(\epsilon)$ in all the calculations that follow, that is, we work in the distinguished limit where viscous, capillary and Marangoni forces already balance, and we choose the size of any *extra* group so as to generate a new distinguished limit where four forces balance.

[1] We note that U is dimensional and that T is nondimensional. It is very convenient to use these two parameters to describe the models, and so we proceed, even though this is not a *true* parameter space.

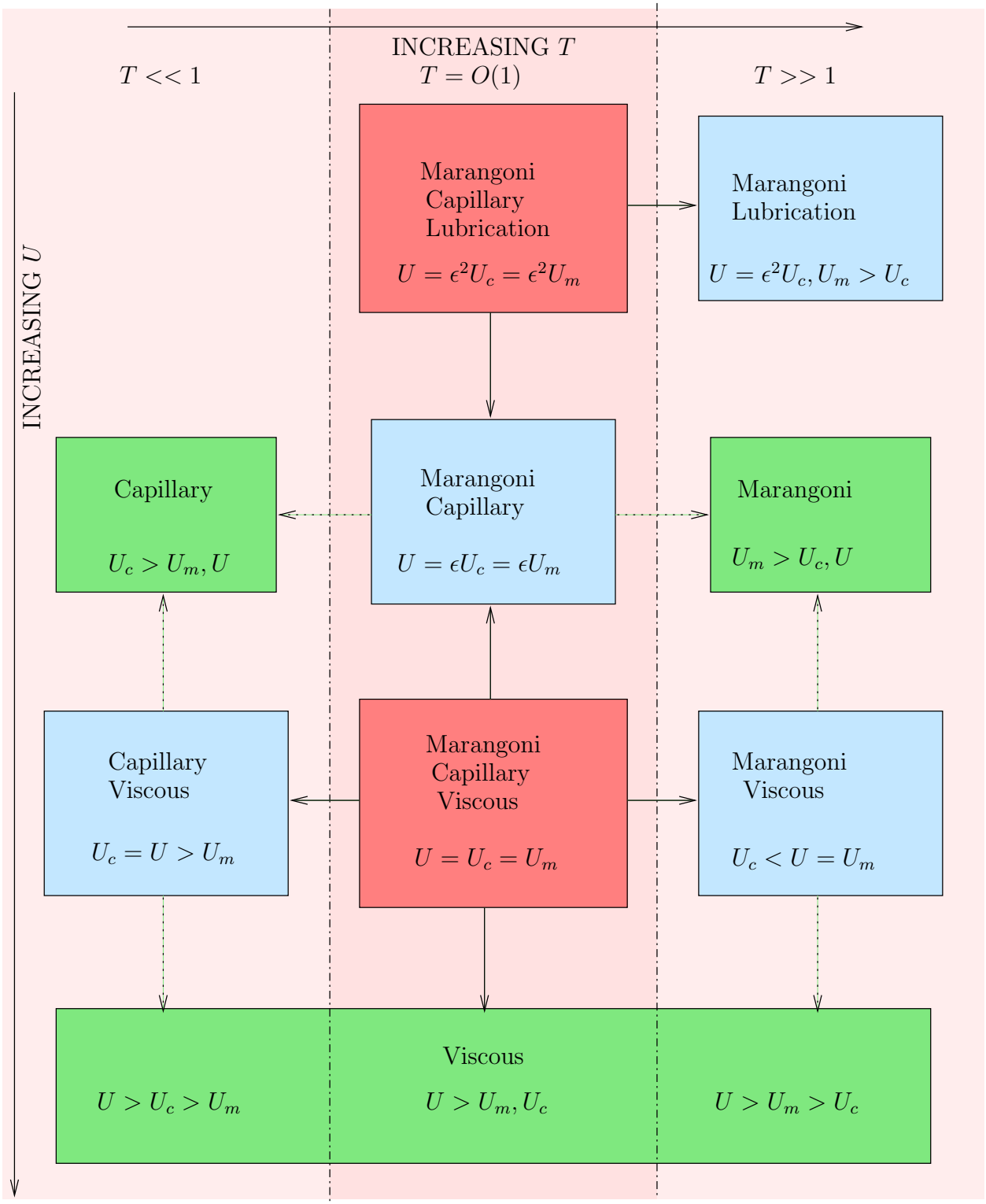

Figure 4.2: Schematic showing where the models lie in U, T space. The red blocks show the distinguished limits, the blue blocks show the intermediate regimes where two mechanisms balance, and the green blocks show the limits in which one mechanism dominates.

	Ma$\sim O(\epsilon^2)$	Ma$\sim O(\epsilon)$	Ma$\sim O(1)$	Ma$\sim O(\epsilon^{-1})$
Ca$\sim O(1)$	Viscous $h_t + (\bar{u}h)_x = 0$ $(4h\bar{u}_x)_x = 0$ $u = \bar{u}$	Viscous/Marangoni $h_t + (\bar{u}h)_x = 0$ $(4h\bar{u}_x)_x + 2\mathcal{M}\sigma_x = 0$ $u = \bar{u}$	Marangoni $h_t + (\bar{u}h)_x = 0$ $\sigma_x = 0$ $u = \bar{u}$	
Ca$\sim O(\epsilon)$	Viscous/Capillary $h_t + (\bar{u}h)_x = 0$ $(4h\bar{u}_x)_x + \frac{\mathcal{C}}{2}hh_{xxx} = 0$ $u = \bar{u}$	Viscous/Capillary/ Marangoni $h_t + (\bar{u}h)_x = 0$ $(4h\bar{u}_x)_x + \frac{\mathcal{C}}{2}hh_{xxx} + 2\mathcal{M}\sigma_x = 0$ $u = \bar{u}$	Marangoni $h_t + (\bar{u}h)_x = 0$ $\sigma_x = 0$ $u = \bar{u}$	Marangoni $h_t + (\bar{u}h)_x = 0$ $\sigma_x = 0$ $u = \bar{u}$
Ca$\sim O(\epsilon^2)$	Capillary $h_{xxx} = 0$	Capillary $h_{xxx} = 0$	Capillary/Marangoni $h_t + (\bar{u}h)_x = 0$ $2\mathcal{M}\sigma_x + \frac{\mathcal{C}}{2}hh_{xxx} = 0$ $u = \bar{u}$	Marangoni $h_t + (\bar{u}h)_x = 0$ $\sigma_x = 0$ $u = \bar{u}$
Ca$\sim O(\epsilon^3)$	Capillary $h_{xxx} = 0$	Capillary $h_{xxx} = 0$	Capillary $h_{xxx} = 0$	Capillary/Marangoni/ Lubrication $h_t + (\bar{u}h)_x = 0$ $2\mathcal{M}\sigma_x + \frac{\mathcal{C}}{2}hh_{xxx} = 0$ $u = \bar{u} + \frac{\bar{C}}{4}h_{xxx}\left(\frac{h^2}{12} - y^2\right)$

Figure 4.3: Table showing regimes.

4.4.1 Gravity

When gravitational forces are included we must introduce a new dimensionless group, the Stokes number $\mathrm{St} = \rho g L^2 \cos\alpha/(\mu U)$, where α is the angle between the x axis and the direction of action of gravity[2]. Following the procedure described earlier, and assuming that $\mathrm{St} \sim O(1)$, we find that the tangential force balance becomes

$$\left(4h_0 u_{0x}\right)_x + \frac{\mathcal{C}}{2} h_0 h_{0xxx} + 2\mathcal{M}\sigma_x + \mathrm{St} h_0 = 0. \tag{4.66}$$

Howell [36], §2.5 details the effects of introducing gravity into such thin film models in the absence of Marangoni forces.

4.4.2 Pressure drops across the film

If we wish to incorporate a difference in pressure across the film, as in the case of a film between two bubbles of different sizes, or in glass bottle manufacture, we must re-write boundary condition (4.10) as

$$\pm\frac{\epsilon}{\mathrm{Ca}}(H_{xx} \pm \frac{1}{2}h_{xx}) = P_{\pm} - p + \frac{2\epsilon^2 u_x(h_x \pm \frac{1}{2}h_x)^2 - 2\epsilon^2 v_x(H_x \pm \frac{1}{2}h_x) - 2u_y(H_x \pm \frac{1}{2}h_x) + 2v_y}{1 + \epsilon^2(H_x \pm \frac{1}{2}h_x)^2}, \tag{4.67}$$

where $P_{\pm}$ represents the nondimensional pressure above and below the film. If we allow the pressure difference, $\Delta P = P_+ - P_-$, to enter the problem at leading order, we modify (4.20) to read

$$\pm\mathcal{C}\left(H_{0xx} \pm \frac{1}{2}h_{0xx}\right) = P_{\pm} - p_0 + 2v_{0y} \qquad \text{on} \qquad y = H_0 \pm \frac{h_0}{2}. \tag{4.68}$$

We integrate the normal momentum balance and apply the above boundary conditions which results in the following equation for the centreline

$$-\Delta P + 2\mathcal{C}H_{0xx} = 0, \tag{4.69}$$

i.e., the centreline is a parabola. The leading order pressure is modified to read

$$p_0 = \frac{P_+ + P_-}{2} - \frac{\mathcal{C}}{2}h_{0xx} - 2u_{0x}. \tag{4.70}$$

The equation for conservation of mass and the longitudinal force balance remain the same. Therefore, the effect of including a pressure drop across the film is to force the centreline to have nonzero curvature.

[2]We assume that α is not so large that both the longitudinal and transverse components of gravity must be included.

4.4.3 Van der Waals forces and disjoining pressure

Long-range molecular forces, due to the interactions between the two liquid surfaces, generate disjoining pressures, which may either stabilise or destabilise the film. Two such forces are termed 'Van der Waals' (attractive) and 'electric double layer' (repulsive): see Middleman [58]. For these forces to be present, the film under consideration must be sufficiently thin (roughly 10-100 Angstroms). We model such forces by including an extra term, $A\phi/(6\pi)$, in the pressure, where ϕ is given by $\phi = 1/h^3$ and A is the Hamaker constant.[3] We assume that $\mathcal{A} = A/(6\pi L^2 \mu U \epsilon^3) \sim O(1)$, and then these forces enter the problem at $O(\epsilon^2)$. The appropriate modification of (4.29) reads

$$-p_{0x} + u_{0xx} + u_{1zz} = \mathcal{A}\left(\frac{1}{h^3}\right)_x. \tag{4.71}$$

On performing the algebra, we find that the longitudinal force balance is

$$(4hu_x)_x + \frac{\mathcal{C}}{2}hh_{xxx} + 2\mathcal{M}\sigma_x + \frac{3\mathcal{A}}{h^3}h_x = 0, \tag{4.72}$$

and the pressure is given by

$$p = -2u_x - \frac{\mathcal{C}}{2}h_{xx} - \frac{\mathcal{A}}{h^3}. \tag{4.73}$$

We have formulated the problem for attractive forces: repulsive forces simply correspond to $\mathcal{A}$ being negative.

4.4.4 Closure of the models

In this section we have presented a number of models for the film thickness h and the velocity u. Some of these formed closed systems, but those of interest contain Marangoni terms. To close these systems, we must make constitutive assumptions about σ. Our approach is to incorporate more chemistry (as described in Chapter 2) and so in §4.5 and §4.6, we couple the surface tension to the concentration of surfactant or volatile component. There are more *ad-hoc* approaches that we could also employ (see §2.4): the simplest is to assume that the surface velocity is zero. In this case, from (4.36), assuming that $\sigma^+ = \sigma^- = \sigma$, we find that

$$\bar{u} = \frac{\bar{\mathcal{C}}}{24}h^2 h_{xxx}, \tag{4.74}$$

and (4.33) reduces to the lubrication equation

$$h_t + \frac{\bar{\mathcal{C}}}{24}\left(h^3 h_{xxx}\right)_x = 0, \tag{4.75}$$

[3]The Hamaker constant $A \sim 10^{-21} - 10^{-19}$ Kg m^2 s^{-2}, see Middleman [58].

see Myers [59]. This approach has been used to model a soap film by Schwartz and Princen [69]. Once h has been found, $\bar{u}$ is given by (4.74), and σ by (4.34).

We might also employ a surface viscosity. As shown below, this can simplify the modelling, but only at the expense of demanding extra experimental evidence which may be difficult to obtain. The constitutive relation is that

$$\sigma = \eta u_x, \tag{4.76}$$

where η is the coefficient of surface viscosity. We nondimensionalise using $\eta = \Lambda\eta'$, where Λ is the typical magnitude of the surface viscosity, and we replace our Marangoni number by another dimensionless group, the viscosity ratio $\mathcal{V}_s = \Lambda/(\epsilon\mu L)$. We note that this is independent of the chosen velocity scale. Thus we obtain two distinguished limits corresponding to §4.3.1.1 and §4.3.1.2. In the first case, the surface velocity is equal to the bulk velocity, and the longitudinal force balance reads

$$\left(\left(4h + 2\mathcal{V}_s\eta\right)\bar{u}_x\right)_x + \frac{\mathcal{C}}{2}hh_{xxx} = 0, \tag{4.77}$$

and it is clear that the surface viscosity enhances the 'Trouton viscosity'. In the second case, the relationship between surface and average velocity is

$$u_s = \bar{u} - \frac{\bar{C}}{24}h^2h_{xxx}, \tag{4.78}$$

and the longitudinal force balance becomes

$$2\mathcal{V}_s\left(\eta\bar{u}_x\right)_x - \mathcal{V}_s\frac{\bar{C}}{12}\left(\eta\left(h^2h_{xxx}\right)_x\right)_x + \frac{\mathcal{C}}{2}hh_{xxx} = 0. \tag{4.79}$$

We must now specify extra h boundary conditions, since our problem for h is now fifth-order.

4.5 Thin film equations: presence of a surfactant

As discussed in the previous chapters, the presence of a surfactant reduces the surface tension of an interface. We also recall that it is energetically favourable for a surfactant to accumulate at a surface rather than remaining in the bulk liquid. We denote the surface surfactant concentration on the top and bottom surfaces by $\Gamma^{\pm}(x,t)$ respectively and the bulk surfactant concentration by $C(x,y,t)$. The field equations and boundary conditions for the concentration fields read (see §2.2)

$$C_t + (\mathbf{u}.\nabla)C = D\nabla^2C, \tag{4.80}$$

with, on $y = H \pm h/2$,

$$\Gamma^{\pm}_t + \frac{(u_s\Gamma^{\pm})_x}{\sqrt{1+(H_x \pm \frac{1}{2}h_x)^2}} = \mp\frac{D}{\sqrt{1+(H_x \pm \frac{1}{2}h_x)^2}}\left(C_y - \left(H_x \pm \frac{h_x}{2}\right)C_x\right), \quad (4.81)$$

$$\sigma^* - \sigma^{\pm} = -RT\Gamma_\infty \ln\left(1 - \frac{\Gamma^{\pm}}{\Gamma_\infty}\right), \quad (4.82)$$

$$\Gamma^{\pm} = \frac{\Gamma_\infty C}{k_2 + C}, \quad (4.83)$$

where D is the diffusion coefficient σ^* is the surface tension of water and Γ_∞ and k_2 are (dimensional) Langmuir coefficients. We must also specify an initial condition and boundary conditions at the ends of the film in order to close the model. Nondimensionalising using $\Gamma^{\pm} = \Gamma^*\Gamma'^{\pm}$, $C = C^*C'$ and the other scalings given in (4.6) earlier, the resulting equations are (dropping primes)

$$\epsilon^2 \mathrm{Pe}(C_t + uC_x + vC_y) = \epsilon^2 C_{xx} + C_{yy}, \quad (4.84)$$

with, on $y = H \pm h/2$,

$$\Gamma^{\pm}_t\sqrt{1+\epsilon^2(H_x \pm \frac{1}{2}h_x)^2} + (u_s\Gamma^{\pm})_x = \mp\frac{S}{\epsilon}\left(C_y + \epsilon^2\left(H_x \pm \frac{h_x}{2}\right)C_x\right), \quad (4.85)$$

$$\frac{\sigma^* - \gamma}{RT\Gamma_\infty} - \frac{\Delta\gamma}{RT\Gamma_\infty}\sigma^{\pm} = -\ln\left(1 - \frac{\Gamma^*\Gamma^{\pm}}{\Gamma_\infty}\right), \quad (4.86)$$

$$\Gamma^{\pm} = \frac{\frac{\Gamma_\infty\lambda}{\Gamma^*}C}{1+\lambda C}, \quad (4.87)$$

where we have three dimensionless groups, the Péclet number, $\mathrm{Pe} = UL/D$, the replenishment number, $S = DC^*/U\Gamma^*$ and $\lambda = C^*/k_2$. We shall decide on our choice of Γ^* and C^* when we come to apply these equations in specific situations. Again there are several intrinsic velocity scales that present themselves in this problem, which come from balancing the various mechanisms in the convection-diffusion problem. As before, we may choose one of these as our velocity scaling, or we may choose U from the boundary conditions. The extra possible velocity scalings are

- the velocity resulting from a balance between longitudinal diffusion and convection,

$$U_p = \frac{D}{L}; \quad (4.88)$$

- the velocity resulting from a balance between diffusion across the film and convection,

$$U_q = \frac{D}{L\epsilon^2} = \frac{U_p}{\epsilon^2}; \quad (4.89)$$

- the velocity resulting from a balance between diffusion from the bulk and convection on the surface,

$$U_s = \frac{DC^*}{\Gamma^*}. \tag{4.90}$$

In classifying the possible regimes, it is useful to form the dimensionless group

$$H_p = \frac{C^* L \epsilon^2}{\Gamma^*} = \frac{U_s \epsilon^2}{U_p}. \tag{4.91}$$

As in §4.3.1, it transpires that we can balance at most three effects and there are two distinguished limits in which this occurs.

4.5.1 Distinguished Limits: three mechanisms balancing

The two distinguished limits are when bulk convection, bulk diffusion and surface convection all balance, in the cases (a) when the concentration is uniform across the film and (b) when the concentration varies across the film. This is analagous to the situation in §4.3.1, where either u was extensional or it varied across the film.

4.5.1.1 Longitudinal diffusion, bulk convection and surface convection

Here, $H_p \sim O(1)$, $U \sim U_p \sim U_s\epsilon^2$, and we have $S \sim O(\epsilon^{-1})$ and $\mathrm{Pe} \sim O(1)$. As in the liquid case, we expand the dependent variables in power series in ϵ^2. We set $\mathcal{S} = 1/(S\epsilon)$, and our leading order problem reads

$$C_{0yy} = 0, \tag{4.92}$$

with, on $y = H_0 \pm \frac{h_0}{2}$,

$$C_{0y} = 0, \tag{4.93}$$

which has the solution

$$C_0 = C_0(x,t), \tag{4.94}$$

i.e., the bulk concentration is constant across the lamella. This is often called the 'well-mixed approximation' (compare with (4.3.1.1) to see the similarity with the u problem). With this form for the bulk concentration, the Langmuir isotherm (4.87) dictates that the surface concentrations $\Gamma_0^{\pm}$ are the same (and equal to Γ_0).

We must proceed to the next order in our expansions to close the model. At $O(\epsilon^2)$, the problem reads

$$\mathrm{Pe}\,(C_{0t} + u_0 C_{0x}) = C_{0xx} + C_{1yy}, \tag{4.95}$$

with, on $y = H_0 \pm h_0/2$,

$$\mp\left(C_{1y} + \left(H_x \pm \frac{h_x}{2}\right) C_{0x}\right) = \mathcal{S}\left(\Gamma_{0t} + (u_s\Gamma_0)_x\right). \tag{4.96}$$

We integrate (4.95) across the film, and apply the boundary conditions (4.96), to yield (dropping zeros)

$$(hC_x)_x - \mathrm{Pe}h\left(C_t + \bar{u}C_x\right) - 2\mathcal{S}\left(\Gamma_t + (u_s\Gamma)_x\right) = 0. \tag{4.97}$$

The first of these terms represents bulk diffusion, the second, bulk convection, and the third, surface convection. Finally we have obtained a closed system; for (4.97) along with the film equations and the constitutive relations (4.86) and (4.87) comprise five equations for h, u, C, Γ and σ. We shall discuss the mathematical structure of such problems in §4.7.

4.5.1.2 Diffusion across the film, bulk convection and surface convection

Here $H_p \sim O(1)$, $U \sim U_s \sim U_q$ and we have $S \sim O(\epsilon)$ and $\mathrm{Pe} \sim O(\epsilon^{-2})$. The problem for $C = C(x, y, t)$ reads

$$P^*\left(C_t + uC_x + vC_y\right) = C_{yy}, \tag{4.98}$$

with, on $y = H \pm h/2$,

$$\mp C_y = \mathcal{S}\left(\Gamma^{\pm}_t + \left(u^{\pm}_s\Gamma^{\pm}\right)_x\right), \tag{4.99}$$

where $P^* = \epsilon^2\mathrm{Pe}$. We must also couple these with (4.86)-(4.87). This limit presents a harder mathemtical model than the previous one. It is analogous to the equations in the diffusive boundary layer in our description of the overflowing cylinder experiment. However, in that case we were able to make progress due to the different scales over which the liquid and the surfactant acted. Here we are not so lucky. An iterative solution scheme might be as follows: we first assume that we know what h, u and v are, and then we solve for C. We infer Γ using the Langmuir isotherm (4.87), and hence find the surface tension gradient. We must then feed this information into the liquid problem and solve again for h, u and v.

We note that we were able to make significant progress in the liquid problem because we set $\mathrm{Re} = 0$. With $\mathrm{Re} \sim 1/\epsilon^2$, we have problems analagous to those for large Pe, and we are unable to make many simplifications.

4.5.2 Intermediate Regimes: Two mechanisms balancing

4.5.2.1 Bulk convection and surface convection

Here, $H_p \sim O(1)$, $U >> U_p \sim U_s\epsilon^2$, and we have $S \sim O(1)$ and $\mathrm{Pe} \sim O(\epsilon^{-1})$. We find that the bulk concentration is well-mixed and that the surface concentrations are the same. So the equation for $C = C(x,t)$ reads

$$\mathrm{Pe}h\left(C_t + uC_x\right) + 2\mathcal{S}\left(\Gamma_t + (u_s\Gamma)_x\right) = 0. \tag{4.100}$$

We must substitute the Langmuir isotherm (4.87) into (4.100) to give a hyperbolic equation for C, and, assuming u and u_s are given, this can be solved for C using an initial condition. Once this is solved, we can read off the surface concentrations.

4.5.2.2 Diffusion across the film and bulk convection

Here, $H_p >> O(1)$, $U \sim U_q << U_s$ and we have $S \sim O(1)$ or larger, $\mathrm{Pe} \sim O(\epsilon^{-2})$. The bulk concentration is not uniform across the film, and we must solve

$$P^*\left(C_t + uC_x + vC_y\right) = C_{yy}, \tag{4.101}$$

with, on $y = H \pm h/2$,

$$C_y = 0, \tag{4.102}$$

to find C (using the procedure described in §4.5.1.2). We then find $\Gamma^{\pm}$ from (4.87).

4.5.2.3 Longitudinal diffusion and surface convection

Here, $H_p << 1$ and $U \sim U_s\epsilon^2 << U_p$ and we have $S \sim O(\epsilon^{-1})$ and $\mathrm{Pe} \sim O(\epsilon)$. The surfactant is well-mixed, and the equation reads

$$\left(hC_x\right)_x + 2\mathcal{S}\left(\Gamma_t + \left(u_s\Gamma\right)_x\right) = 0. \tag{4.103}$$

We must substitute for Γ from the Langmuir isotherm (4.87) into (4.103) in order to solve the problem for $C(x,t)$, and then Γ may be obtained by using (4.87) for a second time.

4.5.2.4 Diffusion across the film and surface convection

Here, $H_p << 1$ and $U \sim U_s << U_q$, and for example $S \sim O(\epsilon)$ and $\mathrm{Pe} \sim O(\epsilon^{-1})$. The concentration of surfactant is not uniform across the film and, with $\mathcal{S}^* = \epsilon/S$, we have

$$C = \frac{1}{2\lambda}\left[\left(1+\frac{y}{h}\right)\left(\frac{\Gamma^+}{\frac{\Gamma_\infty}{\Gamma^*} - \Gamma^+}\right) + \left(1-\frac{y}{h}\right)\left(\frac{\Gamma^-}{\frac{\Gamma_\infty}{\Gamma^*} - \Gamma^-}\right)\right], \tag{4.104}$$

where Γ^+ and Γ^- can be found from solving

$$\left(\Gamma^+ + \Gamma^-\right)_t + \left(u_s^+\Gamma^+ + u_s^-\Gamma^-\right)_x = 0. \tag{4.105}$$

and

$$\left(\Gamma^+ - \Gamma^-\right)_t + \left(u_s^+\Gamma^+ - u_s^-\Gamma^-\right)_x = -\frac{1}{\lambda\mathcal{S}^* h}\left(\frac{\Gamma^+}{\frac{\Gamma_\infty}{\Gamma^*} - \Gamma^+} - \frac{\Gamma^-}{\frac{\Gamma_\infty}{\Gamma^*} - \Gamma^-}\right). \tag{4.106}$$

This model is analagous to the Marangoni dominated model presented in §4.3.3.3, where the velocity was linear across the film.

4.5.3 Regimes where one mechanism dominates

4.5.3.1 Surface convection

Here, $H_p << 1$, $U_s\epsilon^2 << U << U_p$ and we have $S \sim O(1)$ or less, $\mathrm{Pe} \sim O(1)$. The surfactant is well-mixed which forces the surface concentration to be the same on both surfaces, and the field equation at next order reveals

$$\Gamma_t + (u_s\Gamma)_x = 0. \tag{4.107}$$

To find the concentrations Γ and C, we must solve (4.107) to find Γ, and we can then find the (well-mixed) C using the inverted Langmuir isotherm

$$C = \frac{\Gamma}{\lambda\left(\frac{\Gamma_\infty}{\Gamma^*} - \Gamma\right)}. \tag{4.108}$$

4.5.3.2 Bulk convection

Here, $H_p >> 1$, $U \sim U_p << U_s\epsilon^2$ and we have $S \sim O(\epsilon^{-1})$, and $\mathrm{Pe} \sim O(\epsilon^{-1})$. The surfactant is well-mixed which forces the surface concentrations to be the same, and the field equation becomes

$$C_t + uC_x = 0. \tag{4.109}$$

The solution procedure is to find C using (4.109) and to then find Γ using (4.87).

4.5.3.3 Longitudinal diffusion

Here, we let H_p be any size, $U << U_p, U_s\epsilon^2$ and for example we could have $\mathrm{Pe} \sim O(\epsilon)$ and $S \sim O(\epsilon^{-3})$. We find that bulk diffusion governs the distribution of well-mixed surfactant, and the equation that the concentration satisfies is reduced to

$$(hC_x)_x = 0. \tag{4.110}$$

If, for example, the film thickness is spatially constant, the solution to (4.110) is

$$C = \frac{f_1(t)}{h(t)}x + f_2(t), \tag{4.111}$$

where f_1 and f_2 are determined using two end conditions. The surface concentration is then found from (4.87).

4.5.3.4 Convection dominated flows

Here, we have flows where Pe $\sim O(\epsilon^{-3})$ or larger. In this parameter regime, we have a convection-dominated situation, with diffusive boundary layers set up at the two free boundaries (as in the overflowing cylinder). We must solve the outer problem (which is convection-dominated),

$$C_t + uC_x + vC_y = 0, \tag{4.112}$$

and then match to our inner solution which satisfies

$$C_t + uC_x - u(H_x \pm \frac{1}{2}h_x)C_\eta + vC_\eta = C_{\eta\eta}, \tag{4.113}$$

where $H \pm h/2 + \eta = \sqrt{P^*}y$, with, on $\eta = 0$,

$$\mp C_\eta = \frac{S}{\sqrt{P^*}}\left(\Gamma^\pm_t + \left(u^\pm_s\Gamma^\pm\right)_x\right), \tag{4.114}$$

and the adsorption isotherm closes the problem. It seems reasonable to take the obvious solution of (4.112), $C = C_b$, and so we apply the matching condition

$$C \to C_b \qquad \text{as} \qquad \eta \to \pm\infty, \tag{4.115}$$

(where the $\pm$ depends on which surface the boundary layer is on). The solution strategy here depends on the size of $B = S/\sqrt{P^*}$. If $B >> 1$ we solve the surface-convection-dominated problem

$$\Gamma^\pm_t + \left(u^\pm_s\Gamma^\pm\right)_x = 0, \tag{4.116}$$

and then we solve for C in the two boundary layers using the inverted Langmuir isotherm (4.108) to pass information to the boundary layer model. If $B \sim O(1)$ we must first substitute for Γ using the isotherm, and then solve the resulting problem (which balances all three transport mechanisms) for C. Γ is then inferred by using the isotherm for a second time. Finally, if $B >> 1$, we solve the bulk convection and diffusion dominated problem with the boundary condition $C_\eta = 0$ and we then read off Γ from the isotherm.

4.5.4 Summary

We have derived the leading-order equations governing the evolution of both the surface and bulk concentrations, in a variety of parameter regimes. In Figure 4.4, we show how each of the models fits into H_p, U parameter space, and in Figure 4.5 we present a table of the models. Once U has been determined, Pe and S can be calculated, and the appropriate model may be "lifted" from the catalogue. We note that (i) if $\epsilon^2\mathrm{Pe} << 1$, then the surfactant is well-mixed, (ii) if not, but $\epsilon^2\mathrm{Pe} = O(1)$, transverse diffusion and convection balance and the surfactant concentration varies across the film, and (iii) if $\epsilon^2\mathrm{Pe} >> 1$, we have a boundary layer structure.

4.5.5 The no-slip condition

In the limit where the concentration of surfactant is high, the Langmuir isotherm (4.87) implies that the variation in surface concentration is small. So, Γ is of the form

$$\Gamma \sim \frac{\Gamma_\infty}{\Gamma^*}\left(1 - \frac{k_2}{C^*C} + \ldots\right) = \frac{\Gamma_\infty}{\Gamma^*} - \alpha\Gamma_1 + \ldots, \tag{4.117}$$

where $\alpha = k_2\Gamma_\infty/(C^*\Gamma^*)$. Substituting this into (4.85) and expanding the surface velocity in the form $u_s = u_0 + \alpha u_1 + O(\alpha^2)$ yields, on $y = H \pm h/2$,

$$-SC_y \sim \frac{\Gamma_\infty}{\Gamma^*}u_{0x} - \alpha\left(u_0\Gamma_1\right)_x - \frac{\Gamma_\infty}{\Gamma^*}\alpha u_{1x} - \alpha\Gamma_{1t} + O(\alpha^2). \tag{4.118}$$

Hence, the leading order balance depends on the size of S and α (since we assume that $\frac{\Gamma_\infty}{\Gamma^*} \sim O(1)$). This reduces to a no-slip condition if both α and S are small (*i.e.* the surfactant is also relatively insoluble). Such a condition has been employed in this geonetry by previous authors such as Schwartz and Princen [69], but has not previously been justified from any systematic modelling of the free surface properties.

4.5.6 Insoluble surfactants

If insoluble surfactants are present on the film surfaces, but not in the bulk liquid, they move due to surface convection *and* diffusion. The concentration of such a surfactant satisfies

$$\mathrm{Pe}_s\left(\Gamma^\pm_t + \left(u_s\Gamma^\pm\right)_x\right) = \Gamma^\pm_{xx}, \tag{4.119}$$

where Pe_s is the surface Péclet number, and with

$$\frac{\sigma^* - \gamma}{RT\Gamma_\infty} - \frac{\Delta\gamma}{RT\Gamma_\infty}\sigma^\pm = -\ln\left(1 - \frac{\Gamma^\pm}{\Gamma_\infty}\right), \tag{4.120}$$

at the free surface. These surfactants always generate high shear at the free surface.

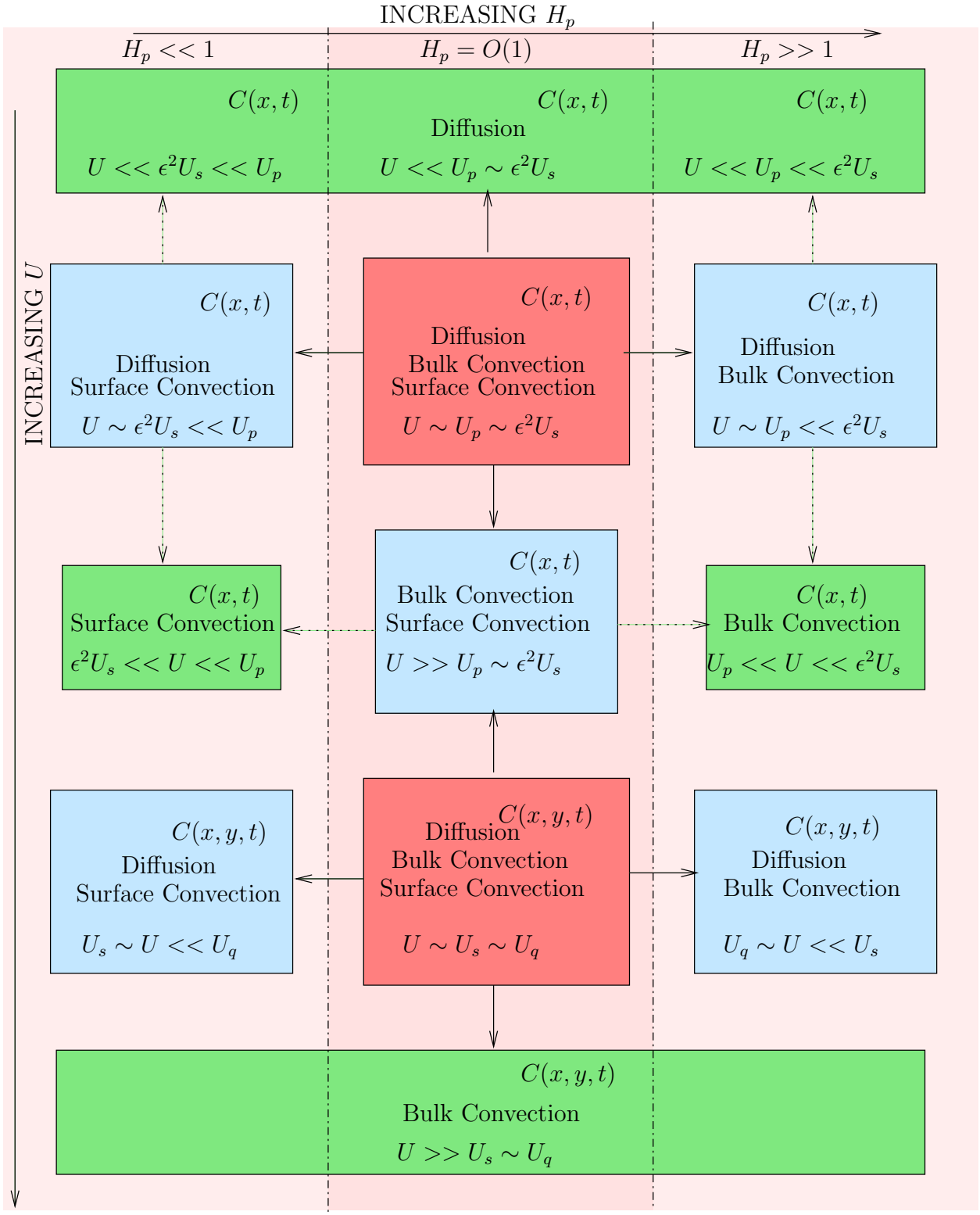

Figure 4.4: Schematic showing where the models lie in U, H_p space. The red blocks show the distinguished limits, the blue blocks show the intermediate regimes where two mechanisms balance, and the green blocks show the limits in which one mechanism dominates.

	$\mathrm{Pe} \sim O(\epsilon)$	$\mathrm{Pe} \sim O(1)$	$\mathrm{Pe} \sim O(\epsilon^{-1})$	$\mathrm{Pe} \sim O(\epsilon^{-2})$	$\mathrm{Pe} \sim O(\epsilon^{-3})$
$\mathrm{S} \sim O(\epsilon^{-2})$	Bulk Diffusion $\Gamma^+ = \Gamma^-$ $(hC_x)_x = 0$ Langmuir gives Γ	Bulk Diffusion and Bulk Convection $\Gamma^+ = \Gamma^-$ $(hC_x)_x - \mathrm{Pe}h(C_t + uC_x) = 0$ Langmuir gives Γ	Bulk Convection $\Gamma^+ = \Gamma^-$ $C_t + uC_x = 0$ Langmuir gives Γ	Bulk Convection and Bulk Diffusion $P^* (C_t + uC_x + vC_y) = C_{yy}$ $C_y = 0$ Langmuir gives $\Gamma^\pm$	Boundary layer problem
$\mathrm{S} \sim O(\epsilon^{-1})$	Bulk Diffusion and Surface Convection $\Gamma^+ = \Gamma^-$ $(hC_x)_x - 2\mathcal{S}(\Gamma_t + (u_s\Gamma)_x) = 0$ Must use Langmuir to solve problem	Bulk Conv. and Diff. Surface Convection $\Gamma^+ = \Gamma^-$ $(hC_x)_x - \mathrm{Pe}h\,(C_t + \bar{u}C_x) - 2\mathcal{S}\,(\Gamma_t + (u_s\Gamma)_x) = 0$ Must use Langmuir to solve problem	Bulk Convection $\Gamma^+ = \Gamma^-$ $C_t + uC_x = 0$ Langmuir gives Γ	Bulk Convection and Bulk Diffusion $P^* (C_t + uC_x + vC_y) = C_{yy}$ $C_y = 0$ Langmuir gives $\Gamma^\pm$	Boundary layer problem
$\mathrm{S} \sim O(1)$	Surface Convection $\Gamma^+ = \Gamma^-$ $\Gamma_t + (u_s\Gamma)_x = 0$ Langmuir gives C	Surface Convection $\Gamma^+ = \Gamma^-$ $\Gamma_t + (u_s\Gamma)_x = 0$ Langmuir gives C	Surface Convection/ Bulk Convection $\Gamma^+ = \Gamma^-$ $\mathrm{Pe}h\,(C_t + \bar{u}C_x) + \mathcal{S}\,(\Gamma_t + (u_s\Gamma)_x) = 0$ Must use Langmuir to solve problem	Bulk Convection and Bulk Diffusion $P^* (C_t + uC_x + vC_y) = C_{yy}$ $C_y = 0$ Langmuir gives $\Gamma^\pm$	Boundary layer problem
$\mathrm{S} \sim O(\epsilon)$	Surface Convection $\Gamma^+ = \Gamma^-$ $\Gamma_t + (u_s\Gamma)_x = 0$ Langmuir gives C	Surface Convection $\Gamma^+ = \Gamma^-$ $\Gamma_t + (u_s\Gamma)_x = 0$ Langmuir gives C	Surface Convection and Bulk Diffusion C Linear across film Coupled equations for Γ^+ and Γ^-	Bulk Conv. and Diff. Surface Convection $P^* (C_t + uC_x + vC_y) = C_{yy}$ $\mp C_y = \mathcal{S}\left(\Gamma^\pm_t + (u^{\pm_s}\Gamma^\pm)_x\right)$ Must use Langmuir to solve problem	Boundary layer problem

Figure 4.5: Table showing regimes.

4.6 Thin film equations: presence of a miscible, volatile component

As stated in Chapter 2 earlier, we denote the volatile component concentration by s, and the nondimensionalised field equation for s reads

$$\epsilon^2 \mathrm{Pe}(s_t + us_x + vs_y) = \epsilon^2 s_{xx} + s_{yy}, \tag{4.121}$$

where Pe is the Péclet number. We nondimensionalise the boundary conditions (2.24) and (2.26) in the usual way, and we obtain

$$s_y - \epsilon^2 \left(H_x \pm \frac{h_x}{2}\right) s_x \pm \epsilon^2 \mathrm{Pe}\mathcal{E} e_\pm (1-s)\sqrt{1+\epsilon^2\left(H_x \pm \frac{h_x}{2}\right)^2} = 0, \tag{4.122}$$

$$v \mp u\left(H_x \pm \frac{h_x}{2}\right) - \left(H_t \pm \frac{h_t}{2}\right) = \mathcal{E} e_\pm \sqrt{1+\epsilon^2\left(H_x \pm \frac{h_x}{2}\right)^2}, \tag{4.123}$$

where $\mathcal{E} = E_0/(U\epsilon)$ is the evaporation number. The modified kinematic condition (4.123) can be used to obtain a modified conservation of mass equation which now takes account of the loss of liquid due to evaporation:

$$h_t + (\bar{u}h)_x + \mathcal{E}(e_+ + e_-) = 0. \tag{4.124}$$

As stated in §2.3, we must specify models for how the evaporation and surface tension vary with concentration, and so we set $e_\pm = s|_{H\pm\frac{h}{2}}$ and $\sigma_x^\pm = -\alpha s_x|_{H\pm\frac{h}{2}}$. So (4.124) becomes

$$h_t + (\bar{u}h)_x + \mathcal{E}(s|_{H+\frac{h}{2}} + s|_{H-\frac{h}{2}}) = 0. \tag{4.125}$$

and boundary condition (4.122) reads

$$s_y - \epsilon^2 \left(H_x \pm \frac{h_x}{2}\right) s_x \pm \epsilon^2 \mathrm{Pe}\mathcal{E} s(1-s)\sqrt{1+\epsilon^2\left(H_x \pm \frac{h_x}{2}\right)^2} = 0, \tag{4.126}$$

where s is evaluated at the two free surfaces. Thus we arrive at a closed system for h, u, and s. The volatile model has a number of similarities to the surfactant model, but is simpler because we only have to consider one concentration field.

As in the liquid and surfactant cases, we consider changing the order of the two parameters Pe and $\mathcal{E}$, and catalogue the numerous models that result. We restrict ourselves to flows where $\mathcal{E} \sim O(1)$ or smaller in cases where the volatile is well-mixed, since conservation of mass forces $s = 0$ when $\mathcal{E}$ violates this size condition. We may obtain a non-zero leading

order solution for s for larger values of $\mathcal{E}$ by considering a shorter timescale than L/U (see §4.6.3.4). We, can, as before, identify several key velocity scalings by balancing various mechanisms:

- a balance between convection and diffusion in the well-mixed limit,

$$U_p = \frac{D}{L}, \tag{4.127}$$

- a balance between convection and diffusion when the volatile is not well-mixed,

$$U_q = \frac{D}{L\epsilon^2} = \frac{U_p}{\epsilon^2}, \tag{4.128}$$

- an evaporation based velocity scale,[4]

$$U_e = \frac{E_0}{\epsilon}. \tag{4.129}$$

We note that U_p and U_q are identical to those specified for the surfactant problem. Here, it is convenient to continue to work with the parameter $\mathcal{E}$. We shall start by deriving the leading-order model in the case where $Pe \sim O(1)$ and $\mathcal{E} \sim O(1)$, when we can obtain a dominant balance between convection, diffusion and evaporation in a well-mixed scenario. We then present the other dominant balance, followed by the intermediate regimes where two forces balance, and, finally, the intermediate regimes where one force dominates.

4.6.1 Distinguished limits: three mechanisms balancing

The distinguished limits are when convection, diffusion and evaporation all balance in the cases (a) when the volatile has uniform concentration across the film and (b) when the volatile has non-uniform concentration across the film.

4.6.1.1 Convection, longitudinal diffusion and evaporation

Here, $\mathcal{E} \sim O(1)$, $U \sim U_p \sim U_e$ and Pe $\sim O(1)$. The leading-order problem reads

$$s_{0yy} = 0, \tag{4.130}$$

with

$$s_{0y} = 0, \tag{4.131}$$

on the free boundaries, which has the solution

$$s_0 = s(x,t), \tag{4.132}$$

[4]This comes from considering the balance in the conservation of mass equation.

so, in this regime, the concentration is well-mixed. This tells us that the evaporation rates on the free boundaries are the same. As previously, we must proceed to order $O(\epsilon^2)$ in the field equation and boundary conditions in order to close the leading order problem. We find

$$\mathrm{Pe}(s_t + us_x) = s_{xx} + s_{1yy}, \tag{4.133}$$

and

$$-s_{1y} - \left(H_x \pm \frac{h_x}{2}\right) s_x \pm \mathrm{Pe}\mathcal{E}s(1-s) = 0, \tag{4.134}$$

on the free surfaces. Integrating (4.133) across the film and applying (4.134), we obtain

$$\left(hs_x\right)_x - \mathrm{Pe}h\left(s_t + \bar{u}s_x\right) - 2\mathrm{Pe}\mathcal{E}s(1-s) = 0, \tag{4.135}$$

as the equation for the leading-order concentration. The first term in (4.135) represents bulk diffusion, the second term represents convection and the third represents evaporation. Coupling (4.135) with the liquid equations, as in the surfactant case, we obtain three coupled nonlinear partial differential equations for the film thickness, velocity and volatile concentration.

4.6.1.2 Convection, diffusion across the film and evaporation

Here, $\mathcal{E} \sim O(1)$, $U \sim U_q \sim U_e$ and we have $\mathrm{Pe} \sim O(\epsilon^{-2})$. The volatile no longer has constant concentration across the film, and it satisfies a problem in which convection, diffusion and evaporation all play a part. We set $P^* = \epsilon^2\mathrm{Pe}$, and the model then reads

$$s_{yy} = P^*\left(s_t + us_x + vs_y\right), \tag{4.136}$$

with

$$s_y \pm P^*\mathcal{E}s(1-s) = 0, \tag{4.137}$$

on the free boundaries. Assuming that u and v are given, we may solve this parabolic equation, with appropriate initial and end-conditions. We then use the relationship between the volatile's concentration and surface tension to feed information back into the problem for the liquid.

4.6.2 Intermediate regimes where two mechanisms balance

4.6.2.1 Convection and longitudinal diffusion

Here, $\mathcal{E} \sim O(\epsilon)$, $U \sim U_p >> U_e$, we have $\mathrm{Pe} \sim O(1)$, and we find the evaporation no longer plays a part in determining the concentration. The volatile is well-mixed, and we are left with a balance between diffusion and convection

$$\left(hs_x\right)_x - \mathrm{Pe}h\left(s_t + \bar{u}s_x\right) = 0. \tag{4.138}$$

This requires two end-conditions and an initial condition for s in order to be solved.

4.6.2.2 Convection and evaporation

In this case, $\mathcal{E} \sim O(1)$, $U \sim U_e >> U_p$ and Pe $\sim O(\epsilon^{-1})$, and the problem becomes dominated by convection and evaporation

$$h\left(s_t + \bar{u}s_x\right) + 2\mathcal{E}s(1-s) = 0. \tag{4.139}$$

The volatile remains well-mixed in this case, and we solve this equation by specifying one end-condition and an initial condition for s.

4.6.2.3 Convection and diffusion across the film

Here $\mathcal{E} \sim O(1)$, $U \sim U_q >> U_e$ and we have Pe $\sim O(\epsilon^{-2})$. We simplify the boundary condition on the free surfaces, and the model for the concentration (which is non-uniform across the film) becomes

$$P^*\left(s_t + us_x + vs_y\right) = s_{yy}, \tag{4.140}$$

with

$$s_y = 0, \tag{4.141}$$

on the free surfaces. In this problem, the transport is dominated by convection and diffusion.

4.6.2.4 Convection and diffusion across the film (and evaporation)

Here, $\mathcal{E} \sim O(\epsilon^{-1})$, $U \sim U_q << U_e$ and Pe $\sim O(\epsilon^{-2})$, conservation of mass dictates that $s|_{h/2} = -s|_{-h/2}$, and the boundary condition says that $s = 0$ or 1 on both the free surfaces. We conclude that the appropriate boundary condition to apply is $s = 0$ and so we have

$$P^*\left(s_t + us_x + vs_y\right) = s_{yy}, \tag{4.142}$$

with

$$s = 0, \tag{4.143}$$

on the free surfaces. Evaporation, in this case, occurs fast enough to remove any volatile component that approaches the surface.

4.6.3 Regimes where one mechanism is dominant

4.6.3.1 Diffusion

Here $\mathcal{E} \sim O(1)$ or less, $U \sim U_e << U_p$ or $U_e << U << U_p$ and we have Pe $\sim O(\epsilon)$ or smaller. The convective terms are negligible and, evaporation terms do not enter the model at leading-order. The volatile is well-mixed, and satisfies merely

$$\left(hs_x\right)_x = 0. \tag{4.144}$$

If, for example, the film thickness is spatially constant, this yields the solution

$$s = \frac{f_1(t)}{h(t)}x + f_2(t), \tag{4.145}$$

where f_1 and f_2 have to be determined using the end conditions (*c.f.* §4.111).

4.6.3.2 Convection (well-mixed)

In this limit, $\mathcal{E} \sim O(\epsilon)$, $U >> U_e, U_p$ and Pe $\sim O(\epsilon^{-1})$ for example, and neither diffusion nor evaporation plays a part in the volatile concentration distribution. The convection-dominated model for the well-mixed surfactant reads

$$s_t + \bar{u}s_x = 0. \tag{4.146}$$

4.6.3.3 Convection dominated flow

Here, $\mathcal{E}$ can be any size, and Pe $\sim O(\epsilon^{-3})$ or larger. As in the surfactant case, the problem is now convection-dominated, and we have diffusive boundary layers at the two free boundaries. The outer convection-dominated problem reads

$$s_t + us_x + vs_y = 0, \tag{4.147}$$

while in the boundary layer, after scaling by $\sqrt{P^*}y = H \pm h/2 + \eta$, we find that

$$s_t + us_x - u(H_x \pm \frac{1}{2}h_x)s_\eta + vs_\eta = s_{\eta\eta}. \tag{4.148}$$

The boundary condition at the free surfaces is

$$s_\eta \pm \sqrt{P^*}\mathcal{E}s(1-s) = 0. \tag{4.149}$$

The solution procedure depends on the size of $\sqrt{P^*}\mathcal{E}$. If this is much bigger than one, then we apply $s = 0$ (by the same argument as in §4.6.2.4). If $\sqrt{P^*}\mathcal{E} \sim O(1)$ then we must use the full boundary condition and if $\sqrt{P^*}\mathcal{E} << 1$, we use $s_\eta = 0$. All cases require the use of initial and end-conditions.

4.6.3.4 Evaporation

Here, $\mathcal{E} \sim O(\epsilon^{-1})$, $U << U_e, U_q$, the volatile component is well-mixed, but the boundary conditions force the leading-order concentration to be zero, *i.e.*, the evaporation takes place fast enough for there to be no volatile component remaining on this timescale (given by L/U). If we wish to follow the evolution of this leading order concentration

on its journey to zero, we must look at an evaporation timescale given by $\epsilon L/U$. Setting $t' = t/\epsilon$, conservation of mass reads

$$h_{t'} + 2Es = 0, \tag{4.150}$$

where the volatile concentration is given by

$$hs_{t'} + 2Es(1-s) = 0. \tag{4.151}$$

We may solve these equations, assuming that $s = s_I < 1$ and $h = 1$ at $t = 0$ to yield

$$h = \frac{1-s_I}{1-s}, \tag{4.152}$$

where s satisfies

$$\frac{s(1-s_I)e^{\frac{1}{1-s}}}{s_I(1-s)} = e^{\frac{1-2Et'}{1-s_I}}. \tag{4.153}$$

Hence,

$$s \to 0 \qquad h \to 1 - s_I \qquad \text{as} \qquad t' \to \infty. \tag{4.154}$$

4.6.4 Summary

We have derived the leading-order equations governing the evolution of the concentration of a volatile component, in a variety of parameter regimes. In Figure 4.6, we show how each of the models fits into $\mathcal{E}$, U parameter space, and in Figure 4.7 we present a table of the models. We note that we have found that it is not possible to balance diffusion and evaporation without convection when the volatile is well-mixed, on the timescale L/U. Once U has been determined, Pe and E can be calculated, and the appropriate model may be "lifted" from the catalogue. As in the surfactant case, (i) if $\epsilon^2\text{Pe} << 1$, the volatile is well-mixed, (ii) if $\epsilon^2\text{Pe} \sim 1$, the volatile concentration varies across the film and (iii) if $\epsilon^2\text{Pe} >> 1$, we have a boundary layer structure at the free surfaces.

4.7 Mathematical Structure of a typical coupled problem

We illustrate the procedure for determining the type of system that we are working with by considering the case of a film containing a well-mixed surfactant, in the parameter regime $\text{Ma} \sim O(1)$, $\text{Ca} \sim O(\epsilon^2)$, $S \sim O(\epsilon^{-1})$, and $\text{Pe} \sim O(1)$ (see §4.3.1.1 and §4.5.1.1). We set $\Gamma = bC$ for convenience, and $S^* = 2b/S\epsilon$, $T = 4b\text{MaCa}/\epsilon^2$. The system reads

$$h_t + (uh)_x = 0, \tag{4.155}$$

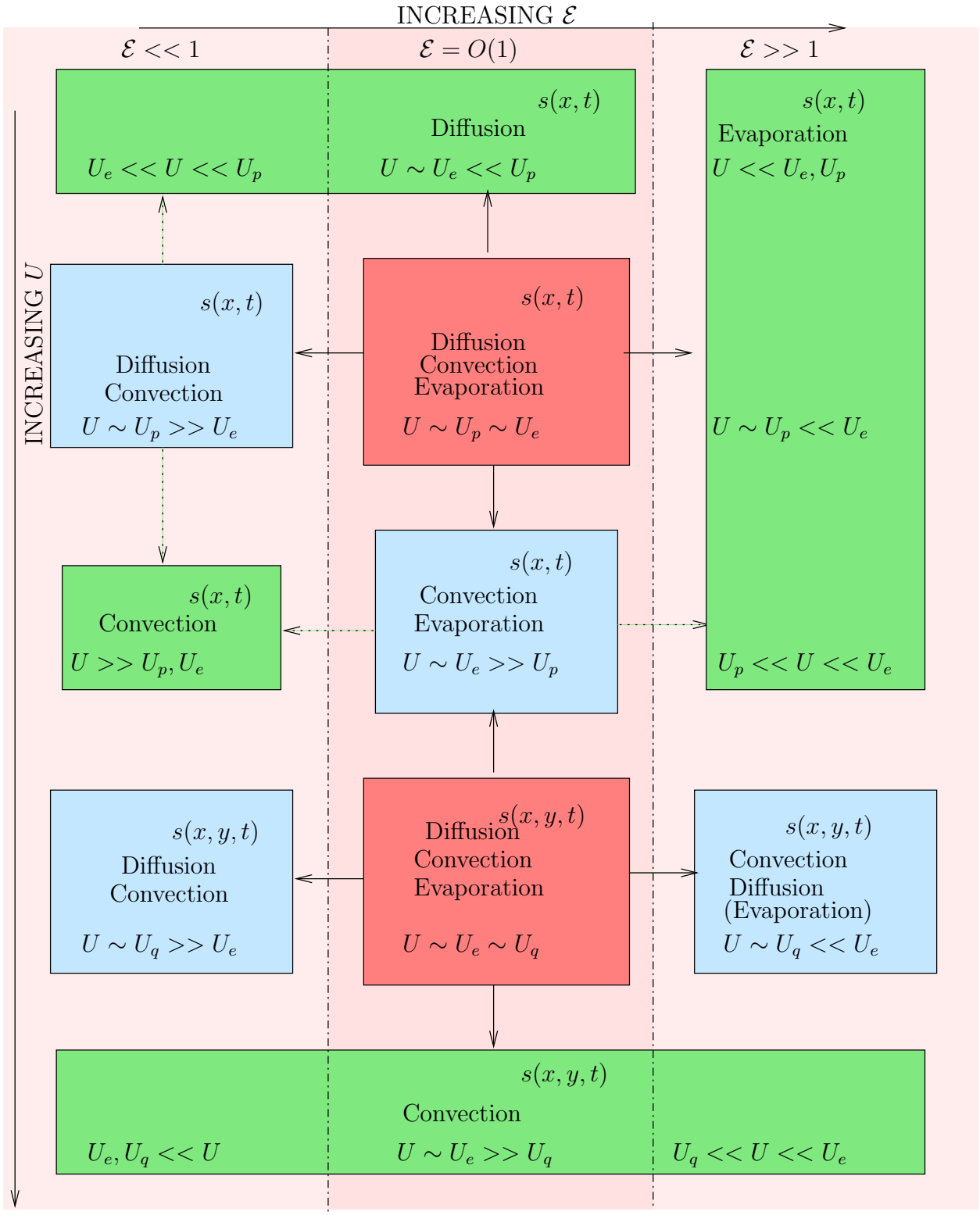

Figure 4.6: Schematic showing where the models lie in U, $\mathcal{E}$ space. The red blocks show the distinguished limits, the blue blocks show the intermediate regimes in which two mechanisms balance, and the green blocks show the regimes in which one force dominates.

	$\mathrm{Pe} \sim O(\epsilon)$	$\mathrm{Pe} \sim O(1)$	$\mathrm{Pe} \sim O(\epsilon^{-1})$	$\mathrm{Pe} \sim O(\epsilon^{-2})$	$\mathrm{Pe} \sim O(\epsilon^{-3})$
$E \sim O(1)$	Evaporation $s = 0$ (Shorter timescale for s evolution)	Evaporation $s = 0$ (Shorter timescale for s evolution)	Evaporation $s = 0$ (Shorter timescale for s evolution)	Convection and Diffusion $P^* (s_t + u s_x + v s_y) = s_{yy}$ $s = 0$	Boundary layer problem
$E \sim O(\epsilon)$	Diffusion $(h s_x)_x = 0$	Convection, Diffusion and Evaporation $(h s_x)_x - \mathrm{Pe}(s_t + (us)_x) - 2\mathrm{Pe}\mathcal{E} s(1-s) = 0$	Convection and Evaporation $h(s_t + u s_x) + 2\mathcal{E} s(1-s) = 0$	Convection, Diffusion and Evaporation $P^* (s_t + u s_x + v s_y) = s_{yy}$ $s_y \pm P^* \mathcal{E} s(1-s) = 0$	Boundary layer problem
$E \sim O(\epsilon^2)$	Diffusion $(h s_x)_x = 0$	Convection and Diffusion $(h s_x)_x - \mathrm{Pe} h(s_t + u s_x) = 0$	Convection $s_t + u s_x = 0$	Convection and Diffusion $P^* (s_t + u s_x + v s_y) = s_{yy}$ $s_y = 0$	Boundary layer problem

Figure 4.7: Table showing regimes.

$$hh_{xxx} = TC_x, \tag{4.156}$$

$$(hC_x)_x - \mathrm{Pe}h\,(C_t + uC_x) - S^*\,(C_t + (uC)_x) = 0, \tag{4.157}$$

which, after setting $g = h_x$, $d = C_x$, integrating (4.156) and writing as a matrix system reads

$$A\mathbf{U}_t + B\mathbf{U}_x = \mathbf{C}, \tag{4.158}$$

where $\mathbf{U} = (h, u, g, C, d)$,

$$A = \begin{pmatrix} 1 & 0 & 0 & 0 & 0 \\ 0 & 0 & 0 & 0 & 0 \\ 0 & 0 & 0 & 0 & 0 \\ 0 & 0 & 0 & 0 & 0 \\ 0 & 0 & 0 & -(\mathrm{Pe}h + S^*) & 0 \end{pmatrix} \qquad B = \begin{pmatrix} u & h & 0 & 0 & 0 \\ 0 & 0 & h & 0 & 0 \\ 1 & 0 & 0 & 0 & 0 \\ 0 & 0 & 0 & 1 & 0 \\ 0 & -S^*C & 0 & -(\mathrm{Pe}hu + S^*) & h \end{pmatrix}, \tag{4.159}$$

and $\mathbf{C}$ is the vector containing all of the non-derivative terms in the system. We consider $\det(\dot{x}A - \dot{t}B) = 0$, where $\dot{}$ denotes differentiation along a characteristic, and we find that

$$-h^3\dot{t}^5 = 0, \tag{4.160}$$

and so conclude that the system has one repeated root ($\dot{t} = 0$) and is therefore parabolic. In fact, all the models that include the surfactant concentration turn out to be parabolic. The parabolic system given above needs initial conditions for C and h, three end-conditions for h, two end-conditions for C and an end-condition for u in order to close the model. In §5.2, we discuss appropriate choices for these conditions in a foam lamella containing a well-mixed surfactant.

The only hyperbolic system is the Trouton model described in §4.3.3.2.

4.8 Conclusion

In this chapter we have presented models for the evolution of thin films between two free surfaces acting under the influence of a number of forces. We may summarise these by writing down equations which contain all the terms: we must then decide on the parameter sizes and hence which terms to keep at leading order. These equations read

$$h_t + (\bar{u}h)_x + \frac{E}{\epsilon}(e_+ + e_-) = 0, \tag{4.161}$$

$$(4h\bar{u}_x)_x + \frac{\epsilon}{2\mathrm{Ca}}hh_{xxx} + \frac{\mathrm{Ma}}{\epsilon}(\sigma^+ + \sigma^-)_x + \mathrm{St}h + \frac{3A^*}{\epsilon^3}\frac{h_x}{h^3} = 0, \tag{4.162}$$

where

$$u = \bar{u} + \frac{\epsilon^3}{4\mathrm{Ca}} h_{xxx} \left(-y^2 + 2Hy - H^2 + \frac{1}{12} h^2 \right) + \frac{\epsilon \mathrm{Ma}}{2} (\sigma^+ - \sigma^-)_x y, \tag{4.163}$$

$$H_{xx} = -\frac{\Delta P \mathrm{Ca}}{2\epsilon}, \tag{4.164}$$

$$P = \frac{P_+ + P_-}{2} - 2u_x - \frac{\epsilon}{2\mathrm{Ca}} h_{xx} - \frac{A^*}{\epsilon^3 h^3}. \tag{4.165}$$

We note that there is no asymptotic limit in which all the terms in (4.161)–(4.165) balance. The shear is generated due to a coupling with:

1. the concentration of surfactant, which satisfies

   - either

     $$\epsilon^2 \mathrm{Pe}(C_t + uC_x + vC_y) = \epsilon^2 C_{xx} + C_{yy}, \tag{4.166}$$

     with, on $y = H \pm h/2$,

     $$\mp S \left(C_y + \epsilon^2 \left(H_x \pm \frac{h_x}{2} \right) C_x \right) = \Gamma_t + (u_s \Gamma)_x, \tag{4.167}$$

   - or

     $$(hC_x)_x - \mathrm{Pe}h \left(C_t + \bar{u} C_x \right) - \frac{2}{\epsilon S} \left(\Gamma_t + (u_s \Gamma)_x \right) = 0, \tag{4.168}$$

   where both models must use, on $y = H \pm h/2$,

   $$\frac{\sigma^* - \gamma}{RT\Gamma_\infty} - \frac{\Delta\gamma}{RT\Gamma_\infty} \sigma^\pm = -\ln\left(1 - \frac{\Gamma}{\Gamma_\infty}\right), \tag{4.169}$$

   $$\Gamma^\pm = \frac{\frac{\Gamma_\infty \lambda}{\Gamma^*} C}{1 + \lambda C}; \tag{4.170}$$

2. the concentration of volatile liquid component, which satisfies

   - either

     $$\epsilon^2 \mathrm{Pe}(s_t + us_x + vs_y) = \epsilon^2 s_{xx} + s_{yy}, \tag{4.171}$$

     with, on $y = H \pm h/2$,

     $$-s_y + \epsilon^2 \frac{h_x s_x}{2} = \epsilon \mathrm{Pe} E e (1 - s) \sqrt{1 + \frac{\epsilon^2 h_x^2}{4}}, \tag{4.172}$$

   - or

     $$(hs_x)_x - \mathrm{Pe}h \left(s_t + \bar{u} s_x \right) - 2 \frac{\mathrm{Pe}E}{\epsilon} e(1 - s) = 0, \tag{4.173}$$

where both models must use, on $y = H \pm h/2$,

$$\sigma_x = -\alpha s_x, \tag{4.174}$$

$$e = s. \tag{4.175}$$

We note that

- The velocity across the film is uniform except when the capillary number is $O(\epsilon^3)$ or when the Marangoni number is $O(\epsilon^{-1})$.
- The centreline is straight unless there is a pressure drop across the film.
- Applying a no-slip boundary condition may only be justified by considering the surfactant problem, and requires that the concentration of surfactant is high, and that it is relatively insoluble.
- The surfactant or volatile component problem can be considerably simplified in parameter regimes where they are well-mixed.
- The possible velocity scales which come from balancing forces are U_m, U_c, U_l, U_p, U_q and either U_s or U_e. The appropriate velocity scale depends on the situation being modelled.
- The coupled system of equations for the longitudinal velocity, thickness of film and concentration of Marangoni-inducing component form a parabolic system of equations.

In the next chapter, we use various forms of these models to describe flow from a lamella into a Plateau border in a foam.

Chapter 5

Foam films

5.1 Introduction

As discussed in Chapter 1, the liquid within a foam is contained within three characteristic structures: lamellae, Plateau borders and nodes. In this chapter, we focus on the flow of liquid from a lamella into a Plateau border. An understanding of this process is fundamental to the understanding of foam collapse, since rupture of lamellae is responsible for bubble coalescence and thus foam deterioration.

Systematic work on lamella drainage has been undertaken by several previous authors. We briefly describe some of the relevant work below.

1. Schwartz and Princen [69] decomposed the liquid into four regions: a Plateau border, a transition region, a laid-down film and a black film; see Figure 5.1. They considered a Plateau border moving away from a lamella at speed $U(t)$ where the liquid interfaces are loaded with surfactant everywhere except the Plateau border. They used this assumption to justify the use of a no-slip boundary condition. They derived a lubrication-style equation for the evolution of the transition region thickness which they solved using matching conditions with both the Plateau border and the laid-down film.

2. Barigou and Davidson [5] also decomposed the liquid into four regions: a border region, two transition regions (one with fully rigid surfaces and one with partially mobile interfaces), and a lamella, see Figure 5.2. They assumed that the Plateau border is immobile and the lamella is free (the converse of the Schwartz and Princen conjecture). They derived a lubrication-style equation for the velocity in region II_1, and they performed a shear balance in region II_2 which they relate to the gradient of surface tension. They discussed the possibility of a sharp border contraction, that is a dimpling effect at the Plateau border end of the lamella, and they concluded that

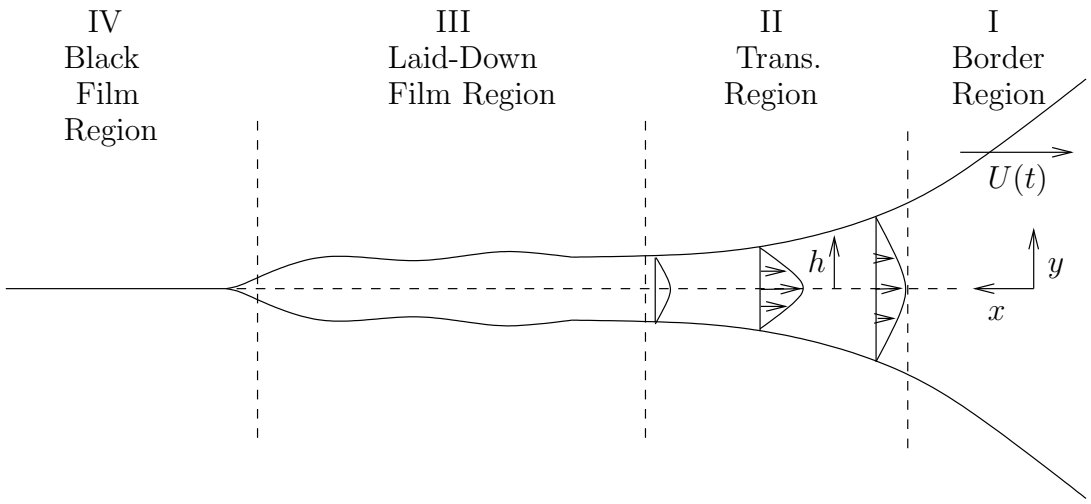

Figure 5.1: Schwartz and Princen's liquid regime.

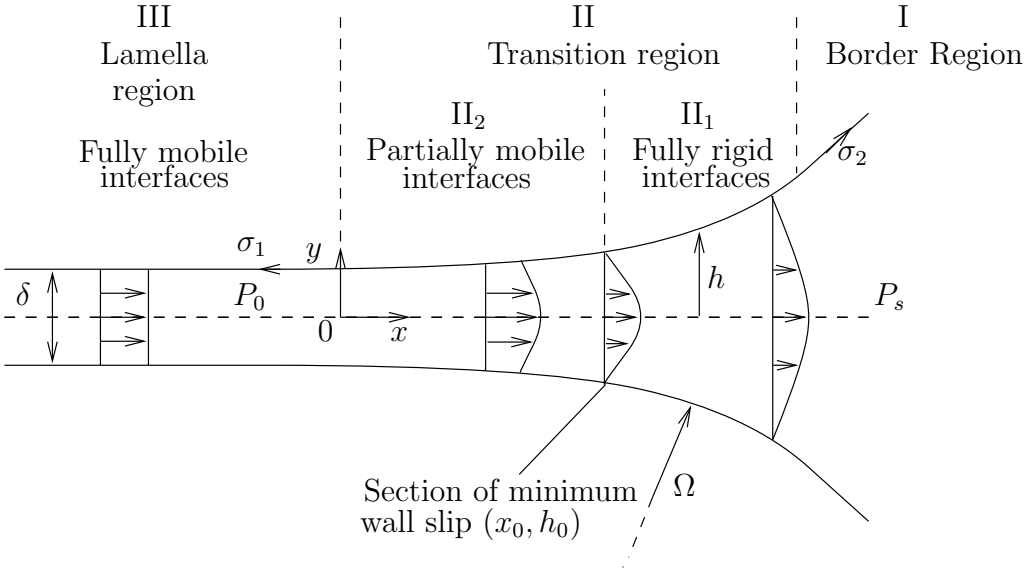

Figure 5.2: Barigou and Davidson's liquid regime.

the pressure distribution in such a configuration is 'physically impossible'. They estimated film thinning by an approximation to the conservation-of-mass equation, and then compared this with experimental evidence.

3. Braun, Snow and Pernisz [13] modelled a vertical film draining under capillary, gravitational and viscous forces. They assumed that the surfactant loads the surface everywhere, and therefore employed the no-slip condition throughout their regions. They matched a time-dependent film onto the static meniscus. Their numerical solutions exhibit dimples close to the meniscus.

A less systematic approach was adopted by Hirasaki, Singh and Miller [71], who assumed

that the flow obeys the radially-symmetric form of the lubrication equation everywhere (but without assuming $u = 0$ on the boundary) and formulated the surfactant problem using convection and diffusion of the bulk surfactant and convection, diffusion and replenishment of surface surfactant. They incorporated surface tension gradients by utilising surface elasticity and surface viscosity, and proposed a *global* force balance to determine the velocity scaling and govern the rate of thinning. The cases of both insoluble and soluble surfactant were considered, and a 'mobility factor' was introduced which allowed calculation of the film drainage time.

As mentioned in Chapter 2 as a motivation for considering the overflowing cylinder, experimental work on *in situ* foam lamellae remains sparse due to the experimental difficulties concerned with probing a foam. However, some work has been carried out on single foam films. Joye, Miller and Hirasaki [43] presented interference patterns from a single film containing surfactant above the critical micelle concentration. They used this evidence to support the claim that foam films thin with a dimple close to the Plateau border (in opposition to Barigou and Davidson [5]). They formulated a model (utilising no-slip everywhere) for the drainage of a foam film draining with constant flux and their numerical solutions develop dimples close to the Plateau border.

Our approach to the problem of lamella drainage is also to decompose the liquid domain into separate regions, and then to match together the solutions in each region. We use the thin film models generated in Chapter 4 to describe the flow of liquid with or without the presence of a surfactant or volatile component. Our work differs from that described above because we do not, *a priori*, assume anything about the surfactant loading at the surface. Indeed, determining the surfactant distribution forms an integral part of our solution procedure.

5.1.1 Relevant parameter sizes

The physical parameters describing the liquid, surfactant or volatile component, and the shape of the bubbles, vary considerably between different foams. Even for chemically identical systems, bubble size can be varied by changing the way that the foam is formed. We list typical parameter sizes for aqueous surfactant solutions in Table 5.1 and for volatile systems in Table 5.2.

μ	$\sim$	10^{-3} Kg m^{-1} s^{-1}	ρ	$\sim$	10^{3} Kg m^{-3}
σ^*	$\sim$	7×10^{-2} N m^{-1}	γ	$\sim$	$2 - 5 \times 10^{-2}$ N m^{-1}
$\Delta\gamma$	$\sim$	$10^{-3} - 10^{-2}$ N m^{-1}	R	$\sim$	8.3 J mol^{-1} K^{-1}
T	$\sim$	298 K	Γ_∞	$\sim$	$1 - 6 \times 10^{-6}$ mol m^{-2}
D	$\sim$	$10^{-10} - 10^{-8}$ m ^{2} s^{-1}	k_2	$\sim$	$0.1 - 0.5$ mol m^{-3}

Table 5.1: Estimated parameter values for aqueous systems containing surfactants.

μ	$\sim$	1×10^{-4} Kg m^{-1} s^{-1}	ρ	$\sim$	7×10^{2} m^{-3}
σ^*	$\sim$	1×10^{-2} N m^{-1}	E_0	$\sim$	$10^{-5} - 10^{-4}$ m s^{-1}
D	$\sim$	5×10^{-9} m^2 s^{-1}			

Table 5.2: Estimated parameter values for volatile systems.

5.1.2 Plan

We start by recapping the case of a pure viscous lamella previously studied by Howell [38]. The solution procedure is to decompose the liquid domain into (i) a viscous lamella, (ii) a capillary-static Plateau border, and (iii) a transition region between the two in which viscous and capillary forces balance. The result is a prediction of the drainage rate of liquid from the lamella into a Plateau border. Thus if, as explained in Chapter 1, we assume that the lamella ruptures at a critical thickness h^{crit}, we obtain a corresponding lamella lifetime.

It transpires that for a typical aqueous system this lifetime is extremely short: around 10^{-3} seconds. In practice, it is a common experience that foam can last much longer than this when some stabilising mechanism is present. Therefore we extend the simple viscous model of Howell to include Marangoni effects due to a surfactant or to a volatile component. This introduces extra parameters into the model and there are a number of asymptotic limits that we can consider. We focus on several such limits which are of interest. We consider a fast diffusing surfactant, for which diffusion, convection and surface convection are all important, a surfactant such as CTAB, for which surface and bulk convection dominate, and an insoluble surfactant, where the motion is governed by surface convection and surface diffusion. We also discuss a lamella stabilised by a volatile component and "a lamella stabilised by a constant surface viscosity".

5.2 Evolution of a thin aqueous film in the absence of surfactant

5.2.1 Introduction and modelling ideas

We first consider the case where there is no surfactant present in the system, and show that such a film has a very short lifetime. Howell [38] has considered the analagous problem of drainage of a bubble near the surface of a viscous liquid, and we follow his methodology in our work here. We restrict ourselves to a two-dimensional geometry and show the liquid domain in Figure 5.3. Our modelling assumption is that the velocity of

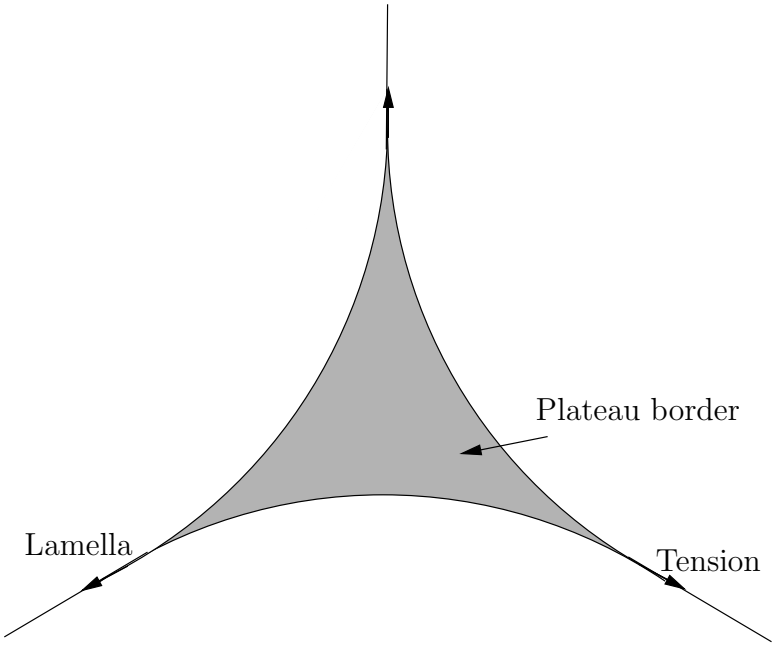

Figure 5.3: The 'outer' picture.

the liquid in the Plateau border is small enough that we may treat the Plateau border as capillary-static (we will check that this assumption is valid *a posteriori* in §5.2.3). Thus its free surfaces have constant mean curvature which, in our two dimensional geometry, implies that they must be circular arcs of constant radius a. These meet tangentially at three points, the points where the lamellae meet the Plateau border. For bubbles of a given size, the radius a is determined by the liquid fraction in the foam (see Chapter 6).

We now look more closely at the lamella, as shown in Figure 5.4. In the lamella, the free surfaces are almost flat and here we suppose that capillary forces are small (we shall, again, check this assumption *a posteriori* in §5.2.3). We therefore have a viscosity-dominated lamella. However, near to the Plateau border, the assumption that capillary

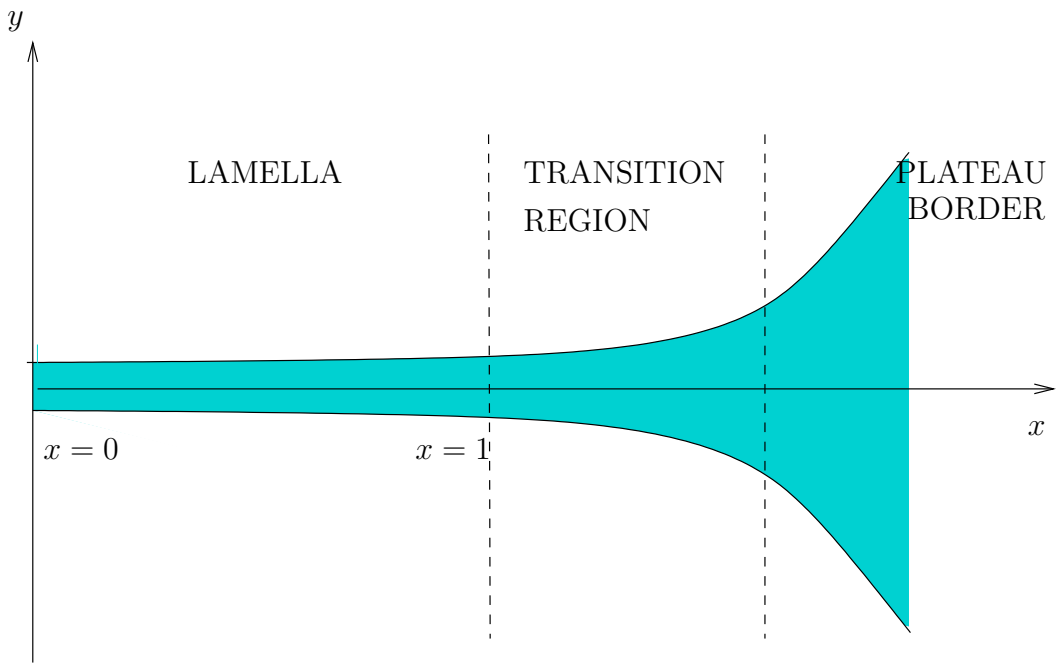

Figure 5.4: The 'inner' picture.

forces are negligible must break down, because here curvature of the film has to increase from practically zero to an $O(1/a)$ amount to match into the Plateau border. In this 'transition region', capillary and viscous forces are both important. We use this balance between viscosity and capillarity in the transition region to decide on the correct velocity scaling.

5.2.2 Model for a film acting under viscosity and capillarity

Recall that the model for a liquid acting under capillary and viscous forces reads (see §4.3.2.2)

$$h_t + (\bar{u}h)_x = 0, \tag{5.1}$$

$$(4h\bar{u}_x)_x + \frac{\epsilon}{2\mathrm{Ca}} h h_{xxx} = 0, \tag{5.2}$$

where the pressure is given by

$$p = -2\bar{u}_x - \frac{\epsilon}{2\mathrm{Ca}} h_{xx}. \tag{5.3}$$

We must now determine the appropriate lengthscale for the transition region and the velocity scaling for the problem, so that we can estimate the size of each of the terms in (5.1) and (5.2) and hence read off the models that hold in each region.

5.2.3 Lengthscale of the transition region and velocity scalings

We find the lengthscale of the transition region from the fact that we must be able to match this region with both the lamella and the Plateau border. As before, we denote the radius of curvature of the Plateau border by a. So, dimensionally, we must have

$$h_{\xi\xi} \sim 1/a, \tag{5.4}$$

where ξ is the dimensional lengthscale in the transition region. We nondimensionalise the transition region thickness with ϵL (ϵ is the aspect ratio of the lamella and L is the length of the lamella), length with δL, and we find $\epsilon h'_{\xi'\xi'}/(\delta^2 L) \sim 1/a$. We therefore take our transition region lengthscale to be

$$\delta L = \sqrt{\epsilon a L}. \tag{5.5}$$

For example, for typical bubbles with the following characteristic dimensions

$$\epsilon \sim 10^{-3}, \qquad L \sim 10^{-3} \text{ m}, \qquad a \sim 4 \times 10^{-4} \text{ m}, \tag{5.6}$$

we find $\delta \sim 0.02$. The aspect ratio of the transition region $\epsilon' = \epsilon/\delta \sim 0.05$ and so our thin film models will hold here too.

We have yet to decide on the velocity scaling, U, for this problem. Our transition region is defined by the fact that viscous and capillary effects balance there, and so this determines our velocity scaling (found by setting $\epsilon'/\text{Ca} = 1$)

$$U = \frac{\gamma}{\mu}\sqrt{\frac{\epsilon L}{a}}. \tag{5.7}$$

For water, $\mu = 1 \times 10^{-3}$ Kg m^{-1} s^{-1} and $\gamma = 7 \times 10^{-2}$ N m^{-1}. We therefore have $U \sim 3.5$ m s^{-1}. So we have the inequalities

$$\epsilon << \epsilon' = \text{Ca} << 1, \tag{5.8}$$

which imply (i) capillarity is negligible in the lamella; (ii) viscous effects are negligible in the Plateau border, and (iii) the two effects balance in the transition region, justifying our initial assumptions.

We read off the model in the lamella from (5.1)-(5.2):

$$h_t + (\bar{u}h)_x = 0, \tag{5.9}$$

$$(4h\bar{u}_x)_x = 0, \tag{5.10}$$

while in the transition region (after performing the scaling $x - 1 = \delta\xi$) we have

$$(\bar{u}h)_\xi = 0, \tag{5.11}$$

$$(4h\bar{u}_\xi)_\xi + \frac{1}{2}hh_{\xi\xi\xi} = 0. \tag{5.12}$$

We note that (5.9)-(5.10) require two boundary conditions on u in order to determine the solution. One condition is the obvious symmetry condition that the velocity must be zero at $x = 0$: the second condition must come from matching with the transition region. Thus our solution procedure in this case is to consider the transition region first, so as to find the rate at which liquid leaves the lamella. We shall then return to solve the lamella problem.

5.2.4 Transition region

We must couple equations (5.11) and (5.12) with boundary conditions at both the lamella and the Plateau border ends of the region. We set constant velocity and thickness at the lamella end and match curvature at the Plateau border end:

$$\bar{u} \to \frac{Q}{h_0}, h \to h_0 \qquad \text{as} \qquad \xi \to -\infty \tag{5.13}$$

$$h_{\xi\xi} \to 1 \qquad \text{as} \qquad \xi \to \infty, \tag{5.14}$$

where Q is the flux from the lamella into the Plateau border, which is to be found. Equation (5.11) implies that the flux is uniform through the transition region

$$\bar{u}h = Q. \tag{5.15}$$

Then (5.12) becomes an ordinary differential equation for h, with Q as a parameter. Crucially, the boundary conditions (5.13) and (5.14) overdetermine the problem; integration of this ordinary differential equation gives rise to a relationship between Q and h_0:

$$Q(h_0) = \frac{3\sqrt{2}h_0^{\frac{3}{2}}}{16}. \tag{5.16}$$

We note that, as the film thins, the flux decreases.

With Q given by (5.16) the transition region model becomes

$$\hat{h}\hat{h}_{\hat{\xi}} = \sqrt{2}\left(\hat{h}^{\frac{3}{2}} - 1\right), \tag{5.17}$$

where $\hat{h} = h/h_0$ and $\hat{\xi} = \xi/h_0^{\frac{1}{2}}$. The solution to (5.17) is

$$2\sqrt{\hat{h}} - \frac{2}{\sqrt{3}}\arctan\left[\frac{1+2\sqrt{\hat{h}}}{\sqrt{3}}\right] + \frac{1}{3}\log\left[\frac{1-2\sqrt{\hat{h}}+\hat{h}}{1+\sqrt{\hat{h}}+\hat{h}}\right] = \sqrt{2}\hat{\xi}, \tag{5.18}$$

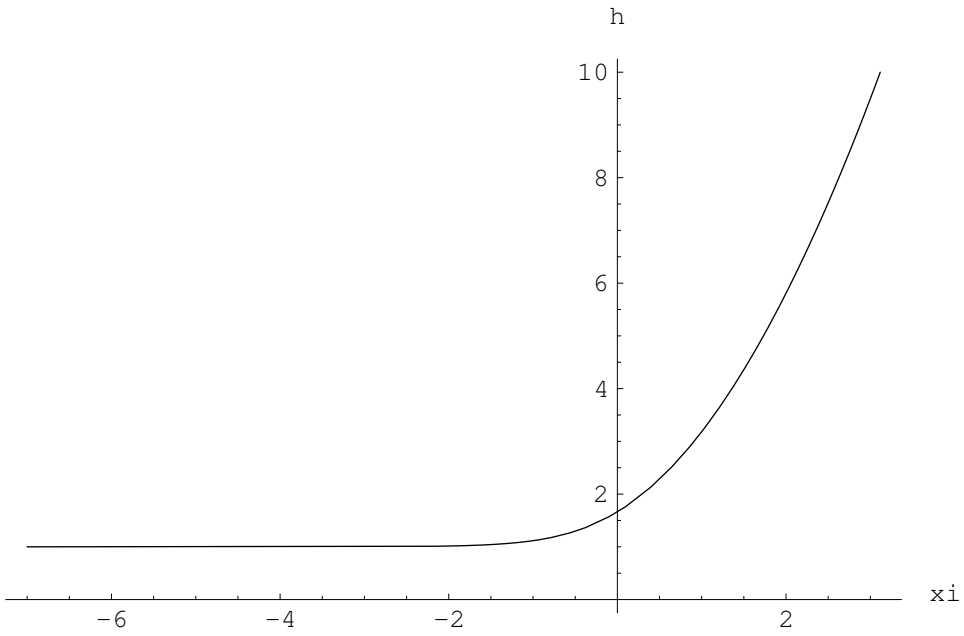

Figure 5.5: Transition region shape.

where the constant of integration (corresponding to translation in ξ) has been set to zero without loss of generality. A plot of the solution is given in Figure 5.5. We note that the profile is monotonic increasing. Finally, we obtain the pressure in the transition region, using the scaled form of (5.3) and the solution in (5.17),

$$p = -\frac{1}{2} + \frac{1}{4\hat{h}^{\frac{3}{2}}} + \frac{1}{4\hat{h}^3}. \tag{5.19}$$

A plot of the pressure distribution is shown in Figure 5.6. The pressure decreases monotonically from zero in the lamella to $-1/2$ in the Plateau border. It is the large negative pressure in the Plateau border (compared with the lamella) which drives the flow and causes the lamella to drain.

5.2.5 Lamella model

We can also solve the lamella model explicitly in this case. In addition to (5.9) and (5.10), we specify boundary conditions describing the symmetry of the system, the flux from the lamella into the Plateau border, and an initial condition to close the model. For simplicity, we set the thickness of the lamella to be initially uniform. We take

$$\bar{u} = 0 \qquad \text{at} \qquad x = 0, \tag{5.20}$$

$$\bar{u} = \frac{Q(h)}{h} = \frac{3\sqrt{2}}{16} h^{\frac{1}{2}} \qquad \text{at} \qquad x = 1, \tag{5.21}$$

$$h = 1 \qquad \text{at} \qquad t = 0. \tag{5.22}$$

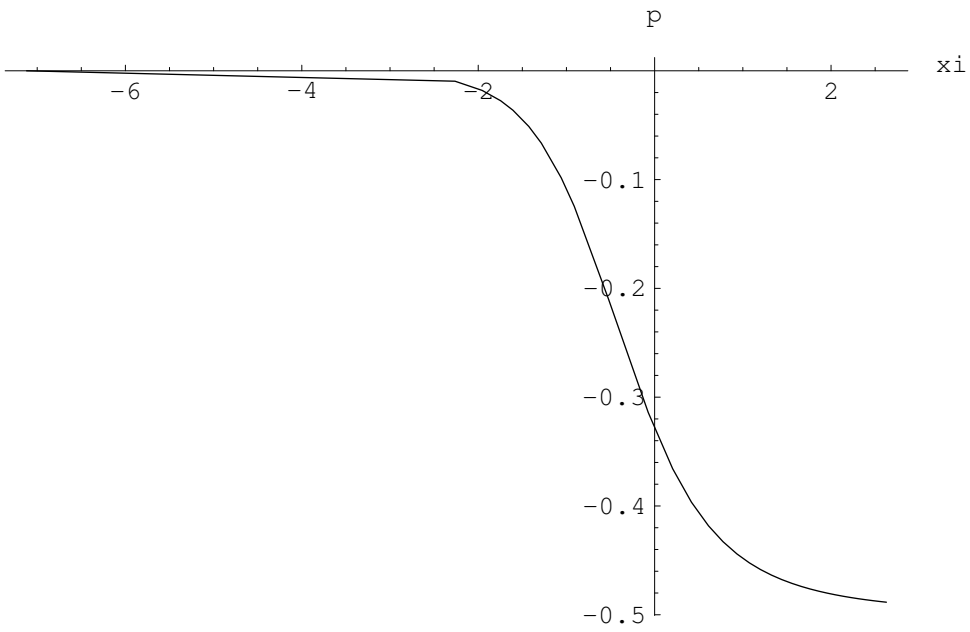

Figure 5.6: Transition region pressure profile.

Under our assumption that the film thickness is spatially uniform initially, we can easily see that it remains so. Then we find that

$$\bar{u} = \frac{3\sqrt{2}}{16} h^{\frac{1}{2}} x, \tag{5.23}$$

and (5.9) provides us with an equation for h

$$h_t + \frac{3\sqrt{2}}{16} h^{\frac{3}{2}} = 0, \tag{5.24}$$

which has the solution

$$h = \left(1 + \frac{3\sqrt{2}}{32} t\right)^{-2}. \tag{5.25}$$

The solution for h given in (5.25) does not tend to zero in finite time. Hence, as noted in Chapter 1, we assume that there is a critical thickness (which is a material property of the film) at which the lamella ruptures. Redimensionalising, we find the lamella lifetime, depending on the critical rupture thickness h_D^{crit},

$$t_D^{\text{crit}} = \frac{32\mu L\sqrt{a}}{3\sqrt{2}\gamma} \left[\left(\frac{1}{h_D^{\text{crit}}}\right)^{\frac{1}{2}} - \left(\frac{1}{h_D^*}\right)^{\frac{1}{2}} \right], \tag{5.26}$$

where the subscript '$_D$' denotes dimensional quantities, and h_D^* is the initial dimensional lamella thickness. If we use suitable values for the parameters, and suppose the film starts with thickness 1μm and ruptures when the thickness reaches 0.1μm, then the time to rupture is $t_D^{\text{crit}} \sim 4 \times 10^{-3}$ s. Clearly, for foam with a lifetime of many seconds or

minutes, the presence of a surfactant or volatile component must alter the dominant balance so as to slow down drainage significantly.

5.2.6 Implications

In this section we have shown how, in a simple case, we can describe the drainage of a lamella into a Plateau border by introducing a transition region between the two in which there are significant curvature changes. In the following sections, we perform a similar decomposition of the liquid domain for cases in which there is surfactant present in the system.

5.3 Evolution of films stabilised by a well-mixed soluble surfactant

We apply an analagous procedure to the case where there is a well-mixed soluble surfactant which is transported by bulk convection, diffusion and surface convection. The general equations for such a system were derived in §4.5.1.1 and to choose the correct leading-order model we must decide on our choice of C^*, Γ^*, and $\Delta\gamma$. To proceed, we make the assumption that the concentration in the Plateau border is constant, C_{Pb} say, on the time-scale of our lamella drainage problem. We justify this assumption in §5.3.2 later. We make the further assumption that C_{Pb} is small and we set $C^* = C_{Pb}$. This simplifies the problem greatly because it allows us to replace the Langmuir isotherm (4.170) with a linear relation, $\Gamma = \eta C$ (where $\eta = \Gamma_\infty/k_2$), known as the Henry isotherm. We recall that we performed a similar linearisation of the Langmuir isotherm in Chapter 3. We are also able to linearise the Frumkin equation (4.169) in this limit too. We choose Γ and $\Delta\gamma$ to remove the constants of proportionality in the Henry isotherm and in the relation between surface tension and the surface concentration, and hence $\Gamma^* = \eta C_{Pb}$ and $\Delta\gamma = RT\eta C_{Pb}$.

We include capillary, Marangoni, viscous, diffusive, convective and replenishing effects in the model. We therefore have (see the summary at the end of Chapter 4)

$$h_t + (\bar{u}h)_x = 0, \tag{5.27}$$

$$(4h\bar{u}_x)_x + \frac{\epsilon}{2\mathrm{Ca}} h h_{xxx} + \frac{2\mathrm{Ma}}{\epsilon}\sigma_x = 0, \tag{5.28}$$

$$(hC_x)_x - \mathrm{Pe}h\left(C_t + \bar{u}C_x\right) - \frac{2}{S\epsilon}\left(\Gamma_t + (u_s\Gamma)_x\right) = 0, \tag{5.29}$$

where

$$u = \bar{u} + \frac{\epsilon^3}{4\mathrm{Ca}} h_{xxx} \left(-y^2 + \frac{1}{12} h^2 \right), \tag{5.30}$$

$$u_s = \bar{u} - \frac{\epsilon^3}{24\mathrm{Ca}} h^2 h_{xxx}, \tag{5.31}$$

$$p = -2\bar{u}_x - \frac{\epsilon}{2\mathrm{Ca}} h_{xx}, \tag{5.32}$$

$$\Gamma = C, \tag{5.33}$$

$$\sigma_x = -\Gamma_x. \tag{5.34}$$

5.3.1 Selection of velocity scale

Again, there are numerous ways that we could select our velocity scale in this case. However, we make the observation that, for velocities of practical interest ($O(10^{-3})$ m s^{-1} say) the reduced capillary number (Ca/ϵ) is small and so viscous forces are negligible everywhere. With small capillary number we have a capillary-static Plateau border, and, since the curvature of the lamella is small, we conclude that the lamella must be dominated by Marangoni forces. Our transition region in this case is therefore where the capillary and Marangoni terms balance. However, we are unable to obtain a velocity scaling from such a balance, since the remaining dimensionless group in (5.28), $T = \mathrm{CaMa}/\epsilon^2 = \Delta\gamma/(\epsilon^2\gamma)$ is independent of the velocity scale chosen.

To ensure a balance in (5.28), we must have a gradient in Γ, which means that we must ensure that there is a nontrivial balance in (5.29). We choose to balance the surface convection and bulk diffusion in the transition region, *i.e.*, we set

$$\frac{S\epsilon}{\delta} = 1, \qquad \text{so} \qquad U = \frac{D}{\eta}\sqrt{\frac{\epsilon L}{a}}. \tag{5.35}$$

If we have chosen the velocity scaling inappropriately, we will find that one of remaining parameters in the system is large and deduce that a different scaling for U is more appropriate (as we find in §5.4 for a lamella stabilised by CTAB). For the moment, we choose to work with an artificial highly diffusive surfactant, with say $D \sim 2 \times 10^{-8}$ m^2 s^{-1}, and $\eta \sim 1 \times 10^{-5}$ m. We estimate $U \sim 1 \times 10^{-4}$ m s^{-1} (we note that this is much smaller than the velocity scaling of the previous section), the reduced Péclet number, $\mathcal{P} = \delta Pe$ is $O(1)$, $\mathrm{Ca} \sim 10^{-6}$, and $\mathcal{T} = T/\delta^2 \sim O(1)$.

Thus the leading-order model that holds in the lamella is

$$h_t + (\bar{u}h)_x = 0, \tag{5.36}$$

$$\sigma_x = 0, \tag{5.37}$$

$$\mathcal{P}hC_t + 2\Gamma_t + \mathcal{P}\bar{u}hC_x + 2(u_s\Gamma)_x = 0, \tag{5.38}$$

$$u = u_s = \bar{u}, \tag{5.39}$$

$$\Gamma = C, \tag{5.40}$$

$$\sigma_x = -\Gamma_x, \tag{5.41}$$

while in the transition region we have

$$(\bar{u}h)_\xi = 0, \tag{5.42}$$

$$hh_{\xi\xi\xi} + \mathcal{T}\sigma_\xi = 0, \tag{5.43}$$

$$(hC_\xi)_\xi - \mathcal{P}h\bar{u}C_\xi - 2\,(u_s\Gamma)_\xi = 0, \tag{5.44}$$

$$u_s = \bar{u} - \tilde{\beta}h^2h_{\xi\xi\xi}, \tag{5.45}$$

$$\Gamma = C, \tag{5.46}$$

$$\sigma_\xi = -\Gamma_\xi, \tag{5.47}$$

where $\mathcal{T} = 4a\Delta\gamma/(\gamma L\epsilon)$ and $\tilde{\beta} = \epsilon'^3/24Ca$. In both the lamella and the transition region, viscous forces are negligible at leading order and the physical structure of the problem is different from the pure liquid film considered in the previous section. Here, the flow is completely governed by what is happening at the free surfaces.

5.3.1.1 Parameter sizes and plan for the rest of this section

We first consider the behaviour of this system of equations by analysing the case where $\mathcal{P}$ and $\mathcal{T}$ are both $O(1)$, but the 'lubrication' parameter $\tilde{\beta} << 1$. We note that these are assumptions that are not, in general, true. If $\mathcal{P} << 1$ we lose the bulk convection term, and if $\mathcal{P} >> 1$ we must choose a different velocity scaling, balancing bulk convection with either diffusion or surface convection. The effect of having a very small or very large $\mathcal{T}$ is that h and C vary over different lengthscales, and we have nested transition regions. However, assuming $\mathcal{P}, \mathcal{T} \sim O(1)$ appears to be the most generic case, where all the terms have the same influence, and so we proceed under this assumption.

Changing $\tilde{\beta}$ has a different effect on the model. With $\tilde{\beta} << 1$, the flow is everywhere extensional, but with $\tilde{\beta} \sim O(1)$, the velocity in the transition region becomes parabolic. Using typical values for the parameters, $\tilde{\beta} \sim 2$ and so, after considering the (simpler) $\tilde{\beta} << 1$ case, we incorporate the effect of $\tilde{\beta} \sim O(1)$ in §5.3.7.

We follow the following plan in the rest of this section. First we consider the Plateau border, and show that our assumptions about the concentration are correct and that its shape is governed by capillary statics. Next, we consider the problem in the lamella, with the aim of relating the concentration in the lamella to its thickness. Following this, we work with the transition region model, using the information already obtained from the lamella and the Plateau border. As in the last section, the aim will be to find the flux of liquid, Q, flowing out from the lamella as a function of lamella thickness h_0. Finally, we return to the lamella problem to find how the thickness varies with time, and, ultimately, the time to rupture. Once this is completed, we consider how the inclusion of a nonzero $\tilde{\beta}$ modifies the problem, and we repeat the transition region analysis to find $Q(h_0)$ and then the time to rupture.

5.3.2 Plateau border

In this subsection we justify our assumption that the surfactant concentration is constant in the Plateau border. To do this, we consider the flux of surfactant leaving the lamella, which is controlled by surface and bulk convection, and reads, in dimensional variables,

$$\text{Flux out} = huC_l\left(1+2\frac{\eta}{h}\right), \tag{5.48}$$

where C_l is the concentration in the lamella. We equate this to the flux into the Plateau border, so

$$\frac{\mathrm{d}C_{Pb}}{\mathrm{d}t} \sim \frac{huC_l}{a^2}\left(1+2\frac{\eta}{h}\right). \tag{5.49}$$

We nondimensionalise in the standard way, to get

$$\frac{\mathrm{d}C_{Pb}}{\mathrm{d}t} \sim \frac{\epsilon L^2}{a^2}QC_l\left(1+\frac{2\eta}{\epsilon Lh}\right). \tag{5.50}$$

Using typical parameter values, we find that $\mathrm{d}C_{Pb}/\mathrm{d}t \sim 10^{-1}QC_l$, and we conclude that, providing $Q \sim O(1)$ or smaller, C_{Pb} is constant on the timescale for lamella drainage. As noted earlier, with the velocity scaling given by (5.35), Ca $\sim O(10^{-6})$ and so our assumption that the Plateau border is dominated by capillary statics is verified, and the Plateau border free surfaces have constant curvature $1/a$.

5.3.3 Lamella model

The lamella model (5.36)-(5.41) may be simplified to read

$$h_t + (uh)_x = 0, \tag{5.51}$$

$$C_x = 0, \tag{5.52}$$

$$(2+\mathcal{P}h)\,C_t + \mathcal{P}uhC_x + 2\,(u_xC) = 0, \tag{5.53}$$

where, since capillary forces are small in this region, $u = \bar{u} = u_s$. We note that (5.52) dictates that $C = C(t)$. So, (5.53) reduces to the following (linear) equation for C,

$$\dot{C} = -\frac{2Cu_x}{2+\mathcal{P}h}. \tag{5.54}$$

We impose the boundary conditions of no flux and symmetry at the lamella's middle, flux conservation with the transition region, and, for simplicity, that the concentration of surfactant and the lamella thickness are both constant initially (the concentration must necessarily be constant at $t = 0$ to satisfy (5.52). If the concentration is not constant, we must consider a problem on a shorter timescale than L/U in which the concentration adjusts), *i.e.*

$$u = 0 \qquad \text{at} \qquad x = 0, \tag{5.55}$$

$$u = \frac{Q}{h} \qquad \text{at} \qquad x = 1, \tag{5.56}$$

$$C = C_I, h = 1 \qquad \text{at} \qquad t = 0. \tag{5.57}$$

As before, Q is the flux of liquid flowing from the lamella into the transition region, and C_I is the initial lamella concentration. The choice of appropriate C_I depends on the "history" of the lamella. Consider the initial formation of the foam as a whole. At the start, the bubbles are almost spherical, with surfactant distributed uniformly. The liquid drains through the foam to form the lamella-Plateau border structure. The concentration of surfactant in the lamella is decreased by the increase in surface area required to generate this evolution of morphology. Therefore, we conjecture that $C_I < 1$ for draining foams (in dimensional terms, this reads $C_I < C_{Pb}$). However, in some laboratory experiments to study single lamellae (see Joye et al. [43]), individual thin films are generated by dipping a ring into surfactant solution. The thin films are automatically forced into the lamella-Plateau border shape although the concentration of surfactant may still be assumed uniform. We therefore allow ourselves to consider $C_I \leq 1$.
We may then solve the system for C to give

$$C = C_I\frac{(2+\mathcal{P})h}{2+\mathcal{P}h}. \tag{5.58}$$

We note that the flux of surfactant from the lamella is given by

$$\text{Flux} = QC\left(\mathcal{P} + \frac{2}{h}\right), \tag{5.59}$$

and so we see that, as the film thins, the transport of surfactant is dominated by surface convection.

As in §5.2, we can also solve for u,

$$u = \frac{Q(h)x}{h}, \tag{5.60}$$

and finally h is given by

$$\int_h^1 \frac{d\mathcal{H}}{Q(\mathcal{H})} = t. \tag{5.61}$$

We return to evaluate this integral once we have determined the flux Q as a function of thickness using the transition region model.

5.3.4 Transition region

We couple (5.42)-(5.47) with boundary conditions that the film thickness, liquid velocity and concentration are constant in the lamella. We read off these values from the lamella model, given the thickness h_0, and they are

$$h \to h_0, \qquad \bar{u} \to \frac{Q}{h_0}, \qquad C \to C_0 = C_I \frac{(2+\mathcal{P})h_0}{2+\mathcal{P}h_0} \qquad \text{as} \qquad \xi \to -\infty. \tag{5.62}$$

We also match curvature of the film and concentration with the Plateau border and we set

$$h_{\xi\xi} \to 1, C \to 1 \qquad \text{as} \qquad \xi \to \infty. \tag{5.63}$$

The corresponding leading-order equations for the liquid velocity, lamella thickness and concentration of surfactant are

$$\bar{u}h = Q, \tag{5.64}$$

$$\mathcal{T}\,(C - C_0) = hh_{\xi\xi} - \frac{h_\xi^2}{2}, \tag{5.65}$$

$$hC_\xi = \mathcal{P}Q\,(C - C_0) + 2Q\left(\frac{C}{h} - \frac{C_0}{h_0}\right), \tag{5.66}$$

We note that the flow in the transition region is quasi-steady. The first of these equations is the integrated conservation of mass equation, the second is the integrated longitudinal force balance, and the third is the integrated surfactant concentration equation. The constants of integration were found by applying the conditions as $\xi \to -\infty$. We note that (5.65) and (5.66) decouple from (5.64): we can solve for C and h and then read off $\bar{u}$ from (5.64).

5.3.4.1 Asymptotic behaviour of solutions at $\pm\infty$

We must check that the boundary conditions that we wish to impose on (5.65)-(5.66) do not over-determine the problem. We first reduce the number of parameters in the problem by setting $\hat{C} = (C - C_0)/C_0$, $\hat{h} = h/h_0$ and $\hat{\xi} = \sqrt{\mathcal{T}C_0/h_0^2}\xi$. The resulting system of equations for $\hat{C}$ and $\hat{h}$ are

$$\hat{C} = \hat{h}\hat{h}_{\hat{\xi}\hat{\xi}} - \frac{\hat{h}_{\hat{\xi}}{}^2}{2}, \tag{5.67}$$

$$\hat{h}\hat{C}_{\hat{\xi}} = \Upsilon Q^* \hat{C} + Q^* \left(\frac{\hat{C+1}}{\hat{h}} - 1 \right), \tag{5.68}$$

where $\Upsilon = \mathcal{P}h_0/2$ and $Q^* = 2Q/(h_0\sqrt{\mathcal{T}C_0})$ and the boundary conditions that we wish to impose now read $\hat{C} \to 0$, $\hat{h} \to 1$ as $\hat{\xi} \to -\infty$, $\hat{h}_{\hat{\xi}\hat{\xi}} \to h_0/(\mathcal{T}C_0)$, $\hat{C} \to (1 - C_0)/C_0$ as $\hat{\xi} \to \infty$. Our plan is to find the behaviour of $\hat{h}$ and $\hat{C}$ as $\hat{\xi} \to \pm\infty$ and then see how many of the number of degrees of freedom the boundary conditions eliminate. We linearise about $\hat{h} \sim a_1\hat{\xi}^2/2$ as $\hat{\xi} \to \infty$ by setting

$$\hat{h} \sim \frac{a_1\hat{\xi}^2}{2} + a_2\hat{\xi} + a_3 + \frac{a_4}{\hat{\xi}} + \frac{a_5}{\hat{\xi}^2} + O\left(\frac{1}{\hat{\xi}^3}\right). \tag{5.69}$$

We note that, in general, we must also look for terms of the form $\hat{\xi}^m e^{-a\hat{\xi}^n}$, but it is easy to show that these terms do not appear. We find the corresponding form for $\hat{C}$ by substituting this into (5.67):

$$\hat{C} \sim a_1a_3 - \frac{a_2^2}{2} + \frac{3a_1a_4}{\hat{\xi}} + \frac{3a_2a_4 + 6a_1a_5}{\hat{\xi}^2} + O\left(\frac{1}{\hat{\xi}^3}\right). \tag{5.70}$$

We are able to find relationships between the coefficients in these expansions using (5.68), and we get the leading order balance

$$-\frac{3}{2}a_1^2a_4 = \Upsilon Q^* \left(a_1a_3 - \frac{a_2^2}{2} \right) - Q^*. \tag{5.71}$$

Imposing the boundary conditions as $\hat{\xi} \to \infty$, we see, trivially, that $a_1 = h_0/(\mathcal{T}C_0)$ and that we must also take $a_1a_3 - a_2^2/2 = (1 - C_0)/C_0$ (from (5.70)). Substituting into (5.71) gives an expression for a_4:

$$a_4 = -\frac{2\mathcal{T}^2C_0^2}{3h_0^2} \left(\Upsilon Q^* \left(\frac{1 - C_0}{C_0} \right) - Q^* \right), \tag{5.72}$$

and we can generate a_5 from (5.68),

$$a_5 = \frac{2\mathcal{T}^3C_0^3}{3h_0^3} \left(\Upsilon Q^* \left(\frac{1 - C_0}{C_0} \right) - Q^* \right) \left(a_2 + \frac{Q^*\Upsilon}{2} \right). \tag{5.73}$$

Since the system exhibits translational invariance, we may set $a_2 = 0$. We can see that once this is done, a_1, $a_3 \ldots$ are all determined uniquely by (5.67) and (5.68) and the boundary conditions. We re-write these expansions in the original variables, and they then read (with error $O(1/\xi^3)$)

$$h \sim \frac{\xi^2}{2} + \left(1 - \frac{C_I(2+\mathcal{P})h_0}{2+\mathcal{P}h_0}\right)\mathcal{T} + 2\left(-\mathcal{P} + C_I(2+\mathcal{P})\right)\frac{Q\mathcal{T}}{3\xi} - \left(-\mathcal{P} + C_I(2+\mathcal{P})\right)\frac{\mathcal{P}\mathcal{T}Q^2}{3\xi^2}, \tag{5.74}$$

$$C \sim 1 + 2\left(-\mathcal{P} + C_I(2+\mathcal{P})\right)\frac{Q}{\xi} - 2\left(-\mathcal{P} + C_I(2+\mathcal{P})\right)\frac{\mathcal{P}Q^2}{\xi^2}. \tag{5.75}$$

We note that, for $C_I = \mathcal{P}/(2+\mathcal{P})$, the coefficients of the small terms in these expansions vanish, and that, for $C_I < \mathcal{P}/(2+\mathcal{P})$, $C \to 1$ from below, while if $C_I > \mathcal{P}/(2+\mathcal{P})$, $C \to 1$ from above.

We conclude that, for a given set of parameters including the unknown h_0 and Q, there is a unique solution (up to translation) leaving $\xi = \infty$.

At the other end of the range, we linearise about $\hat{h} = 1$, setting $\hat{h} \sim 1 + ae^{\lambda\hat{\xi}}$. Substituting this into (5.67) gives

$$\hat{C} \sim a\lambda^2 e^{\lambda\hat{\xi}}, \tag{5.76}$$

and we obtain an equation for λ by substituting into (5.68):

$$\lambda^3 - (\Upsilon + 1)Q^*\lambda^2 + Q^* = 0. \tag{5.77}$$

Setting $\chi = \lambda\sqrt{1+\Upsilon}$, and $q = Q^*(1+\Upsilon)^{\frac{3}{2}}$, the cubic can be simplified to

$$\chi^3 - q\chi^2 + q = 0. \tag{5.78}$$

Now the structure of the solution depends on the sign of Q^*. Motivated by the purely viscous calculation of §5.2, and on physical grounds, we anticipate that Q^* should be positive, *i.e.* the liquid should flow *from* the lamella *into* the Plateau border. Therefore we assume that $q > 0$ and deduce that (5.78) has at least one negative real root, $\chi = -\chi^*(q)$ say, where

$$\chi^* = -\frac{q}{3} + \frac{2^{\frac{1}{3}}q^2}{3f(q)} + \frac{f(q)}{2^{\frac{1}{3}}3}, \tag{5.79}$$

and

$$f(q) = \left(27q - 2q^3 + 3\sqrt{3}q\sqrt{27 - 4q^2}\right)^{\frac{1}{3}}. \tag{5.80}$$

The other two roots are, in terms of χ^*,

$$\chi_\pm = \frac{\chi^*}{2(1-\chi^{*2})}\left(1 \pm \sqrt{4\chi^{*2} - 3}\right), \tag{5.81}$$

which are real if $\chi^* > \sqrt{3}/2$ and form a conjugate pair with positive real part if $\chi^* < \sqrt{3}/2$. The corresponding behaviour for $\hat{h}$ and $\hat{C}$ is monotonic decay in the former case and oscillatory decay in the latter.

The corresponding condition on q for oscillatory behaviour reads

$$q = \frac{2Q}{h_0\sqrt{TC_0}}\left(1 + \frac{\mathcal{P}h_0}{2}\right)^{\frac{3}{2}} < \frac{3\sqrt{3}}{2}. \tag{5.82}$$

and using (5.62), this condition reads

$$\mathcal{B} = \frac{4\sqrt{2}Q\left(1 + \frac{\mathcal{P}h_0}{2}\right)^2}{3\sqrt{3}\sqrt{\mathcal{T}C_I(2+\mathcal{P})}h_0^{\frac{3}{2}}} < 1. \tag{5.83}$$

So, as we approach $-\infty$, we find that we must suppress one growing mode (the one given by $\chi = -\chi^*$), and the other two modes decay either monotonically or in an oscillating fashion, as dictated by (5.83). In either case, for a given set of parameters (including h_0 and Q), there is a one-parameter family of solutions leaving $\hat{\xi} = -\infty$ (as in Tuck and Schwartz [75]) of the form

$$\hat{h} \sim 1 + \alpha\left(e^{\hat{\xi}\chi_-} + e^{\hat{\xi}\chi_+}\right), \tag{5.84}$$

where α is a free parameter and translational invariance has been used to make the coefficients of the two exponentials the same.

We consider two possible numerical procedures for solving the problem. One alternative is to start from $\hat{\xi} = -\infty$ (in practice, some large negative value), in which case we have two shooting parameters, α (*c.f.* (5.84)) and Q to vary, and two conditions $\hat{h}_{\hat{\xi}\hat{\xi}} \to h_0/\mathcal{T}C_0$ and $\hat{C} \to (1 - C_0)/C_0$ to satisfy as $\hat{\xi} \to \infty$. Thus it is at least plausible that the problem is well posed and that Q is uniquely determined. The method that we prefer to employ, however, is to start from $\hat{\xi} = \infty$ (again, really a large positive value), in which case we only have one free parameter Q, which we vary in order to satisfy $\hat{h} \to 1$ as $\hat{\xi} \to -\infty$.

We note that, since Q is not known *a priori*, we are not able, given a set of parameters, to decide whether or not we would expect oscillating solutions before attempting the numerical solution.

5.3.5 Summary

We summarise the results presented above before obtaining numerical solutions of the transition region model.

- There is a relationship between the concentration and thickness in the lamella which reads
$$C_0 = C_I \frac{(2+\mathcal{P})h_0}{2+\mathcal{P}h_0}. \tag{5.85}$$

- The behaviour at the Plateau border end of the transition region depends on the size of
$$\mathcal{K} = \frac{\mathcal{P}}{(2+\mathcal{P})C_I}. \tag{5.86}$$
This condition does not depend on h_0 or Q. If $\mathcal{K} > 1$, then $C \to 1$ from below. If $\mathcal{K} < 1$, we have $C \to 1$ from above, and since the concentration in the lamella is less than that in the Plateau border (except possibly at $t = 0$), we must have $C_\xi = 0$ somewhere, and hence C must be nonmonotonic.

- The behaviour at the lamella end of the transition region is determined by the size of
$$\mathcal{B} = \frac{4\sqrt{2}Q\left(1+\frac{\mathcal{P}h_0}{2}\right)^2}{3\sqrt{3}\sqrt{\mathcal{T}C_I(2+\mathcal{P})}h_0^{\frac{3}{2}}}. \tag{5.87}$$
If $\mathcal{B} < 1$, we expect oscillating solutions as we approach the lamella. If $\mathcal{B} > 1$, we expect monotonic behaviour as we approach the lamella.

- We appear to have a well-posed system which, upon numerical solution, will yield the flux Q for each given value of h_0, $\mathcal{P}$,$\mathcal{T}$ and C_I. Our plan is to solve for $Q(h_0)$ with all the other parameters fixed, and then find the evolution of the lamella using (5.61).

The flow of information is shown in Figure 5.7. The arrows show how the information is transmitted between the regions, and shows that we pass information about the surfactant concentration into the transition region from both the lamella and the Plateau border, and we pass information about the liquid from the Plateau border into the transition region and then into the lamella.

5.3.6 Results and discussion

We solve the transition region system (5.65)-(5.66) to obtain $Q = Q(h_0)$. To demonstrate two classes of solutions to the transition region model, we start by keeping h_0, $\mathcal{P}$ and $\mathcal{T}$ fixed while varying C_I. First, we use $h_0 = 0.8$, $\mathcal{P} = 5$, $\mathcal{T} = 5$, $C_I = 0.5$, and we find that $Q = 0.4292$. We calculate $\mathcal{B} = 1.405 > 1$, and so we expect monotonic behaviour as $\xi \to -\infty$. We also have $\mathcal{K} > 1$, and so expect $C \to 1$ from below as $\xi \to \infty$. The film thickness and surfactant concentrations are shown in Figure 5.8. They exhibit monotonic increase in both h and C, as predicted. We call such solutions 'monotonic'. Secondly, we

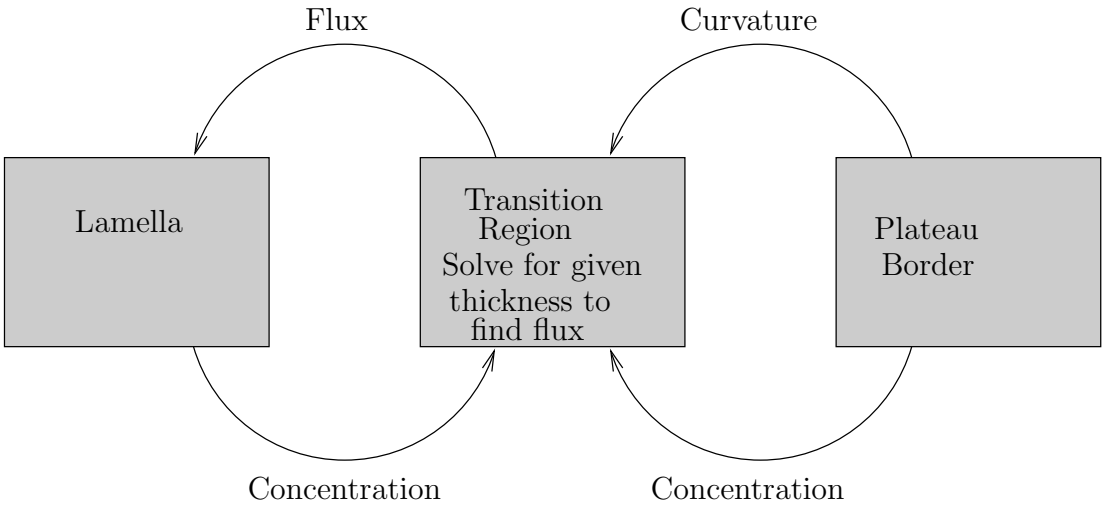

Figure 5.7: Flowchart showing information routes.

set $C_I = 1$, and we find that $Q = 0.0349$. We calculate $\mathcal{B} = 0.0808 < 1$, and so we expect the solution to oscillate as we approach $-\infty$. We also have $\mathcal{K} < 1$ and so we expect $C \to 1$ from above as $\xi \to \infty$. The film thickness and concentration of surfactant in this case are shown in Figure 5.9. Both the film thickness and the surfactant concentration are nonmonotonic, as expected. We call such solutions 'dimpled'.

We show plots of the surface convective flux $2QC/h$, bulk convective flux $\mathcal{P}QC$ and the diffusive flux $-hC_\xi$ when $h_0 = 0.8$, $\mathcal{P} = 5$, $\mathcal{T} = 5$, and $C_I = 0.5$ in Figure 5.10. We see that the diffusive flux is always negative, *i.e.*, diffusion transports surfactant from the Plateau border into the lamella, and that the convective fluxes are both positive, indicating that they transport surfactant from the lamella to the Plateau border. We note that bulk convection appears to be the dominant mechanism.

We repeat this procedure for the same parameters but setting $C_I = 1$, and we show the results in Figure 5.11. Here, bulk convection and surface convection again transport surfactant from the lamella into the Plateau border, but now transport by diffusion is more complicated. We remember that the concentration profile in this parameter regime is nonnomotonic, and that the concentration achieves a maximum within the transition region. We see that diffusion transports surfactant out from this maximum (both towards the Plateau border and further into the transition region).

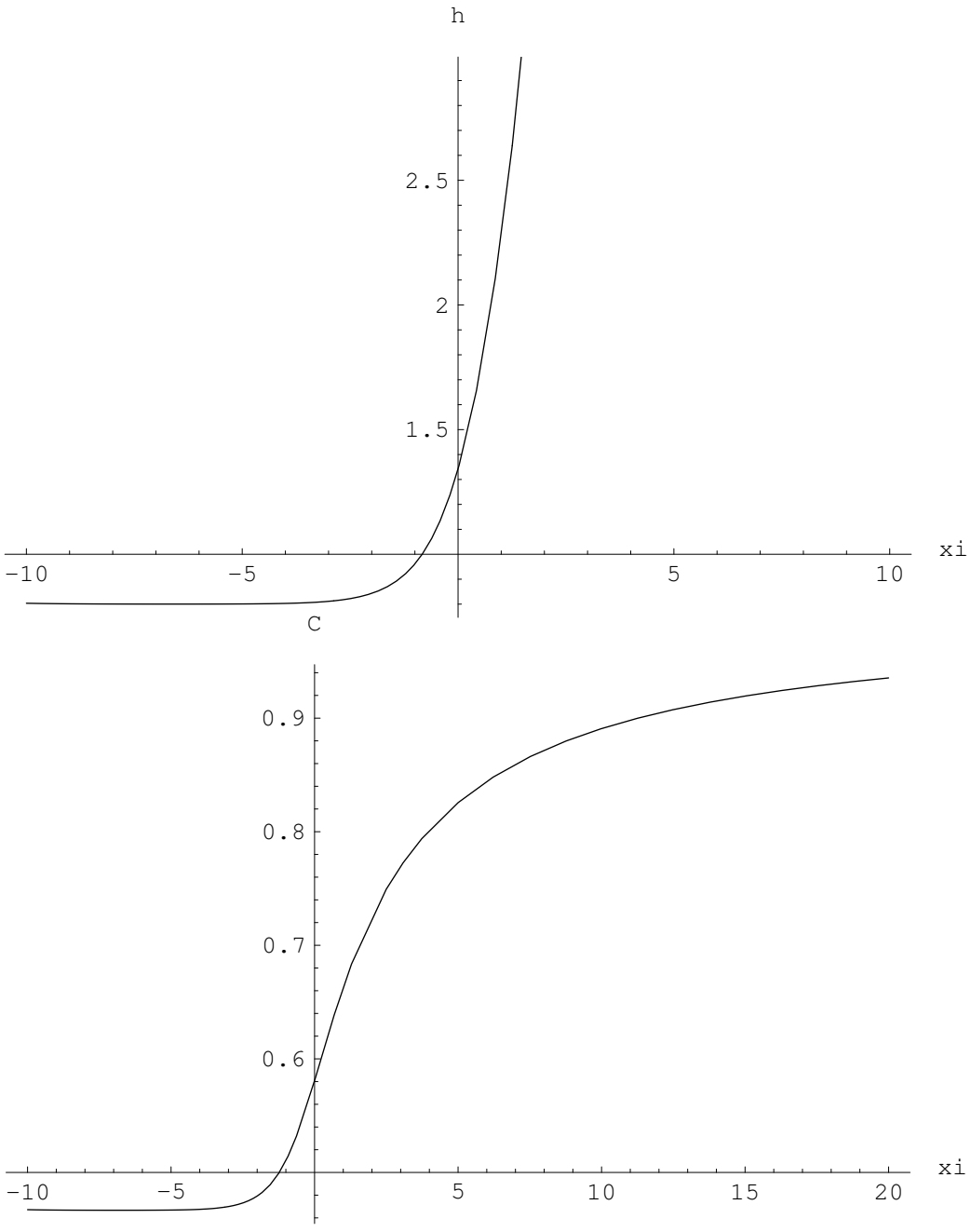

Figure 5.8: Results for thickness and concentration in a monotonic solution.

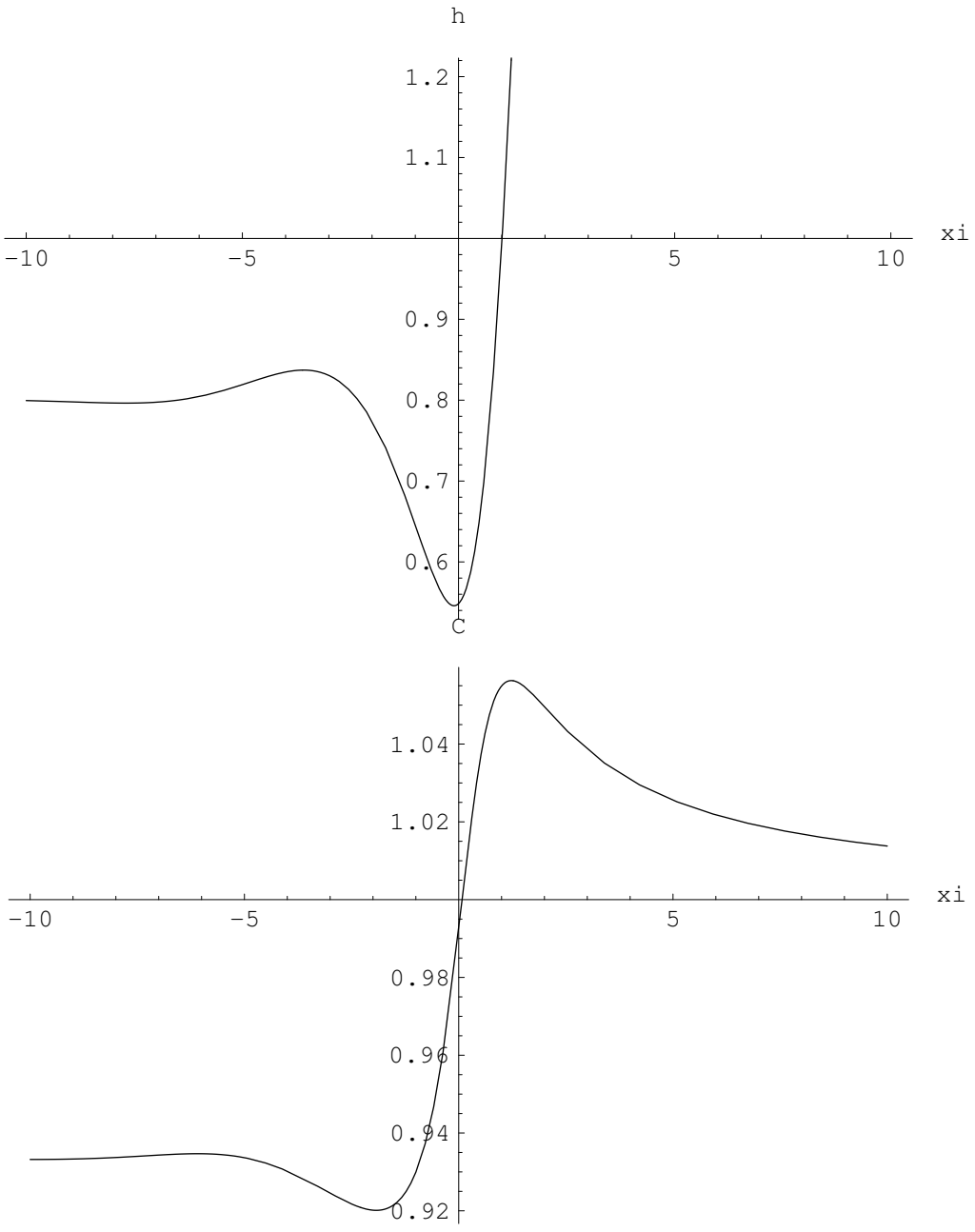

Figure 5.9: Results for thickness and concentration in a dimpled solution.

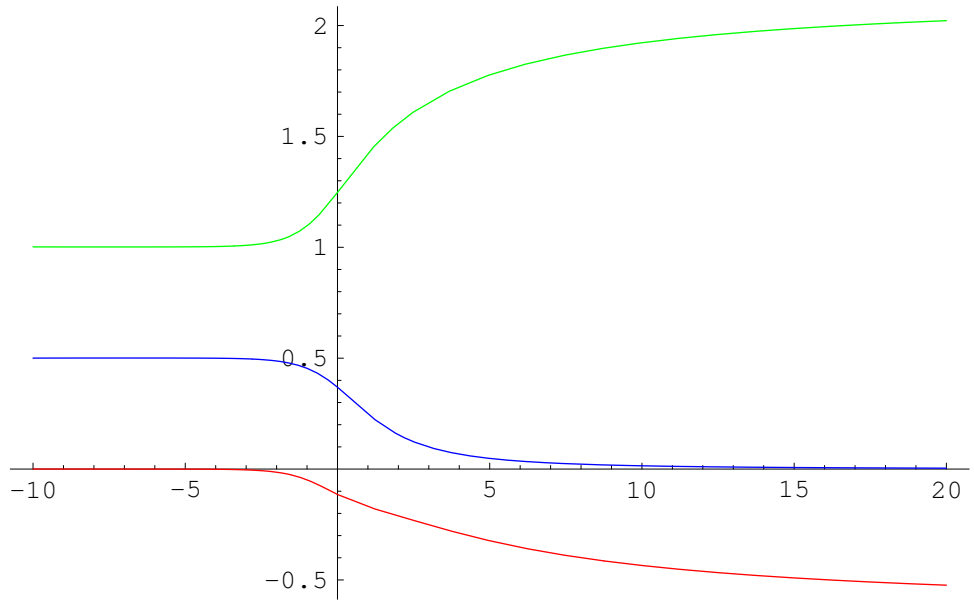

Figure 5.10: Surface convection (blue), bulk convection (green) and bulk diffusion (red) for a monotonic solution.

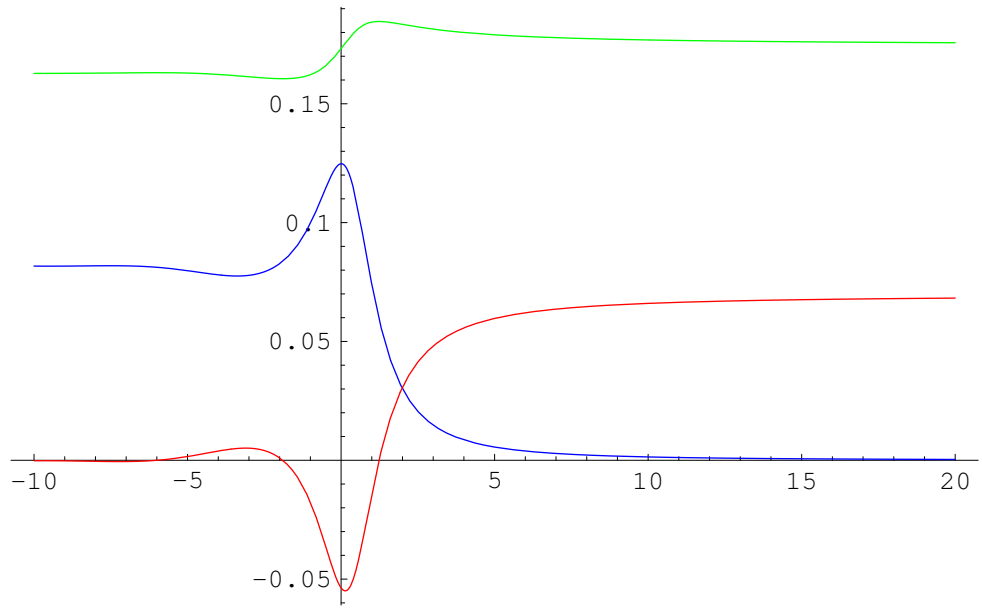

Figure 5.11: Surface convection (blue), bulk convection (green) and bulk diffusion (red) for a nonmonotonic solution.

We may examine the behaviour of each of these mechanisms for large ξ by substituting the appropriate expansions from §5.3.4.1. We find

$$\mathcal{P}QC \sim \mathcal{P}Q + 2\mathcal{P}(-\mathcal{P} + C_I(2+\mathcal{P}))\frac{Q^2}{\xi} + O\left(\frac{1}{\xi^2}\right), \tag{5.88}$$

$$2Q\frac{C}{h} \sim \frac{4Q}{\xi^2} + O\left(\frac{1}{\xi^2}\right), \tag{5.89}$$

$$-hC_\xi \sim -(-\mathcal{P} + C_I(2+\mathcal{P}))Q + 2(-\mathcal{P} + C_I(2+\mathcal{P}))\frac{\mathcal{P}Q^2}{\xi} + O\left(\frac{1}{\xi^2}\right), \tag{5.90}$$

i.e., as $\xi \to \infty$, the bulk convection term tends to the constant $\mathcal{P}Q$ from below if $\mathcal{K} > 1$, the surface convection term always tends to zero from above, and the diffusion term tends to the constant $(-\mathcal{P} + C_I(2+\mathcal{P}))$ which is negative if $\mathcal{K} > 1$. These behaviours are supported by the numerical solutions above.

We now calculate the pressure in the transition region using

$$p = -\frac{1}{2}h_{xx}. \tag{5.91}$$

As we would expect, in a monotonic solution, shown in red in Figure 5.12, we see that the pressure decreases monotonically from 0 to $-1/2$. In a dimpled solution, shown in blue in Figure 5.12, we see that the pressure variation is non-monotonic.

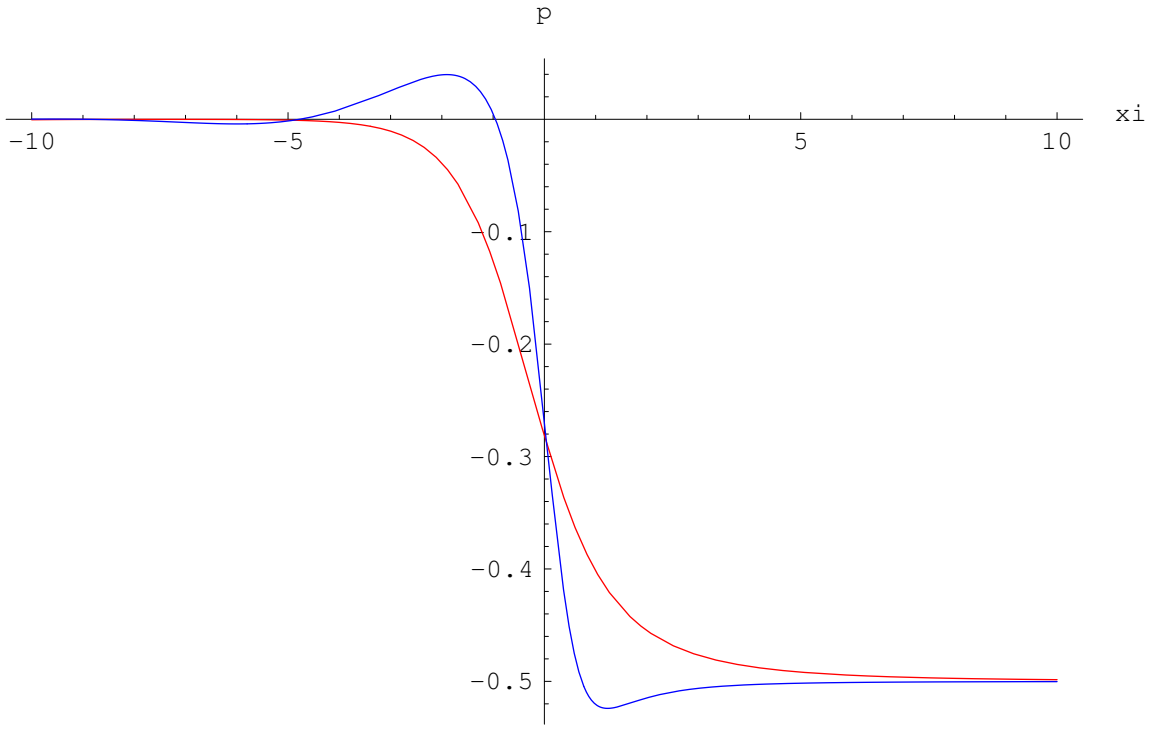

Figure 5.12: Pressure in a monotonic solution (red) and a dimpled solution (blue).

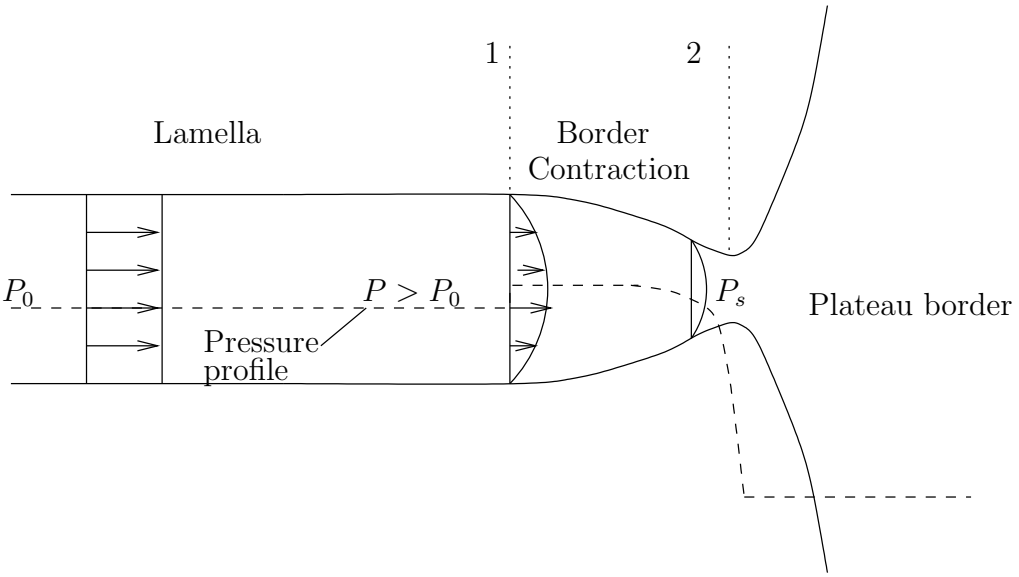

Figure 5.13: Barigou and Davidson's rejected transition region.

Notice that in the latter case there is a maximum of pressure in the transition region, *i.e.*, the pressure increases to a value greater than zero before a sudden decrease to a value just below $-1/2$. The pressure then tends to $-1/2$ from below. We compare this pressure distribution with that dismissed by Barigou and Davidson [5], shown in Figure 5.13. Since they have a sharp change in boundary structure at the start of the transition region (a change from a stress-free boundary in the lamella to a 'no-slip' boundary in the transition region), they have a 'step rise in pressure' at the 'inlet to the contraction zone'. It is this step that they reject as unphysical. Our results have a gradual change in stress at the surface and we obtain a smooth profile for the pressure when we have a dimpled solution. We therefore see no reason to reject this type of solution on the basis of the pressure profile.

We now generate $Q = Q(h_0)$ for a given set of parameters. We take $\mathcal{P} = 0.5$, $\mathcal{T} = 0.5$, $C_I = 0.1$, and we vary h_0 from 1 to 0.1 (to tie in with the initial and critical values used in §5.2 earlier). Here, we have $\mathcal{K} > 1$, and so we expect $C \to 1$ from below as $\xi \to \infty$. The variation is shown in Figure 5.14. Surprisingly, the flux *increases* as h_0 decreases, in contrast with the surfactant-free case.

We show the thickness of the transition region for h_0 between 0.1 and 1 (using these parameters) in Figure 5.15, and we show some of the corresponding concentrations in Figure 5.16. These may be thought of as "time snapshots" of the transition region as the lamella drains from $h = 1$ to $h = 0.1$. We calculate $\mathcal{B}$ for each of the snapshots. We find that, for $h_0 = 0.6$ and larger, we have $\mathcal{B} < 1$, while for the other solutions, we have

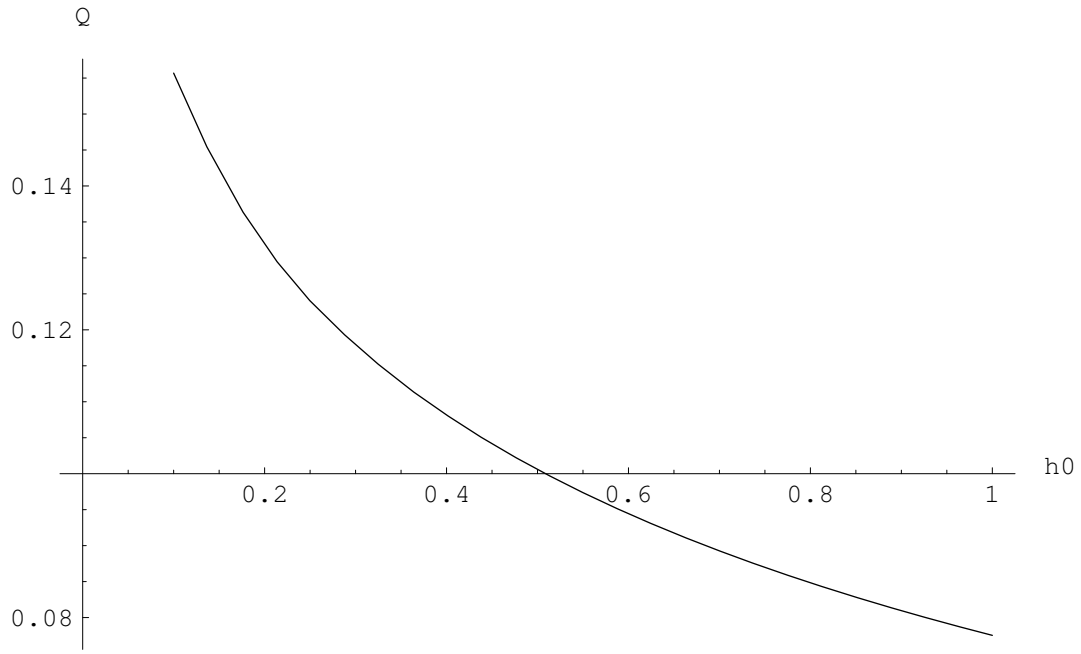

Figure 5.14: Graph showing Q as a function of h_0 for $\mathcal{P} = 0.5$, $\mathcal{T} = 0.5$, $C_I = 0.1$.

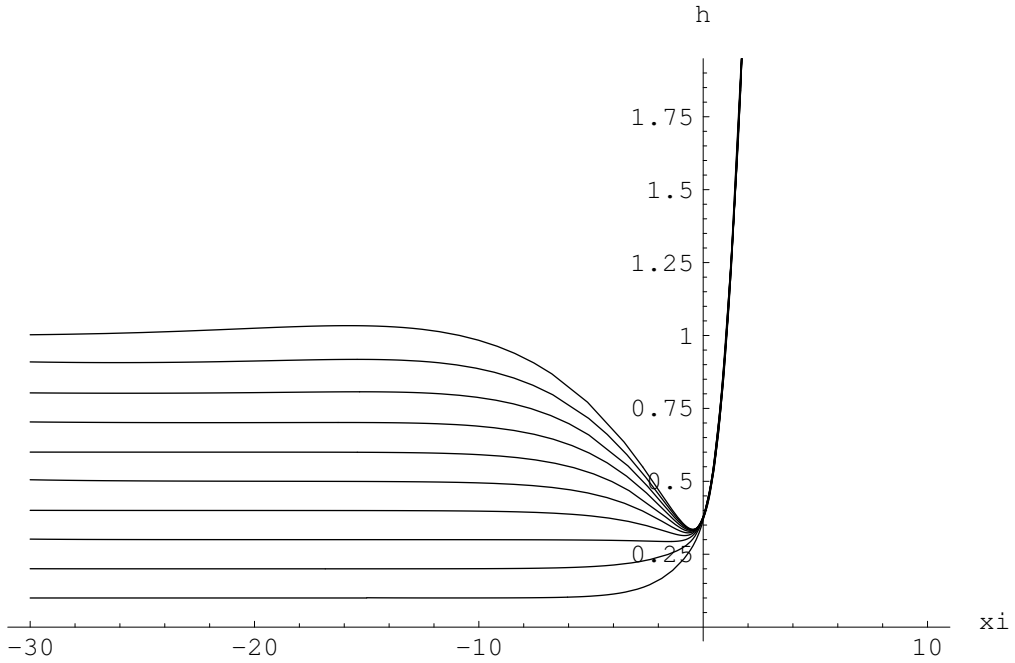

Figure 5.15: Transition region thickness for various values of h_0, with $\mathcal{P} = 0.5$, $\mathcal{T} = 0.5$, $C_I = 0.1$.

$\mathcal{B} > 1$. If we examine the solutions closely for large negative ξ, we see that the solutions agree with this prediction. We note that condition (5.87) for oscillatory solutions contains the factor $Q/h_0^{\frac{3}{2}}$, and that this factor increases as h_0 decreases, with the flux as shown in Figure 5.14. Hence, (5.87) dictates that the oscillations as $\xi \to -\infty$ die away as the film

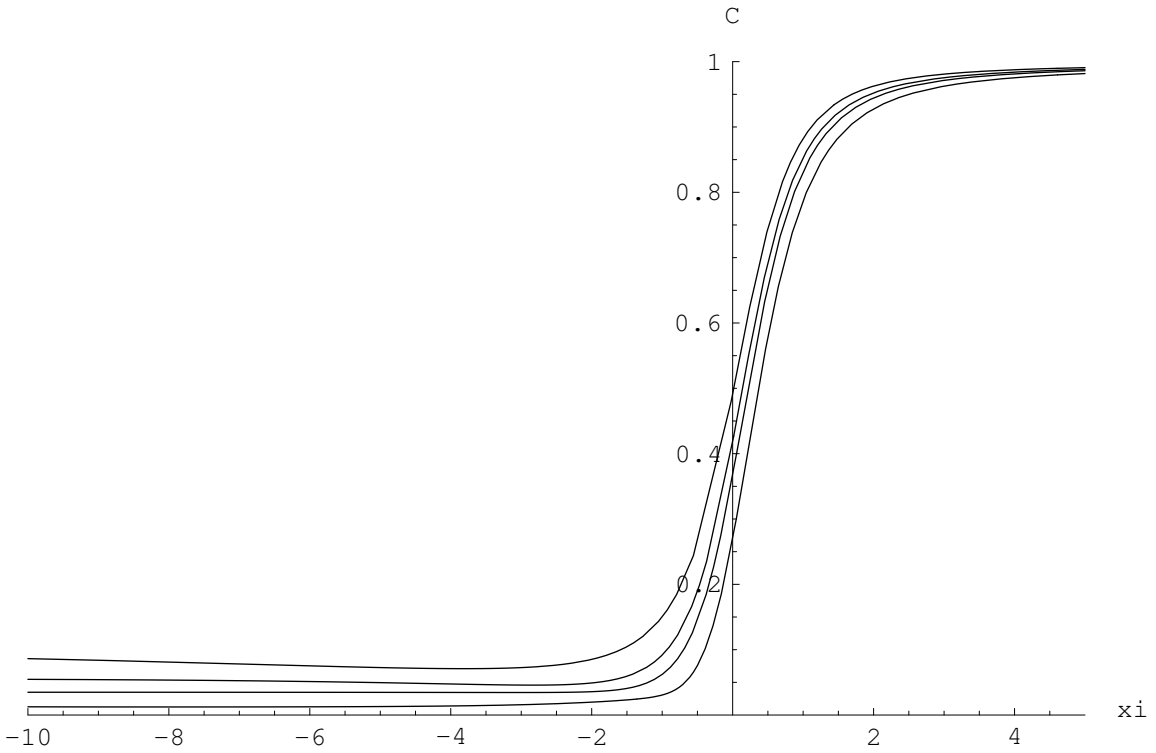

Figure 5.16: Concentration in the transition region for various values of h_0, with $\mathcal{P} = 0.5$, $\mathcal{T} = 0.5$, $C_I = 0.1$

thins. This is supported by this numerical evidence. However, we note that, for $h_0 = 0.5$, 0.4 and 0.3, a single oscillation remains close to $\xi = 0$ even after the small oscillations have died away. We have thus far been unable to explain this using asymptotics.

We are now in a position to determine the time taken for the lamella to drain. We (numerically) integrate (5.61), and find that the time taken for the lamella to reach its critical thickness, $h^{crit} = 0.1$, is $t = 9.085$. A graph of lamella thickness h against time is shown in Figure 5.17. We note that, from the graph, it appears that h tends to zero in finite time. Whether this does in fact occur depends on the behaviour of Q as $h_0 \to 0$, and we return to this point in §5.3.6.1 below. We redimensionalise the time to rupture using the timescale $L/U = 10$s. Hence $t_D^{\text{crit}} \sim 90$ s for the parameter values chosen here. This is at least in the right ball park, and is certainly much closer to the timescale for rupture of a typical foam film than the prediction of §5.2.

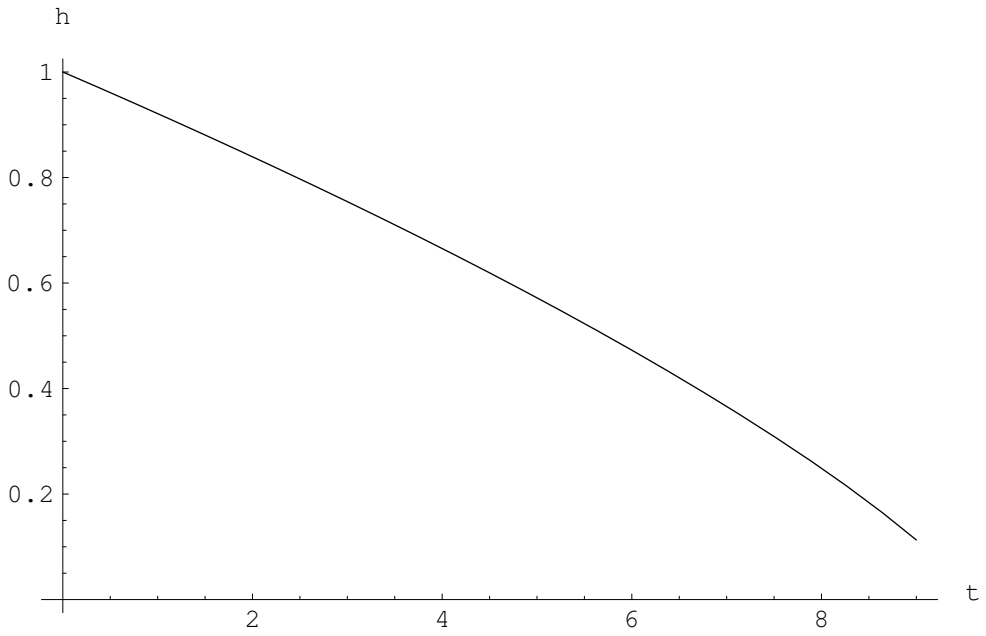

Figure 5.17: Graph showing lamella thickness versus time for $\mathcal{P} = 0.5$, $\mathcal{T} = 0.5$, and $C_I = 0.1$.

5.3.6.1 Unexpected results

While attempting numerical solutions to the transition region model, we found the following surprising behaviour. We noticed that, for some parameter regimes, Q appears to tend to infinity at a finite value of h_0. We illustrate such behaviour in the case when we have $C_I = 0.5$, $\mathcal{P} = 5$, and $\mathcal{T} = 5$, shown in Figure 5.18. We were unable to find a value of Q for $h_0 \leq 0.58$. At first, we dismissed these results as erroneous, but such behaviour can in fact be justified asymptotically. For convenience, we combine (5.65) and (5.66) to eliminate C, giving

$$h^3 h''' = Q(\mathcal{P}h + 2)\left(hh'' - \frac{1}{2}h'^2\right) + 2Q\mathcal{T}C_0\left(1 - \frac{h}{h_0}\right), \tag{5.92}$$

with

$$h \to h_0 \qquad \text{as} \qquad \xi \to -\infty, \tag{5.93}$$

$$h \sim \frac{1}{2}\xi^2 + \mathcal{T}(1 - C_0) \qquad \text{as} \qquad \xi \to \infty. \tag{5.94}$$

We then reduce the order of the problem by setting $h'^2 = G(h)$. (Note that the solutions of interest here are all monotonic, so there is no problem defining $G(h)$). The problem becomes

$$\sqrt{G}G_{hh} = \frac{Q}{h^3}(2 + \mathcal{P}h)\left(hG_h - G\right) + \frac{4Q\mathcal{T}C_0}{h^3}\left(1 - \frac{h}{h_0}\right), \tag{5.95}$$

where

$$G(h_0) = 0, \qquad G'(h_0) = 0, \tag{5.96}$$

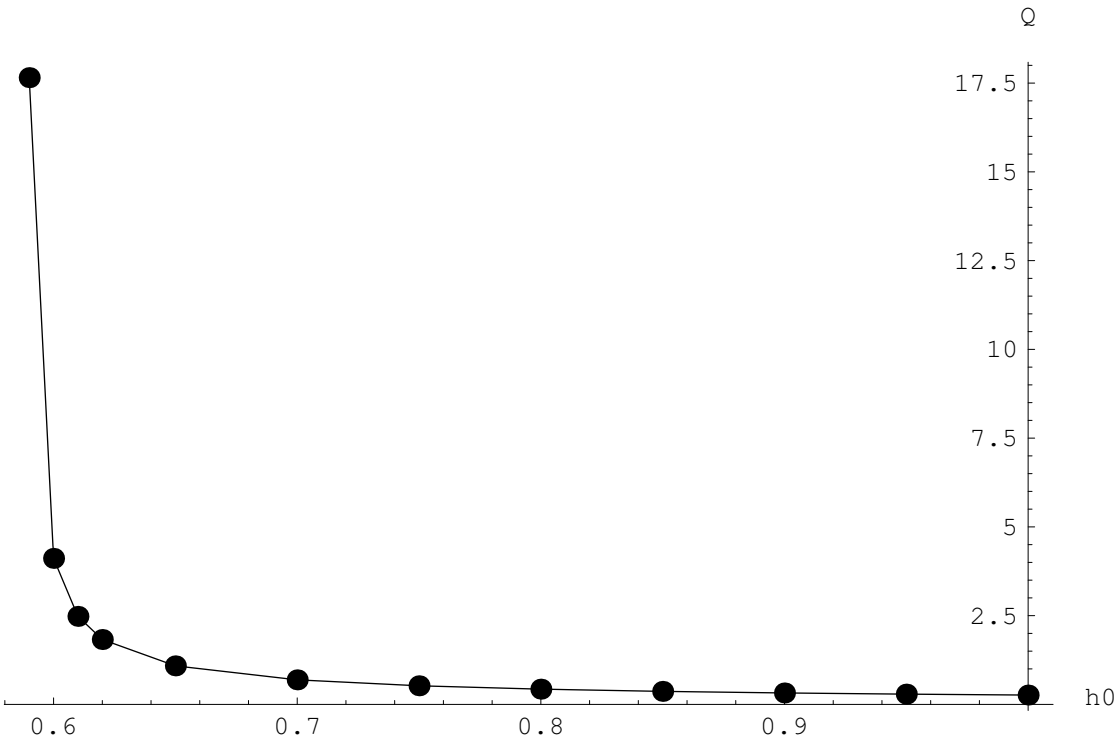

Figure 5.18: Graph showing Q against h_0 for $C_I = 0.5$, $\mathcal{P} = 5$, and $\mathcal{T} = 5$.

$$G \sim 2h - 2\mathcal{T}(1 - C_0) \qquad \text{as} \qquad h \to \infty. \tag{5.97}$$

In our earlier approach, we varied h_0 and found the corresponding value for Q. Here, we use the opposite idea, *i.e.*, we let $Q \to \infty$, and see if we can deduce a value for h_0.

First, we consider the problem near to the Plateau border. We note that (5.95) is singular as $Q \to \infty$, *i.e.*, to lowest order the highest derivative disappears. However, as h becomes large to match with the Plateau border this term comes back in at leading order. The appropriate scaling is $h = Q^2\hat{h}$, $G = Q^2\hat{G}$, and we arrive at

$$\hat{h}^3\sqrt{\hat{G}}\hat{G}_{\hat{h}\hat{h}} = \left(\mathcal{P}\hat{h} + \frac{2}{Q^2}\right)(\hat{h}\hat{G}_{\hat{h}} - \hat{G}) + \frac{4\mathcal{T}C_0}{Q^2}\left(\frac{1}{Q^2} - \frac{\hat{h}}{h_0}\right), \tag{5.98}$$

with

$$\hat{G} \sim 2\hat{h} - \frac{2\mathcal{T}(1 - C_0)}{Q^2} \qquad \text{as} \qquad \hat{h} \to \infty. \tag{5.99}$$

We seek an outer solution as an asymptotic expansion in powers of $1/Q^2$, and the leading-order problem reads

$$\hat{h}^3\sqrt{G_0}G_{0\hat{h}\hat{h}} = \frac{1}{2}\mathcal{P}\hat{h}(\hat{h}G_{0\hat{h}} - G_0). \tag{5.100}$$

It is fortunate that we can spot a solution to (5.100) which also satisfies the boundary condition as $\hat{h} \to \infty$, namely

$$G_0 = 2\hat{h}. \tag{5.101}$$

We need not look for a more general solution since we have already established that the solution eminating from ∞ is unique. Comparing terms of $O(1/Q^2)$, we find

$$\sqrt{2\hat{h}}G_{1\hat{h}\hat{h}} = \frac{\mathcal{P}}{\hat{h}^2}(\hat{h}G_{1\hat{h}} - G_1) - \frac{4\mathcal{T}C_0}{h_0 h^2}. \tag{5.102}$$

This has the solution

$$G_1 = \frac{1}{2\mathcal{P}^2}\left(\hat{h}\left(\alpha_1 - \frac{\sqrt{2}\mathcal{P}(\alpha_1-\alpha_2)}{\sqrt{\hat{h}}}e^{-\frac{\sqrt{2}\mathcal{P}}{\sqrt{\hat{h}}}} + (\alpha_2-\alpha_1)e^{-\frac{\sqrt{2}\mathcal{P}}{\sqrt{\hat{h}}}}\right)\right) - \frac{4\mathcal{T}C_0}{\mathcal{P}h_0}. \tag{5.103}$$

We want $G_1 \sim -2\mathcal{T}(1-C_0)$ as $\hat{h}\to\infty$, so we set $\alpha_2 = 0$, and

$$\alpha_1 = \frac{8\mathcal{T}C_0}{\mathcal{P}h_0} - 4\mathcal{T}(1-C_0). \tag{5.104}$$

Therefore $\hat{G}$ reads

$$\hat{G} \sim 2\hat{h} + \frac{1}{\mathcal{P}^2Q^2}\left(\frac{8\mathcal{T}C_0}{\mathcal{P}h_0} - 4\mathcal{T}(1-C_0)\right)\left(\hat{h} - (\hat{h}+\mathcal{P}\sqrt{2\hat{h}})e^{-\sqrt{\frac{2}{\hat{h}}}\mathcal{P}}\right) - \frac{4\mathcal{T}C_0}{\mathcal{P}h_0Q^2} + O\left(\frac{1}{Q^4}\right). \tag{5.105}$$

We obtain a matching condition for the inner problem by susbtituting $\hat{G} = G/Q^2$, $\hat{h} = h/Q^2$ and thus the two-term outer expansion of the two-term inner solution must read

$$G \sim -\frac{4\mathcal{T}C_0}{\mathcal{P}h_0} + 2h + \left(\frac{8\mathcal{T}C_0}{h_0\mathcal{P}^3Q^2} - \frac{4\mathcal{T}(1-C_0)}{\mathcal{P}^2Q^2}\right)h, \tag{5.106}$$

as $h\to\infty$.

We now consider (5.95) in the limit $Q\to\infty$. We seek an asymptotic solution in powers of $1/Q$, and the leading-order equation reads

$$hG_h - G + \frac{4\mathcal{T}C_0}{(2+\mathcal{P}h)}\left(1 - \frac{h}{h_0}\right) = 0, \tag{5.107}$$

which has the solution

$$G = \alpha h + \frac{1}{4h_0}\left[8\mathcal{T}C_0h_0 + (8\mathcal{T}C_0 + 4\mathcal{T}C_0h_0\mathcal{P})h\log\left(\frac{h}{2+\mathcal{P}h}\right)\right]. \tag{5.108}$$

Applying the matching condition (5.106) at leading-order, we obtain

$$G = 2h\left[1 + \frac{C_I(2+\mathcal{P})\mathcal{T}}{2}\log\left(\frac{\mathcal{P}h}{2+\mathcal{P}h}\right)\right] + \frac{2\mathcal{T}C_I(2+\mathcal{P})h_0}{2+\mathcal{P}h_0}. \tag{5.109}$$

We remember that here we are trying to find h_0 as a function of Q (in the limit as $Q\to\infty$) and to do so we apply the left-hand boundary conditions $G(h_0) = 0$ and $G'(h_0) = 0$. We set

$$h_0 = h_c + \frac{h_{c1}}{Q} + \frac{h_{c2}}{Q^2} + \ldots, \tag{5.110}$$

so that h_c is the value of h_0 (if it exists) at which Q approaches infinity, and satisfies $G(h_c) = 0$, *i.e.*

$$2h_c\left[1 + \frac{C_I\mathcal{T}(2+\mathcal{P})}{2}\log\left(\frac{\mathcal{P}h_c}{2+\mathcal{P}h_c}\right)\right] + \frac{2\mathcal{T}C_I(2+\mathcal{P})h_c}{2+\mathcal{P}h_c} = 0. \tag{5.111}$$

For given C_I, $\mathcal{P}$ and $\mathcal{T}$, (5.111) has two nonnegative solutions for h_c, one of which is $h_c = 0$. However, this can be rejected since one can readily show that $G'(0) \neq 0$. The other, positive, solution for h_c does satisfy $G'(h_c) = 0$. For $\mathcal{T} = 5$, $\mathcal{P} = 5$, and $C_I = 0.5$, this gives $h_c = 0.587$. So, our numerical observations that $Q \to \infty$ for h_0 around 0.59 appear to have been justified. With $\mathcal{T} = 0.5$, $\mathcal{P} = 0.5$, and $C_I = 0.1$, we calculate $h_c = 4.4 \times 10^{-7}$. Clearly, in our calculations we did not make h_0 small enough to notice the presence of this h_c. We note that the existence of h_c, however small, explains why the flux increases as h_0 decreases.

In general, the positive solution of (5.111) can be written as

$$\tilde{h}_c = \mathcal{P}h_c = F(\mathcal{T}^*), \tag{5.112}$$

where $\mathcal{T}^* = C_I\mathcal{T}(2+\mathcal{P})$, and F is given by

$$\mathcal{T}^* = -\frac{2(2+F(\mathcal{T}^*))}{(2+F(\mathcal{T}^*))\log\left[\frac{2+F(\mathcal{T}^*)}{F(\mathcal{T}^*)}\right] + 2}. \tag{5.113}$$

We show the solution to (5.113) in Figure 5.19. We note that, as $\mathcal{T}^* \to 0$, $F \to 0$, and we find that the behaviour is

$$F \sim 2e^{-1-\frac{2}{\mathcal{T}^*}} \qquad \text{as} \qquad \mathcal{T}^* \to 0, \tag{5.114}$$

and in particular if $\mathcal{T}^*$ is small, F is exponentially small. This is the reason why we did not notice the presence of h_c when we took $C_I = 0.1$, and $\mathcal{T} = \mathcal{P} = 0.5$ earlier. We also note that, as $\mathcal{T}^* \to \infty$, $F \to \infty$, and

$$F \sim \sqrt{\mathcal{T}^*} \qquad \text{as} \qquad \mathcal{T}^* \to \infty, \tag{5.115}$$

and so, for large enough $\mathcal{T}^*$, we are in a situation where $h_c > 1$ (*i.e.*, the critical thickness is above the starting thickness of the lamella) and we cannot even start to follow the evolution of h.

Of course, in practice the flux cannot become infinite on physical grounds. We anticipate that, as Q becomes large, some physical effects that have thus far been neglected become important. Moreover, these should then describe the behaviour of Q for $h < h_c$. There

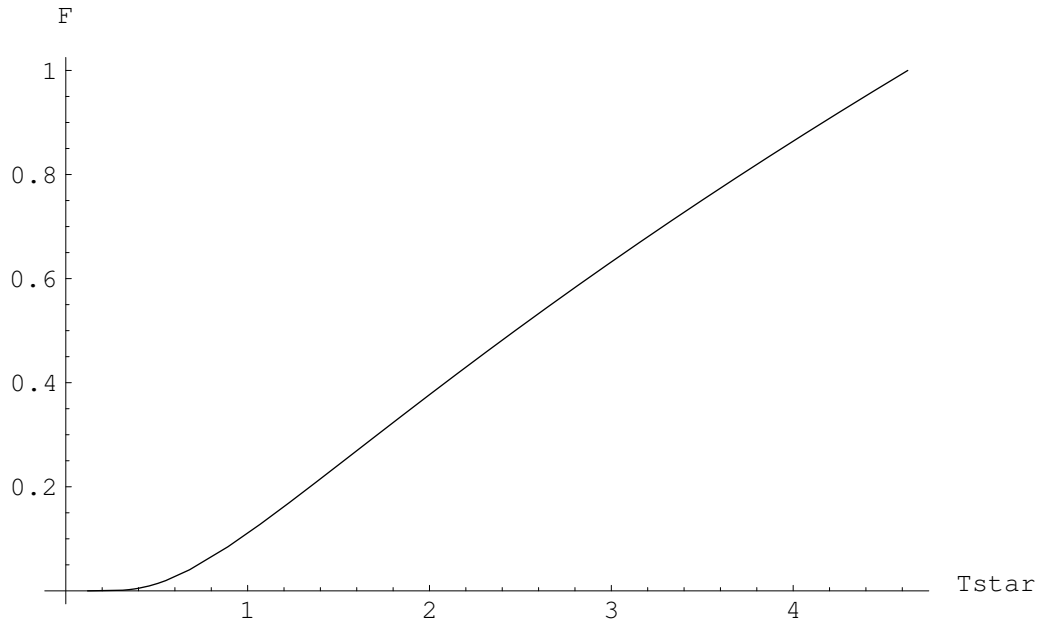

Figure 5.19: Graph showing how the function F varies with T^*

is more than one candidate for the relevant extra effect; for example, it could be inertia, but we will only assess the effect of the viscous term that was neglected in (5.43). When this term is included, the transition region model reads

$$uh = Q, \tag{5.116}$$

$$-\nu Q\left(\frac{h_\xi}{h}\right)_\xi + hh_{\xi\xi\xi} - \mathcal{T}C_\xi = 0, \tag{5.117}$$

$$hC_\xi = \mathcal{P}Q(C - C_0) + 2Q\left(\frac{C}{h} - \frac{C_0}{h_0}\right), \tag{5.118}$$

where $\nu = 8\delta\mathrm{Ca}/\epsilon$. Using our velocity scaling, $\nu \sim 4 \times 10^{-5} << 1$. As previously, we re-write the problem as one equation for h, which reads

$$h^3h''' = Q(2+\mathcal{P}h)\left(hh'' - \frac{1}{2}h'^2\right) + 2\mathcal{T}C_0\left(1 - \frac{h}{h_0}\right) + \nu Q\left(h\left(\frac{h'}{h}\right)' - 2Q\frac{h'}{h} - \mathcal{P}Qh'\right). \tag{5.119}$$

We set $G = h'^2$, and the problem becomes

$$h^3\sqrt{G}G_{hh} = Q(2+\mathcal{P}h)(hG_h - G) + 4\mathcal{T}QC_0\left(1 - \frac{h}{h_0}\right) + \nu Q\left(G_h - \frac{2G}{h} - Q\left(\frac{4}{h} + 2\mathcal{P}\right)\sqrt{G}\right). \tag{5.120}$$

We can see that for $Q \sim O(1)$, we have the problem that we have just considered, but for $Q \sim O(1/\nu)$ the viscous terms come in and we have the equation

$$hG_h - G + \frac{4\mathcal{T}C_0}{2+\mathcal{P}h}\left(1 - \frac{h}{h_0}\right) - \frac{2}{h}\tilde{Q}\sqrt{G} = 0, \tag{5.121}$$

where $\tilde{Q} = \nu Q$. We note that $\tilde{Q}$ is the viscous scaled flux that we considered in §5.2. We hope that the solution to this equation will provide insight into what happens to the solution after the lamella thickness has reached h_c. In any case, since the flux becomes very large at this thickness, we assume that the rest of the drainage occurs on the (much faster) viscous timescale, and so the film thins to the rupture thickness very quickly.

We conclude by summarising the behaviour of the solution that we have uncovered in this subsection.

- We are able to find a solution to the surfactant problem (5.65)-(5.66) providing h_0 is larger than a critical value h_c given by

$$\left[1 + \frac{C_I \mathcal{T}(2+\mathcal{P})}{2} \log\left(\frac{\mathcal{P}h_c}{2+\mathcal{P}h_c}\right)\right] + \frac{\mathcal{T}C_I(2+\mathcal{P})}{2+\mathcal{P}h_c} = 0. \tag{5.122}$$

- As $h_0 \to h_c$ from above, $Q \to \infty$.

- To find the behaviour of solutions once the lamella has thinned to h_c, we must include more physics; we considered introducing the viscous terms. We obtain a new model that holds when viscous effects are significant.

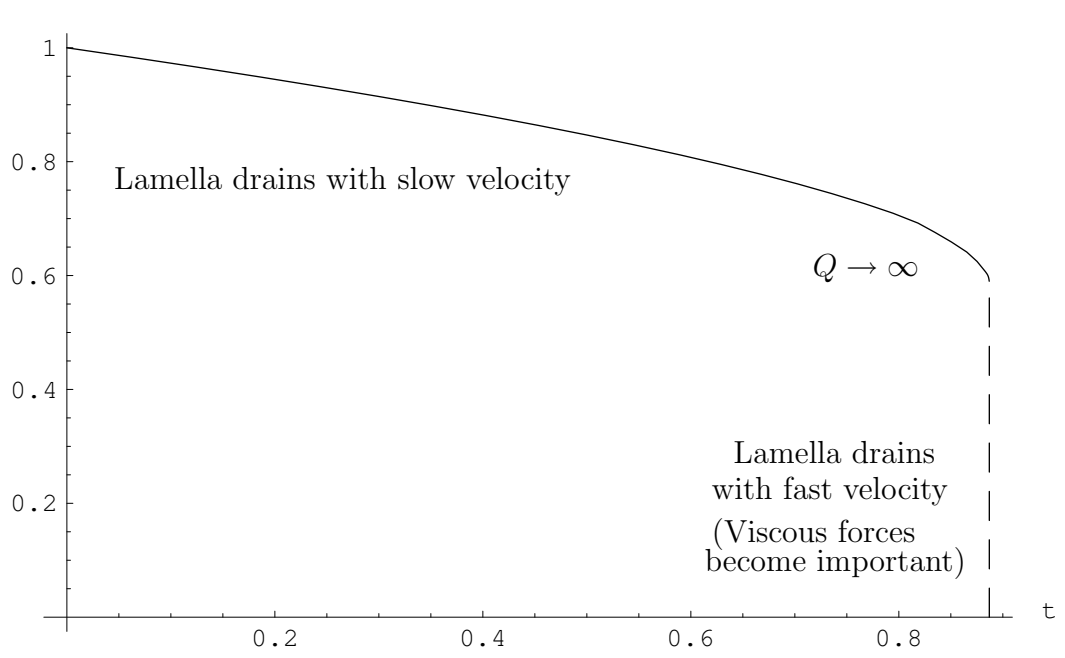

Figure 5.20: Schematic showing how the thickness of a lamella changes with time. The upper part of the curve was calculated for $C_I = 0.5$, $\mathcal{P} = 5$, $\mathcal{T} = 5$.

- We hypothesise that the film thins from h_c to h^{crit} on the fast viscous timescale and we show a schematic of our conjecture for the variation of the film thickness with time in Figure 5.20.

We conjecture that if $h_c > 1$, the surfactant is unable to prolong the life of the film, since for $h_0 = 1 < h_c$, we are already in the regime that requires a viscous velocity scaling.

5.3.7 Including the 'lubrication' term

We now take into account the effect of nonzero $\tilde{\beta}$ on the solution. If $\tilde{\beta} = O(1)$, then the lamella model remains the same but the transition region model is modified. We have

$$\bar{u}h = Q, \tag{5.123}$$

$$\mathcal{T}(C - C_0) = hh_{\xi\xi} - \frac{h_\xi^2}{2}, \tag{5.124}$$

$$(1 + \beta\mathcal{T}C)hC_\xi = \mathcal{P}Q(C - C_0) + 2Q\left(\frac{C}{h} - \frac{C_0}{h_0}\right), \tag{5.125}$$

where $\beta = 2\tilde{\beta}$, with

$$h_{\xi\xi} \to 1, \qquad C \to 1, \qquad \text{as} \qquad \xi \to \infty, \tag{5.126}$$

$$h \to h_0, \qquad u \to \frac{Q}{h_0}, \qquad C \to C_0, \qquad \text{as} \qquad \xi \to -\infty, \tag{5.127}$$

and

$$u = \bar{u} + 3\beta\left(-y^2 + \frac{1}{12}h^2\right)h_{\xi\xi\xi}, \tag{5.128}$$

$$C_0 = \frac{C_I(2 + \mathcal{P})}{2 + \mathcal{P}h_0}h_0. \tag{5.129}$$

5.3.7.1 Behaviour as $\xi \to \pm\infty$

In order to check that the problem is well-posed, we must again consider the asymptotic behaviour of this system. We scale $C = C_0 + C_0\hat{C}$, $h = h_0\hat{h}$ and $\xi = h_0/\sqrt{\mathcal{T}C_0}\hat{\xi}$, and the system of equations becomes

$$\hat{C} = \hat{h}\hat{h}_{\hat{\xi}\hat{\xi}} - \frac{\hat{h}_{\hat{\xi}}^2}{2}, \tag{5.130}$$

$$\left(1 + \beta^* + \beta^*\hat{C}\right)\hat{h}\hat{C}_{\hat{\xi}} = Q^*\Upsilon\hat{C} + Q^*\left(\frac{\hat{C} + 1}{\hat{h}} - 1\right), \tag{5.131}$$

where, as before, $\Upsilon = \mathcal{P}h_0/2$, $Q^* = 2Q/(h_0\sqrt{\mathcal{T}C_0})$, and we have the extra parameter $\beta^* = \beta\mathcal{T}C_0$. On substituting

$$\hat{h} = \frac{a_1\hat{\xi}^2}{2} + a_2\hat{\xi} + a_3 + \frac{a_4}{\hat{\xi}} + \frac{a_5}{\hat{\xi}^2} + O\left(\frac{1}{\hat{\xi}^3}\right), \tag{5.132}$$

(again, we do not explicitly search for exponentially small terms), we find that

$$\hat{C} = a_1a_3 - \frac{a_2^2}{2} + \frac{3a_1a_4}{\hat{\xi}} + \frac{3a_2a_4 + 6a_1a_5}{\hat{\xi}^2} + O\left(\frac{1}{\hat{\xi}^3}\right). \tag{5.133}$$

Using (5.131),

$$a_4 = -\frac{2\left(Q^*\Upsilon\left(a_1a_3 - \frac{a_2^2}{2}\right) - Q^*\right)}{3a_1^2\left(1+\beta^*+\beta^*\left(a_1a_3-\frac{a_2^2}{2}\right)\right)}, \tag{5.134}$$

$$a_5 = -\frac{a_2a_4}{a_1} - \frac{\left(\frac{a_4Q^*\Upsilon}{2a_1} + \frac{3a_1a_4^2\beta^*}{4}\right)}{1+\beta^*+\beta^*\left(a_1a_3-\frac{a_2^2}{2}\right)}, \tag{5.135}$$

which reduce to (5.72) and (5.73) when β^* is set to zero. Imposing boundary conditions as $\hat{\xi} \to \infty$, we see that $a_1 = h_0/(\mathcal{T}C_0)$ and $a_1a_3 - a_2^2/2 = (1-C_0)/C_0$. Hence, imposing $a_2 = 0$ by translational invariance, we see that the solution satisfying the conditions at $\hat{\xi} = \infty$ is unique.

If we look for stability of $\hat{h} = 1$ by substituting $\hat{h} = 1 + ae^{\lambda\hat{\xi}}$ as $\hat{\xi} \to -\infty$, we obtain

$$(1+\beta^*)\,\lambda^3 = Q^*(\Upsilon+1)\lambda^2 - Q^*, \tag{5.136}$$

as the equation for λ. In this case, we may reduce (5.136) to (5.78) by setting $\chi = \lambda\sqrt{\Upsilon+1}$ and $q = Q^*(1+\Upsilon)^{\frac{3}{2}}/(1+\beta^*)$. We therefore expect oscillations of the solution as we approach minus infinity if

$$\frac{2Q\left(1+\frac{\mathcal{P}h_0}{2}\right)^{\frac{3}{2}}}{h_0\sqrt{\mathcal{T}C_0}(1+\beta\mathcal{T}C_0)} < \frac{3\sqrt{3}}{2}, \tag{5.137}$$

i.e., if

$$\mathcal{B} = \frac{4\sqrt{2}Q\left(1+\frac{\mathcal{P}h_0}{2}\right)^2}{3\sqrt{3}h_0^{\frac{3}{2}}\sqrt{\mathcal{T}C_I(2+\mathcal{P})}\left(1+\frac{\beta\mathcal{T}C_I(2+\mathcal{P})h_0}{2+\mathcal{P}h_0}\right)} < 1. \tag{5.138}$$

We either have two real roots indicating monotonic behaviour or a conjugate pair suggesting oscillatory behaviour as we approach the lamella. Again, we have a one-parameter family of solutions eminating from $\hat{\xi} = -\infty$. We conclude that we are not over-specifying the problem, and that, as before, the most convenient numerical solution procedure is to start from $\hat{\xi} = \infty$ and vary Q until $\hat{h} \to 1$ as $\hat{\xi} \to \infty$.

5.3.7.2 Surface and centre-line velocities as $\xi \to \infty$

We use asymptotics to examine the behaviour of the velocities as we approach the Plateau border. Scaling $h = h_0h'$, $y = h_0y'$, $\xi = h_0/(\sqrt{\mathcal{T}C_0})\xi'$ and $u = (\mathcal{T}C_0)^{\frac{3}{2}}u'$, we have (dropping primes)

$$u' = \frac{\mathcal{Q}}{h'} + 3\beta h'_{\xi'\xi'\xi'}\left(\frac{1}{12}h'^2 - y'^2\right), \tag{5.139}$$

where $\mathcal{Q} = Q/(h_0(\mathcal{T}C_0)^{\frac{3}{2}})$. Calling u'_{cl} the velocity of the liquid at the centreline, we have the following expressions for u'_s and u'_{cl}

$$u'_s = \frac{\mathcal{Q}}{h'} - \frac{\beta}{2}h'^2 h'_{\xi'\xi'\xi'}, \tag{5.140}$$

$$u'_{cl} = \frac{\mathcal{Q}}{h'} + \frac{\beta}{4}h'^2 h'_{\xi'\xi'\xi'}. \tag{5.141}$$

Using (5.69),

$$u'_s \sim \frac{3a_1^2 a_4\beta}{4} + \frac{3a_5 a_1^2\beta}{\xi'} + \frac{\frac{2\mathcal{Q}}{a_1} + \frac{\beta}{2}(6a_1a_3a_4 + 15a_1^2a_6)}{\xi'^2} + O\left(\frac{1}{\xi'^3}\right), \tag{5.142}$$

$$u'_{cl} \sim -\frac{3a_1^2 a_4\beta}{8} - \frac{3a_5 a_1^2\beta}{2\xi'} + \frac{\frac{2\mathcal{Q}}{a_1} - \frac{\beta}{4}(6a_1a_3a_4 + 15a_1^2a_6)}{\xi'^2} + O\left(\frac{1}{\xi'^3}\right), \tag{5.143}$$

and we use the expression for a_4 given by (5.72) to decide whether we have $u'_s > 0$, $u'_{cl} < 0$ or $u'_s < 0$, $u'_{cl} > 0$ as $\xi' \to \infty$. If we set

$$\mathcal{D} = \frac{\mathcal{P}h_0}{2}\left(\frac{2+\mathcal{P}h_0}{C_I(2+\mathcal{P})h_0} - 1\right) - 1 = \frac{2+\mathcal{P}h_0}{2}(\mathcal{K}-1), \tag{5.144}$$

then we have $u'_s > 0$ if $\mathcal{D} < 0$ and vice versa, *i.e.*, $u'_s > 0$ if $\mathcal{K} < 1$. In the special case where $C_I = \mathcal{P}/(2+\mathcal{P})$ (*i.e.*, $\mathcal{K} = 1$), both a_4 and a_5 are zero, but $a_6 = -Q^*\mathcal{T}/(h_0(1+\beta^*+\frac{2\beta^*}{\mathcal{P}h_0})) \neq 0$. Here, we have u'_s, $u'_{cl} \to 0$ as $\xi' \to \infty$, where u'_{cl} always approaches from above and u'_s approaches from above providing

$$\frac{\mathcal{P}\mathcal{T}(1+\beta\mathcal{T})}{15\beta(2+\mathcal{P}h_0)^2} > 1. \tag{5.145}$$

5.3.7.3 Summary

In addition to the points raised in §5.3.5, we have

- The condition for oscillating solutions as $\xi \to -\infty$ is

$$\mathcal{B} = \frac{4\sqrt{2}Q\left(1+\frac{\mathcal{P}h_0}{2}\right)^2}{3\sqrt{3}h_0^{\frac{3}{2}}\sqrt{\mathcal{T}C_I(2+\mathcal{P})}\left(1+\frac{\beta\mathcal{T}C_I(2+\mathcal{P})h_0}{2+\mathcal{P}h_0}\right)} < 1. \tag{5.146}$$

- The surface velocity is positive as we approach the Plateau border if $\mathcal{K} < 1$, and the centre-line velocity is negative. If $\mathcal{K} > 1$, then the surface velocity is negative and the centreline velocity is positive. We therefore expect eddies to be set up at the entrance to the Plateau border, with direction of rotation being determined by $\mathcal{K}$.

5.3.7.4 Results and discussion

We solve the transition region model and, again, see the two classes of solution. Here, since the liquid velocity is no longer extensional, we can visualise the flow easily by plotting the velocity field. To do this, we must use the vertical velocity, which reads,

$$v = \frac{Q}{h^2} h_x y - \beta h_{xxxx} \left(\frac{h^2}{4} y - y^3 \right) - \frac{\beta}{2} h h_x h_{xxx} y. \tag{5.147}$$

With $\mathcal{T} = 5$, $\mathcal{P} = 5$, $C_I = 0.5$, $h_0 = 0.8$ and $\beta = 1$, we find that $Q = 2.008$. We calculate $\mathcal{B} = 1.97 > 1$ and hence we expect no oscillations. We note that, as before, $\mathcal{K} > 1$, and so we expect that $C \to 1$ from below and that $u_s < 0$, $u_{cl} > 0$ as $\xi \to \infty$. We show the transition region shape and the velocity field in the region in Figure 5.21 (we do not show the monotonic increasing concentration profile). We observe a monotonic solution in which the velocity decreases as the liquid approaches the Plateau border, and the centre-line velocity is positive while the surface velocity becomes negative. Eddies are set up at the entrance to the Plateau border which drive liquid down the transition region walls while returning it along the centre-line.

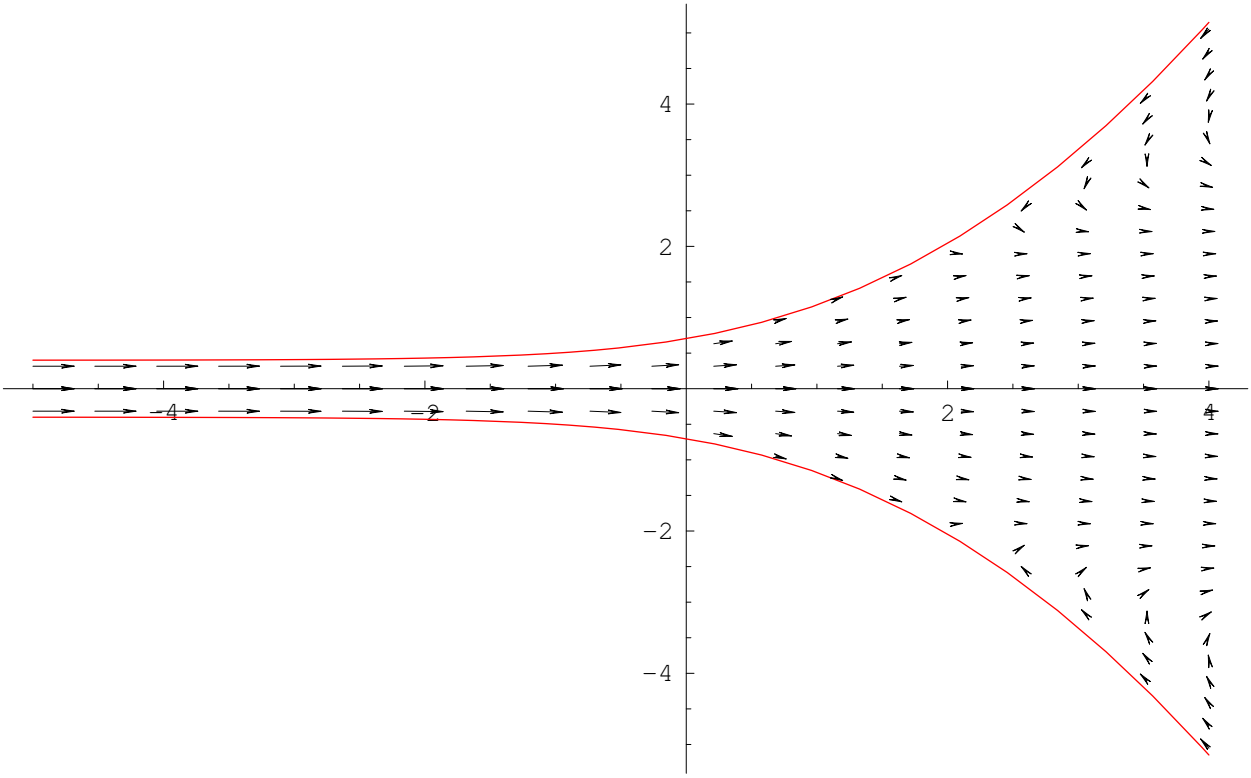

Figure 5.21: Velocity field for a solution where $\mathcal{K} > 1$.

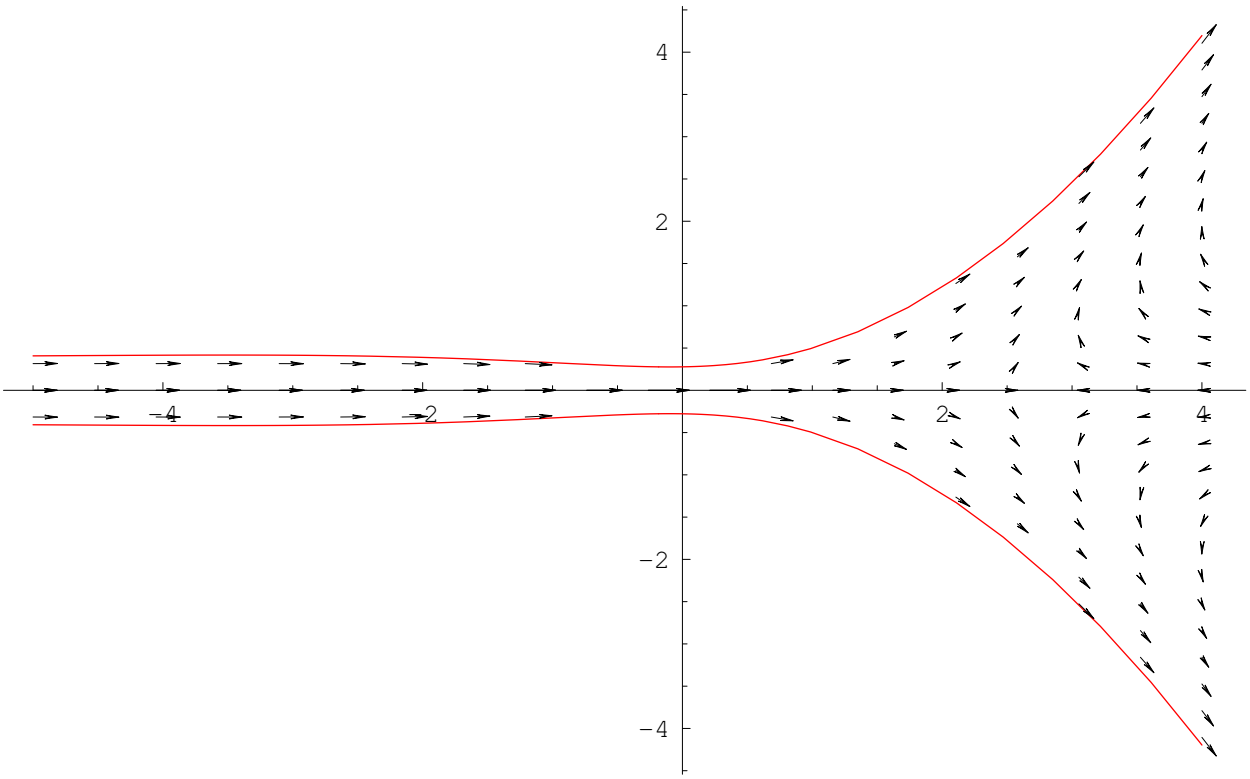

Figure 5.22: Velocity field for a solution where $\mathcal{K} < 1$.

With $\mathcal{T} = 5$, $\mathcal{P} = 5$, $C_I = 1.0$, $h_0 = 0.8$ and $\beta = 1$, we find $Q = 0.2095$. We calculate $\mathcal{B} = 0.086 < 1$, predicting oscillations, and since $\mathcal{K} < 1$, we expect that $u_s > 0$ and $u_{cl} < 0$ as $\xi \to \infty$. Plots of the transition region shape, along with velocity field are shown in Figure 5.22. We observe a dimpled solution in which the velocity decreases in magnitude as the liquid aproaches the Plateau border, and the velocity beomes negative on the centre-line, and is always positive along the free surfaces. In contrast to the previous case, eddies are now set up which send the liquid in the opposite direction, that is, the liquid moves into the Plateau border along the walls and out along the centreline.

We stress that the cases $u_s > 0$, $u_s < 0$ are *not* dependent on whether or not we have a dimpled solution, but merely on whether $\mathcal{K} \gtrless 1$. We examine the effects of increasing the value of β from zero to one in the two cases we presented earlier. Surface velocities and the centreline velocities for $\beta = 0$ (black), 0.2 (red), 0.4 (green), 0.6 (blue), 0.8 (purple) and 1.0 (cyan) are shown in Figure 5.23. When $\beta = 0$ the liquid velocity is everywhere positive. With nonzero β, we note that in the $\mathcal{K} > 1$ case (with C_I and $\mathcal{P}$ fixed), increasing β from zero creates a stagnation point which travels down the free surface from infinity. The centreline velocity remains positive everwhere in this case. When $\mathcal{K} < 1$, increasing β from zero creates a stagnation point on the centreline which travels in from infinity.

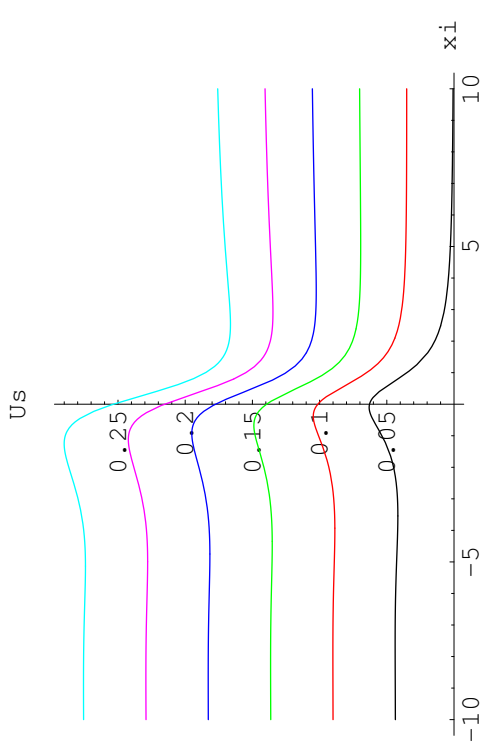

(b) u_s for $\mathcal{K} < 1$

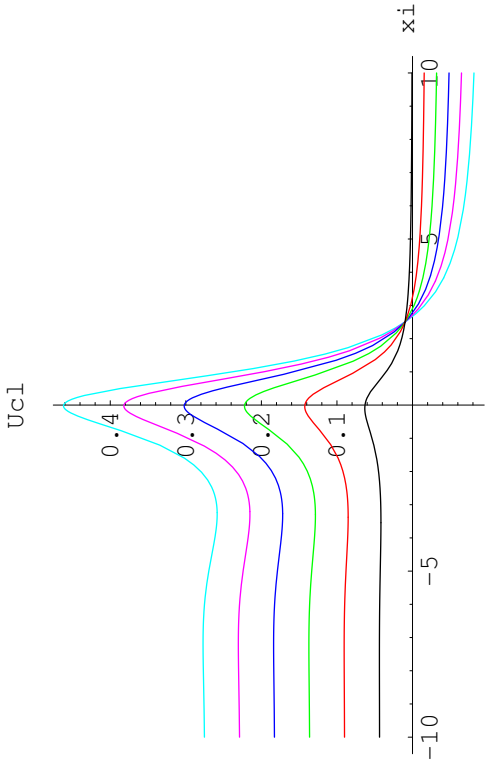

(d) u_{cl} for $\mathcal{K} < 1$

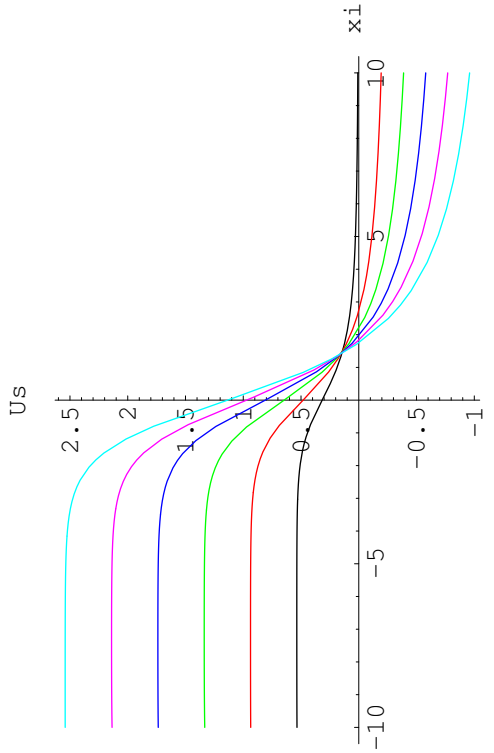

(a) u_s for $\mathcal{K} > 1$

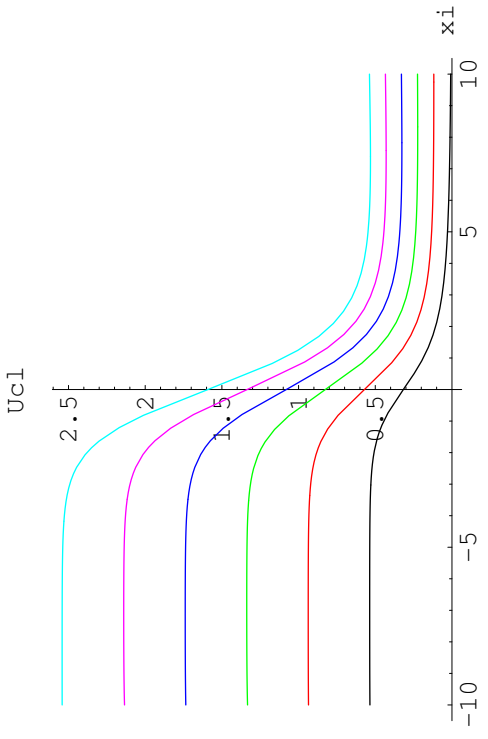

(c) u_{cl} for $\mathcal{K} > 1$

Figure 5.23: Graphs showing surface velocities and centreline velocities in the cases $C_I < P/(2+\mathcal{P})$ (figures (a) and (c)) and $C_I > P/(2+\mathcal{P})$ (figures (b) and (d)), for $\beta = 0$ (black), 0.2 (red), 0.4 (green), 0.6 (blue), 0.8 (purple), and 1.0 (cyan).

The surface velocity remains positive everywhere in this case.

We proceed to generate $Q = Q(h_0)$ for a given set of parameters. We take $\mathcal{P} = 0.5$, $\mathcal{T} = 0.5$, $C_I = 0.1$, and $\beta = 1$, and we vary h_0 from 1 down to 0.1. The variation of Q with h_0 is shown in Figure 5.24. As previously, we see that Q increases as h_0 decreases.

We briefly comment on the behaviour of the solution as $Q \to \infty$. In this case, we combine (5.124)-(5.125) to give

$$\left(1 + \beta\mathcal{T}C_0 + \beta\left(hh'' - \frac{1}{2}h'^2\right)\right)h^3h''' = Q(\mathcal{P}h + 2)\left(hh'' - \frac{1}{2}h'^2\right) + 2Q\mathcal{T}C_0\left(1 - \frac{h}{h_0}\right), \tag{5.148}$$

and the boundary conditions remain the same, viz (5.93)-(5.94). Here, we do not attempt to analyse asymptotically this equation in the limit as $Q \to \infty$. Rather, we note that the condition (5.122) giving h_c in the extensional flow case was obtained by considering the leading-order inner problem in the limit as $Q \to \infty$, and that (5.148) has the same leading-order behaviour. We therefore have the same condition for h_c, namely (5.122). We note that this is a preliminary result and that we have yet to check that the matching with the outer problem can be completed without any complications.

Finally, we integrate (5.61), to give $h = h(t)$ as shown in Figure 5.25 and calculate the time taken for the lamella to reach its critical thickness, which is $t = 8.82$, which we redimensionalise to give $t_D^{\text{crit}} = 88$ s. Comparing this to the case $\beta = 0$, we see that the inclusion of the parabolic velocity profile has resulted in a slight decrease in the rupture time. We stress that the main effect of including the lubrication term is that it either retards the surface flow and accelerates the centre-line flow, or vice versa, depending on the magnitude of $\mathcal{K}$.

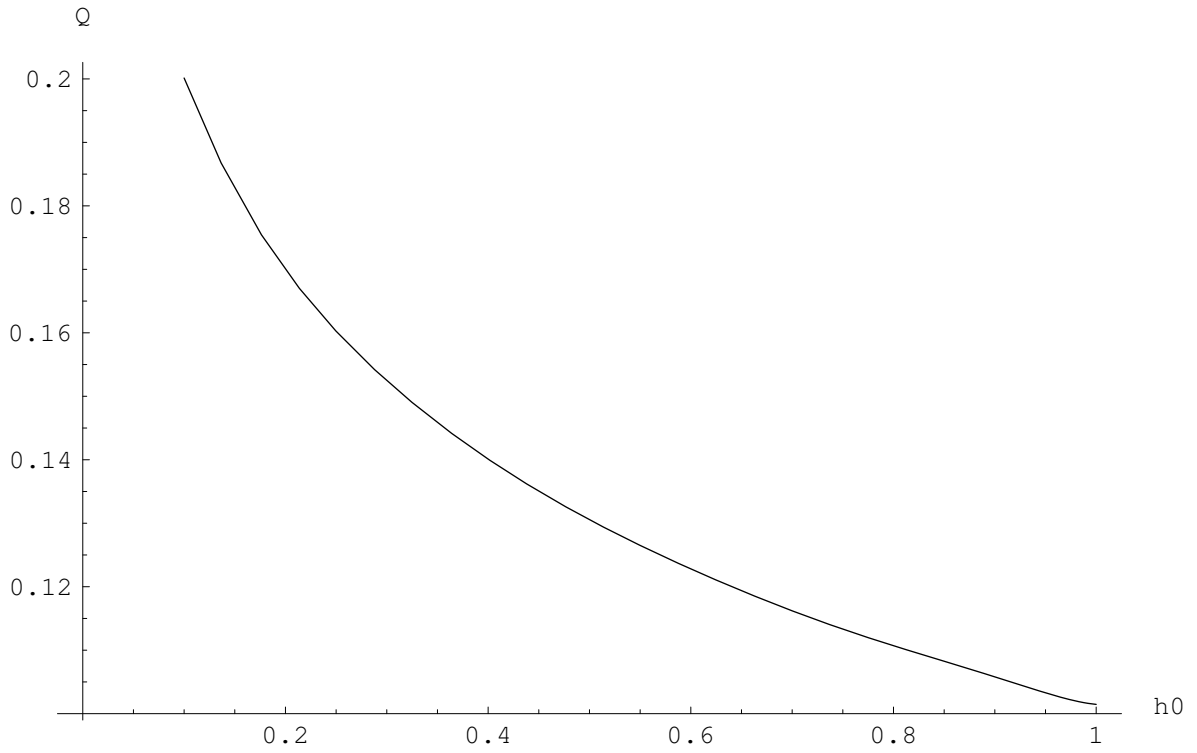

Figure 5.24: Graph showing Q as a function of h_0 for $\mathcal{P} = 0.5$, $\mathcal{T} = 0.5$, $C_I = 0.1$, and $\beta = 1$.

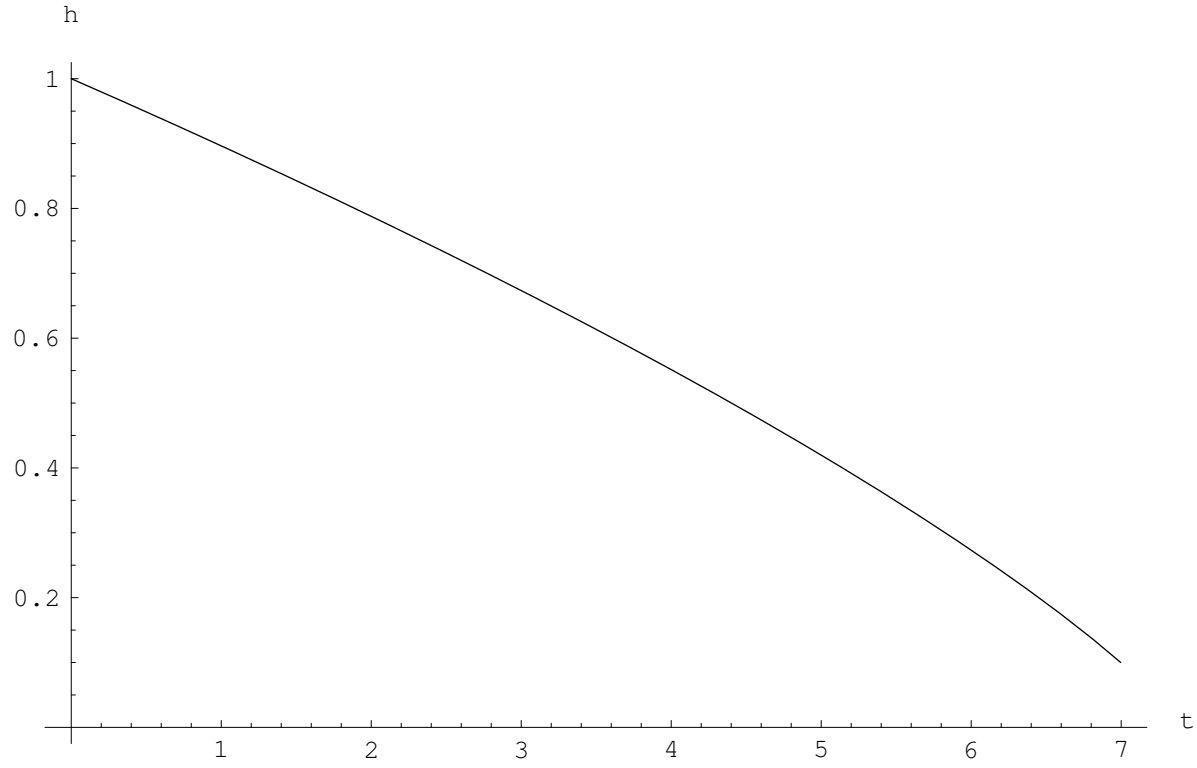

Figure 5.25: Graph showing lamella thickness with time for $\mathcal{P} = 0.5$, $\mathcal{T} = 0.5$, $C_I = 0.1$ and $\beta = 1.0$.

5.3.8 Conclusions

We present a summary of the important results and behaviour of the solutions that we have uncovered in this section.

- We identified a relationship between the lamella concentration and thickness, which we used in the solution of the transition region model.
- In the summary §5.3.5, we presented conditions on two key parameters, $\mathcal{K}$ and $\mathcal{B}$ which determine the behaviour at the Plateau border end and lamella end of the transition region respectively, in the case when $\beta = 0$. The corresponding conditions when $\beta \sim O(1)$ were given in §5.3.7.3.
- We examined numerical solutions to the transition region model and showed that they had the behaviour predicted by the key parameters.
- The solutions fall into three categories: monotonic solutions, solutions that are nonmonotonic but tend monotonically to the lamella thickness, and nonmonotonic solutions that oscillate as the lamella is approached.
- We obtained the flux of liquid from the lamella into the transition region, as a function of lamella thickness, for a given set of parameters.
- We solved the lamella model, using this flux, to obtain a time to critical thickness, which on redimensionalising, was 90 seconds in the $\beta = 0$ case, and was slightly reduced in the $\beta = 1$ case.
- We found (numerically) that, for some parameter values, the flux tends to infinity at a finite lamella thickness. We were able to predict this thickness by considering the $Q \to \infty$ limit of the model. We conjectured that viscosity enters the model when Q became sufficiently large, and enables the lamella to carry on thinning.
- We saw that, when β is nonzero, eddies are set up in the transition region which draw liquid into the Plateau border along the centreline in one case, and along the free surfaces in another. The size of $\mathcal{K}$ determines which scenario occurs.

In the following two sections, we present and solve the models for a lamella stabilised by CTAB and an insoluble pulmonary surfactant. The methodology used is identical to that in this section, so we omit the bulk of the details.

5.4 Example: evolution of a thin film stabilised by CTAB

We use the ideas of the previous section to look at drainage of a lamella stabilised by CTAB. We recall that for CTAB, $D \sim 5 \times 10^{-10}$ m^2 s^{-1}, and if we proceed using the velocity scaling given in (5.35) we find that $U \sim 2.5 \times 10^{-6}$ m s^{-1}. We calculate Pe ~ 0.05 but $\beta \sim 2500$. Since $\epsilon \sim 10^{-3}$, including such a large β is asymptotically dubious. We conclude that the velocity used in §5.3 is inappropriate in this case. We note that we must still have a nontrivial balance in the surfactant equation in the transition region or we will not have gradients in the concentration field and hence a Marangoni stabilisation. To obtain (5.35), we balanced diffusion with surface convection in the transition region, while assuming that the resulting Péclet number would be $O(1)$ (with respect to ϵ). Here, we choose to balance diffusion to the surface and surface convection while assuming that Pe $\sim O(\epsilon^{-1})$. With this in mind, we set

$$S = 1 \qquad U = \frac{D}{\eta}, \tag{5.149}$$

which gives $U \sim 5 \times 10^{-5}$ m s^{-1}. Our timescale here is $T = L/U = 20$ s. We calculate the parameter values, and find that Pe $\sim 100 \sim O(\epsilon^{-1})$, $\tilde{\beta} \sim 5$, Ca $\sim 10^{-6}$ and $\mathcal{T} \sim O(1)$ (for $C \sim O(10^{-3}) - O(10^{-2})$ mol m^{-3}) and so we use the model given in §4.5.2.1 for flows where Pe $\sim O(\epsilon^{-1})$ and $S \sim O(1)$. We set ϵPe $= \mathcal{P}^*$, and we operate in an intermediate regime where diffusion may be neglected. Our plan, again, is to consider the Plateau border first, then the lamella and finally to match between the two.

5.4.1 Plateau Border

Here, we check that the concentration may be considered constant in the Plateau border. We follow the ideas of §5.3.2. The flux out is, again, due to bulk and surface convection, and, since (5.50) is independent of the velocity scale chosen, we read off that $\mathrm{d}C_{Pb}/\mathrm{d}t \sim 10^{-1}QC_l$, *i.e.* the concentration in the Plateau border is constant on the lamella drainage timescale. We also calculate Ca $\sim 10^{-6}$ and so we also conclude that the Plateau border shape is governed by capillary statics.

5.4.2 Lamella

In the lamella, the model is identical to that described in §5.3.3, and so we read off

$$C = \frac{C_I(2 + \mathcal{P}^*)h}{2 + \mathcal{P}^* h}, \tag{5.150}$$

$$u = \frac{Q(h)}{h}x, \tag{5.151}$$

$$\int_h^1 \frac{d\mathcal{H}}{Q(\mathcal{H})} = t. \tag{5.152}$$

5.4.3 Transition region

Our transition region model reads

$$(\bar{u}h)_\xi = 0, \tag{5.153}$$

$$hh_{\xi\xi\xi} = \mathcal{T}C_\xi, \tag{5.154}$$

$$\mathcal{P}^* h\,(uC_\xi) + 2\,(u_s C)_\xi = 0, \tag{5.155}$$

where

$$u_s = \bar{u} - \frac{\beta}{2}h^2 h_{\xi\xi\xi}, \tag{5.156}$$

as before. We might, in the first instance, think that we would be unable to apply two conditions on the concentration problem, since we have lost the diffusion term from (5.155). However, we remember that the lubrication part of the surface convection term also provides a second derivative (for C), and so we have *not* reduced the order of the problem by neglecting diffusion.

Equations (5.153)-(5.155) can be simplified to

$$hh_{\xi\xi} - \frac{h_\xi^2}{2} = \mathcal{T}(C - C_0), \tag{5.157}$$

$$\beta\mathcal{T}hCC_\xi = \mathcal{P}^* Q(C - C_0) + 2Q\left(\frac{C}{h} - \frac{C_0}{h_0}\right). \tag{5.158}$$

We note that we are able to obtain (5.158) from (5.125) by dividing through by β in (5.125) and then taking the limit $\beta \to \infty$ while $Q/\beta \sim O(1)$. Hence, the asymptotic solutions presented in §5.3.7 can be easily modified to cater for our current situation (by removing the constant 1 that occurs in the denominators of a_4 and a_5, for example), and we have a unique solution (up to translation) leaving $\xi = \infty$.

We set $Q^* = \frac{Q}{\beta}$, and work with Q^* in our numerical simulations. We take $\mathcal{T} = 1$, $\mathcal{P}^* = 0.1$ $\beta = 10.4$ and $C_I = 0.1$, and we vary h_0 from 0.1 to 1 as before, to find Q^* as a function of h_0. We show the behaviour in Figure 5.26.
We find that

$$\int_{0.1}^1 \frac{d\mathcal{H}}{Q^*} = 3.61, \tag{5.159}$$

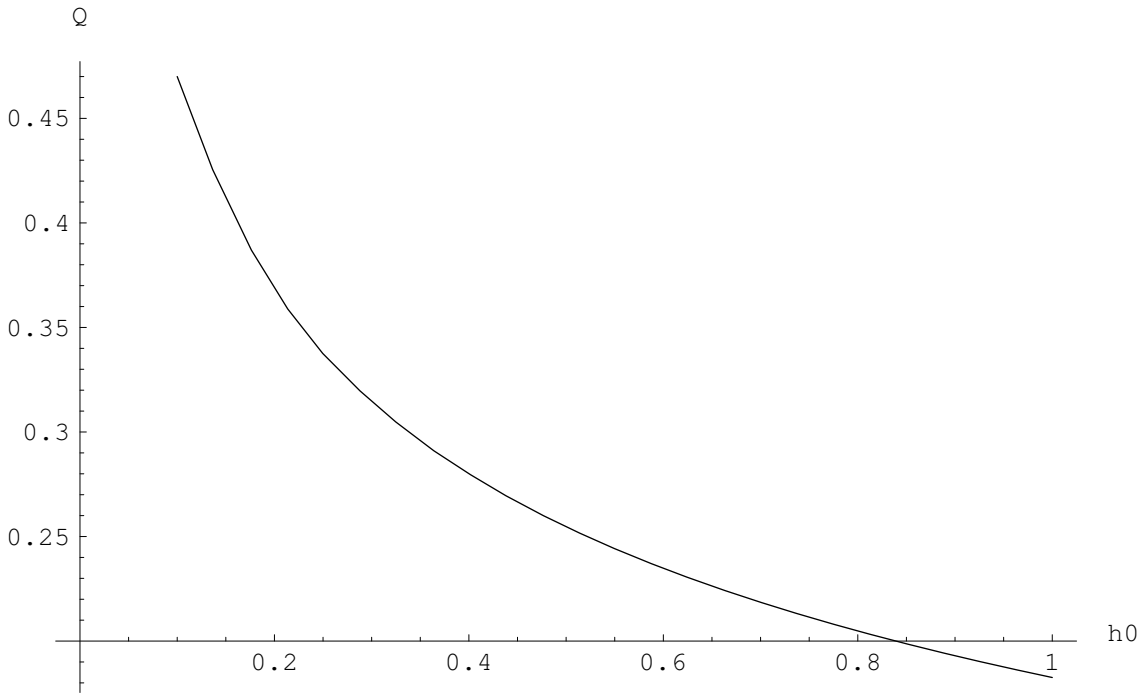

Figure 5.26: Graph showing the variation of Q^* with h_0 for $\mathcal{T} = 1$, $\mathcal{P}^* = 0.1$ and $C_I = 0.1$

and so the time to rupture $t = 3.61/\beta = 0.347$. Hence, redimensionalising, we find that $t_D^{\text{crit}} = 6.94$ s.

We note that as $Q \to \infty$, (5.157)-(5.158) has the same leading-order behaviour as (5.92) and so the critical thickness defined by (5.111) applies to this problem too.

5.4.4 Implications

We found a rupture time for a lamella stabilised by a dilute CTAB solution to be about 7 seconds. We note that this is a plausible time for collapse of such a film. We comment that neglecting the diffusion term has resulted in a model which exhibits the same qualitative behaviour as shown in the previous section (where diffusion was included).

We shall use the function $Q(h_0)$ found in this section in the next chapter when describing a macroscopic foam model.

5.5 Example: evolution of films stabilised by insoluble surfactants

In the presence of an insoluble surfactant, we include viscous, capillary, Marangoni, convective and diffusive effects. Assuming symmetry about the centerline, we have

$$h_t + (\bar{u}h)_x = 0, \tag{5.160}$$

$$(4h\bar{u}_x)_x - \frac{2\mathrm{Ma}}{\epsilon}\Gamma_x + \frac{\epsilon}{2\mathrm{Ca}}hh_{xxx} = 0, \tag{5.161}$$

$$\mathrm{Pe}_s(\Gamma_t + (u_s\Gamma)_x) = \Gamma_{xx}, \tag{5.162}$$

where

$$u_s = \bar{u} - \frac{\epsilon^3}{24\mathrm{Ca}}h^2h_{xxx}, \tag{5.163}$$

$$p = -2\bar{u}_x - \frac{\epsilon}{2Ca}h_{xx}. \tag{5.164}$$

We note that in this model we include surface diffusion, which has thus far been neglected. For realistic velocities we expect the viscous term in (5.161) to be negligible compared to the other two terms (taking $U \sim 10^{-4}$ m s^{-1} for example, the viscous term is $O(10^{-2})$) and when we neglect this term, the problem is somewhat degenerate unless we include the surface diffusion term (for example, there is no intrinsic velocity scale).

We choose our velocity scaling by balancing surface diffusion and convection in the transition region, which tells us that

$$U = \frac{D_s}{\sqrt{\epsilon aL}}. \tag{5.165}$$

Using a value for D_s for a pulmonary surfactant , given by Halpern and Grotberg [32], of 1×10^{-8} m^2 s^{-1}, we find that $U \sim 5 \times 10^{-4}$ m s^{-1}. We calculate $\tilde{\beta} \sim 0.5$ and, with a choice of $\Delta\gamma \sim 5 \times 10^{-5}$ N m^{-1}, we have $\mathcal{T} \sim 1.6$. We find our timescale $T = L/U = 2$ s. The model that holds in the lamella reads

$$h_t + (uh)_x = 0, \tag{5.166}$$

$$\Gamma_x = 0, \tag{5.167}$$

$$\Gamma_t + (u\Gamma)_x = 0, \tag{5.168}$$

while in the transition region we have

$$(\bar{u}h)_\xi = 0, \tag{5.169}$$

$$\mathcal{T}\Gamma_\xi = hh_{\xi\xi\xi}, \tag{5.170}$$

$$(u_s\Gamma)_\xi = \Gamma_{\xi\xi}, \tag{5.171}$$

where

$$u_s = \bar{u} - \tilde{\beta}h^2 h_{\xi\xi\xi}. \tag{5.172}$$

Again, we consider the Plateau border first, then the lamella, and then the transition region.

5.5.1 Plateau border

Here, the flux of surfactant from the lamella into the Plateau border is entirely due to surface convection. Therefore

$$\frac{\mathrm{d}\Gamma_{Pb}}{\mathrm{d}t} \sim \frac{hu\Gamma_l}{a^2}, \tag{5.173}$$

where Γ_l is the concentration in the lamella. Nondimensionalising, we find that

$$\frac{\mathrm{d}\Gamma_{Pb}}{\mathrm{d}t} \sim \frac{\epsilon L^2}{a^2} Q\Gamma_l, \tag{5.174}$$

and we calculate $\mathrm{d}\Gamma_{Pb}/\mathrm{d}t \sim 6 \times 10^{-3} Q\Gamma_l$ and so we conclude that Γ is constant in the Plateau border on the lamella drainage timescale. Here, Ca $\sim 10^{-5}$ and so we also conclude that the Plateau border is dominated by capillary statics.

5.5.2 Lamella

The tangential force balance (5.167) immediately integrates to give $\Gamma = \Gamma(t)$. If we assume that $h = 1$ and $\Gamma = \Gamma_I$ initially, the solution is

$$\Gamma = \Gamma_I h, \tag{5.175}$$

with

$$u = \frac{Q(h)}{h}x, \tag{5.176}$$

and $h(t)$ is given by

$$\int_h^1 \frac{d\mathcal{H}}{Q(\mathcal{H})} = t. \tag{5.177}$$

We use the relationship between Γ and h in the transition region, and shall return to find the time to rupture once we have found $Q(h)$.

5.5.3 Transition region

We simplify the system by integrating (5.169), (5.170) and (5.171) and then, substituting for u_s, obtain

$$\bar{u}h = Q, \tag{5.178}$$

$$\mathcal{T}(\Gamma - \Gamma_0) = hh_{\xi\xi} - \frac{h_\xi^2}{2}, \tag{5.179}$$

$$\Gamma_\xi = \frac{Q}{1 + \tilde{\beta}\mathcal{T}h\Gamma}\left(\frac{\Gamma}{h} - \frac{\Gamma_0}{h_0}\right), \tag{5.180}$$

where we have applied the conditions that $h \to h_0$ and $\Gamma \to \Gamma_0$ as $\xi \to -\infty$. Here, it is clear that, with $\tilde{\beta} = 0$, the surfactant distribution equation (5.180) cannot admit a solution which has $\Gamma \to \Gamma_0$ as $\xi \to -\infty$ *and* $\Gamma \to 1$ as $\xi \to \infty$. Thus, we conclude that we must include $\tilde{\beta} \neq 0$ in the model.

5.5.4 Asymptotics of the transition region

We examine the behaviour of the system and we find that there is a unique solution leaving $\xi = \infty$. We examine the behaviour as $\xi \to -\infty$ and we find that there is a one parameter family of solutions. As in the previous cases, we have either monotonic or oscillating behaviour, and the condition for oscillations now reads

$$\mathcal{B} = \frac{2Qh_0^2}{3\sqrt{3}\sqrt{\mathcal{T}\Gamma_I h_0}(1 + \tilde{\beta}\mathcal{T}\Gamma_I h_0^2)} < 1. \tag{5.181}$$

We may use the asymptotic form of the solution as $\xi \to \infty$ to find the surface and centreline velocities as the liquid approaches the Plateau border. We find that

$$h^2 h_{\xi\xi\xi} \sim \frac{Q\Gamma_I}{\tilde{\beta}} + O\left(\frac{1}{\xi}\right), \tag{5.182}$$

for large ξ, so

$$u_s \sim \Gamma_I Q + O\left(\frac{1}{\xi}\right), \qquad u_{cl} = -\frac{\Gamma_I Q}{2} + O\left(\frac{1}{\xi}\right), \qquad \text{as} \qquad \xi \to \infty, \tag{5.183}$$

i.e., we *always* have flow out along the free surfaces and back along the centreline, for $Q > 0$. We note that this is counter-intuitive, and that this is a manifestation of the fact that the concentration tends to 1 from above as $\xi \to \infty$.

5.5.5 Solution

We illustrate the solution in the limit when $\tilde{\beta}$ becomes large compared to one. This is analagous to choosing the velocity scaling by setting $\tilde{\beta} = 1$ and then taking the limit $\mathrm{Pe} \to 0$. The surfactant model is then governed wholly by surface convection. In this case, we set $\mathcal{Q} = \frac{Q}{\tilde{\beta}\mathcal{T}}$, and (5.180) becomes

$$\Gamma_\xi = \frac{\mathcal{Q}}{h\Gamma}\left(\frac{\Gamma}{h} - \Gamma_I\right). \tag{5.184}$$

We employ the same solution procedure as previously, we choose the parameters parameters $\mathcal{T} = 0.5$ and $\Gamma_I = 0.1$ (and $\tilde{\beta} = 10$), and we solve the system to find $\mathcal{Q}$ for each h_0. We then solve the lamella model to find the time to rupture. For $\mathcal{T} = 0.5$ and $\Gamma_I = 0.1$, we show the graph of $\mathcal{Q}$ vs h_0 in figure 5.27. We calculate that

$$\int_{0.1}^{1} \frac{dh}{\mathcal{Q}} = 6.27, \tag{5.185}$$

and so,

$$\int_{0.1}^{1} \frac{dh}{Q} = \frac{6.27}{\mathcal{T}\tilde{\beta}} = t. \tag{5.186}$$

For $\tilde{\beta} = 10$, we have $t = 1.25$ and so, redimensionalising, we have $t_D^{\mathrm{crit}} = 2.5$ s. Again, this time is plausible for the drainage of a real lamella. We note that we have not yet considered the $Q \to \infty$ problem in this case.

5.6 Preliminary model: film stabilised by a well-mixed volatile component

In this section we present our thoughts on modelling a lamella stabilised by a well-mixed volatile component, but do not solve the problems arising. We include viscous, capillary and Marangoni effects, and also mass transfer across the surfaces. Here, we have two physical effects that we can use to select a velocity scaling; evaporation and convection. Since we wish to examine the behaviour generated by the ability of this component to evaporate, we use the evaporation number to determine the velocity scaling. In fact, we assume that the Plateau border is governed by capillary statics (as before) and that the concentration of the volatile component is constant there (we check that these are valid assumptions in §5.6.1). We are left with a choice of either (a) having evaporation in the lamella and not in the transition region, or (b) having no volatile in the lamella (to leading order) and then having evaporation in the transition region. We choose to work with the

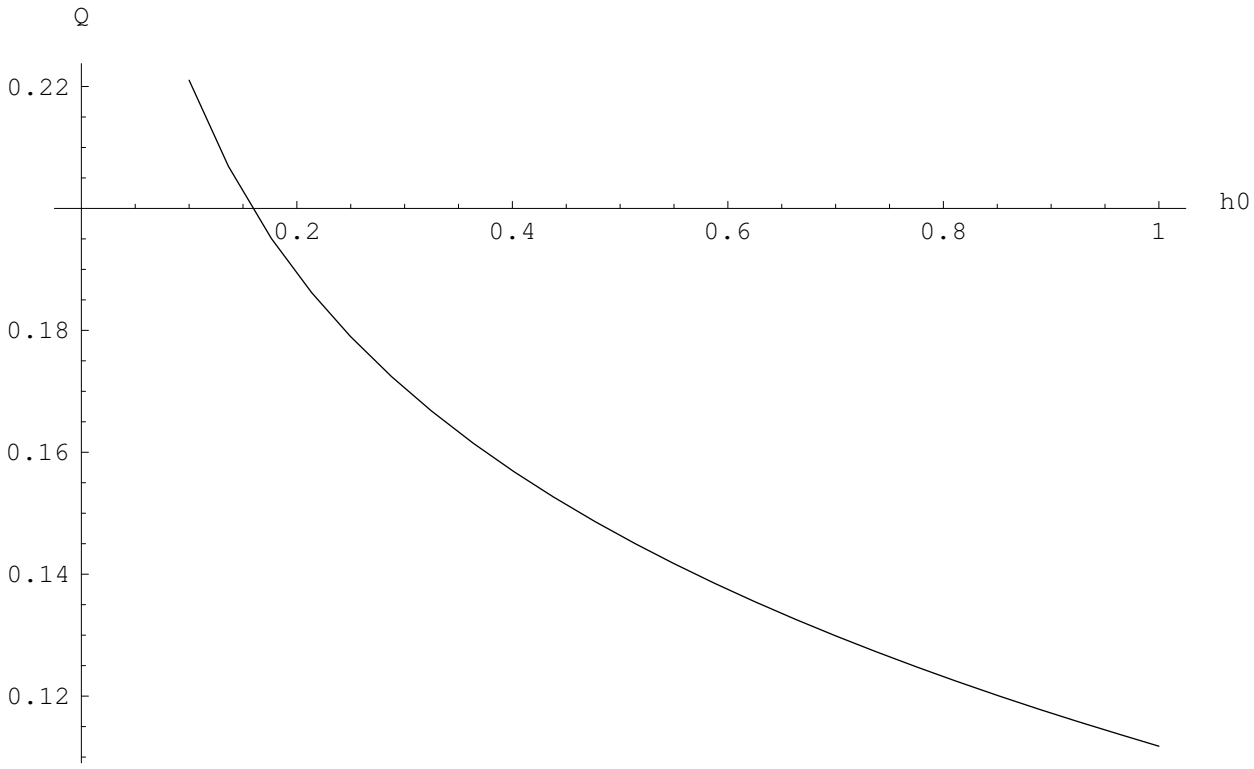

Figure 5.27: Graph showing the variation of $\mathcal{Q}$ with h_0 when $\mathcal{T} = 0.5$ and $\Gamma_I = 0.1$

former (since, when we attempted the latter, we were unable to effect the matching of the transition region into the Plateau border). We therefore set

$$U = \frac{E_0}{\epsilon}. \tag{5.187}$$

We note that this is fast ($U \sim 0.01$ m s^{-1} for $E_0 \sim 1 \times 10^{-5}$ m s^{-1} and $\epsilon \sim 10^{-3}$) and that the associated timescale is 10^{-1} s. We further assume that the Péclet number $\mathrm{Pe} \sim O(1/\delta)$ (*i.e.*, that the volatile has a large diffusivity).

The general model reads (see the summary in §3.8),

$$h_t + (\bar{u}h)_x + 2\mathcal{E}s = 0, \tag{5.188}$$

$$(4h\bar{u}_x)_x - \frac{2\mathrm{Ma}}{\epsilon}s_x + \frac{\epsilon}{2\mathrm{Ca}}hh_{xxx} = 0, \tag{5.189}$$

$$(hs_x)_x - \mathrm{Pe}h\left(s_t + \bar{u}s_x\right) - 2\mathrm{Pe}\mathcal{E}s(1-s) = 0. \tag{5.190}$$

Hence, using the velocity scaling (5.187), the leading-order lamella model reads

$$h_t + (uh)_x + 2s = 0, \tag{5.191}$$

$$s_x = 0, \tag{5.192}$$

$$h\left(s_t + us_x\right) + 2s(1-s) = 0, \tag{5.193}$$

while in the transition region we have

$$uh = Q, \tag{5.194}$$

$$hh_{\xi\xi} - \frac{1}{2}h_\xi^2 = \mathcal{T}(s - s_0), \tag{5.195}$$

$$hs_\xi - \mathcal{P}Q(s - s_0) = 0, \tag{5.196}$$

where s_0 is the lamella concentration.

5.6.1 Plateau border

We calculate the flux from the lamella into the Plateau border. The flux out from the lamella is due to convection, and so

$$\frac{\mathrm{d}s_{Pb}}{\mathrm{d}t} \sim \frac{uh}{a^2}s_l, \tag{5.197}$$

where s_l is the concentration in the lamella. On nondimensionalising (5.197) reads

$$\frac{\mathrm{d}s_{Pb}}{\mathrm{d}t} \sim \frac{\epsilon L^2}{a^2}Qs_l \sim 6 \times 10^{-3}Qs_l. \tag{5.198}$$

Hence, the concentration in the Plateau border can be considered constant. We also calculate that $\mathrm{Ca} \sim 10^{-4}$ and so we conclude that the Plateau border shape is governed by capillary statics.

5.6.2 Lamella model

Since the consequence of (5.192) is that $s = s(t)$, for simplicity we seek a solution where $h = h(t)$, and, applying $uh = Q$ at $x = 1$, we find that

$$u = \frac{Q(h)}{h}x, \tag{5.199}$$

and the problem for h and s reads

$$h_t + Q + 2s = 0, \tag{5.200}$$

$$hs_t + 2s(1-s) = 0, \tag{5.201}$$

which we couple with the conditions $h = 1$ and $s = s_I$ at $t = 0$. Once Q has been found from the transition region, the evolution of h and s is determined by (5.200) and (5.201).

5.6.3 Transition region

As previously, we consider how many boundary conditions we are imposing on the system. We set

$$h \sim \frac{a_1}{2}\xi^2 + a_2\xi + a_3 + \frac{a_4}{\xi} + \frac{a_5}{\xi^2} + O\left(\frac{1}{\xi^3}\right), \tag{5.202}$$

as $\xi \to \infty$. We find that

$$s = s_0 + \frac{1}{\mathcal{T}}\left(a_1 a_3 - \frac{a_2^2}{2}\right) + \frac{3a_1a_4}{\mathcal{T}\xi} + \frac{3a_2a_4 + 6a_1a_5}{\mathcal{T}\xi^2} + O\left(\frac{1}{\xi^3}\right). \tag{5.203}$$

Using the boundary conditions

$$h_{\xi\xi} = 1 \qquad s = s_{pb} \qquad \text{as} \qquad \xi \to \infty, \tag{5.204}$$

we find that $a_1 = 1$, $a_3 = \mathcal{T}(s_{pb} - s_0)$ and we may set $a_2 = 0$ due to translational invariance. We use (5.196) to find the other constants in the expansion. For example,

$$a_4 = -\frac{2}{3}\mathcal{T}(s_{pb} - s_0). \tag{5.205}$$

The solution is, given all the parameters, again uniquely determined by the conditions at $\xi = \infty$.

As $\xi \to -\infty$, we linearise about the thickness h_0 and the concentration s_0, assumed known. We set $h = h_0(1 + ae^{\lambda\xi})$, and we find that $s = s_0 + h_0^2 a\lambda^2 e^{\lambda\xi}/\mathcal{T}$. We use (5.196) to find an equation for λ,

$$\lambda^2\left(\lambda - \frac{\mathcal{P}Q}{h_0}\right) = 0, \tag{5.206}$$

and so we have $\lambda = \mathcal{P}Q/h_0$ or zero. Thus there is a single decaying solution as $\xi \to -\infty$ and, once translational invariance is eliminated, this implies that there is a unique solution eminating from $\xi = -\infty$. This differs from all our previous models in which there was a one-parameter family of solutions coming out of $\xi = -\infty$, and implies that in general the present problem is not well posed.

To attempt to explain why we have lost the degree of freedom, we include the so-far neglected viscous term, and repeat our search for the behaviour at minus infinity. The model in this case reads

$$-\nu Q\frac{h_\xi}{h} + hh_{\xi\xi} - \frac{h_\xi^2}{2} = \mathcal{T}(s - s_0), \tag{5.207}$$

$$hs_\xi = \mathcal{P}Q(s - s_0), \tag{5.208}$$

where $\nu = 8\mu E_0\delta/(\epsilon^2\gamma)$. When we substitute for $h = h_0(1 + ae^{\lambda\xi})$, we find that λ satisfies

$$\lambda^3 - \lambda^2\left(\frac{\nu Q}{h_0^2} + \frac{\mathcal{P}Q}{h_0}\right) + \frac{\nu\mathcal{P}Q^2}{h_0^3}\lambda = 0. \tag{5.209}$$

The roots of this equation are

$$\lambda = 0, \frac{\nu Q}{h_0^2}, \frac{\mathcal{P}Q}{h_0}, \tag{5.210}$$

and so we see that we recover the roots given above in the limit as $\nu \to 0$. The implication is that there is a region between the lamella and the transition region in which viscous effects must be included no matter how small ν is. In this way, two decaying solutions as $\xi \to -\infty$ are recovered and thus the problem is rendered (at least potentially) well posed.

5.6.4 Implications

In this section we have presented a preliminary model for a thin film containing a volatile component. Some more careful asymptotic analysis of the effect of the viscous term is required before we can proceed with a numerical solution.

5.7 Films stabilised by the presence of surface viscosity

In this section we discuss the use of surface viscosity in place of our Marangoni-induced stress. It is our aim here to show that this simplification of the model, while enabling an exact solution to the problem which has a plausible rupture time, does not result in a solution which exhibits the behaviour that we have uncovered in §5.3. The liquid model (see §4.4.4) reads

$$h_t + (\bar{u}h)_x = 0, \tag{5.211}$$

$$(4h\bar{u}_x)_x + 2\mathcal{V}_s\left(\eta u_{sx}\right)_x + \frac{\epsilon}{2\mathrm{Ca}}hh_{xxx} = 0. \tag{5.212}$$

We suppose that $\Lambda \sim 2 \times 10^{-7}$ Kg s^{-1} in line with Dey et al. [27] although we note that this parameter appears to vary widely in the literature (for example Bikerman [11] has surface viscosity of 3×10^{-5} Kg s^{-1}). Hence, the viscosity ratio is $O(\epsilon^{-1})$.

To effect our decomposition of the liquid domain, we assume that the Plateau border is governed by capillary-statics and that the lamella is governed by surface viscosity (and we check that these assumptions hold *a posteriori*). We must then generate a balance between capillarity and surface viscosity in the transition region between the two. This determines the velocity scale, which we find by setting $\mathcal{V}_s\mathrm{Ca}\delta/\epsilon = 1$ whence

$$U = \frac{\gamma\epsilon'\epsilon L}{\Lambda}. \tag{5.213}$$

With the magnitude of surface viscosity given above and taking $\gamma = 7 \times 10^{-2}$ N m^{-1}, we find that $U \sim 1.8 \times 10^{-2}$ m s^{-1}. We also have Ca $\sim \epsilon'^2$, so $\bar{u} = u_s = u$. We note that, since the capillary number is small, we have verified that the Plateau border is governed by capillary-statics and that the lamella is dominated by surface viscosity, as assumed earlier.

In general, $\eta = \eta(C)$, but for illustrative purposes we proceed by assuming that the surface viscosity is constant (in line with a number of authors, see Braun et al. [12] for example), and, without loss of generality, $\eta = 1$. We do not, therefore, need to consider the surfactant problem at all, and we follow the layout of §5.2 for a pure liquid, *i.e.*, we consider the transition region first and then the lamella second.

5.7.1 Transition region

After making the $x - 1 = \delta\xi$ scaling, in the transition region we have

$$uh = Q, \tag{5.214}$$

$$2\left(u_\xi\right)_\xi + \frac{1}{2} h h_{\xi\xi\xi} = 0, \tag{5.215}$$

which we couple with the boundary conditions

$$h \to h_0, u \to \frac{Q}{h_0}, \qquad \text{as} \qquad \xi \to -\infty, \tag{5.216}$$

$$h_{\xi\xi} \to 1 \qquad \text{as} \qquad \xi \to \infty. \tag{5.217}$$

We integrate (5.215), and apply the boundary conditions to yield

$$h_\xi = B\sqrt{h} - \frac{8Q}{5h^2}. \tag{5.218}$$

As in §5.2 earlier, applying the condition as $\xi \to \infty$ gives $B = \sqrt{2}$, and we obtain the relationship between Q and h_0 from (5.218),

$$Q = \frac{5\sqrt{2} h_0^{\frac{5}{2}}}{8}. \tag{5.219}$$

We note that Q decreases as h_0 decreases, in line with the surfactant-free case, and in contrast to the Marangoni-stabilised films.
We scale $\xi = \sqrt{h_0}\hat{\xi}$ and $h = h_0\hat{h}$, and we obtain

$$\hat{h}^2 \hat{h}_{\hat{\xi}} = \sqrt{2}\left(\hat{h}^{\frac{5}{2}} - 1\right), \tag{5.220}$$

which we integrate to yield

$$\sqrt{2}\hat{\xi} = 2\sqrt{\hat{h}} - \frac{1}{5}\sqrt{2(5+\sqrt{5})}\arctan\left[2\sqrt{\frac{2}{5+\sqrt{5}}}\left(\frac{1}{4}(1-\sqrt{5})+\sqrt{\hat{h}}\right)\right] -$$
$$\frac{1}{5}\sqrt{2(5-\sqrt{5})}\arctan\left[2\sqrt{\frac{2}{5-\sqrt{5}}}\left(\frac{1}{4}(1+\sqrt{5})+\sqrt{\hat{h}}\right)\right] + \frac{2}{5}\log[-1+\sqrt{\hat{h}}] -$$
$$\frac{1}{10}(1-\sqrt{5})\log\left[1+\frac{1}{2}(1-\sqrt{5})\sqrt{\hat{h}}+\hat{h}\right] - \frac{1}{10}(1+\sqrt{5})\log\left[1+\frac{1}{2}(1+\sqrt{5})\sqrt{\hat{h}}+\hat{h}\right]. \quad (5.221)$$

The transition region thickness given by (5.221) is shown in Figure 5.28. As in the pure

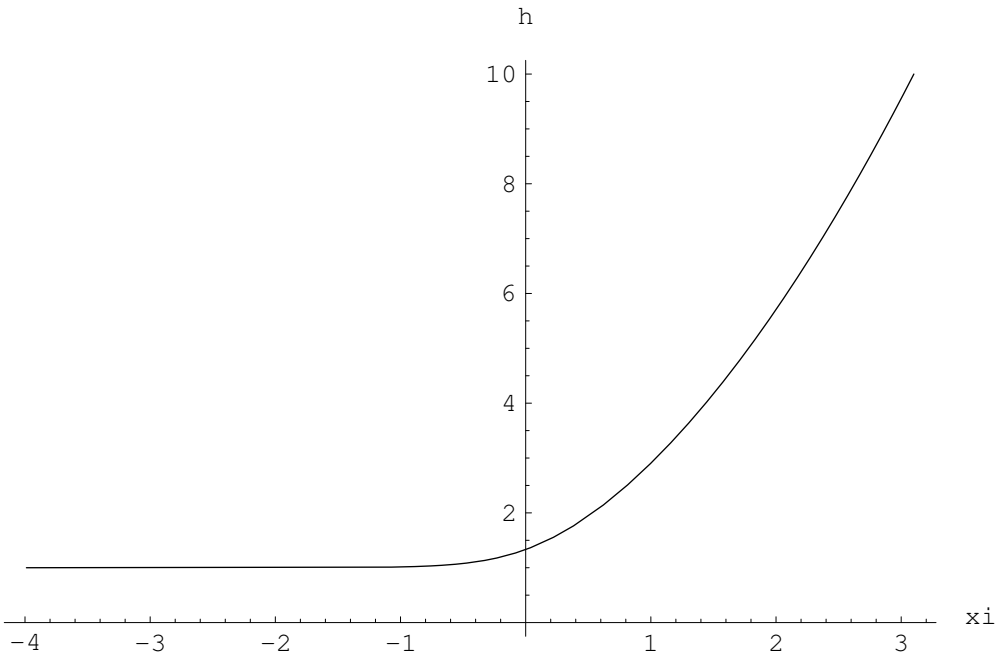

Figure 5.28: Transition region shape

water case earlier, this shape is monotonic.

5.7.2 Lamella model

In the lamella, we have

$$h_t + (uh)_x = 0, \quad (5.222)$$

$$u_{xx} = 0, \quad (5.223)$$

coupled with the initial and boundary conditions

$$u = 0 \qquad \text{at} \qquad x = 0, \quad (5.224)$$

$$u = \frac{Q}{h} \qquad \text{at} \qquad x = 1, \quad (5.225)$$

$$h = 1 \qquad \text{at} \qquad t = 0. \quad (5.226)$$

We assume that h is spatially independent and solve for u to give

$$u = \frac{5\sqrt{2}}{8} h^{\frac{3}{2}} x. \tag{5.227}$$

The equation for h then reads

$$h_t + \frac{5\sqrt{2}}{8} h^{\frac{5}{2}} = 0, \tag{5.228}$$

which has solution

$$h = \left(1 + \frac{15}{8\sqrt{2}} t\right)^{-\frac{2}{3}}, \tag{5.229}$$

whence

$$u = \frac{5\sqrt{2}}{8\left(1 + \frac{15}{8\sqrt{2}} t\right)} x. \tag{5.230}$$

We redimensionalise, and rearrange to find the time to rupture

$$t_D^{crit} = \frac{16\Lambda\sqrt{a}L}{15\sqrt{2}\gamma} \left(\left(\frac{1}{h_D^{crit}} \right)^{\frac{3}{2}} - \left(\frac{1}{h_D{}^*} \right)^{\frac{3}{2}} \right). \tag{5.231}$$

We calculate the critical time to rupture, $t_D^{crit} = 1.3$ s, given that the critical thickness for rupture is 0.1μm.

Thus, while the inclusion of a constant surface viscosity in place of our Marangoni term has enabled us to obtain an exact solution to the problem, which has a rupture time consistent with our Marangoni models, it has not produced the same behaviour of solution as our previous work, namely the dimpled solutions which are also seen in some experiments and the increase of the flux as the film thins.

In the case where the surface viscosity is larger, so that $u_s \neq \bar{u}$, we are unable to find an exact form for the solution even when the surface viscosity is constant, and we must resort to a numerical solution. If we allow the surface viscosity to vary with concentration too, we have the added problem that we must specify the constitutive relation for $\eta = \eta(\Gamma)$. If we assume that the relationship is linear, then the coupled problem reads

$$C\left(2\frac{Q}{h} - \beta h^2 h_{\xi\xi\xi}\right)_\xi + h h_{\xi\xi} - \frac{h_\xi^2}{2} = 0, \tag{5.232}$$

$$h C_\xi = PQ(C - C_0) + 2Q\left(\frac{C}{h} - \frac{C_0}{h_0}\right) - \beta C h^2 h_{\xi\xi\xi}. \tag{5.233}$$

The flux Q is now present in both equations, and the longitudinal force balance (5.232) has higher-order derivatives than before. This system is as complicated as the Marangoni formulations and so there is no benefit in considering it any further.

5.8 Conclusions

In this chapter, we have studied a number of models for the drainage of thin films in the presence of surfactants or volatile components. In each case, we have decomposed the liquid domain into a capillary-static meniscus, a time-dependent thinning film and a quasi-steady transition region between the two. We draw the following conclusions.

- In the absence of a Marangoni component, the drainage is governed by a balance between capillary and viscous forces. We found that the flux from the lamella into the transition region is given by $Q = 3\sqrt{2}h_0^{\frac{3}{2}}/16$. So, Q tends to zero as h_0 tends to zero. We found that $h \sim t^{-2}$, and concluded that h does not tend to zero in finite time. Imposing a critical rupture thickness, we found the time to rupture is of the order of 4×10^{-3} s.

- In the presence of a highly diffusive surfactant, the drainage is governed by a balance between Marangoni and capillary forces, and bulk diffusion, convection and surface convection. We first worked in the limit where the lubrication term is negligible. We were able to find a relationship between the concentration and thickness in the lamella. We solved the transition region problem numerically, and found that the flux *increases* as thickness decreases, suggesting rupture in finite time. We saw two types of solution: monotonic and nonmonotonic. The nonmonotonic solutions sometimes have oscillatory exponentially decaying behaviour, as predicted from analysing the behaviour as the lamella is approached. We found a rupture time of approximately 90 s.

- In some parameter regimes, we found that the flux becomes very large as the lamella thickness approaches a critical value. We were able to find this value by considering the limit as $Q \to \infty$. We hypothesised that, once this value has been reached, some neglected physics, such as viscous forces, must be re-introduced and the lamella ruptures very quickly.

- In the limit where the lubrication term is nonnegligible, the longitudinal velocity is parabolic across the transition region, and, when $\mathcal{K} > 1$, an eddy is produced which rotates in such a way that the liquid leaves the transition region along its centreline, and returns along the film's walls. When $\mathcal{K} < 1$ the eddy rotates in the opposite sense. We calculated that a rupture time for a typical set of parameters is 88 s.

- We formulated the model which describes a lamella stabilised by a surfactant like CTAB. Here, we found that diffusion is not important (and that neglecting this

term does not reduce the order of the problem) and we observe similar behaviour to that described above. We solved the transition region model numerically using realistic parameters for a dilute CTAB solution, and we found that the rupture time is 6.9 s.

- For an insoluble surfactant, we concluded that we must *always* have a parabolic profile for the velocity in the transition region. Again, there are monotonic and nonmonotonic solutions, but now we found that there is flow out along the free surfaces and back along the centreline for all fluxes $Q > 0$. We used typical parameter sizes for a pulmonary surfactant and calculated a rupture time of 2.5 s.

- We presented a model for a lamella stabilised by a volatile component. We plan to study the behaviour of this model in the future.

- In the presence of a constant surface viscosity, we found an analytic form for the flux. Here it reads $Q = 5\sqrt{2}h_0^{\frac{5}{2}}/8$, and hence the flux tends to zero as $h_0 \to 0$. We found that a lamella drains with thickness $h \sim t^{-\frac{2}{3}}$, which does not tend to zero in finite time. However, employing the rupture criterion, we calculated a rupture time of 0.66 s. We noted that including the surface viscosity term, while producing a plausible drainage time, did not capture the behaviour that we uncovered in our Marangoni work. We also noted that, since $\eta = \eta(\Gamma)$ in general, the problem for a surface-viscosity-stabilised lamella would be as complicated as that for a Marangoni-stabilised one.

In all these situations, the introduction of a Marangoni stress increases the time to the critical thickness, and also results in a flux that *increases* as the lamella thickness decreases.

We may extend this work in a number of ways. Firstly, we may relax the small concentration approximation, that is, use nonlinear relationships between C, Γ, and σ. This would result in a more complicated system in the transition region. Our solution procedure in this instance would be identical to that we have previously detailed and we would expect the results to be qualitatively the same. There are other regimes that we have not considered. For example, some surfactants may have small enough diffusivity that they will not be well-mixed in the transition region. In this limit, we would have to solve a two-dimensional problem for the concentration in the transition region. Obviously, more work is required in the interpretation of the critical thickness and importantly, in analysing the model including viscous terms to see whether the lamella continues to thin on this faster timescale.

In this chapter we have examined the microscopic flow between a lamella and a Plateau border in a foam. In the next chapter we use the knowledge of this drainage process when formulating several *ad-hoc* models for macroscopic foam drainage.

Chapter 6

Plateau border flow, macroscopic models and foam destruction

6.1 Introduction

In this chapter we present an overview of two other aspects of foam modelling, namely

- Flow within Plateau borders and macroscopic models.
- Effectiveness of foam destruction methods.

Our approach is different from that adopted in the previous chapters. Here, we concentrate on formulating phenomenological models. We hope that such models will give us insight into some macroscopic foam properties.

6.2 Plateau border flow

The bulk flow of liquid within a dry foam is through the network of Plateau borders, where gravitational forces are strong enough to drain the liquid through the foam. Previous work on the subject has been concerned with predicting (i) the height to which a foam will rise, (ii) the amount of liquid leaving the base of a standing foam, (iii) the hold-up of a foam (that is, the amount of the gaseous phase contained within the foam). Desai and Kumar [25], for example, present both experimental and modelling work on flows through foams. They note that models for Plateau border flow using no-slip boundary conditions at the Plateau border walls predict velocities significantly smaller than those they find experimentally (which are of the order of 5×10^{-3} m s^{-1} for bubble diameters of 1×10^{-2} m). They present a model for flow through a network of pipes of triangular cross-section, where the velocities at the vertices of these triangles are taken to be zero, and the velocity on the rest of the free surfaces obeys a surface-viscosity-controlled momentum balance.

Narsimhan [60] and Bhakta and Ruckenstein [10] include drainage from lamellae (using the lubrication equation for the thin film) into a model which couples conservation of liquid in the lamellae with conservation of liquid in the Plateau borders (which they allow to deform) and assumes given forms for the velocities in each region. They use a disjoining pressure to describe the difference in pressure between the lamellae and Plateau borders, and generate predictions about the film hold-up, and the height of a foam as it is formed. All these papers assume that the Plateau borders are either vertical or at a specified (single) angle, based on a uniform dodecahedron. Podual, Kumar and Gangdi [67] work with a modified tetrakaidecahedron, which has square, pentagonal and hexagonal faces, and they include transport along horizontal, vertical and oblique Plateau borders. They compare experimental results to their numerical solutions for the liquid drained from a foam.

Verbist and Weaire [76], Verbist, Weaire and Kraynik [77] and Grunnet-Jepsen, Darton and Whalley [21] all generate similar models, although they neglect the flow from the lamellae into the Plateau borders. They derive a partial differential equation for the evolution of the Plateau border area, assuming that the velocity obeys Darcy's law with the pressure controlled by surface tension and gravity. They discuss steady and travelling wave solutions to the equation.

We present Verbist and Weaire's derivation as an example of all the work described above. They suppose that the Plateau borders form a network of N independent vertical pipes, each with cross-sectional area $A(z,t)$ and having average velocity $u(z,t)$ in the direction of the pipe. Conservation of mass then reads

$$A_t + (uA)_z = 0. \tag{6.1}$$

The assumption that the net pressure gradient balances the viscous drag gives

$$\rho g + \gamma \left(\frac{1}{R}\right)_z - \frac{\eta^* u}{A} = 0, \tag{6.2}$$

where η^* is the effective viscosity of the liquid in the channel. This takes account of the stiffening of the Plateau border walls due to the presence of a surfactant. The pressure has been taken as equal to the excess capillary pressure. Here, R is the radius of curvature of each of the Plateau border walls as in Figure 6.1. R is related to A using

$$R = \frac{\sqrt{A}}{\left(\sqrt{3} - \frac{\pi}{2}\right)^{\frac{1}{2}}} = \sqrt{\frac{A}{C_1}}, \tag{6.3}$$

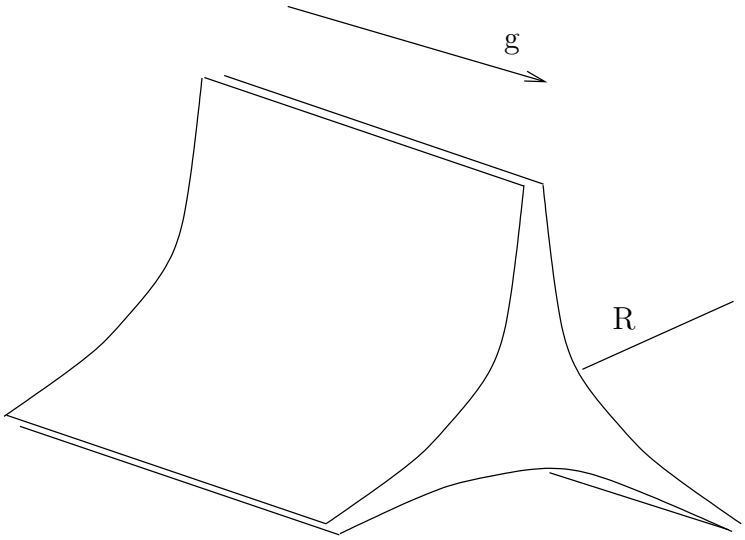

Figure 6.1: A Plateau border aligned with its centreline in the direction of gravity.

which defines C_1, the Plateau border parameter. Hence, the following equation gives the evolution of the Plateau border area

$$A_t + \left(\frac{\rho g A^2}{\eta^*} - \frac{\sqrt{C_1}\gamma}{2\eta^*} A^{\frac{1}{2}} A_z \right)_z = 0. \tag{6.4}$$

Verbist et al. [77] call this equation the 'Foam Drainage Equation'. We make the following observations.

- No account is taken of lamella drainage.
- Gravity acts to decrease the Plateau border area, while surface tension acts to increase the area.

In the next section, we use the limit $\eta^* \to 0$ to formulate a model for Plateau border flow which incorporates zero shear at the walls.

6.2.1 An *ad-hoc* model for drainage of a Plateau border incorporating zero shear on the walls

We choose to work in the limit of the model (6.1)-(6.2) in which the effective viscosity may be set to zero. This may be seen as analogous to choosing to work with a zero shear boundary condition in place of no slip. Thus, our nondimensional model for the Plateau border cross-sectional area and the velocity of the liquid in the Plateau border, with z measured vertically upwards from the bottom node of the Plateau border, reads

$$A_t + (uA)_z = 0, \tag{6.5}$$

$$BA + \left(\sqrt{A}\right)_z = 0, \tag{6.6}$$

where B is the Bond number, given by $B = \rho g\sqrt{A_0}L/(\sqrt{C_1}\gamma)$, L is the length of the Plateau border, and A_0 is a typical cross-sectional area. We note that this system has the obvious general solution

$$A = \frac{1}{(a_1(t) + Bz)^2} \qquad u = -\frac{a_1'(t)}{B} + \beta(t)(a_1(t) + Bz)^2. \tag{6.7}$$

We have, so far, neglected drainage from the lamellae into the Plateau borders. To include these terms, we modify the conservation of mass equation (6.5) to read

$$A_t + (Au)_z = \frac{3U_{drain}h_0L}{U_{pb}A_0}Q\left(h\right), \tag{6.8}$$

where U_{drain} is the lamella drainage velocity given in Chapter 5, U_{Pb} is a typical velocity of the liquid in the Plateau border, h_0 is the lamella thickness scaling, the factor of three corresponds to the number of lamellae draining into the Plateau border, and Q is the flux from a lamella into the Plateau border, as given in one of the many parameter regimes of the last chapter. We note that there is no intrinsic velocity scale present in (6.6). Thus the appropriate velocity scaling must be externally specified through the boundary conditions that we apply at the end of the Plateau borders, where they meet the nodes. We use (6.6) and (6.8) in the next section where we generate a macroscale model for a foam.

6.2.2 Application to foam build-up

6.2.2.1 Experimental set up

In this section, we present a rough model to describe foam build-up in an experimental rig. The rig has a square cross section and is shown in Figure 6.2. Gas is supplied at the bottom of the rig, at a speed of approximately $U_{sup} \sim 5 \times 10^{-2}$ m s^{-1}, and the surfactant solution in the rig begins to foam above the distributor. The bubbles that form at the bottom of the rig are nearly spherical, while at the top of the rig the bubbles are more polyhedral. The situation is dynamic, with bubbles rising in random patterns, but the foam forms a 'head' of constant height, approximately 40 cm, after an initial build up period. Given the material properties of the surfactant solution, and the gas velocity, we would like to be able to predict this height, and also the foam coarseness.

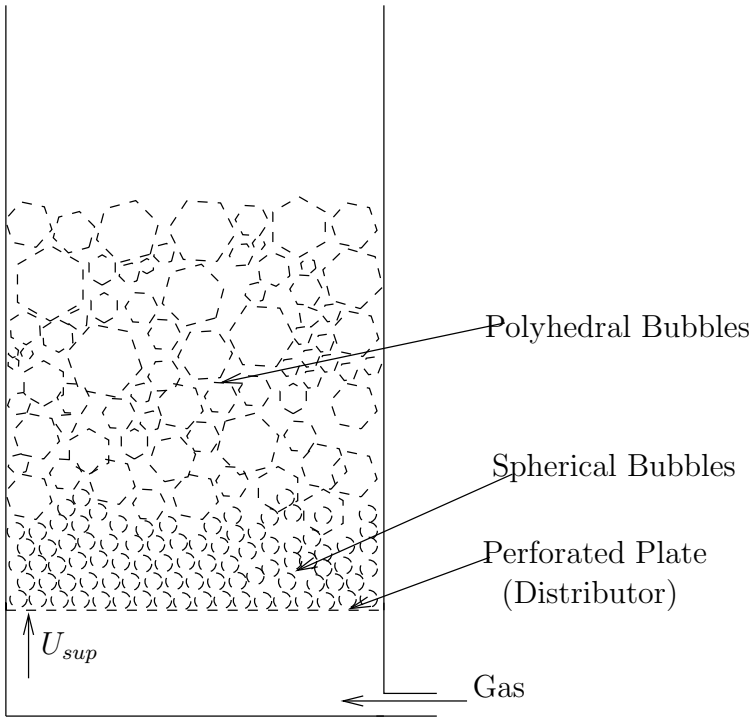

Figure 6.2: Diagram showing the foam rig.

6.2.2.2 Foam Height

We are able to make an initial estimate for the height of the foam, assuming that the bubbles are convected with the velocity of the gas supply until such time as they rupture. Hence,

$$H = T_{Rupt} U_{sup}. \tag{6.9}$$

With our rupture time for a lamellae stabilised by $CTAB$, given in §5.4, of 6.9 seconds, and a flow speed of 5 cm s^{-1}, we have that $H^d = 34.5$ cm. We are encouraged by the fact that this is the same order of magnitude as the height that is seen experimentally.

6.2.2.3 Homogenisation

We wish to construct a simple model which describes the foam coarseness (*i.e.* the area of the Plateau borders and the thickness of the lamellae) in the rig, the concentration of surfactant in the rig, and the height to which the foam rises. We formulate conservation equations for α, the volume fraction of the foam occupied by Plateau borders, β, the volume fraction occupied by the lamellae, and $1 - \alpha - \beta$, the volume fraction of the gaseous phase. Thus,

$$\alpha_t + (u_{Pb}\alpha)_z = q, \tag{6.10}$$

$$\beta_t + (u_l\beta)_z = -q, \tag{6.11}$$

$$-\alpha_t - \beta_t + (u_g(1-\alpha-\beta))_z = 0, \tag{6.12}$$

where q is the flux of volume fraction leaving the lamellae and entering the Plateau borders, u_{Pb} is the velocity of the liquid in the Plateau borders, u_l is the velocity of the liquid in the lamellae and u_g is the gas velocity. For convenience later, we now combine (6.10) and (6.11) to give

$$\alpha_t + \beta_t + (u_{Pb}\alpha)_z + (u_l\beta)_z = 0. \tag{6.13}$$

We suppose that each of the bubbles has the same number of associated lamellae and Plateau borders. We do this for simplicity but we note that this does not adequately describe the fact that bubbles are formed with random shapes. Further, we suppose that there are N such bubbles per unit volume. We call N_{Pb} the average number of Plateau borders per bubble (that is, the total number of Plateau borders in a unit volume/total number of bubbles, which depends on the geometrical properties of the bubble shape chosen and the typical volume of the bubbles produced by the distributor), N_l the average number of lamellae per bubble (defined in a similar way to N_{Pb}), A_l the area of the lamellae faces, h the average lamellae thickness, A the average area of the Plateau border and L the length of the Plateau border.

We suppose that all of these parameters are constant, but we can easily see that A_L, L and N need not be. Indeed we would expect A_L and L to increase from the bottom of the rig, and for N to decrease. Allowing N to vary due either to diffusion of gas between bubbles or to lamellae rupture within the foam will be the subject of future work.

Since there are three lamellae draining into each Plateau border, the volume fraction of liquid entering the Plateau borders is given by three times the product of the flux from a single lamella, the average number of Plateau borders per bubble and the number of bubbles per unit volume. Hence

$$q = 3Q_D L N N_{Pb}, \tag{6.14}$$

where Q_D is the dimensional form of the flux Q defined in the previous chapter. We note that, in general, this depends on the lamella thickness, the Plateau border area and the concentration of surfactant. We relate the volume fractions α and β to A and h respectively using

$$\alpha = N N_{Pb} L A \qquad \beta = N N_l A_L h. \tag{6.15}$$

Thus we are able to write the system as

$$h_t + (u_l h)_z = -\frac{3Q_D L N_{Pb}}{A_l N_l}, \tag{6.16}$$

$$N_{Pb}L\left(A_t + (u_{Pb}A)_z\right) + N_l A_L\left(h_t + (u_l h)_z\right) = 0, \tag{6.17}$$

$$\left(NN_{Pb}L(u_{Pb} - u_g)A + NN_l A_l(u_l - u_g)h + u_g\right)_z = 0. \tag{6.18}$$

We note that we have three equations for the five unknowns h, A, u_l, u_{Pb} and u_g. We must specify two constitutive relations to close this system. We choose to use the dimensional form of the quasi-steady relationship for A given in (6.6)

$$\sqrt{C_1}\gamma A_z + \rho g L A^{\frac{3}{2}} = 0, \tag{6.19}$$

and we set the simplest possible condition on the velocity of the lamellae: that it is identical to the gas velocity, and so

$$u_l = u_g. \tag{6.20}$$

Thus we now have five equations (6.16)-(6.20) for the five unknowns. Finally, we suppose that the surfactant present in the Plateau border is convected with the liquid in the Plateau border, and that the concentration in the lamella is given by the relationship that we found in the previous chapter, so

$$C_t^{Pb} + u_{Pb}C_z^{Pb} = 0, \tag{6.21}$$

$$C_l = \frac{C_I\left(1 + \frac{2\eta}{\epsilon L}\right)h}{2\eta + h}. \tag{6.22}$$

We have ignored the flux of surfactant from the lamella into the Plateau border, since we have already established in the previous chapter that this is negligible, and we have also ignored diffusion, since we can easily see that the associated Peclet number will be high. As the concentration of surfactant in the lamella decouples from the rest of the problem, we shall henceforth not explicitly discuss it. We also take the constant solution to (6.21), *i.e.* $C = C_0$, the concentration of the surfactant solution added to the system.

We are interested in the steady state of the system (once the constant head, height H, has formed). Henceforth, we set all time derivatives equal to zero. In order to close the model we must now decide on appropriate boundary conditions to apply. We suppose that we know the gas velocity at the bottom of the rig, and that the distributor produces bubbles with known lamella thickness and Plateau border area. We suppose that the top surface is determined by the condition that this is where the lamellae rupture. Finally, we assert that the net liquid content in the foam does not change once the steady state has been reached. Thus, the conditions read

$$u_g(0) = U_{sup}, \tag{6.23}$$

$$A(0) = A_0, \tag{6.24}$$

$$h(0) = h_0, \tag{6.25}$$

$$h(H) = h_D^{crit}, \tag{6.26}$$

with the further condition that the total liquid flux is zero.

We note that we have not chosen to specify the pressure at the top surface of the foam (which one might think would be a plausible boundary condition). In fact, we allow there to be a discontinuity in the pressure at the top surface, which we attribute to the curvature at the top surface.

We assume that the rig has width W (which is 20 cm) and we nondimensionalise with

$$A = A_0 A' \qquad h = h_0 h', \tag{6.27}$$

$$(u_{Pb}, u_g) = U_{sup}(u'_{Pb}, u'_g) \qquad z = W z'. \tag{6.28}$$

The nondimensionalised system reads

$$(u_g h)_z = -\frac{Q(h)}{\mathcal{F}}, \tag{6.29}$$

$$u_{Pb} A + \mathcal{G} u_g h = 0, \tag{6.30}$$

$$\mathcal{L}(u_{Pb} - u_g)A + u_g = (1 - \mathcal{L}(\mathcal{G} + 1)), \tag{6.31}$$

$$A_z + B A^{\frac{3}{2}} = 0, \tag{6.32}$$

where $\mathcal{F} = A_L U_{sup} N_l/(3LWU_{drain}N_{Pb})$, $\mathcal{G} = N_L A_L h_0/(N_{Pb} L A_0)$ and $\mathcal{L} = N N_{Pb} L A_0$. The boundary conditions become

$$u_g(0) = 1, \tag{6.33}$$

$$A(0) = 1, \tag{6.34}$$

$$h(0) = 1, \tag{6.35}$$

$$h(H) = h^{crit}. \tag{6.36}$$

The solution to (6.32) and (6.34) is

$$A = \frac{1}{(1 + Bz)^2}, \tag{6.37}$$

and we use (6.30) and (6.31) to give

$$u_g = \frac{1 - \mathcal{L}(\mathcal{G} + 1)}{1 - \mathcal{L}(\mathcal{G}h + A)} \qquad u_{Pb} = -\frac{\mathcal{G}h(1 - \mathcal{L}(\mathcal{G} + 1))}{A(1 - \mathcal{L}(\mathcal{G}h + A))}, \tag{6.38}$$

The final step is to solve (numerically) for the thickness h using

$$\left(\frac{(1 - \mathcal{L}(\mathcal{G} + 1))h}{1 - \mathcal{L}(\mathcal{G}h + A)}\right)_z = -\frac{Q(h)}{\mathcal{F}}. \tag{6.39}$$

As noted in Chapter 1, the total volume fraction of the liquid phase is small and thus we simplify the system by letting $\mathcal{L} \to 0$ (recall that $\mathcal{L}$ is the volume fraction of liquid in the Plateau borders at the bottom of the rig) while keeping B, $\mathcal{F}$ and $\mathcal{G} \sim O(1)$. Thus, in addition to (6.37), we have

$$u_g = 1, \tag{6.40}$$

$$u_{Pb} = -\mathcal{G}h(1 + Bz)^2, \tag{6.41}$$

$$z = \mathcal{F} \int_h^1 \frac{d\mathcal{H}}{Q(\mathcal{H})}, \tag{6.42}$$

$$H = \mathcal{F} \int_{h^{crit}}^1 \frac{d\mathcal{H}}{Q(\mathcal{H})}. \tag{6.43}$$

We note that the average Plateau border area and the average lamellae thickness decrease towards the top of the rig, *i.e.*, the foam becomes coarser.

In principle, given an experiment, we are now in the position to determine the physical characteristics of the foam in the rig. We can use the techniques of the previous chapter to determine the flux function (which depends on h, C and A), and then we would use the model presented in this section to determine the height of the top surface, average Plateau border area and average lamella thickness (and hence coarseness).

6.3 Foam destruction

In this section, we consider two experiments in which foam destruction occurs.

6.3.1 First experimental set up

The first involves the foam rig described in §6.2.2. Here, it was found (Sun [73]) that, if the rig was modified so that a sample of foam could be collected from the top, then the solution that was obtained from this sample acted as an antifoam, *i.e.*, when the solution was poured back into the foam rig, the foam height decayed rapidly to a tenth of its original size, remained at this level for a few minutes, and then slowly rose again, see Figure 6.3.

6.3.1.1 Homogenised model

We consider the amount of surfactant in the collected sample. The number of moles of surfactant collected are equal to the number of moles in a lamella multiplied by the number of lamellae (N_l) plus the number of moles in a Plateau border multiplied by the

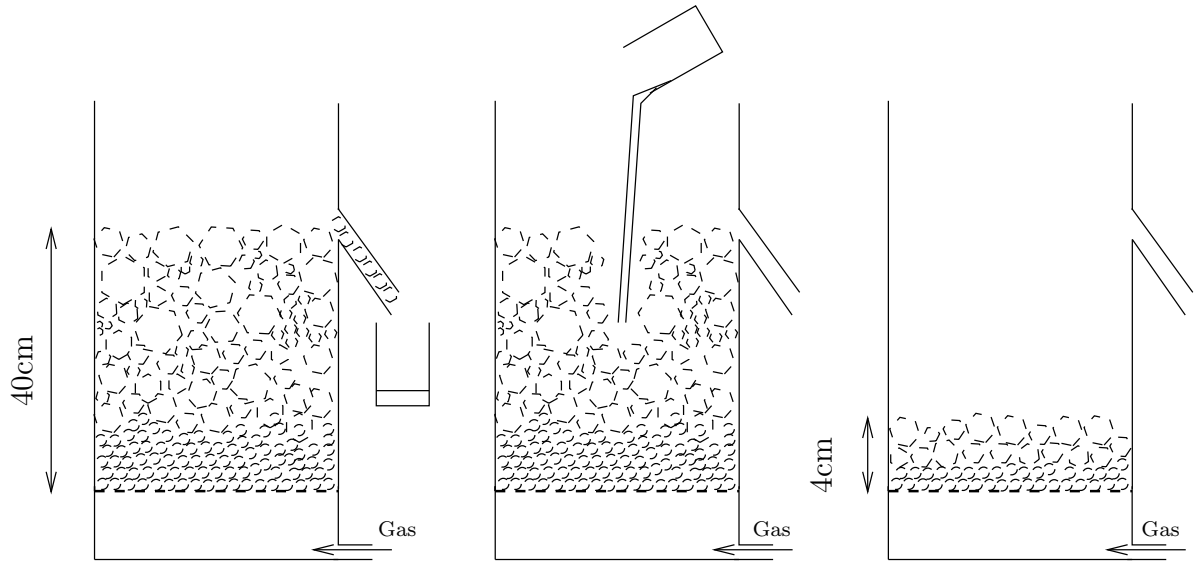

Figure 6.3: Antifoam production: the top layer of foam was removed and allowed to break down. The solution was added to the foam and it dramatically reduced its height

number of Plateau borders (N_{Pb}). We must also take account of the surfactant adsorbed onto the surface. We work in dimensional variables, and then the number of moles of surfactant contained in a lamella, M_l, is given by

$$M_l(z) = \frac{C_I(2+\mathcal{P})h(z)C^{Pb}}{2\epsilon L + \mathcal{P}h(z)}h(z)A_L + \frac{C_I\eta(2+\mathcal{P})h(z)C^{Pb}}{2\epsilon L + \mathcal{P}h(z)}2A_L, \tag{6.44}$$

and the number of moles of surfactant in a Plateau border, M_{Pb}, is given by

$$M_{Pb}(z) = C^{Pb}A(z)L + \eta C^{Pb}\pi\sqrt{\frac{A(z)}{C_1}}L, \tag{6.45}$$

Hence, the total number of moles is

$$\begin{aligned} N_{\text{Moles}} &= N_l M_l + N_{Pb}M_{Pb} && (6.46)\\ &= C^{Pb}\left(N_l A_L C_I\left(\frac{2\eta}{\epsilon L}+1\right)h(z) + N_{Pb}LA(z)\left(1+\frac{\pi\eta}{\sqrt{C_1A(z)}}\right)\right), && (6.47)\end{aligned}$$

where we have used $\mathcal{P} = L\epsilon/\eta$. The volume of liquid present is given by

$$V(z) = N_{Pb}LA(z) + N_l A_L h(z), \tag{6.48}$$

and so the total average concentration at any z station is

$$C(z) = \frac{C^{Pb}}{1+F(z)}\left(C_I\left(1+\frac{2\eta}{\epsilon L}\right) + F(z)\left(1+\frac{\eta\pi}{\sqrt{C_1A(z)}}\right)\right), \tag{6.49}$$

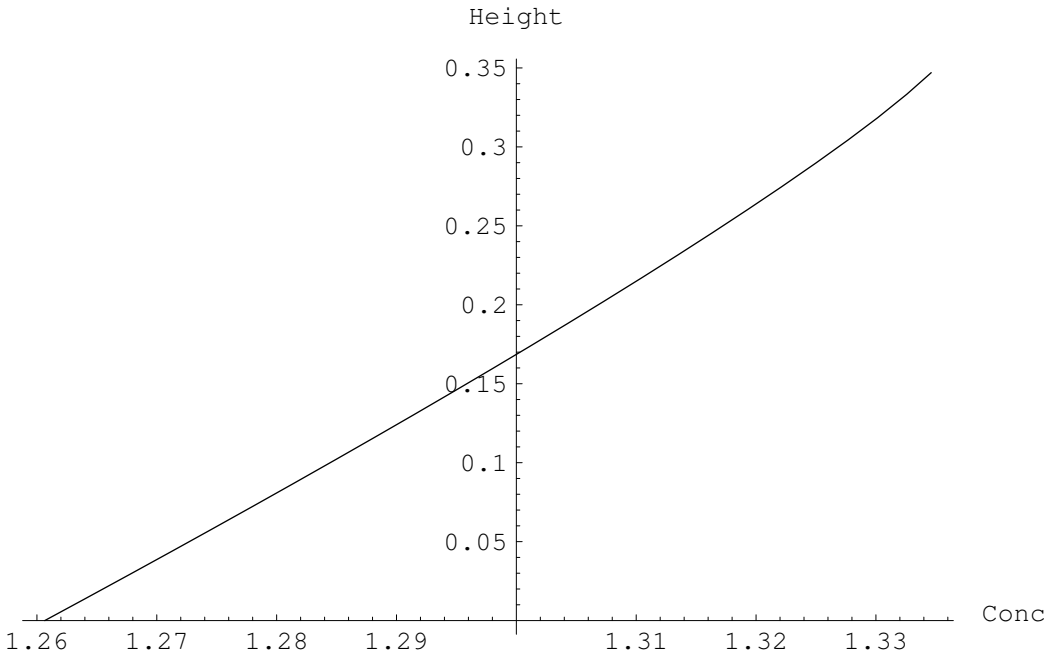

Figure 6.4: Graph showing how the total average surfactant concentration varied in the rig. The height is in metres and the concentration is in moles per cubic metre.

where $F(z) = N_{Pb}LA(z)/(N_l A_L h(z))$. Using the solutions for A and h given by (6.37) and (6.42), we use typical values of the parameters to find that

$$C(H) \sim 1.34C_0 \qquad C(0) \sim 1.26C_0 \tag{6.50}$$

i.e., $C(H) > C(0)$, where C_0 is the concentration of the surfactant solution.

The variation of C in the rig is shown in Figure 6.4. We may thus view the rig as a distillation column, since the average concentration of surfactant at the top of the foam is greater than at the bottom. When the solution is poured back into the rig, its concentration is closer to that of the foam at the top of the rig than that at the bottom. The solution therefore destroys the lower levels of the foam, and the height decreases. The foam that remains is the foam that was at the top of the column. Now the solution at the bottom of the rig will equilibrate reasonably fast (because the volume of the solution being poured back in is small), and so new foam that tries to form at the bottom of the rig will be in equilibrium with the bulk liquid, but out of equilibrium with the foam that has remained. Thus the generation of new foam will be hindered until such time as the concentration of surfactant in the remaining foam has equilibrated with the bulk concentration. After this time, the foam will be able to grow again.

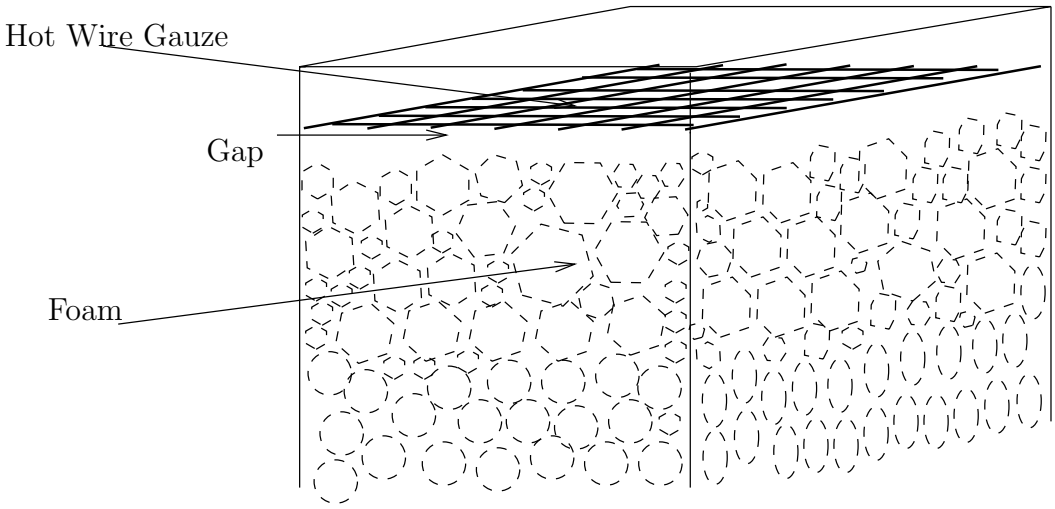

Figure 6.5: Schematic showing the hot gauze restricting the growth of a foam.

6.3.2 Second experimental set up

The second experiment uses a hot gauze (Darton [19]), see Figure 6.5.[1] The wire spacing is of the same order of magnitude as the bubble diameters. Foam is generated in the rig and allowed to rise up below a hot grid of wires. Providing the temperature is hot enough, the foam was unable to flow through the gauze. It was found that higher concentrations of surfactant require higher temperatures to contain the foam. It was also noted that there is a gap of a few millimetres between the top of the foam and the gauze.

Here, there is a mechanism that we have not considered before, namely the effect of temperature on surface tension. A change in temperature affects the surface tension in two ways. Firstly, a change from 80 to 100 degrees centigrade, say, alters the surface tension of water from about 63 mN m^{-1} to about 59 mN m^{-1} (Darton [20]). Secondly, such a change in temperature also affects the behaviour of the surfactant (recall that the relationship between σ and Γ, (2.19) contains a T factor). Both these mechanisms result in a *reduction* of the surface tension of a surfactant solution, and so there is a gradient of surface tension between hot and cold spots in a liquid which draws liquid towards the cold spot.

6.3.2.1 Microscopic model

We present preliminary ideas about the destruction of a lamella using hot wires. We restrict ourselves to the case where the surface tension varies linearly with temperature,

[1] A more recent experiment uses a spiral tube, see Stone [72].

θ, (Adamson [1])

$$\sigma = E_s \left(1 - \frac{\theta}{\theta_c}\right), \tag{6.51}$$

where E_s is a measure of the surface energy and θ_c is the critical temperature (that is, the temperature associated with the triple point of the solution). We assume that the temperature of the film is not sufficient to boil the liquid.

We model the temperature in the liquid in a lamella assuming that it obeys a convection-diffusion equation, and that, at the free surfaces, we have a radiation boundary condition (see Crank [16]). The model reads

$$D\nabla^2\theta = \theta_t + (\mathbf{u}.\nabla)\theta, \tag{6.52}$$

with, at the free surface,

$$D\theta_n = -H(\theta - \theta_{AIR}), \tag{6.53}$$

where H is a heat transfer coefficient. We study the situation in which the temperature is well-mixed and diffusion, convection and the transfer to the air term all balance. This requires the thermal Peclet number $\mathrm{Pe}_T = UL/D \sim O(1)$, and the radiation parameter $K^* = H/(D\epsilon) \sim O(1)$. We nondimensionalise and, as in the previous cases, must proceed to $O(\epsilon^2)$ in the field equation and boundary condition in order to close the model. We find that the temperature $\theta = \theta(x,t)$ satisfies

$$(h\theta_x)_x = \mathrm{Pe}_T h\,(\theta_t + u\theta_x) + K^*(2\theta - \theta_{AIR} - \theta_{BUB}), \tag{6.54}$$

where θ_{BUB} is the temperature of the air in the bubble, and θ_{AIR} is the temperature above the foam (see Figure 6.6).

To solve for the temperature field in a lamella geometry would require the decomposition of the liquid domain as described in the previous chapter, and the coupling of (6.54) with equations for conservation of mass, longitudinal force balance and surfactant concentration. Here, we simply make qualitative suggestions about how this mechanism could result in accelerated lamella rupture.

We suppose that the lamella is at temperature θ_c and the Plateau border has a different (lower) temperature (the Plateau border has the lower temperature because it contains more liquid). In this case, we will have a transition region between the two in which the temperature changes. However, here, provided the temperatures are large enough that surfactant-generated Marangoni forces are of the same size or smaller than those brought about by the temperature change, the surface tension is *lower* in the lamella than in

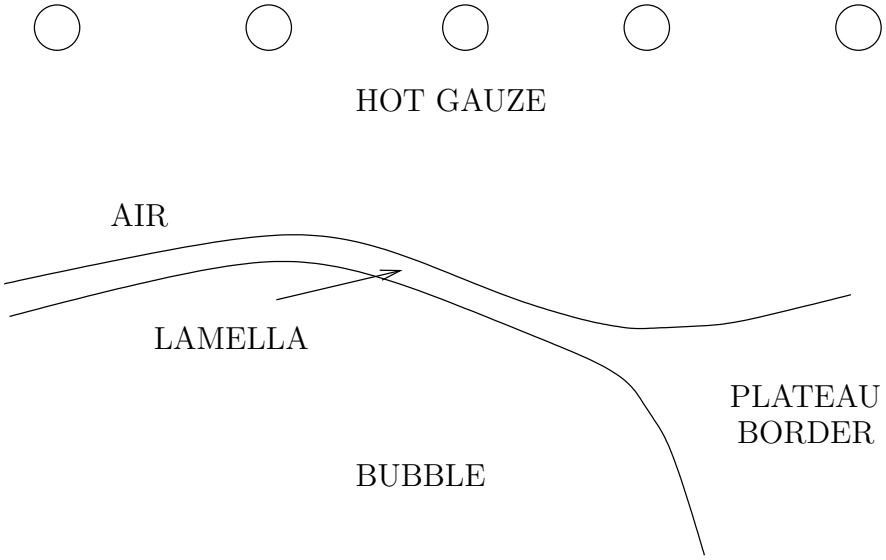

Figure 6.6: Close-up of lamella at the surface of the foam, with the hot gauze above

the Plateau border, and so this temperature difference enhances the drainage caused by capillary forces, and the lamella thins rapidly.

6.4 Short-comings of the models

Our approach in this chapter has been less systematic than in previous ones. Ultimately, we must back up our modelling by more rigorous derivations of our models. In the case of the Plateau border flows, this will require the extension of the work in Cummings and Howell [17] to include the evolution of non-axisymmetric fibres that have cusps. In our modelling, we have neglected the nodes that are present within the foam. These Plateau border junctions have an associated curvature and shape which will affect the liquid flow. In future modelling, these should also be taken into account.

Chapter 7

Conclusion

In this chapter we give a brief summary of the main results that we have obtained and we then propose some extensions to this work. We also discuss some experiments that are suggested by our modelling work.

7.1 Review of thesis

In Chapter 1 we presented an overview of foaming situations, foam structure and foam properties, and discussed some of the general literature on various aspects of foam modelling.

In Chapter 2, we presented models for surfactant solutions and for volatile-inert systems. In the surfactant case, we showed how to formulate the model for adsorption at the free surface, and discussed the variation of surface tension with surface concentration. In the volatile-inert system, we incorporated bulk and evaporative mass transfer into our model and also discussed the variation of surface tension with composition.

In Chapter 3 we formulated a model to describe the flow of liquid and the distribution of surfactant in the overflowing cylinder experiment. The general structure of the problem is as follows

- gravity is strong enough to keep the top surface flat;
- the bulk flow is dominated by inertia; we solved the inviscid problem to find the "outer" flow;
- convection dominates surfactant transport and thus the surfactant concentration is constant throughout most of the cylinder;

- there are hydrodynamic and diffusive boundary layers at the free surface where the effects of viscosity and diffusivity become important; the diffusive boundary layer is much thinner than the hydrodynamic boundary layer;
- at the free surface, the system selects its own length scale and velocity scale which are therefore independent of the radius of the cylinder and the flux of liquid imposed at depth; this agrees with experimental evidence.

The most puzzling aspect of the model is that it appears to admit a one-parameter family of solutions. When we fixed this parameter using experimental data, the rest of the solution agreed well with experiments. However, we have been unable to find a mathematical criterion to select the value of the arbitrary constant. We hypothesise that neglect of rim effects was the most likely cause of the indeterminacy.

In Chapter 4, we derived models for thin films between two free surfaces acting under the influence of viscosity, capillarity, and surface tension gradients. We found that

- there are two distinguished limits in the liquid problem: one where viscous, capillary and Marangoni effects balance, and one where capillary, Marangoni and lubrication effects balance. There is no limit in which both viscosity and lubrication effects are important;
- there are two distinguished limits for the surfactant (or volatile) problem: one where longitudinal diffusion, convection and surface convection (or evaporation) balance, and one where lateral diffusion, convection and surface convection (or evaporation) balance;

The dominant physical effects are determined by the relative sizes of the corresponding dimensionless parameters, and we tabulated all the possible relevant combinations.

In Chapter 5 we used the models that we derived in Chapter 4 to describe the flow of liquid from a lamella into a Plateau border. In each case we decoupled the liquid regime into a time-dependent lamella, a capillary-static Plateau border and a quasi-steady transition region between the two. We showed the following.

- A surfactant-free lamella draining under the influence of viscosity and constant surface tension ruptures extremely quickly.
- The distinguished limit most appropriate to the problem of foam lamella drainage contains Marangoni, capillary and lubrication effects. In this limit, the liquid is retarded by surface tension gradient effects and thus exhibits a much longer lamella lifetime.

- Our theoretical estimated rupture times are broadly in line with experiments.
- One interesting prediction of our models was that the film thins slowly down to a critical thickness, after which it ruptures very rapidly.

We also obtained the film thickness and surfactant concentration profiles in each case, and the velocity field in the liquid.

In Chapter 6, we adopted a more phenomenological approach in obtaining bulk models for foams. We presented a model for drainage of liquid through a foam including surface tension, gravity and transport from the lamellae into the Plateau borders. Our model for a continuously regenerated foam gave a height of the correct order of magnitude. We also discussed how foam removed from the top of the rig could be used as an antifoam, and how a hot gauze could cause foam destruction.

7.2 Future work

In this thesis we have considered situations in which a Marangoni shear at a free surface enhances or retards the flow. There are numerous other situations which could benefit from our modelling approach. For example, as commented on in Chapter 3, another experiment used to measure the properties of expanding surfaces uses a jet of surfactant solution. The solution is 'shot' from a nozzle at high velocity, and measurements of surface velocities and concentrations are taken close to the point of exit from the nozzle (and out as far as the jet remains horizontal). The situation here is different from the overflowing cylinder set-up for a number of reasons: the most important difference is that here the surfactant at the surface is not in equilibrium with the surfactant below the surface. The case where the surface tension takes much longer to reach its equilibrium value than the jet does to reach an effective uniform velocity has been previously studied by Harper [34]. The liquid configuration is shown in Figure 7.1.

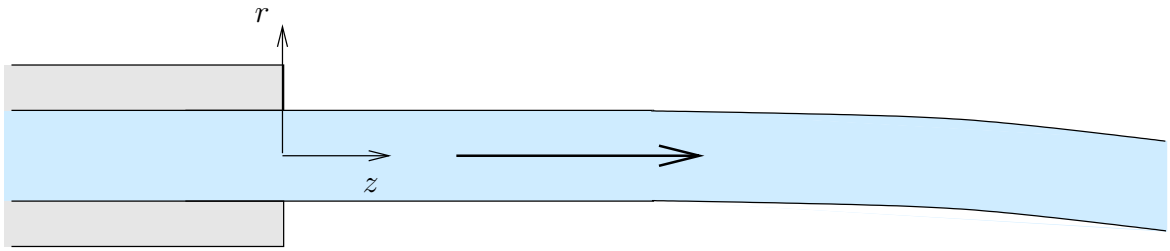

Figure 7.1: The jet experiment.

The liquid velocity at the exit from the nozzle is of the order of several metres per second, but the liquid velocity profile is unknown in the nozzle itself. A crucial part of the modelling of the system is to determine the correct velocity profile at the exit. The surfactant distribution in the nozzle is more straightforward. Since the surfactant does not adsorb onto the surfaces in the apparatus, we have $C = C_b$ and $\Gamma = 0$ for $z \leq 0$. Outside the nozzle, the liquid must adjust itself to take account of the change from a no-slip boundary condition to one of continuity of tangential stress. The liquid velocity profile will change to plug flow at distance down the stream, while the surfactant will equilibrate with the surface. The surfactant distribution at the surface will have the opposite effect to that in the overflowing cylinder. Here, we have the surface concentration increasing as z increases, and we expect a surface tension gradient to be established which retards the flow close to the surface. The study of such a system would be useful since, in a foam, the surface tension gradient generates a flow which opposes the main flow of the liquid.

In the rest of this section we restrict ourselves to suggestions of future work that follow directly from the work in this thesis.

- Overflowing Cylinder

  We reiterate that finding the undetermined parameter in the overflowing cylinder model, possibly by solving the coupled boundary layer problems on the finite domain of the cylinder is the next (and most important) step towards a complete description of the liquid flow and surfactant distribution. Another extension to this work would be to look above the critical micelle concentration, utilising a convection-diffusion problem for both the bulk and micellar surfactant with interactions between the two, as well as adsorption onto the surface. This could be checked against the (already existing) experimental work.

- Models for thin films

  Our work on thin films acting under Marangoni, viscous and capillary effects could be extended to include other physical effects such as inertia and disjoining pressure. Such effects could become important, for example, in the final thinning phase of foam films.

- Lamellae with surfactants

  We formulated our models for the drainage of foam lamellae in the limit of small concentration. For foam containing higher surfactant concentrations, we would have to include the nonlinear relationships between surface tension, surface concentration

and subsurface concentration, but we would expect the problem to exhibit the same qualitative behaviour as the model that we have considered. The study of the critical blow-up thickness discovered in §5.3.6.1 also deserves considerably more attention, in particular, to see whether or not viscosity will enable the film to continue thinning past the critical thickness.

- Lamellae with volatiles

  The model for drainage of a lamella stabilised by volatile components is at a preliminary stage. Carrying out a detailed study of the region where viscous effects become important (by looking at (5.207)-(5.208)) is obviously the next thing to do here.

- Destabilisation of foam films

  In Chapter 6 we discussed the destabilisation of foam films using an antifoam or heat. Development of the thin film theory to include (i) a point source of a "strong" surfactant or (ii) heat transfer, would enable us to make progress towards a full description of foam destruction in industrially relevant situations.

- Macroscopic models

  Our Plateau border work could be extended to include the effect of the nodes. Hopefully, this would determine a velocity scale for the problem on the microscale of one Plateau border. Our macroscopic model for the foam rig needs refining and checking against experimental observations of the heights reached and the foam coarseness.

A natural extension of this work would be to couple the changes in Plateau border area into the lamella model (remember that, at present, our model assumes that the area is constant).

7.3 Experiments that would provide extra insight into foam modelling

There are numerous experiments that would provide valuable information for foam modelling. We briefly detail these below.

- Chapter 3

  The overflowing cylinder experiments could be repeated with two modifications. Firstly, the use of a cylinder with a much larger radius, 20 cm say, might highlight

any variation of the surface properties with radius (which have not been seen by varying the radius between 3 and 5 cm). Secondly, the use of an overflowing trough might allow us to check the validity of a two-dimensional version of the model.

The overflowing cylinder could also be used to check the behaviour of the volatile-inert system in the presence of an expanding free surface, which could provide valuable insight into the modelling of expanding free surfaces in hydrocarbon foams.

- Chapter 5

  Any non-invasive experiments that could be carried out on individual lamellae would provide a wealth of data that we could check against the predictions of our model. For example, the direction of the surface flow could be checked, as could the dimpling in the film.

- Chapter 6

  Taking samples of the foam at various levels in the foam rig would enable us to verify whether our crude model for the surfactant distribution in the foam is correct. Checking whether it is the top or bottom layer of foam which remains when the surfactant solution is added would test our hypothesis about why the foam is destroyed.

7.4 Discussion

In this thesis we have developed models for describing the evolution of free surfaces under the influence of surfactants. We have succeeded in systematically modelling the liquid flow and surfactant distribution in the microstructure of a foam and thereby explained how lamellae can be stabilised by the presence of surfactant. This provides a key building block for the fundamental understanding of why an intrinsically unstable foam can persist after it has been formed. The final goal, which has yet to be achieved satisfactorily, is to predict the macroscopic constitutive properties by systematically averaging the microstructure.

Bibliography

[1] A.W. Adamson. *Physical chemistry of surfaces, 4th Ed.* J Wiley and Sons, 1982.

[2] P.W. Atkins. *The Elements of Physical Chemistry.* Oxford University Press, 1992.

[3] J.H. Aubert, A.M. Kraynik, and P.B. Rand. Aqueous foams. *Scientific American*, **254**(5):58–66, 1986.

[4] C.W. Bamforth. Foaming in beer and breweries: problems, challenges and solutions. In *Froths and Foams in Biotechnology.* Process engineering, Biotechnology and Separation Science and Technology Groups, SCI, 1997.

[5] M. Barigou and J.F. Davidson. Soap film drainage: Theory and experiment. *Chem. Eng. Sci.*, **49**(11):1807–1819, 1994.

[6] G.K. Batchelor. *An introduction to fluid dynamics.* Cambridge University Press, 1967.

[7] D.J.M. Bergink-Martens, H.J. Bos, and A. Prins. Surface dilation and fluid-dynamical behaviour of Newtonian liquids in an overflowing cylinder. ii. surfactant solutions. *J. Coll. Int. Sci.*, **165**:221–228, 1994.

[8] D.J.M. Bergink-Martens, H.J. Bos, A. Prins, and B.C. Schulte. Surface dilation and fluid-dynamical behaviour of Newtonian liquids in an overflowing cylinder. i. pure liquids. *J. Coll. Int. Sci.*, **138**:1–9, 1990.

[9] D.J.M. Bergink-Martens, H.J. Bos, A. Prins, and A.F. Zuidberg. Surface dilational behaviour of surfactant solutions. *Coll. Surf.*, **65**:191–199, 1992.

[10] A. Bhakta and E. Ruckenstein. Modelling the generation and collapse of aqueous foams. *Langmuir*, **12**:3089–3100, 1996.

[11] J.J. Bikerman. *Foams.* Springer-Verlag, 1973.

[12] R.J. Braun, S. Naire, S. Snow, and U.C. Pernisz. Drainage of a thin free film. Preprint, 1998.

[13] R.J. Braun, S. Naire, S. Snow, and U.C. Pernisz. Gravitational drainage of a tangentially-immobile thick film. Submitted: J. Coll. Int. Sci., 1998.

[14] C.J.W. Breward, R.C. Darton, P.D. Howell, and J.R. Ockendon. Modelling foam drainage. *I Chem E Symposium Series*, **142**:1009–1019, 1997.

[15] C.-H. Chang and E.I. Frances. Adsorption dynamics of surfactants at the air-water interface: a critical review of mathematical models and mechanisms. *Colloids Surfaces A: Physicochem. Eng. Aspects*, **100**:1–45, 1995.

[16] J. Crank. *The Mathematics of Diffusion.* Oxford University Press, 1973.

[17] L.J. Cummings and P.D. Howell. On the evolution of nonaxisymmetric viscous fibres with surface tension, inertia and gravity. *J. Fluid Mech.*, **389**:361–389, 1999.

[18] R.C. Darton. Foams in distillation columns. *Private communication*, 1995.

[19] R.C Darton. Foam destruction using a hot wire gauze. *Private communication*, 1997.

[20] R.C. Darton. Surface tension changes with temperature. *Private Communication*, 1999.

[21] R.C. Darton, H. Grunnet-Jepsen, P.D. Thomas, and P.B. Whalley. Foam stability and structure in adsorption and distillation. AIChE, 1994.

[22] R. Dautov, K.G. Kornev, and Mourzenko V. Foam patterning in porous media. *Phys. Rev. E*, **55**(6):6929–6944, 1997.

[23] A. De Wit, D. Gallez, and C.I. Christov. Nonlinear evolution equations for thin liquid films with insoluble surfactants. *Phys. Fluids*, **6**:3256–3265, 1994.

[24] K. Denbigh. *The Principles of Chemical Equilibrium, 4th Ed.* Cambridge University Press, 1981.

[25] D. Desai and R. Kumar. Flow through a plateau border of cellular foam. *Chem. Eng. Sci.*, **37**:1361–1370, 1982.

[26] J. Dewynne, J.R. Ockendon, and P. Wilmott. On a mathematical model for fibre tapering. *SIAM J. Appl. Math.*, **49**(4):983–990, 1989.

[27] D. Dey, J.M. Boulton-Stone, A.N. Emery, and J.R. Blake. Experimental comparisons with a numerical model of surfactant effects on the burst of a single bubble. *Chem. Eng. Sci.*, **52**(16):2769–2783, 1997.

[28] T. Erneux and S.H. Davis. Nonlinear rupture of free films. *Phys. Fluids A*, **5**:1117–1122, 1993.

[29] D.P. Gaver and J.B. Grotberg. The dynamics of a localised surfactant on a thin film. *J. Fluid. Mech.*, **213**:127–148, 1990.

[30] K.A. Gillow. *Modelling an experiment to study surface dilation effects.* Master's thesis, Mathematics Department, Oxford, 1995.

[31] H. Grunnet-Jepsen, R.C. Darton, and P.B. Whalley. Modelling foaming behaviour. In R. Agrawal and L. Dall-Bauman, editors, *Recent Developments and future opportunities in separations technology.* AIChE annual meeting at Miami Beach, AIChE, 1995. Paper 19b.

[32] D. Halpern and J.B. Grotberg. Dynamics and transport of a localised soluble surfactant on a thin film. *J. Fluid Mech.*, **237**:1–11, 1992.

[33] J. F. Harper. On spherical bubbles rising steadily in dilute surfactant solutions. *Q. J. Mech. Appl. Math.*, **27**(1):87–100, 1974.

[34] J.F. Harper. Surface ages in vibrating jet experiments. *Chem. Eng. Sci.*, **28**:323–325, 1973.

[35] J.F. Harper. The rear stagnation point of a bubble rising steadily in a dilute surfactant solution. *Q. J. Mech. Appl. Math.*, **41**:203–213, 1988.

[36] P.D. Howell. *Extensional thin layer flows.* DPhil thesis, Mathematics Department, Oxford, 1994.

[37] P.D. Howell. Models for thin viscous sheets. *Euro. J. Appl. Math.*, **7**:321–343, 1996.

[38] P.D. Howell. The draining of a two-dimensional bubble. *J. Engrg. Math.*, **35**:251–272, 1999.

[39] S.D. Howison, J.A. Moriarty, J.R. Ockendon, E.L. Terrill, and S.K. Wilson. A mathematical model for drying paint layers. *J. Engrg. Math.*, **32**:377–394, 1997.

[40] M.P. Ida and M.J. Miksis. Thin film rupture. *Appl. Math. Lett.*, **9**:35–40, 1996.

[41] O.E. Jensen. The spreading of insoluble surfactant at the free surface of a deep fluid layer. *J. Fluid Mech.*, **293**:349–378, 1995.

[42] O.E. Jensen and J.B. Grotberg. Insoluble surfactant spreading on a thin viscous film: shock evolution and film rupture. *J. Fluid Mech.*, **240**:259–288, 1995.

[43] J.-L. Joye, C.A. Miller, and G.J. Hirasaki. Dimple formation and behavior during axisymmetrical foam film drainage. *Langmuir*, **8**:3083–3092, 1992.

[44] K.G. Kornev. Capillary pinning of foam in porous media. *JETP*, **80**(6):1049–1055, 1995.

[45] K.G. Kornev and V.N. Kurdyumov. Foams in porous media as a problem in polymer physics. *JETP*, **79**(2):251–261, 1994.

[46] A.M. Kraynik. Foam flows. *Ann. Rev. Fluid Mech.*, **20**:325–357, 1988.

[47] A.M. Kraynik and D.A. Reinelt. The linear elastic behaviour of a bidisperse Weaire-Phelan soap foam. *Chem. Eng. Comms.*, **150**:409–420, 1996.

[48] A.M. Kraynik and D.A. Reinelt. The linear elastic behaviour of dry soap films. *J. Coll. Int. Sci.*, **181**:511–520, 1996.

[49] A.M. Kraynik and D.A. Reinelt. The microrheology of wet foams. Private Communication, 1996.

[50] A.M. Kraynik and D.A Reinelt. Elastic-plastic behaviour of a Kelvin foam. In D. Weaire and C. Frank, editors, *The Kelvin problem*. Taylor and Francis, 1997.

[51] V.G. Levich. *Phisicochemical Hydrodynamics*. Prentice-Hall, 1962.

[52] S. Manning-Benson. *The dynamics of surfactant adsorption*. DPhil thesis, Physical and Theoretical Chemisrty Laboratory, Oxford, 1998.

[53] S. Manning-Benson. Velocity data fits. *Private Communication*, 1998.

[54] S. Manning-Benson, C.D. Bain, and R.C. Darton. Measurement of dynamic interfacial properties in an overflowing cylinder by ellipsometry. *J. Coll. Int. Sci.*, **189**:109–116, 1997.

[55] S. Manning-Benson, C.D. Bain, R.C. Darton, D. Sharpe, J. Eastoe, and P. Reynolds. Invasive and non-invasive measurements of dynamic surface tensions. *Langmuir*, **13**:5808–5810, 1997.

[56] S. Manning-Benson, S.R.W. Parker, C.D. Bain, and J. Penfold. Measurement of the dynamic surface excess in an overflowing cylinder by neutron reflection. *Langmuir*, **14**:990–996, 1998.

[57] E.B. Matzke. The three-dimensional shape of bubbles in foam-an analysis of the role of surface forces in three dimensional cell shape determination. *Am. J. Botany*, **33**:58–80, 1946.

[58] S. Middleman. *Modeling axisymmetric flows*. Academic Press, 1995.

[59] T.G. Myers. Thin films with high surface tension. *SIAM Rev.*, **40**(3):441–462, 1998.

[60] G. Narsimhan. Unsteady state drainage of a standing foam. *AIChE Symposium Series*, **86**(277):76–86, 1990.

[61] C. Nexhip. Slag foams. *Private Communication*, 1997.

[62] H. Ockendon and J.R. Ockendon. *Viscous Flow*. Cambridge University Press, 1995.

[63] A. Oron, S.H. Davis, and S.G. Bankoff. Long-scale evolution of this liquid films. *Rev. Mod. Phys.*, **69**(3):931–980, 1997.

[64] A.B. Pandit and J.F. Davidson. Hydrodynamics of the rupture of thin liquid films. *J. Fluid. Mech.*, **212**:11–24, 1990.

[65] J.R.A. Pearson. *Mechanics of Polymer Processing*. Kluwer Academic Publishers, 1985.

[66] J. Plateau. *Statique expérimentale et théorique des liquides soumis aux seules forces moléculaires*. Gauthier-Villars, 1873.

[67] K. Podual, R. Kumar, and K.S. Gandhi. A new model for drainage of static foams. *Chem. Eng. Sci.*, **51**(9):1393–1403, 1996.

[68] D.A. Reinelt and A.M. Kraynik. Simple shearing flow of a dry Kelvin soap foam. *J. Fluid Mech.*, **311**:327–342, 1996.

[69] L.W. Schwartz and H.M. Princen. A theory of extensional viscosity for flowing foams and concentrated emulsions. *J. Coll. Int. Sci.*, **118**:201–211, 1987.

[70] G. Shugai. *Micromechanics of foam flows*. PhD thesis, Stockholm, 1998.

[71] G. Singh, G.J. Hirasaki, and C.A. Miller. Effect of material properties on the drainage of symmetric, plane parallel, mobile foam films. *J. Coll. Int. Sci.*, **184**:92–105, 1996.

[72] J. Stone. Foam destruction using a hot wire spiral. *Private communication*, 1999.

[73] K-H. Sun. Experimental observations in the foam rig. *Private communication*, 1997.

[74] W. Thompson (Lord Kelvin). On the division of space with minimum partitional area. *Phil. Mag.*, **24**:503–514, 1887.

[75] E.O. Tuck and L.W. Schwartz. A numerical and asymptotic study of some third-order ordinary differential equations relevant to draining and coating flows. *SIAM Rev.*, **32**(3):453–469, 1990.

[76] G. Verbist and D. Weaire. A soluble model for foam drainage. *EuroPhys. Lett.*, **26**:631–634, 1994.

[77] G. Verbist, D. Weaire, and A.M. Kraynik. The foam drainage equation. *J. Phys.: Condens. Matter*, **8**:3715–3731, 1996.

[78] D. Weaire and J.P. Kermode. Computer simulation of a two-dimensional soap froth i. Method and motivation. *Phil. Mag. B*, **48**(3):245–259, 1983.

[79] D. Weaire and J.P. Kermode. Computer simulation of a two-dimensional soap froth ii. Analysis of results. *Phil. Mag. B*, **50**(3):379–395, 1984.

[80] D. Weaire and R. Phelan. A counter-example to Kelvin's conjecture on minimal surfaces. *Phil. Mag. Lett.*, **69**:107–110, 1994.

[81] S.K. Wilson. The levelling of paint films. *IMA J. Appl. Math.*, **50**:149–166, 1993.

[82] F.J. Zuiderweg and A. Harmens. The influence of surface phenomena on the performance of distillation columns. *Chem. Eng. Sci.*, **9**:89–108, 1958.